HEAT EXCHANGER FOULING
BY PRECIPITATION OF CALCIUM PHOSPHATES

By

ATMAJEET SINGH

B.Tech., Indian Institute of Technology, New Delhi, INDIA

A THESIS IN PARTIAL FULFILMENT OF

THE REQUIREMENTS FOR THE DEGREE OF

MASTER OF APPLIED SCIENCE

in

THE FACULTY OF GRADUATE STUDIES

(Department of Chemical Engineering)

We accept this thesis as conforming

to the required standard

THE UNIVERSITY OF BRITISH COLUMBIA

October 1992

In presenting this thesis in partial fulfilment of the requirements for an advanced degree at the University of British Columbia, I agree that the Library shall make it freely available for reference and study. I further agree that permission for extensive copying of this thesis for scholarly purposes may be granted by the head of my department or by his or her representatives. It is understood that copying or publication of this thesis for financial gain shall not be allowed without my written permission.

Department of CHEMICAL ENGG.

The University of British Columbia
Vancouver, Canada

Date 15th Oct. 92

DE-6 (2/88)

ABSTRACT

The fouling characteristics of artificially hardened waters containing calcium and orthophosphate ions were investigated. The water was circulated through a steam heated double pipe heat exchanger under turbulent flow conditions. Inlet water temperatures were about 20 to 25°C and the phosphate content about 100 ppm. Experiments were carried out to ascertain the effects of pH, velocity, surface temperature and concentrations of the calcium and the orthophosphate on the fouling process. The fouling behaviour was recorded in terms of the fouling resistance-time curve which was calculated from the time dependence of the overall heat transfer coefficients. Under the constant heat flux condition imposed, the fouling resistance was generally linear in time; however, asymptotic fouling was observed in some cases.

The fouling rate was found to be a very strong function of the pH over the range 6.5 to 8.0. The rate was also found to be exponentially dependent on the calculated surface temperature. The initial fouling rate increased linearly with the velocity and with the concentrations of scale forming species. Deposit thickness increased with heated length of the stainless steel test section. In most cases, the deposit was a dense crystalline scale, which had a Ca/P molar ratio of 1.35 ± 0.15. The results are discussed in terms of the ionic equilibrium involved and the solubility and crystallisation kinetics from the literature. It is apparent that the rate of phosphate precipitation is influenced both by surface reaction and mass transfer in the range of the variables studied. Findings are compared with the few prior phosphate fouling studies from the literature. Scale density is reported, and its thermal conductivity estimated using the fouling resistance measurements.

TABLE OF CONTENTS

LIST OF TABLES

LIST OF FIGURES

APPENDIX III

APPENDIX IV

ACKNOWLEDGEMENTS

I would like to express my indebtedness to Dr. A.P. Watkinson for his beneficial guidance and support throughout the duration of this research work.

I am also thankful to the workshop staff and the electrical workshop for their help in installation and maintenance jobs. Special thanks are also due to Mr. Horace Lam of the stores for his help in ordering and procuring chemicals and parts. I am grateful to my wife Paramjeet for her unlimited cooperation and care to help me in completing this project.

Financial support provided by NSERC is also gratefully acknowledged.

§1. INTRODUCTION

In general, heat exchanger fouling can be defined as the phenomenon of any undesirable deposition or solidification on the heat transfer surface, caused by the presence in the fluids of substances that either tend to accumulate at or react with the surface. Thermal fouling may be promoted by a temperature gradient near the heat transfer surface. The term scaling is usually used to describe the formation of a dense, crystalline deposit, which adheres well to the heat transfer surface. Fouling is a more general term and can include deposition of non-crystalline as well as crystalline solids. Fouling has been classified into six different types by Epstein (1), based on the mechanism by which it occurs. These are as follows:

1. Precipitation Fouling : the precipitation, on the heat transfer surface, of normal or inverse solubility solutes due to supersaturation.

2. Particulate Fouling : the deposition of suspended solids that are already present in a fluid bulk onto a heat transfer surface caused by the concentration gradient and/or gravity.

3. Chemical Reaction Fouling : the formation of solid products due to chemical reactions which occur at the heat transfer surface. The metallic surface may act as a catalyst but not as a reactant.

4. Corrosion Fouling : the reaction of the heat transfer surface with the process fluid resulting in corrosion products. The corrosion may enhance formation of the fouled layer by other mechanisms.

5. Biofouling : the accumulation and possible growth of biological organisms and their byproducts on a heat exchanger surface.

6. Freezing Fouling : the solidification of a pure liquid or components of a liquid as an outcome of a heat transfer surface being cooled below the freezing point of the fluid or any of its components.

Hasson (2) defines precipitation fouling as " the phenomenon of a solid layer deposition on a heat transfer surface, arising primarily from the presence of dissolved inorganic salts in the flowing solution which exhibit supersaturation under the process conditions " . Precipitation fouling is quite common in industrial cooling water systems (3,4). The most common deposits which occur in cooling water systems are calcium carbonate, calcium sulphate, calcium phosphate, magnesium silicate, and silica (5). Among the less frequent ones are iron oxide, zinc phosphate, calcium fluoride and iron carbonate. Calcium carbonate is by far the most common scale found in cooling water systems. The degree of scaling depends on calcium hardness and bicarbonate alkalinity. Calcium sulphate occurs less commonly than calcium carbonate. If carbonates and sulphates are both present, only when all the carbonate is precipitated will calcium deposit as a sulphate. Magnesium silicate scale is quite rare and is formed as a two step

process : magnesium hydroxide precipitates first, which reacts with suspended and dissolved silica to form a dense, hard-to-remove scale. Since silica solubility increases with temperature and pH, this type of scale is found in the cold regions of heat exchangers. Silica will generally precipitate only if its concentration is above 150 ppm; this value constitutes a threshold limit for cooling water systems (5).

In industrial heat transfer operations, significant fouling can occur because of deposition of calcium orthophosphate salts (3). The problem of phosphate in waters can be due to high concentration factors used in recirculating cooling water systems due to local water shortage; use of low quality make-up water, for example, an end product of a sewage treatment facility; and use of waters with residues from organic phosphonate corrosion and fouling inhibitors. Also, river or lake water can accumulate phosphates from agricultural run-off.

Several phosphate-containing organic phosphonates ($-PO(OH)_2$) and polyphosphates (e.g. $Na_2P_2O_7$, sodium pyrophosphate) are used in cooling water systems to reduce corrosion (9,12). Some of these are as follows:

1) 1-hydroxyethylidene-1-1-diphosphonic acid (HEDP)
2) Amine tris methylene phosphonic acid (AMP)
3) Ethylene diamine tetramethylene phosphonic acid (EDTP)
4) Hexamethylene diamine tetramethylene phosphonic acid (HMTD)

These compounds are effective scaling inhibitors for calcium carbonate and calcium

sulphate scaling. In addition to that, these phosphonates also act as corrosion inhibitors in many cooling water applications. However, these compounds can be oxidised by the different oxidisers e.g. chlorine present in the cooling water. The products of their oxidation are orthophosphate ions which can give rise to the problem of phosphate scaling in water containing significant amounts of calcium hardness. Under normal conditions, the organic phosphonates are less likely to degrade into orthophosphate ions than are the inorganic polyphosphates, e.g. Na_3PO_4, that are used for the same purpose.

The fouling of heat exchangers caused by precipitation of inverse solubility salts, such as calcium phosphates, gives rise to various deleterious effects. The efficiency of heat exchange can be reduced significantly, resulting in energy losses. Cleaning costs can be high and production rates reduce by shutdowns. There may be an increase in the pumping costs due to increased surface roughness caused by fouling and due to reduced cross-sectional area available for flow. Also, fouling may enhance corrosion of the heat transfer surface.

Phosphate fouling can occur with relatively low levels of soluble phosphates (5-10 ppm as PO_4^{3-}) in industries employing condensers and evaporators (3,4). This can result in huge financial costs due to production interruptions, labour costs for cleaning, etc. For example, the losses at a 2000 MW power station because of phosphate fouling were estimated to be 6 million dollars for 1975 (3). Fouling of heat exchangers by all causes has been estimated by Smith and Dirks to cost somewhere between 4.2 and 10 billion dollars per year in the U.S. alone (6). Thackery (7) suggested that fouling costs in the U.K. were about 0.73-1.20 billion dollars in

1979.

Phosphate fouling is of considerable concern to the dairy industry also. During milk processing, calcium phosphates are deposited on plate heat exchangers, which along with denatured proteins can aggravate the problem.

Following are some approaches to deal with precipitation fouling (8):

1. Development of theoretical models for quantitative prediction of fouling rates under different sets of conditions. These could identify conditions to minimise fouling.

2. Modification of the flow pattern and/or equipment geometry to minimise fouling, e.g. increasing the velocity by recirculation, bypassing the process fluid, using fluidised bed heat exchangers instead of shell and tube type, etc.

3. On-line control of fouling using antifoulants or additives that minimise deposit formation.

4. Mechanical and chemical methods to remove deposits after they have formed.

The major factors which affect precipitation fouling have been well recognised by many authors and are as follows:

1. Water chemistry : the concentration of ionic species that participate in the precipitation process and pH that determines the distribution of different dissolved species significantly influences the fouling process. For a definite water chemistry, varying pH can significantly alter the fouling rate since the distribution of anionic species changes, and the solubility limit may be exceeded.

2. Surface and bulk temperatures : since the depositing salts in most cooling water flow situations have inverse solubility, an increase in surface temperature can increase the fouling rate. In the case where deposition is purely mass transfer controlled, increasing the temperature would produce little change.

3. Velocity : the effect of velocity on the fouling rate depends on the type of fouling and must be established by experiments. In general, increasing the velocity tends to decrease the fouling rate (6).

4. Nature of the heating surface : the tube material becomes most important in the case of corrosion fouling, but could affect precipitation fouling as well. Surface finish can affect the nucleation delay time, the attachment of the deposits, and the labour costs of the cleaning operation. In general, excluding surface roughness effects, if the tube material doesn't act either as a catalyst or as a reactant, it should have little effect on the rate of fouling. In a study on phosphate fouling done by Knudsen et. al. (9), it was found that different metal surfaces (stainless steel, 90/10 copper nickel and admiralty

brass) had practically no effect on the fouling rate. Carbon steel in the beginning of the fouling process showed a higher rate of fouling due to formation of a corrosion film.

Since precipitation fouling is a costly phenomenon in many types of industry e.g. food and kindred products, wood and paper products, chemical and allied industries, petroleum refineries and electricity generation, it is worthwhile to quantitatively assess the effects of various variables on the fouling rate and to develop theoretical models of the process. This has been done to a considerable extent for deposition of calcium carbonate, calcium sulphate and some other salts. However, previous studies in phosphate deposition are rather limited. In this work an attempt has been made to interpret results from prior experimental findings, to establish new experimental data, and to interpret all these results using fundamentals of precipitation equilibria and kinetics, heat transfer and fluid flow.

§ 2. THEORY

2.1 Definitions of Solubility and Supersaturation

Solubility of a salt in a fluid is defined as the maximum concentration of the salt in that fluid that can remain for an infinite time in a dissolved state without being precipitated. Solubility is a function of temperature, pH and the nature and extent of other components present. For most salts, the solubility increases with temperature, but for some salts, e.g., calcium carbonate and phosphates, it decreases with temperature. These salts are said to have inverse solubility characteristics. The solubility product is defined as the product of the concentration of all the ions raised to their respective stoichiometric coefficients at the saturation condition. According to the "common ion effect", precipitation of a salt can take place if the solubility product is exceeded. A solution is said to be supersaturated under such conditions. Thus, one of the prerequisites of precipitation fouling is creation of a supersaturation potential. Hasson (2) lists various cases that may lead to supersaturation:

1. A dissolved salt is concentrated beyond its solubility limits at a particular temperature.

2. A solution containing a dissolved salt is either cooled below or heated above its normal solubility temperature, depending on whether the salt shows normal or inverse solubility with temperature. This can occur locally in a system.

3. Streams of different compositions are mixed together so that the ionic product of one of the potentially scale forming salts exceeds its solubility product at that temperature.

2.2 General Mechanism of Precipitation Fouling in a Heat Exchanger

Considering the situation where water containing potential scale forming ions such as calcium and orthophosphate flows adjacent to a hot heat transfer surface, local supersaturation may occur because of the temperature profile that exists near the heat transfer surface. The metal surface provides an excellent site for nucleation. The following steps may be involved in the subsequent scaling process:

1. Diffusion of the calcium and phosphate ions from the bulk to the solid-liquid interface.

2. Nucleation and precipitation of calcium phosphate salts on the heat transfer surface. These processes may or may not be physically and chemically well-defined. In other words, the deposit may be crystalline or non-crystalline in nature, and of a definite or variable stoichiometric composition.

3. Removal phenomena may occur due to shear stresses applied by the fluid on the depositing layer or by thermal stresses caused by temperature variations over time.

4. Aging phenomena that can either harden or loosen the deposit may occur, for

example, by the increasing temperature. Phase transformation of the crystals can also take place during the process. The deposits can also become detached due to thermal stresses caused by temperature variations over time.

2.3 Heat Transfer in a Double Pipe Heat Exchanger (DPHE) During Fouling

As a vertical double pipe heat exchanger is used to monitor the fouling process in this work, it is of interest to analyze the heat transfer process for this situation where steam is on the tube side and water is flowing countercurrently in the annular space. This unit is run at a constant heat flux with time as fouling proceeds, by raising the pressure on the steam side. The following assumptions are made:

1. Steady state operation occurs in the clean condition and pseudo-steady state operation occurs in the fouling condition.

2. One-dimensional radial heat conduction takes place through the tube wall. Axial heat losses are neglected.

3. Radiation heat transfer is neglected.

4. The heat exchanger is perfectly insulated.

5. The steam is pure having no air mixed with it. The condensate drains freely from the tube side of the heat exchanger, resulting in no build-up.

6. On the water side, the entry effects on the boundary layer are neglected.

7. The fouling is purely precipitative in nature and any entrainment or particulate fouling caused by either bulk precipitation, recycle of removed particulates or foreign contaminants in water is negligible.

8. The fouled layer is of uniform thickness, bulk density, chemical composition, and thermal conductivity. The tube is uniformly covered with the foulant layer during a run.

9. The thermal conductivity of the fouled layer is not significantly influenced by changes in temperature or moisture occlusion. This is because the calculated thermal conductivity corresponds to that of a wet deposit whose temperature varies from the tube-scale interface temperature to the scale-water interface temperature.

The heat flow in a clean heat exchanger can be expressed by:

$$Q = U_o A_o \Delta T_{lm} \tag{2-1}$$

where:

Q = the rate of heat transfer

U_o= overall heat transfer coefficients based on the outside area

ΔT_{lm}= log mean temperature difference

The log mean temperature difference is determined by:

$$\Delta T_{lm} = \frac{(\Delta T)_{x=L} - (\Delta T)_{x=0}}{\ln \frac{(\Delta T)_{x=L}}{(\Delta T)_{x=0}}} \tag{2-2}$$

The overall heat transfer coefficient is given by:

$$\frac{1}{U_{oc}} = \frac{1}{h_{co}} + \frac{(D_{to} - D_{ti}) A_o}{2 k_m A_{lm}} + \frac{A_o}{h_{ci} A_i} \tag{2-3}$$

where the subscripts o and i denote outer and inner surface, respectively and:

h_c = convective heat transfer coefficient

k_m = thermal conductivity of the tube material

D_{ti} , D_{to} = the inside and outside diameters of the tube

A_i , A_o = the inside and outside surface areas of the tube

A_{lm} = the log mean area of the heat transfer surface

The inside and outside convective heat transfer coefficients depend on the geometry of the heat exchanger, the flow velocity, the specific heat, the viscosity and the thermal conductivity of the fluids and the tube material. Except for viscosity these heat transfer coefficients increase with increases in the values of the other two cited fluid properties which,

in turn, are functions of temperature. In Appendix II, a calculation method is outlined to give a "theoretical" overall coefficient, based on established equations for inside and outside heat transfer coefficients.

Equation (2-1) can be expressed as:

$$Q = \frac{\Delta T_{lm}}{\frac{1}{U_o A_o}} = \frac{Temperature\ Driving\ Force}{Total\ Heat\ Transfer\ Resistance} \qquad (2\text{-}4)$$

The denominator in equation (2-4) represents the overall thermal resistance of a clean heat exchanger. In order to calculate the overall thermal resistance of a fouled heat exchanger, the unsteady state fouling resistances are arbitrarily added to the steady state heat transfer resistances, expressed by:

$$\frac{1}{U_{od}} = \frac{1}{h_{co}} + \frac{(D_{to}-D_{ti})A_o}{2k_m A_{lm}} + \frac{A_o}{h_{ci}A_i} + R_{fo} + \frac{R_{fi}A_o}{A_i} \qquad (2\text{-}5)$$

where R_f is called the fouling resistance and the subscript d denotes the dirty (or fouled) heat exchanger.

Combining equations (2-3) and (2-5) yields:

$$\frac{1}{U_{od}} = \frac{1}{U_{oc}} + R_{fo} + \frac{R_{fi}A_o}{A_i} \qquad (2\text{-}6)$$

The overall clean heat transfer coefficient for a constant heat flux heat exchanger can be

assumed to be independent of the fouling process and constant over time assuming that the steam side coefficient is constant over time, i.e. the steam temperature rise with time which is used to keep the heat flux constant has negligible effect on the steam side coefficient. The surface roughness effect caused by the fouled layer is not corrected for, and is therefore incorporated into the fouling resistance.

In the present case of using building steam in the DPHE, there is practically little fouling on the steam side. Hence,

$$R_f = R_{fo} = \frac{1}{U_{od}} - \frac{1}{U_{oc}} \tag{2-7}$$

In practice, if one starts with a clean heat exchanger at time=0, the overall heat transfer coefficient decreases with time. Hence, the fouling resistance increases with time, as expressed by:

$$R_f(t) = \left[\frac{1}{U_{od}} - \frac{1}{U_{oc}}\right]_{time=t} \tag{2-8}$$

In practice, the rate of the heat flow varies slightly from time to time, and since condensation is occurring inside the tube, the inside heat transfer coefficient and hence the overall heat transfer coefficient will vary. This is not generally a problem for pure sensible heat transfer where the overall heat transfer coefficient does not vary significantly with the heat transfer rate. The assumption of constant clean overall heat transfer coefficient can cause some

errors in the computation of the fouling resistance. As shown in Table II-1 (Appendix II), the 'theoretical' overall heat transfer coefficients, each one calculated for a particular velocity and rate of heat transfer, agree moderately well with the measured values. The variation of the clean heat transfer coefficient with respect to the rate of heat transfer was determined experimentally by carrying out various clean runs at fixed velocities and varying steam temperatures. A straight line was fitted to the U_{oc} versus Q data using linear regression methods and the slope of the straight line was substituted in the following equation to give the variation of the rate of heat transfer versus time.

$$(U_{oc})_{time=t} = (U_{oc})_{time=0} + (\frac{dU_{oc}}{dQ})\Delta Q \tag{2-9}$$

where:

$$\Delta Q = Q_{time=t} - Q_{time=0} \tag{2-10}$$

This calculation permits $R_f(t)$ to be determined if Q and hence U_{oc} changes slightly during the experiment.

The thermal resistance of a cylindrical deposit having D_{to} and D_{fo} as inside and outside diameters is:

$$R = \frac{(D_{fo}-D_{to})A_o}{2k_f A_{lm}} = \frac{x_f A_o}{k_f A_{lm}} \tag{2-11}$$

where x_f is the thickness of the cylindrical deposit and the log mean area is given by:

$$A_{lm} = \frac{A_{fo} - A_o}{\ln(\frac{A_{fo}}{A_o})} = \frac{2\pi L x_f}{\ln(1+\frac{2x_f}{D_{to}})} \tag{2-12}$$

If $x_f \ll D_o$, A_{lm} can be approximated to A_o.

$$\therefore \quad R_f \approx \frac{x_f}{k_f} \tag{2-13}$$

For a mass deposition rate of foulant onto the tube, the fouling resistance build-up can be expressed by differentiation of equation (2-13):

$$\frac{dR_f}{d\theta} = \frac{1}{k_f}\frac{dx_f}{d\theta} = \frac{\dot{m}_{net}}{\rho_f k_f A_o} = \frac{\dot{w}_{net}}{\rho_f k_f} \tag{2-14}$$

where ρ_f is the bulk density, $\dot{m}_{net}$ and $\dot{w}_{net}$ are the net rate of mass deposition in kg/s and the net flux of mass deposition in kg/m^2.s, respectively, and A_o is area of deposition on the heat transfer surface.

The net rate of deposition in the Kern-Seaton model (11,12) is expressed as the difference between a deposition term and a removal term as given by the following equation:

$$\dot{m}_{net} = \dot{m}_{deposition} - \dot{m}_{removal} \tag{2-15}$$

The removal term is expressed as a function of fluid shear stress, τ, the deposit thickness, x_f , and a constant representing the mechanical strength of the adhering material, M.

The net growth velocity of the layer formation can, therefore, be expressed by:

$$\frac{dx_f}{d\theta} = \frac{\dot{w}}{\rho_f} - \frac{x_f \tau}{M} \tag{2-16}$$

From (2-14) and (2-16), we obtain:

$$\frac{dR_f}{d\theta} = \frac{\dot{w}}{\rho_f k_f} - \frac{x_f \tau}{M k_f} = \frac{\dot{w}}{\rho_f k_f} - \frac{R_f \tau}{M} \tag{2-17}$$

Integration with initial condition $\theta=0$, $R_f=0$ and boundary condition as $\theta \rightarrow \infty$, $R_f \rightarrow R_f^*$ yields:

$$R_f = R_f^* \left(1 - e^{\frac{\theta}{\theta_c}}\right) \tag{2-18}$$

where θ_c is called the time constant and is given by:

$$\theta_c = \frac{M}{\tau} \tag{2-19}$$

and asymptotic resistance, R_f^*, is expressed by:

$$R_f^* = \frac{\dot{w} M}{\rho_f k_f \tau} \tag{2-20}$$

Substituting (2-19) and (2-20) in (2-17) yields:

$$\frac{dR_f}{d\theta} = \frac{R_f^*}{\theta_c} - \frac{R_f}{\theta_c} \qquad (2\text{-}21)$$

In the case of low velocity runs and for very adherent scale deposits, θ_c becomes very large and the removal term becomes insignificant resulting in a linear behaviour given by:

$$\frac{dR_f}{d\theta} = \frac{\dot{w}}{\rho_f k_f} \qquad (2\text{-}22)$$

2.4 Types of Fouling Curves

The fouling curve under a given set of conditions is usually studied by recording the experimental fouling resistance as a function of time. The most commonly obtained shapes of the curves are linear, asymptotic and falling rate as shown in Figure 2-1.

The general shape of the curve can be rationalised in terms of equation (2-15). The linear curve represents the case where the removal rate is negligible relative to the deposition process and the deposition process is constant w.r.t. time, or when the difference in the deposition and removal process is constant over time. The asymptotic curve arises when $\dot{m}_{net}$ becomes zero. This can result when the net rate decreases with time, because of either decrease in the deposition rate or increase in removal rate or both, until the deposition rate equals the removal rate. The falling rate curve arises from an intermediate condition between these two extremes, i.e. deposition rate decreases with zero or negligible removal, or a constant deposition rate and

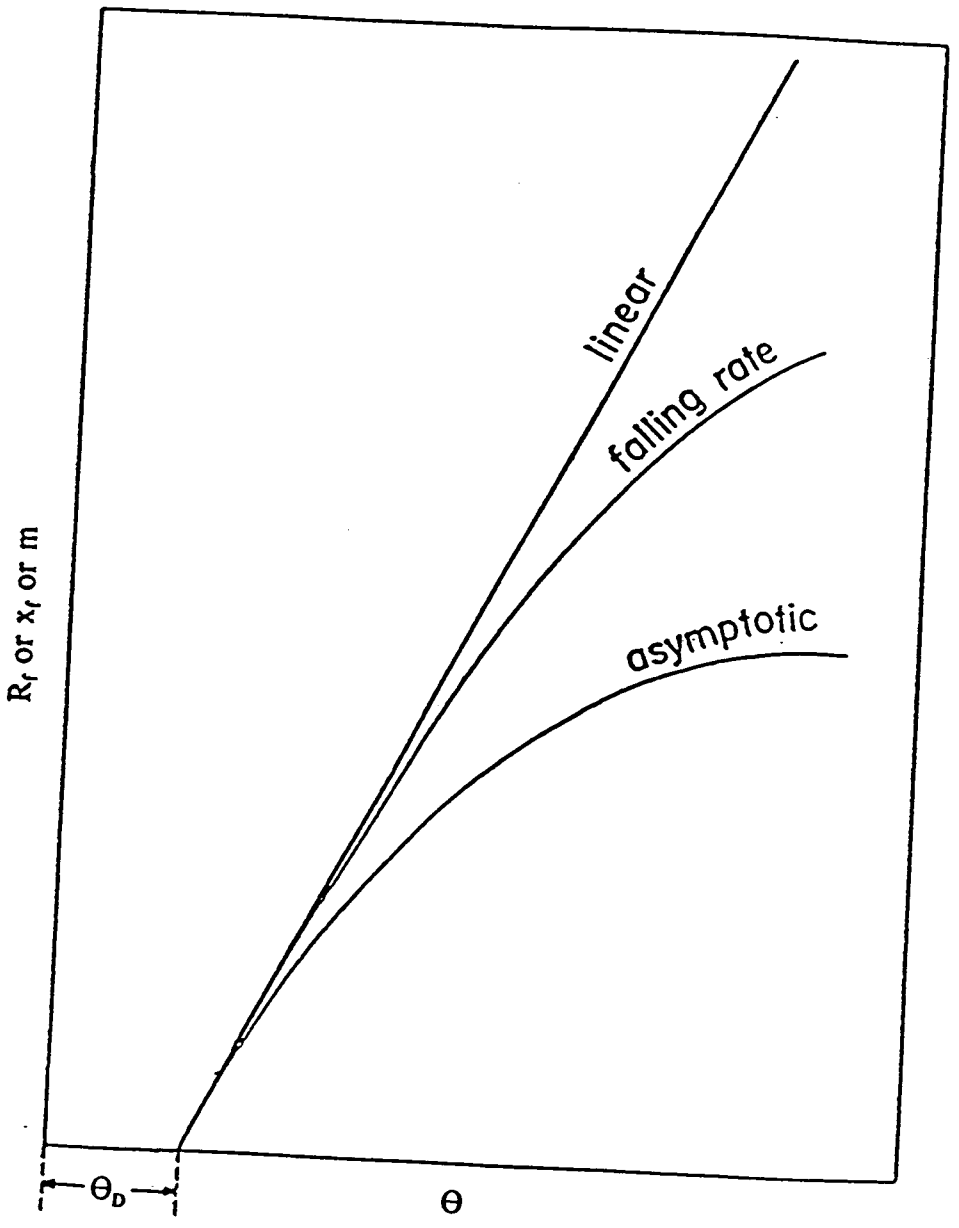

FIGURE 2-1 TYPES OF FOULING CURVES

an increasing removal rate.

2.5 Chemistry of Calcium Phosphates:Equilibrium Considerations

The calcium-phosphorus aqueous system involves some 13 ionic species (12). The distribution of these species is a function of temperature, pH and the total calcium and phosphate concentrations. It is of interest to calculate the concentrations of these species in the aqueous system.

The following sets of relationships should be taken into account in solutions from which calcium phosphates precipitate:

(i) Phosphate species and water equilibria:

$$H_3PO_4 \rightleftarrows H_2PO_4^- + H^+ \qquad K_1 \qquad (2\text{-}23)$$

$$H_2PO_4^- \rightleftarrows HPO_4^{2-} + H^+ \qquad K_2 \qquad (2\text{-}24)$$

$$HPO_4^{2-} \rightleftarrows H^+ + PO_4^{3-} \qquad K_3 \qquad (2\text{-}25)$$

$$H_2O \leftrightarrows H^+ + OH^- \qquad K_w \qquad (2\text{-}26)$$

(ii) Ion-pair equilibria:

$$Ca^{2+} + OH^- \leftrightarrows CaOH^+ \qquad K_4 \qquad (2\text{-}27)$$

$$Ca^{2+} + H_2PO_4^- \leftrightarrows CaH_2PO_4^+ \qquad K_5 \qquad (2\text{-}28)$$

$$Ca^{2+} + HPO_4^{2-} \rightleftarrows CaHPO_4^o \qquad K_6 \qquad (2\text{-}29)$$

$$Ca^{2+} + PO_4^{3-} \rightleftarrows CaPO_4^- \qquad K_7 \qquad (2\text{-}30)$$

The concentration of all different species can be calculated using the following equations:

(i) Equation for total calcium species:

$$T_{Ca} = (Ca^{2+}) + (CaOH^+) + (CaH_2PO_4^+) + (CaHPO_4^o) + (CaPO_4^-) \qquad (2\text{-}31)$$

(ii) Equation for total orthophosphate species:

$$T_{PO4} = (H_3PO_4^o) + (H_2PO_4^-) + (HPO_4^{2-}) + (PO_4^{3-}) + (CaH_2PO_4^+) + (CaHPO_4^+) + (CaPO_4^-) \qquad (2\text{-}32)$$

where the brackets represent the concentration in moles/liter and T_{Ca} and T_{PO4} are the total calcium and phosphate concentrations obtained by an analysis of equilibrium solutions.

(iii) Equation for elecro-neutrality:

$$\sum z_i f_i C_i = 0 \tag{2-33}$$

(iv) Equilibrium relationships:

$$\frac{(H_2PO_4^-)(H^+)}{(H_3PO_4)} f_M = K_1 \tag{2-34}$$

$$\frac{(HPO_4^{2-})(H^+)}{(H_2PO_4^-)} f_D = K_2 \tag{2-35}$$

$$\frac{(PO_4^{3-})(H^+)}{(HPO_4^{2-})} \cdot \frac{f_T f_M}{f_D} = K_3 \tag{2-36}$$

$$\frac{(H^+)(OH^-)}{(H_2O)} f_M^2 = K_w \tag{2-37}$$

$$\frac{(CaOH^+)}{(Ca^{2+})(OH^-)} \cdot \frac{1}{f_D} = K_4 \tag{2-38}$$

$$\frac{(CaH_2PO_4^+)}{(Ca^{2}+)(H_2PO_4^-)} \cdot \frac{1}{f_D} = K_5 \tag{2-39}$$

$$\frac{(CaHPO_4^o)}{(Ca^{2+})(HPO_4^{2-})} \cdot \frac{1}{f_D^2} = K_6 \tag{2-40}$$

$$\frac{(CaPO_4^-)}{(Ca^{2+})(PO_4^{3-})} \cdot \frac{f_M}{f_D f_T} = K_7 \tag{2-41}$$

$$pH = -\log[(H^+)f_M] \tag{2-42}$$

where K_1-K_7 are thermodynamic equilibrium constants. Let $\bar{K}_1$-$\bar{K}_7$ be the corresponding equilibrium constants based on activities. Activity coefficients of monovalent, divalent and trivalent ions are denoted respectively by f_M, f_D and f_T. The ions having equal charges are assumed to have the same activity coefficients. Undissociated molecules are assumed to have an activity coefficient of unity.

The activity coefficients of various ionic species in solution of ionic strength I are calculated from the Debye-Hückel-Davies equation(13):

$$-\log f_i = Az_i^2\left[\frac{\sqrt{I}}{\sqrt{I+1}} - 0.3I\right] = Az_i^2 F(I) \tag{2-43}$$

for $I < 0.1$ mol/L and where f_i is the activity coefficient of a species having a charge i and A is a temperature dependent collection of constants.

In their interionic theory, Debye and Hückel calculated the electrical contribution to the free energy, and the mean activity coefficient of the ions on a mole fraction scale was given by the limiting law (13,14):

$$\log f = -|z_+ z_-| A\left[\frac{\sqrt{I}}{\sqrt{I+1}} - 0.3I\right] \tag{2-44}$$

where:

$$A = \frac{(2N\pi e^6)^{\frac{1}{2}}}{2.3026\,(10k\epsilon T)^{\frac{3}{2}}} \tag{2-45}$$

At 25°C, the value of A equals 0.509. Hence, for the monovalent ion:

$$-\log f_M = 0.51 \times F(I) \tag{2-46}$$

For the divalent ion:

$$-\log f_D = 2.04 \times F(I) \tag{2-47}$$

For the trivalent ion:

$$-\log f_T = 4.59 \times F(I) \tag{2-48}$$

The ionic strength of a solution is expressed by:

$$I = \frac{1}{2} \sum z_i^2 M_i \tag{2-49}$$

where M_i is the molality of i^{th} component and z_i is the charge.

In the present case, artificially hardened water is prepared by dissolving technical grade KH_2PO_4 and $CaCl_2.2H_2O$. Hence, the ionic strength of the solution can be expressed by:

$$I = 4(Ca^{2+}) + 9(PO_4^{3-}) + (CaOH^+) + (CaH_2PO_4^+) + (CaPO_4^-) + (H_2PO_4^-) + 4(HPO_4^{2-}) + (K^+) + (Cl^-) + (H^+) + (OH^-) \quad (2\text{-}50)$$

The ionic equilibrium is described by the equations (2-31) - (2-41), (2-46) - (2-48) and (2-50). The above 15 equations contain the following 28 variables:

T_{Ca} ; (K^+) ; (Ca^{2+}) ; T_{PO4} ; (Cl^-) ; (H_3PO_4) ; $(H_2PO_4^-)$; (HPO_4^{2-}) ; (PO_4^{3-}) ; $(CaH_2PO_4^+)$; $(CaHPO_4^0)$; $(CaPO_4^-)$; $(CaOH^+)$; (H^+) ; (OH^-); K_1 , K_2 , K_3 , K_4 K_5 , K_6 , K_7 , K_w , F(I) , I , f_M , f_D , f_T

In an experiment at a given temperature the four concentrations T_{Ca}, T_{PO4}, K^+, Cl^- and the pH are known. From the literature K_w and K_1 to K_7 are known. Therefore the system of equations can be solved to give all the unknown species concentrations. However, the solution to the above set of equations can also be obtained by using a trial and error method to estimate the ionic strength as given below. The ionic strength of the solution depends on the concentration of various species and vice versa. An iterative procedure is therefore used. As an initial approximation:

$$2I = 9T_{PO4} + 4T_{Ca} + (K^+) + (Cl^-) + (H^+) + (OH^-) \quad (2\text{-}51)$$

This value of I can be used in equations (2-46) - (2-48) to find different activity coefficients. All concentrations are calculated using the mass action relationships as derived below:

Subtracting (2-32) from (2-31) gives:

$$T_{Ca} - T_{PO4} = (Ca^{2+}) + (CaOH^{+}) - (H_3PO_4) - (H_2PO_4^{-}) - (HPO_4^{2-}) - (PO_4^{3-}) \tag{2-52}$$

Eliminating ($CaOH^+$), ($H_2PO_4^-$), (HPO_4^{2-}) and (PO_4^{3-}) from equation (2-50) and by using equations (2-33) to (2-38) gives:

$$T_{Ca} - T_{PO4} = (Ca)^{2+}[1 + \bar{K}_4] - (H_3PO_4) \cdot [1 + \frac{\bar{K}_1}{(H^+)} + \frac{\bar{K}_1\bar{K}_2}{(H^+)^2} + \frac{\bar{K}_1\bar{K}_2\bar{K}_3}{(H^+)^3}] \tag{2-53}$$

or:

$$(Ca^{2+}) - C_1 \cdot (H_3PO_4) = C_2 \tag{2-54}$$

where:

$$C_1 = \frac{1}{1 + \bar{K}_4(OH^-)} \cdot [1 + \frac{\bar{K}_1}{(H^+)} + \frac{\bar{K}_1\bar{K}_2}{(H^+)^2} + \frac{\bar{K}_1\bar{K}_2\bar{K}_3}{(H^+)^3}] \tag{2-55}$$

and:

$$C_2 = \frac{T_{Ca} - T_{PO4}}{[1 + \bar{K}_4(OH^-)]} \tag{2-56}$$

From equations (2-31) and (2-38) to (2-41), it follows that:

$$T_{Ca} = (Ca^{2+}) + \bar{K}_4(Ca^{2+})(OH^-) + \bar{K}_5(Ca^{2+}) \cdot \frac{\bar{K}_1(H_3PO_4)}{(H^+)} + \bar{K}_6(Ca^{2+}) \cdot \frac{\bar{K}_1\bar{K}_2(H_3PO_4)}{(H^+)^2} + \bar{K}_7(Ca^{2+}) \cdot \frac{\bar{K}_1\bar{K}_2\bar{K}_3(H_3PO_4)}{(H^+)^3} \quad (2\text{-}57)$$

or:

$$T_{Ca} = (Ca^{2+})[C_3 + C_4(H_3PO_4)] \quad (2\text{-}58)$$

where:

$$C_3 = 1 + \bar{K}_4(OH^-) \quad (2\text{-}59)$$

and:

$$C_4 = \frac{\bar{K}_5\bar{K}_1}{(H^+)} + \frac{\bar{K}_6\bar{K}_1\bar{K}_2}{(H^+)^2} + \frac{\bar{K}_7\bar{K}_1\bar{K}_2\bar{K}_3}{(H^+)^3} \quad (2\text{-}60)$$

Solving equations (2-54) and (2-58) simultaneously gives the following quadratic equation in (H_3PO_4), denoted by x:

$$x^2 + C_5x + C_6 = 0 \quad (2\text{-}61)$$

where:

$$C_5 = \frac{C_2C_4 + C_3C_1}{C_1C_4} \quad (2\text{-}62)$$

and:

$$C_6 = \frac{C_2C_3 - T_{Ca}}{C_1C_4} \tag{2-63}$$

which on solution gives:

$$x = \frac{-C_5 + \sqrt{C_5^2 - 4C_6}}{2} \tag{2-64}$$

Once (H_3PO_4) is known, the concentrations of the various calcium and phosphate species can be calculated using equations (2-34) to (2-41). These values are then substituted in equation (2-50) to get a new value of I. This new value is then used to calculate a new set of activity coefficients. This cycle is repeated until the difference in two successive values of I is less than 0.01% . Since the value of I no longer remains an unknown the electoneutrality equation (2-33) can be used as a check on the calculated values.

The calculation of the solution concentrations thus involves solving the equations described above. The input requirements are the specifications of total calcium and total orthophosphate concentrations, pH, temperature and concentrations of the chloride and potassium ionic species present.

2.6 Distribution of Various Ionic Forms of Phosphate Species

In order to estimate the distribution of various ionic forms of phosphate species, it is necessary to understand the chemistry of dissociation of the phosphoric acid. Because the

mathematics of a polyprotic acid such as phosphoric acid is quite involved, a simplified approach will be considered.

Phosphoric acid can dissociate in three steps as represented by equations (2-23) to (2-25), the dissociation constants for the three successive reactions being K_1, K_2 and K_3. The activity coefficients are assumed to be unity. Depending on the pH of the solution, the polyprotic acid may exist mainly in its undissociated form or one or more of its ionic forms. The distribution as a function of pH and at a constant temperature (25°C in the present case) can easily be determined using equations (2-34) to (2-36) and a total mass balance on phosphate given by equation (2-69).

If T_{PO4} and pH (or concentration of H^+) are known, there are four equations in four unknowns. Let α_i denote the ratio of the concentration of the species i to the total analytical concentration and the subscripts 0,1,2 and 3 denote the fractions present as H_3PO_4, $H_2PO_4^-$, HPO_4^{2-} and PO_4^{3-} , respectively. Solving the above four equations yields:

$$\alpha_3 = \left[1 + \frac{\bar{K}_1}{(H^+)} + \frac{\bar{K}_1 \bar{K}_2}{(H^+)^2} + \frac{\bar{K}_1 \bar{K}_2 \bar{K}_3}{(H^+)^3}\right]^{-1} \tag{2-65}$$

$$\alpha_2 = \alpha_3 . \frac{\bar{K}_1}{(H^+)} \tag{2-66}$$

$$\alpha_1 = \alpha_3 . \frac{\bar{K}_1 \bar{K}_2}{(H^+)^2} \tag{2-67}$$

$$\alpha_0 = \alpha_3 . \frac{\bar{K}_1 \bar{K}_2 \bar{K}_3}{(H^+)^3} \qquad (2\text{-}68)$$

The mass balance equation can also be expressed as:

$$\alpha_o + \alpha_1 + \alpha_2 + \alpha_3 = 1 \qquad (2\text{-}69)$$

Figure 2-2 is a graph of the various fractions as a function of pH. It may be observed that at no range of pH, the phosphoric acid is present in more than two species. Hence the mathematics gets simplified in this case, mainly because the successive ionization constants are such that $K_1 \gg K_2 \gg K_3$. The various fractions can be easily obtained from this graph by drawing a vertical line at any pH. This graph has four regions from left to right belonging to H_3PO_4 , $H_2PO_4^-$, HPO_4^{2-} , PO_4^{3-}, respectively. The fraction of a vertical line falling in that region is the fraction of phosphoric acid existing as that species. Thus at pH = 7.0, the solution would contain roughly 55% of the total phosphate as $H_2PO_4^-$ and 45% as HPO_4^{2-}

Another useful and popular representation is a logarithmic concentration diagram or a pC-pH diagram. Such a diagram for 0.01 molar phosphoric acid (or any of its salts) is drawn in Figure 2-3. It has a similar appearance as the superimposed species distribution diagram. However, it can be seen that at very low concentrations of the phosphate ions, the lines abruptly change their slopes from ± 1 to ± 2 .

For the crystallization process, the extent of supersaturation is of interest. Once the concentration of all the species is calculated the supersaturation potentials (S) and the degree of

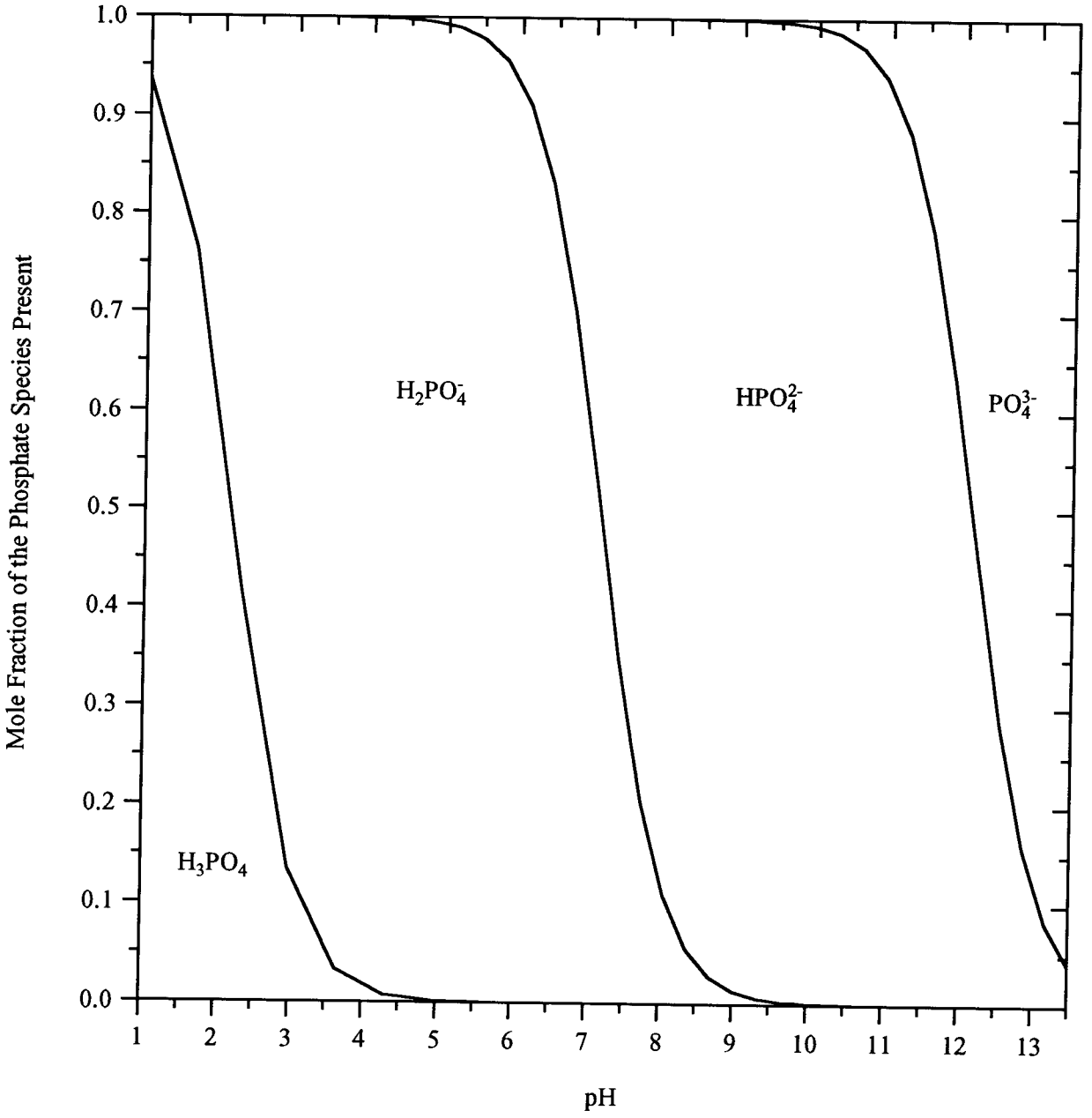

FIGURE 2-2 DISTRIBUTION OF VARIOUS PHOSPHATE SPECIES AS A FUNCTION OF pH AT 25 DEGREE CELSIUS

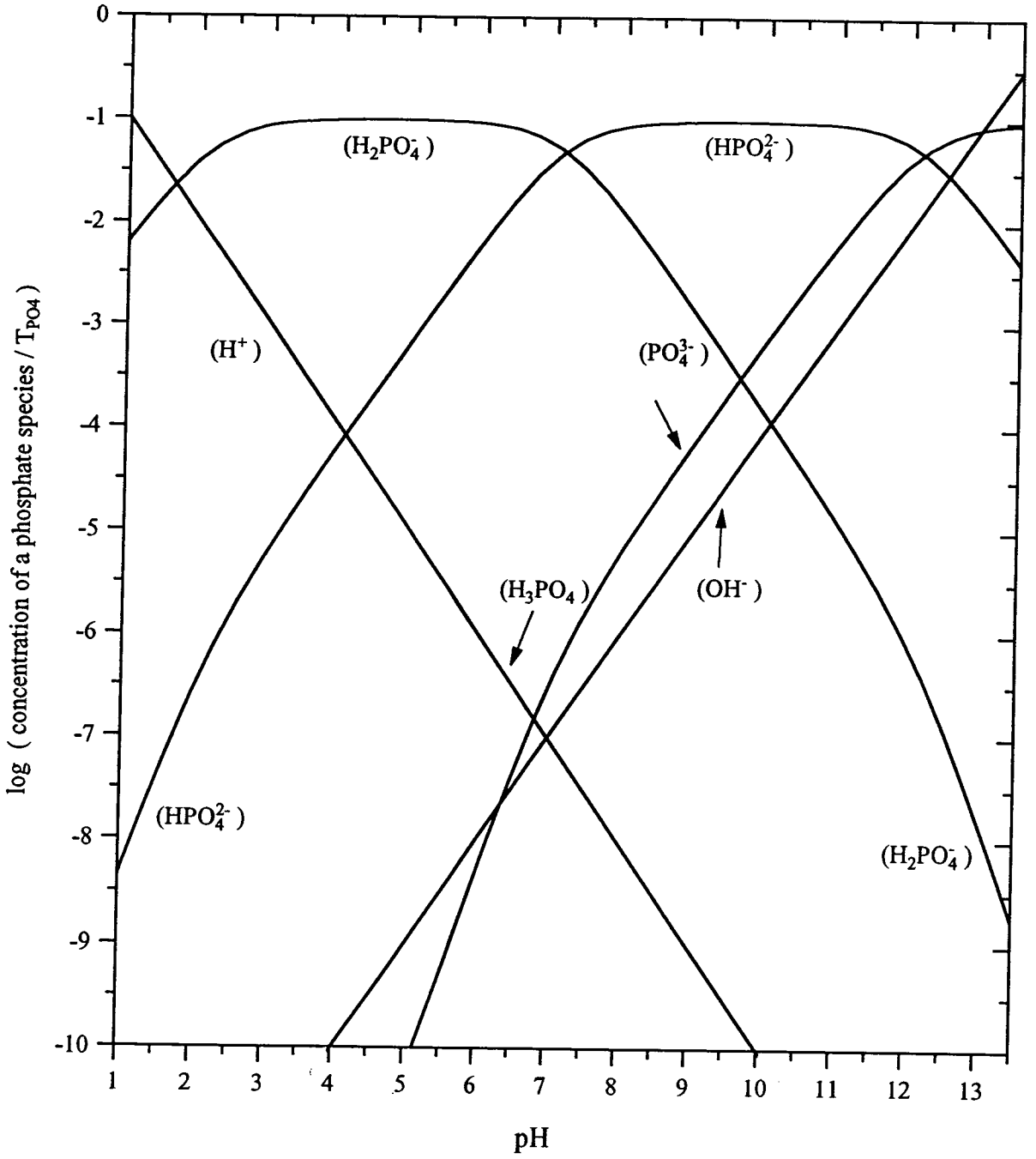

FIGURE 2-3 LOGARITHMIC CONCENTRATION DIAGRAM FOR THE PHOSPHATE SPECIES, ASSUMING 0.1 M PHOSPHORIC ACID

supersaturation (β) of various calcium phosphates, namely dicalcium phosphate dihydrate (DCPD), tricalcium phosphate (TCP), octacalcium phosphate (OCP), and hydroxyapatite (HAP) are calculated as follows:

$$S_{DCPD} = (Ca^{2+})(HPO_4^{2-}) - \frac{K_{sp1}}{f_2^2} \tag{2-70}$$

$$S_{TCP} = (Ca^{2+})^3(PO_4^{3-})^2 - \frac{K_{sp2}}{f_2^3 f_3^2} \tag{2-71}$$

$$S_{OCP} = (Ca^{2+})^4(PO_4^{3-})^3(H^+) - \frac{K_{sp3}}{f_2^4 f_3^3 f_1} \tag{2-72}$$

$$S_{HAP} = (Ca^{2+})^5 (PO_4^{3-})^3(OH^-) - \frac{K_{sp4}}{f_2^5 f_3^3 f_1} \tag{2-73}$$

OCP is sometimes written as $Ca_8H_2(PO_4)_3.5H_2O$. It may be noted that since activity coefficients are fractions, neglecting them can cause considerable computational errors.

Similarly,

$$\beta_{DCPD} = \frac{(Ca^{2+})(HPO_4^{2-})}{\frac{K_{sp1}}{f_2^2}}) \tag{2-74}$$

$$\beta_{TCP} = \frac{(Ca^{2+})^3(PO_4^{3-})^2}{\frac{K_{sp2}}{f_2^3 f_3^2}} \tag{2-75}$$

$$\beta_{OCP} = \frac{(Ca^{2+})^4(PO_4^{3-})^3(H^+)}{\frac{K_{sp3}}{f_2^4 f_3^3 f_1}} \tag{2-76}$$

$$\beta_{HAP} = \frac{(Ca^{2+})^5(PO_4^{3-})^3(OH^-)}{\frac{K_{sp4}}{f_2^5 f_3^3 f_1}} \tag{2-77}$$

Values of the solubility products at 25°C are given below (15):

$K_{sp1} = 1.05\text{x}10^{-8} \times e^{943.7/T(K)} = 2.49\text{x}10^{-7}$ $(mol/L)^2$

$K_{sp2} = 1.15\text{x}10^{-29}$ $(mol/L)^5$

$K_{sp3} = 1.25\text{x}10^{-47}$ $(mol/L)^7$

$K_{sp4} = 1.8\text{x}10^{-58}$ $(mol/L)^9$

Note that the temperature dependencies are generally not established except for K_{sp1}. According to Brown (17),"the application of solubility principles even to a simple ternary system $Ca(OH)_2$-H_2PO_4-H_2O is far more complex than is usually thought". There are many factors contributing to the situation. Orthophosphoric acid is both a weak acid and a polybasic acid. The presence of impurities and other metal ions, such as magnesium, formation of a large number of ion-pair complexes, and the existence of various solid forms (molecular composition) in which

calcium phosphates can precipitate will complicate matters. According to Nancollas (15), the precipitation process depends on pH, supersaturation, ionic strength, temperature and the nature and extent of the solid phases that are already present. Even if the solubility product of a particular phase is exceeded, the precipitation kinetics may vary depending upon the above factors. Metastable phases may persist for very long time, with no precipitation occurring (15). The various calcium phosphate phases can undergo considerable transformations over time (18).

In cooling water systems, hydroxyapatite (abbreviated as HAP), $Ca_4(PO_4)OH$ (a dense white solid) is the form of salt that is commonly identified. But it is not this phase that is initially precipitated. The phase that precipitates initially is popularly known as amorphous calcium phosphate, abbreviated as ACP. This amorphous phase has a broad and diffuse X-Ray diffraction pattern. The lack of crystallinity may be explained due to water of crystallinity present. Some authors (15,17,19) have proposed $Ca_8H_2(PO_4)_6.5H_2O$ (Octacalcium Phosphate), abbreviated as OCP to be the precursor phase. This amorphous phase transforms to crystalline hydroxyapatite over time.

2.7 Solid Forms of Calcium Phosphates

There are five solid calcium phosphates that are relatively stable in aqueous systems. The order of decreasing solubilities of these salts are:

		Ca/P
$CaHPO_4.2H_2O$	dicalcium phosphate dihydrate (DCPD or brushite)	1.00

$CaHPO_4$	anhydrous dicalcium phosphate (ADCP or monetite)	1.00
$Ca_8H_2(PO_4)_6.5H_2O$	octacalcium phosphate (OCP)	1.33
$Ca_3(PO_4)_2$	tricalcium phosphate (TCP)	1.50
$Ca_5(PO_4)_3(OH)$	hydroxyapatite (HAP)	1.67

The solubilities of various calcium phosphates at 25°C are plotted as a function of pH in Figure 2-4. It can be seen that HAP becomes more soluble than DCPD if the solution pH is below 4.3. Such points, known as singular points, depend on the concentration of other components. Below pH 4.8, for example, the most stable salt is $CaHPO_4$. Further reducing the pH to 4.3 leads to DCPD being more soluble than HAP. Under extremely acid conditions, solubilities of two monocalcium phosphates namely $Ca(H_2PO_4)_2$ and $Ca(H_2PO_4)_2.2H_2O$ may become less than that of DCPD. Following is a brief description of calcium phosphates (17):

Hydroxyapatite appears most commonly in boilers using hard water containing phosphate ions or when soluble sodium phosphates are used to precipitate any residual hardness in the boiler water during a process called internal treatment. This form of calcium phosphate is the principal constituent in tooth, bone and many naturally occurring minerals, including rock phosphate. It has a well defined structure that can be found in literature (17). Octacalcium phosphate has considerable similarity (in structure) with hydroxyapatite. Hence, it has been proposed to be a precursor to hydroxyapatite. Hydroxyapatite is considered to form through three mechanisms:

(a) OCP is precipitated first by hydrolysis of $CaHPO_4.2H_2O$ or by titration of a calcium

solution with a phosphate solution at room temperature and neutral pH. After this, OCP can be hydrolysed to hydroxyapatite by boiling or by treating with an alkaline solution. If the crystals are large, hydrolysis may be difficult because of coating with hydroxyapatite and a mixed composition may be obtained.

(b) HAP can also be directly precipitated without an intermediate phase (OCP), for example, in lakes and rivers. However, the kinetics of such a process would be extremely slow.

(c) A combination of the above processes occurs. For example, a unit-cell-thick precipitation layer on a crystal of HAP subsequently hydrolyses to a double-unit-cell-thick layer of HAP. Such a mechanism was proposed because of structural similarities between OCP and HAP.

2.8 Kinetics of Crystallisation of Calcium Phosphates

The chemistry of calcium phosphates in general and HAP in particular is of significant interest because of its relevance to many diverse fields such as water geochemistry, sedimentation mineralogy, fertilizer and food technology, osteology, urology, dental sciences and last but not least, heat exchanger fouling (23).

The stoichiometry of the initial precipitate obtained by mixing solutions containing orthophosphate ions never corresponds to HAP, which is the final crystalline phase obtained in many applications. The molar Ca/P ratio of the initial amorphous precipitate is always less than the value of 1.66 for HAP (22), and usually has a value of about 1.45, which corresponds to that

of TCP (12,22). This phase lacks a crystalline order and hence, its molecular structure and solubility products are not defined.

There is a great deal of uncertainty as to the forms of calcium phosphate precipitating as a function of the variables of the system in which the precipitation is occurring. From Figure 2-4, the position of singular points (at which two or more phases coexist with each other) depends on pH and the ionic strength of the solution. The apparent solubility products for a particular phase may differ significantly if it gets coated with a more acid calcium phosphate, resulting in misleading interpretation of the solubility behavior of the phosphate phase. Thermodynamic analysis cannot predict whether, in a reasonable time, precipitation of a particular phase will occur or not. The kinetic factors become important in determining which phases are actually precipitating as a function of the variables of the system.

The kinetics of calcium phosphate crystal growth has been studied by Nancollas in detail using constant composition techniques, by injecting well characterised seeds of DCPD or HAP and observing the concentration change with time. These methods are claimed by the author to be highly reproducible, in contrast with the method in which heterogenous nucleation occurs on the impurities, which results in less precise measurements. While DCPD, OCP and ACP are proposed to be precursors to the formation of thermodynamically stable HAP, their transformation process into HAP is also little understood (17,22).

At the pH value below about 6.0, as can be seen from Figure 2-4, DCPD and HAP are

the only thermodynamically stable phases present. The kinetics of precipitation of DCPD using the seeded growth technique was studied by Nancollas using a metastable solution (22). The following rate expression was found to fit the experimental data:

$$\frac{dT_{Ca}}{d\theta} = -ksN^2 \qquad (2\text{-}78)$$

where k is the specific reaction rate constant, s is a term proportional to the number of DCPD growth sites and N is the number of moles of DCPD to be precipitated before the equilibrium is reached. The kinetic expressions for the precipitation of other phosphate phases such as OCP and HAP are not given by the author. In order to demonstrate the uncertainty in the nature of the initially precipitating phases, the author carried out four sets of experiments at pH 7.4 and 37°C. At this pH all four types of calcium phosphates can precipitate. At supersaturation corresponding to level c in Figure 2-5 a solid with Ca/P ratio of 1.45 was obtained. This solid was definitely not TCP. When the supersaturation of the metastable solution was increased from the level c to level b keeping everything else constant, the Ca/P ratio of the initial precipitate was obtained as 1.33. The fact that OCP was precipitating was confirmed by x-ray and infra-red techniques. At very high supersaturation corresponding to level a in Figure 2-5, DCPD was produced initially. At low supersaturation level d, HAP is precipitated giving the Ca/P ratio of 1.66, which indicates that HAP can precipitate directly at low supersaturation without the need for the precursor formation. The above experiments clearly indicate that the levels of supersaturation determine the nature of the initially precipitating phosphate phases.

In another paper by Nancollas, the kinetics of precipitation of DCPD using the same

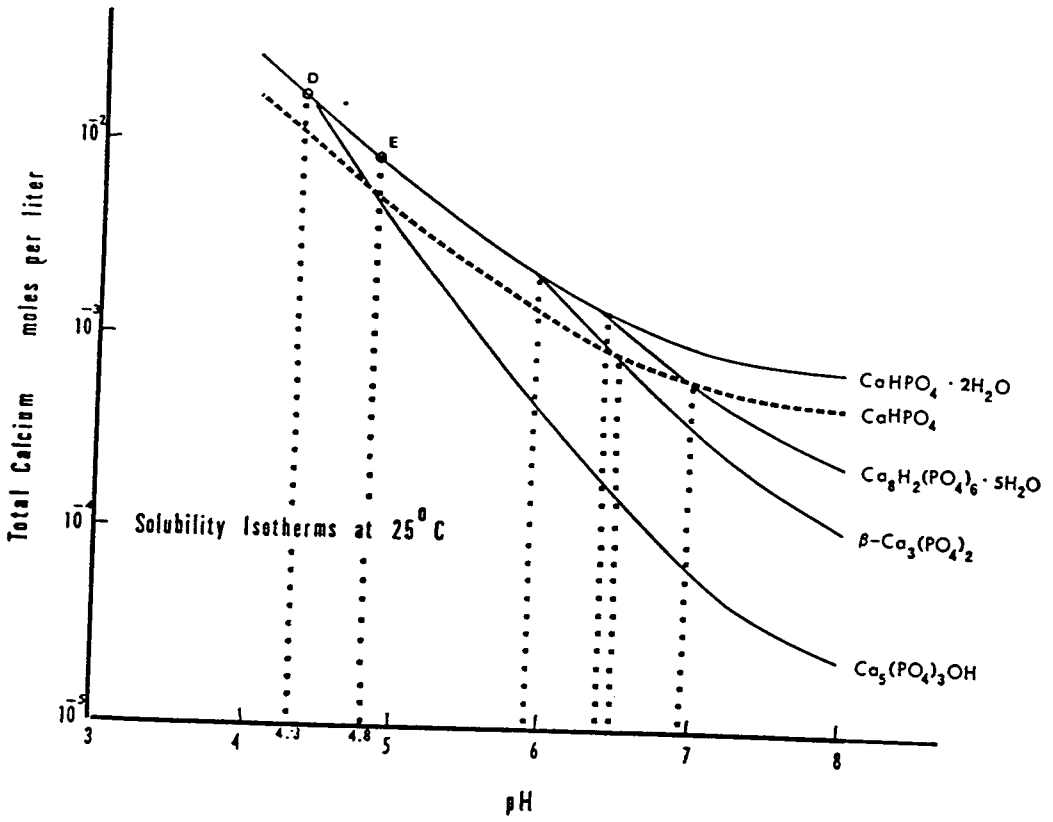

FIGURE 2-4 SOLUBILITIES OF VARIOUS PHOSPHATES AS A FUNCTION OF pH AT 25°C (17)

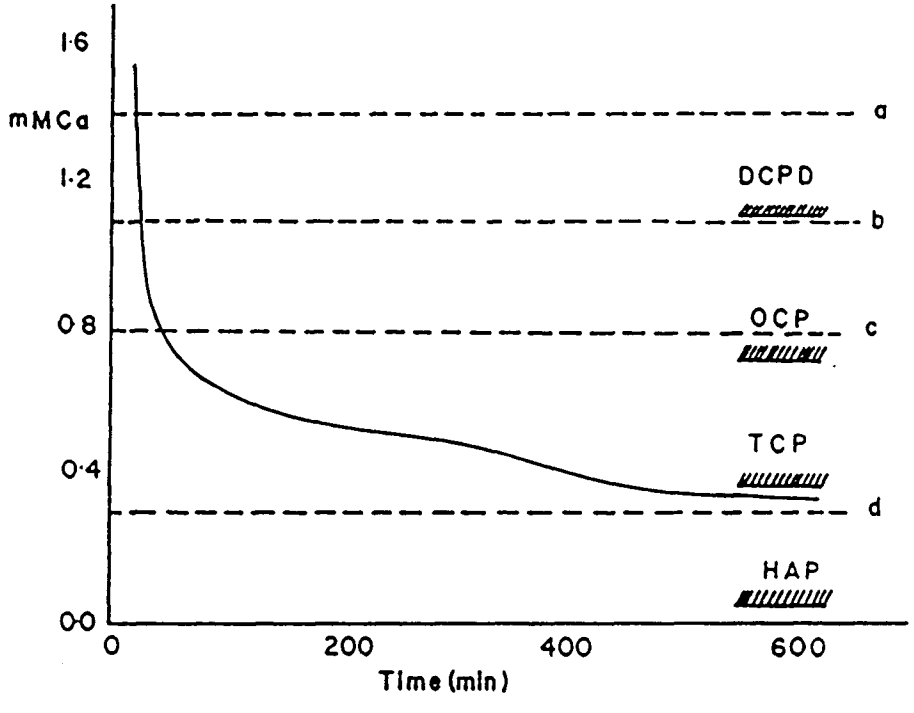

FIGURE 2-5 TOTAL CALCIUM VERSUS TIME IN GROWTH OF HAP CRYSTALS AT pH 7.4, 37°C (15)

techniques was described by the following equation (21):

$$-\left(\frac{w_i}{w}\right)^{\frac{2}{3}} \frac{dT_{Ca}}{d\theta} = ks[(Ca^{2+})(HPO_4^{-}) - \frac{K_{sp}}{f_M^2}] \qquad (2\text{-}79)$$

where w_i and w are the weights of the seed material initially and at any instant of time. The overall rate of crystallisation was considered to be mainly surface reaction controlled. A considerable change in the stirring rate in a batch reaction vessel resulted in negligible changes in the reaction rate constant.

In an earlier paper, Nancollas used the following expression to interpret the DCPD kinetics at similar experimental conditions using the same techniques (20). The following expression was fitted to the experimental data:

$$-\frac{dm}{d\theta} = ks[(Ca^{2+})^{\frac{1}{2}}(HPO_4^{2-})^{\frac{1}{2}} - \frac{K_{sp}^{\frac{1}{2}}}{f_M}] \qquad (2\text{-}80)$$

where the symbols have their usual meanings as above.

The rate was found to be markedly dependent on the rate of stirring, indicating a strongly diffusion controlled process. In none of the papers, however, were the explicit values of the rate constants specified. It is surprising that different empirical expressions fit so well the experimental data for the same kinetics.

At pH values of less than 5.6, the DCPD kinetics have been studied because it is the only

phosphate precipitating. As the pH is increased to 7.4 (the physiological value), the crystallisation of calcium phosphates is much more complicated. There are discontinuities in the growth curves, which is very different from the growth curve of the DCPD. In a typical experiment by Nancollas, ACP was found to precipitate as confirmed by scanning electron micrography. As proposed by the author, the discontinuities were probably due to superposition of a number of reactions in parallel, each one taking place at a different rate.

The concentration of seed material also plays an important role in the precipitation kinetics. In another study done by Nancollas (22), a solution supersaturated w.r.t. both DCPD and HAP, the addition of small amounts of HAP seed crystals resulted in the crystallisation of DCPD . At high concentrations of seed crystals, DCPD was not formed. The explanation offered was that at high concentration of chemicals, the calcium and phosphate concentrations fell too steeply to prevent the heterogenous nucleation of DCPD.

The concentration of Mg has an important part in the precipitation kinetics of calcium phosphates (18). In the presence of Mg and at low pH, ACP and DCPD are precipitated. The initial phases are unstable and undergo further transformations. The transformation of ACP to HAP is influenced by the amount of Mg added. Magnesium acts as a crystal poison and inhibits nucleation. Even in the presence of Mg, DCPD nucleates at any pH between 5.5-8.0 . Sometimes DCPD can coexist with OCP in a limited range of pH. Metastable phases can remain unchanged for a significant time period. The evolution process is affected by the concentration of Mg.

The crystal inhibitors are supposed to act through the following mechanisms (22):

1) The concentrations of one of the potentially scale forming species can decrease if the additive forms a stable chemical complex.

2) Adsorption of the additive takes place at the preferential sites of growth, leading to a reduction in the growth process and affecting the crystal structure significantly.

3) The additive may change the ionic strength of the solution, which in turn affects the solubility of the precipitating phase. In practice, the concentrations of the additives is considerably less than that which would affect the ionic strength.

The organic phosphonates and polyphosphates are very effective crystal growth inhibitors even at a concentration as low as 5×10^{-8} mol/L. The remarkable effect of these additives at a concentration of only 0.5 ppm in inhibiting the growth of calcite crystals was demonstrated by Nancollas (22). The reaction was almost 100 % inhibited. At an additive concentration of about 1 ppm, less than 1% of the seed surface was covered by the additive. This suggests that only a tiny fraction of the growth units actively participate in the crystallisation process. By studying the kinetics of calcite growth in the presence of an inhibitor, it was shown by Nancollas that the rate constant is significantly affected by the presence of the inhibitors.

2.9 Related Studies in the Area of Phosphate Fouling

In the area of phosphate fouling, relatively less work has been done as compared with other kinds of precipitation fouling such as calcium carbonate and calcium sulphate fouling. The

previous work (3,4,9,23) is mainly concerned with the performance of various organic and polyphosphate corrosion inhibitors. As mentioned earlier, the chemistry of calcium phosphate precipitation is very complicated and unpredictable and hence a fundamental approach to develop theoretical models is lacking in all of the above cited references.

Knudsen et al (9) studied the effects of various variables e.g. pH, velocity and surface temperature on the hard water fouling process both in the presence and absence of polyphosphate and phosphonate corrosion inhibitors with the purpose of establishing the overall effect of the inhibitors. The fouling process was found to be strongly dependent on these variables. The deposit obtained by the authors was described to be some form of calcium phosphate, but the chemical or physical structure was not mentioned. No attempt was made to explain the results or model the fouling process. The authors mainly concentrated on monitoring the performance of adding HEDP to the cooling water systems resulting in reduced corrosion but simultaneously giving rise to phosphate fouling.

In related work (23) by Barton et al, the rate of deposition of DCPD on a heat transfer surface was studied at one fixed set of conditions . The experimental results of the rate of DCPD deposition were not reproducible, varying by a factor of about 10 for the same set of conditions. A mathematical model was proposed to predict the rates of deposition or the rate of fouling under this particular set of conditions. However, a fundamental approach was lacking and the reaction constant for the deposition process was derived by equating the calculated rate of deposition to the observed rate of deposition. The theoretical model as such is supposed to be

valid over the limited set of conditions specified in the paper. The wide fluctuations in the observed rate of deposition were attributed to variations in density and porosity of the deposit, resulting in varying values of thermal conductivity. The values of thermal conductivity or density were not specified in their paper.

Humphris (4) studied the problem of phosphate scaling in power station condensers. He concluded that lowering the pH of the cooling water was an effective way to prevent the phosphate fouling. He assumed that the deposits were $CaHPO_4$, but there was no evidence to support this assumption. A nomogram was developed to predict the pH at which the calcium phosphate would precipitate, given the calcium and phosphate content of the water. By adding a required amount of an acid, the actual pH of the water was manipulated to a value just below the extracted value from the monograph.

Parry et al (3) studied a similar problem of calcium phosphate scaling in power station condensers. The operating solution adopted was to lower the pH of the circulating water from 8.6 to 7.5, which resulted in a 97% reduction in scaling. Addition of one of thirty available commercial additives, namely a polycarboxylic acid, was chosen for a plant test. Addition of about 2 ppm of the additive reduced the scaling by about 96%. The advantage of using the additive rather than acid treatment using sulphuric acid is that overdosing would not damage the steel and concrete structures of the cooling water circuits.

Further details of the above studies are given in the "Results and Discussion" section.

§ 3. EXPERIMENTAL APPARATUS

3.1 Water Flow Loop

The apparatus was originally constructed by Sheikholeslami (32) and was substantially modified for the current work. The process flow diagram is shown in Figure 3-1. Water is pumped from the storage tank by means of a Cole-Parmer model K-7084-20 centrifugal pump coupled with a totally enclosed fan cooled (TEFC) 3/4 HP motor. The suction header is 51 mm reinforced PVC pipe. The rest of the piping is also made up of rigid PVC to avoid corrosion build-up in the system and has an ID of 38.1 mm.

The flow of the water from the pump is controlled by a manual valve and is metered via either a Brooks model R-12M-25-4 rotameter or a magnetic flow meter (the calibration curves can be found in the Appendix I). The test fluid flows upwards through the annular space of the double pipe heat exchanger. The heat exchanger is 1.4 metres long and consists of two concentric tubes made of stainless steel. The shell is flanged at both ends to the stainless steel headers. In between the steel headers and the heat exchanger shell, there are two short pyrex glass pipe sections having the same ID as the shell, which allow for the visual observation of the fouling process. Pressure drop is measured by manometers over a length of 0.6 m. Results are discussed in Appendix II-6.

The artificially hardened water is heated by steam flowing downwards through the inner

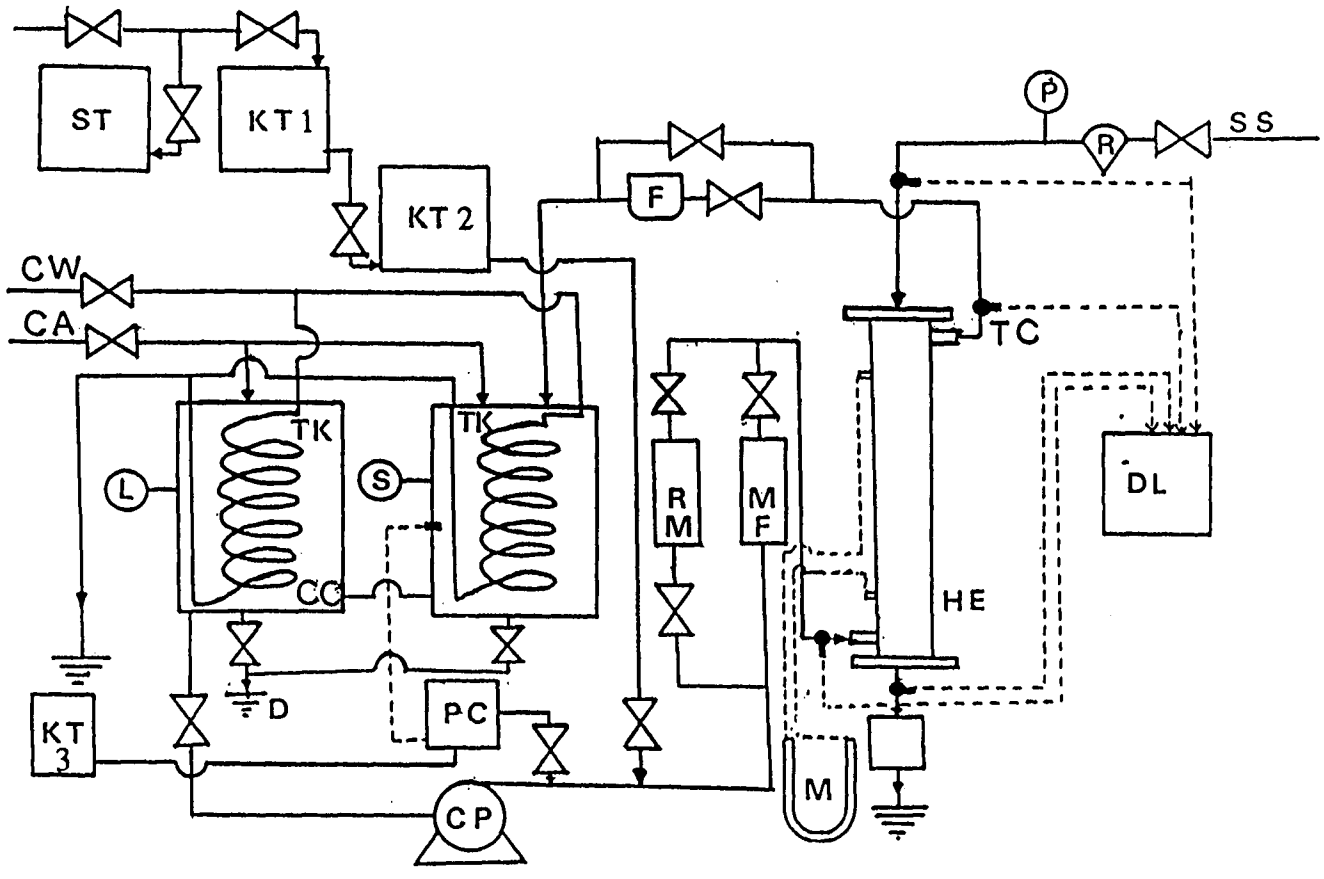

CA Compressed Air
CP Centrifugal Pump
CC Cooling Coil(s)
CW Cooling Water
D Drain(s)
DL Datalogger
F Filter
HE Heat Exchanger
KT KOH Tank(s)
L Level Gage
MF Magnetic Flowmeter
M Manometer
P Pressure Gage
PC PH Controller
RM Rotameter
R Pressure Reducer
S Sampling Point
SS Steam Supply
ST Salt Make-up Tank
TK Supply Tank
TC Thermocouple

FIGURE 3-1 PROCESS FLOW DIAGRAM OF THE APPARATUS

tube. The water enters and leaves the heat exchanger in a direction perpendicular to the axis of the heat exchanger. The heated test fluid returns to the supply tank where it is cooled by exchanging heat with building supply water which flows inside a helical coil made-up of stainless steel.

The test fluid is filtered to remove any particulates formed due to bulk precipitation process as well as any chunks of the deposits from the fouled tube as fouling progresses. The filter can be bypassed, if desired. The filter housing has a Mikro-Klean 25 or 50 microns cartridge which separates particulates from the test fluid. The particulates can be collected and removed at the end of a run.

3.2 pH Control System

The pH for a particular run is controlled automatically except at the very start of a run where a manual control is used. One hundred c.c. of 8 mol/L KOH solution is diluted to 20 litres and is stored in tank KT1 . Five litres of this solution flows by gravity into tank KT2 where it is again diluted to 20 litres. This 0.01 mol/L KOH solution is slowly fed (at the rate of about $<$ 1 litre per minute) into the circulating water suction header, with vigorous air sparging, to ensure uniform mixing. This initial control in raising the pH is manual. A Cole-Parmer Series 7142 proportional type pH controller is used to make the final adjustments to attain the starting pH. This unit also controls the pH during the run. The feed tank for the automatic controller contains 0.04 mol/L KOH solution. The pH controller is calibrated before

each run using standard buffer solutions.

3.3 Steam Supply System

The steam supply comes from the building steam header. A solenoid valve is fitted upstream of the heat exchanger which closes if a power failure occurs, and has to be energised again in order to be opened again when the power supply resumes, in order to protect the equipment from getting damaged by the steam. A needle valve is used to control the steam pressure at the entrance to the heat exchanger and, hence, the temperature in the inside tube of the DPHE. The condensate is collected and removed via #60 Clark type steam trap and is rejected into the mat. The steam outlet line has a steam trap bypass line that can be used as steam condensate drain line while the experiment is in progress. Flow rate of the condensate can be measured manually by means of a receiver and a timer.

3.4 Storage and Supply Tanks

The test fluid for a particular run is prepared in and recirculated from two 230-L PVC tanks. The suction header of the centrifugal pump is 51 mm ID and is connected to both tanks via 51 mm NPT bulk head fittings, also made up of PVC to avoid corrosion. Drain lines are connected to the pump suction header and to the bottom of both tanks. All piping, except the pump section header, is made of PVC and is 25.4 mm ID. One of the tanks has a valve connected at mid-height for sampling during a run. Both tanks are equipped with stainless steel

cooling coils of 18 m length each and 12.7 mm OD. The coil diameter is about 30 cm each. A level gage fitted to one of the tanks permits determination of the volume of the water in the tanks.

3.5 Heat Exchanger

A schematic diagram of the double pipe heat exchanger is shown in Figure 3-2. The 1.4 m long stainless steel heat exchanger shell is 38.1 mm in ID, and comprises of a central S.S. section of 90 cm length which is flanged at both ends to pyrex glass sections, having the same ID as the shell, to allow visual observation of the fouling process. The inner tubes are of two types, both 19.1 mm in OD, but differing in their ID. The two thicknesses were used to vary the temperature of the fouling surface. The thin one has an ID of 16.7 mm and the thick one has an ID of 13.7 mm. The materials of construction of the tubes are S.S. Type 304 and S.S. Type 321, respectively. Both tubes are plain and smooth finished. The dimensions and the thermal conductivities of the tubes are summarised in Table 3-1 .

Table 3-1 SUMMARY OF THE DIMENSIONS OF TUBES

Tube Type	Material of Construction	I.D. (mm)	O.D. (mm)	A_o (m^2)	R_m m^2K/kW	k_m (W/mK)
Thin	SS 304	16.7	19.1	0.084	0.077	16.6
Thick	SS 321	13.7	19.1	0.084	0.194	16.4

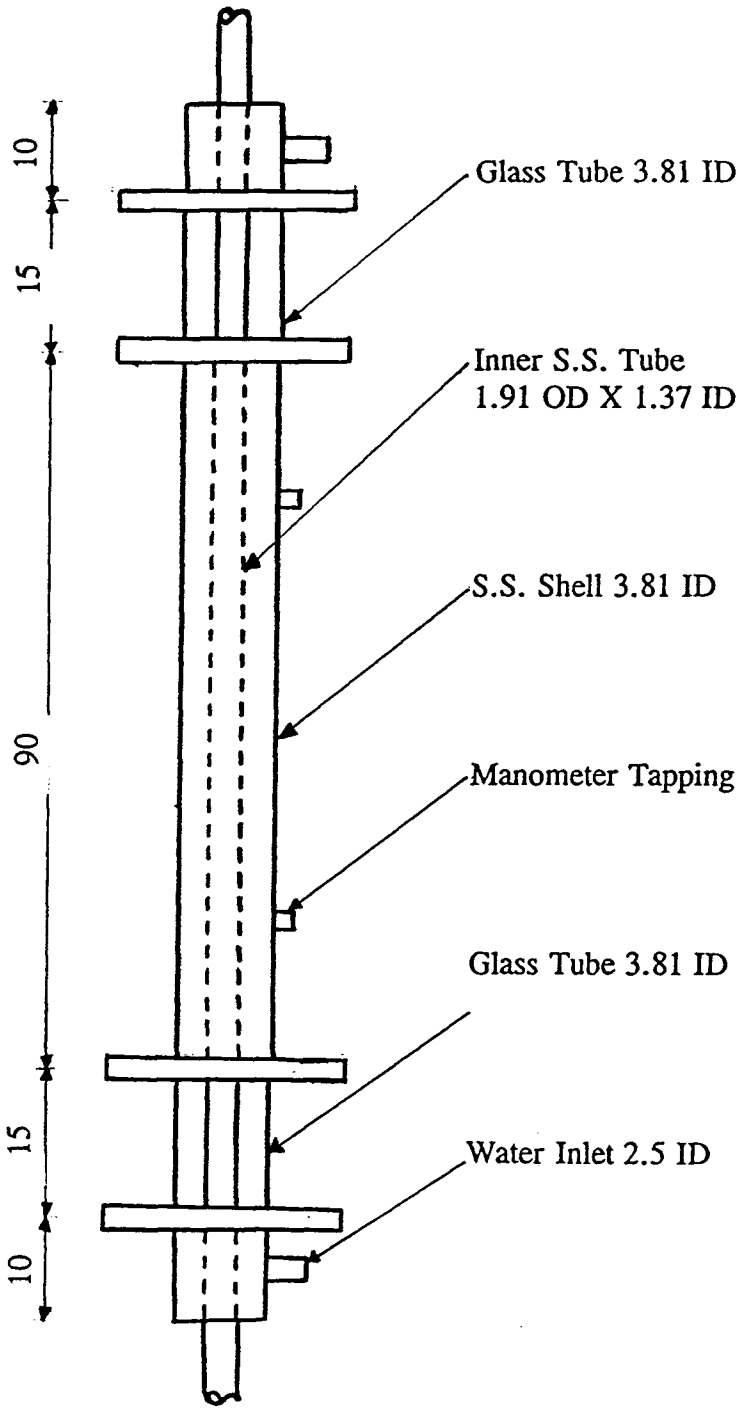

All dimensions are in cm.

FIGURE 3-2 SCHEMATIC DIAGRAM OF THE HEAT EXCHANGER

3.6 Temperature Measurements

The inlet and outlet temperature of water and steam are measured using sheathed J-type Iron-Constanton thermocouples. The thermocouples are connected to a switch, which, in turn, is connected to a DORIC Digitrend datalogger that can either record voltage output of the thermocouples or the temperature directly, at specified intervals of time such as one hour.

The temperature is displayed using an Omega DP 41-TC panelmeter having an accuracy of 0.2°C . The thermocouples were calibrated using a Hewlett Packard model 2801 quartz thermometer using a standard ice-bath and a constant temperature bath. A photograph of the apparatus is shown in Figure 3-3.

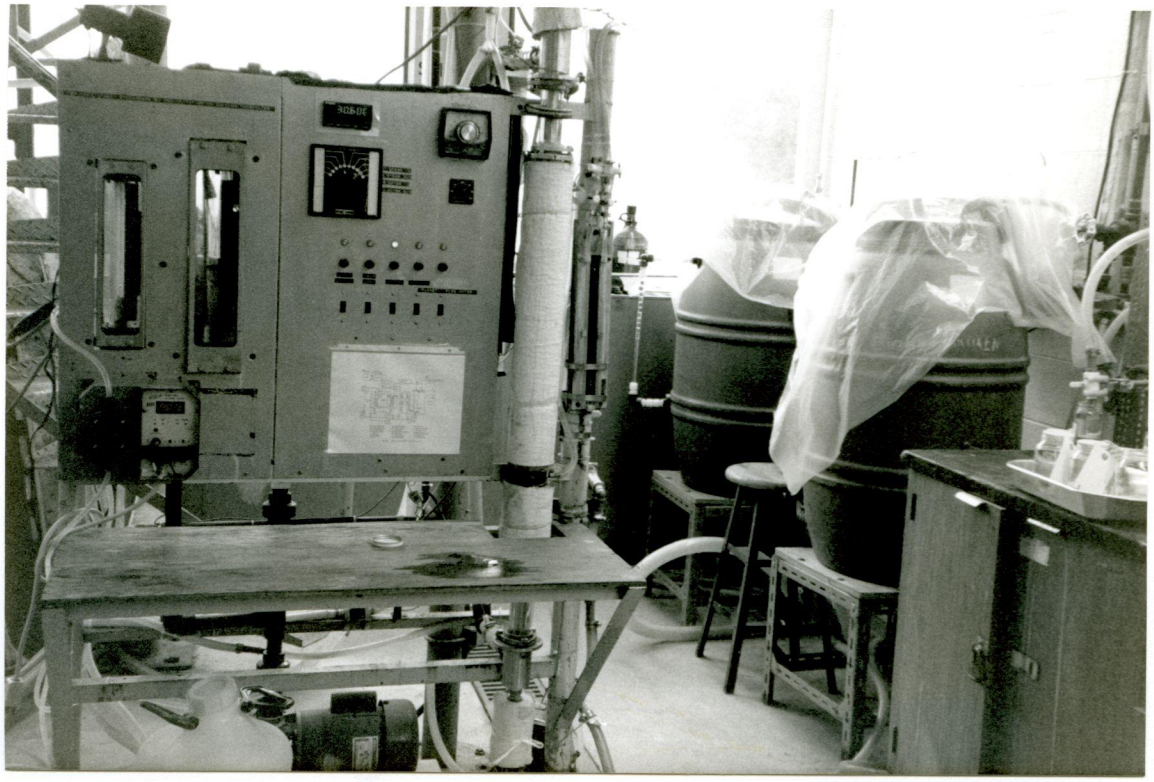

FIGURE 3-3 FRONT PHOTOGRAPH OF THE APPARATUS

§ 4. EXPERIMENTAL PROCEDURES

4.1 General Strategy

The feed tanks were filled with tap water to a level corresponding to the desired total system volume. The pump was turned on, as was the steam and the cooling water. All the temperatures were monitored until steady state was achieved. A measured weight of technical grade $CaCl_2.2H_2O$ was then added to the tank, accompanied with violent agitation caused by sparging of air at about 15 psi gage to promote rapid and complete mixing. After about 15 minutes, a concentrated 4-litre solution containing a known weight of KH_2PO_4 was added, and the mixing was continued. The pH of the resulting solution was always less than the desired pH for all the runs. Hence, the pH was raised by adding KOH solution first manually and then under automatic pH control with the vigorous sparging of air to avoid local high-pH pockets. The first water sample was then taken. Several water samples were subsequently taken and analyzed during each run, and make-up chemicals were added to keep the water analysis as constant as possible. In all cases where chemicals were added initially or as make-up doses, they were completely dissolved in water before addition to the supply tanks and they were added very slowly and with high turbulence by sparging air to avoid local supersaturation pockets and the resulting precipitation that might occur. Step-by-step procedural details for the runs are given in § 4.4 .

4.2 Calcium Content of the Solutions

Hardness, or calcium content, is measured using the EDTA Titrimetric Method (24,25). When EDTA (ethylenediaminetetraacetic acid or its salts) is added to water containing both Ca^{++} and Mg^{++} ions, it preferentially combines with Ca^{++} . Hence, calcium can be determined by making pH so high that Mg^{++} is precipitated as its hydroxide. An indicator changes colour when all the Ca^{++} has reacted with EDTA.

The Erichrome Blue Black indicator is prepared by grinding together in a mortar 200 mg powdered dye and 100 g solid NaCl to 40 to 50 mesh. Standard EDTA titrant of 0.01 mol/L is prepared by weighing and dissolving 3.723 g analytical reagent-grade EDTA in 1000 mL distilled water. Standard EDTA titrant is equivalent to 400.8 μg Ca/1.00 mL

Because of the high pH used, the sample should be titrated immediately after addition of alkali and indicator. Hard waters with alkalinity higher than 300 mg $CaCO_3$/L are analyzed by taking a sample less than 50 c.c. and diluting to 50 c.c.

To carry out the analysis, about 2.0 c.c. of 1.0 mol/L NaOH is added to bring the pH to between 12 and 13. Then 0.1 to 0.2 g of the indicator is added and the sample is stirred thoroughly. The EDTA titrant is added slowly, preferably dropwise, with a continuous shaking of the flask until the colour changes from red through purple to bluish purple to a pure blue with no trace of bluish-purple tint. The calcium hardness can be calculated using the following

expression:

$$\frac{mg}{L}\ CaCO_3 = \frac{A \times B \times 1{,}000}{mL\ sample} \qquad (4\text{-}1)$$

where:

A = mL titrant for sample

B = mg $CaCO_3$ equivalent to 1.00 mL. EDTA at the calcium indicator end point

4.3 Phosphate Content of Solutions

Total orthophosphate is measured using the Vanadomolybdophosphoric acid Colorimetric Method (24,25) . In a dilute solution containing orthophosphate ions, ammonium molybdate reacts under acidic conditions to form molybdophosphoric acid. In the presence of vanadium, yellow vanadomolybdophosphoric acid is formed. The intensity of the yellow colour is proportional to the phosphate concentration.

Vandate-molybdate reagent is made by mixing two solutions: one made by dissolving 25 g ammonium molybdate, $(NH_4)_6Mo_7O_{24}.4H_2O$), in 300 mL distilled water, and the other made by dissolving 1.25 g ammonium metavandate, NH_4VO_3, by heating to boiling in 300 mL distilled water. This solution is cooled to room temperature and 300 mL of concentrated HCl is added. After mixing both solutions, a dilution to one liter is done by adding distilled water.

The sample to be analyzed for phosphate, 35 mL or less, containing less than 1.0 mg

phosphorus is put into a 50-mL volumetric flask. 10 mL of vandate-molybdate reagent is added and the sample is diluted to the mark. The reference or the blank solution is prepared by using distilled water instead of the sample. After at least 10 minutes, the absorbance is measured using a spectrophotometer at 470 nm wavelength and 1 cm path length. A calibration curve is plotted by diluting a standard phosphate solution and measuring absorbance versus known concentration of the phosphate. The calibration curve, Figure I-2, is shown in Appendix I.

4.4 Step-by-step Procedure for a Scaling Run

(1) Weigh the required amounts of KH_2PO_4 and $CaCl_2.2H_2O$ and dissolve them in 4 L water, separately.

(2) Fill the supply tanks to an appropriate level corresponding to a known volume, typically about 350 L.

(3) Start the pump and manually adjust the flow rate to the desired value.

(4) Open the steam valve and manually adjust the steam pressure and hence, the temperature to the desired value.

(5) Open the cooling water flow, in the cooling coil, inside the supply tanks to its maximum value.

(6) Turn on the temperature panelmeter to observe the various temperatures as a function of time.

(7) Calibrate the pH controller and adjust the set point at the desired value.

(8) After the steady state has been reached, as made evident by constant

temperature readings, add the $CaCl_2.2H_2O$ solution with continuous sparging with compressed air at about 10 psi gage pressure. Wait for about 15 minutes and then add the solution of KH_2PO_4 slowly, using a plastic funnel passing through the hole in the centre of the top lids of both the tanks. Sparge with air for at least 15 minutes.

(9) Feed the KOH solution manually by opening a valve using tank #2. Keep the flow rate below about 1L/min.

(10) Reduce the pressure of the sparging air to about 2 psi gage After the pH of the test fluid has reached within $\pm$ 1 units of the set point pH, commission the pH controller.

(11) Turn on the datalogger. Set the clock and program the period and output of recording sequence.

(12) Register the time when the pH of the test fluid becomes equal to the pH set point.

(13) Keep a watch on all the temperatures and the test fluid rotameter reading. Note down the temperature rise of the water, since this corresponds to a particular value of heat duty of the exchanger. Note down the manometric height differential.

(14) Try to keep the heat flux constant by controlling the steam pressure, since as the fouling proceeds, heat transfer rate will decrease and the outlet temperature of the water will fall.

(15) Take a water sample after every 12-24 hours and analyze it for total

orthophosphate and total calcium using the procedures outlined above. If there is a significant decrease in the concentration of either calcium or phosphate ions, or both, over time, add make-up chemicals to keep the water chemistry nearly constant. The chemicals are added after draining out 20 litres of the test fluid and slowly adding the make-up into the suction line of the pump, accompanied with air sparging at 10 psi gage pressure.

The amounts of chemicals to be added are calculated using the following expressions:

$$wc = \frac{(\theta + 1)}{\theta}\left\{\left[\frac{C(0) - C(\theta)}{C(0)}\right] wc(0) + \frac{20}{V}\frac{C(\theta)}{C(0)} \times wp(0)\right\} \qquad (4\text{-}2)$$

$$wp = \frac{(\theta + 1)}{\theta}\left\{\left[\frac{P(0) - P(\theta)}{P(0)}\right] wp(0) + \frac{20}{V}\frac{P(\theta)}{P(0)} wp(0)\right\} \qquad (4\text{-}3)$$

where:

wc, wp = weights of calcium and phosphate salts to be added

C(0), P(0) = concentrations of calcium and phosphate at the start of a run

$C(\theta)$, $P(\theta)$ = concentrations of calcium and phosphate at time θ

$\theta + 1$ = time (from the start) of the addition of the salts in hours

V = total recirculating volume in liters

(16) Take water samples after the addition process is complete and analyze them for the calcium and phosphate contents.

(17) Feed the data into the computer program and calculate the heat flux, the

overall heat transfer coefficient and the fouling resistance as a function of time for each reading.

(18) After there is no longer an appreciable change in the fouling resistance, or the steam pressure reaches its maximum value, terminate the run.

(19) Shut off the steam to the tube by manually closing the needle valve and by cutting off the power supply to the solenoid valve.

(20) Turn off the pump and the cooling water supply to the cooling coil. Drain the supply tanks through both bottom and side exits and let the system cool down.

(21) Turn off the pH controller and immerse the submersible electrode in water to prevent the drying of the tip.

(21) Shut off the datalogger and collect the recorded output.

(22) Disconnect the steam connection at the top of the heat exchanger and the steam trap connection at the bottom. Unscrew the bolts of the flanges of the heat exchanger and unscrew the thermocouple connection. Remove the tube from the heat exchanger. Inspect the layer on the tube for its hardness, uniformity and removability. Measure the thickness of the tube as a function of length using a micrometer screw gage. Scrape off the scale with a spatula and weigh it and store it for future analysis.

(24) Have the calcium and phosphate content of the scale determined by the inductive coupled plasma (ICP) analysis at a commercial laboratory. Measure the bulk density using a specific gravity bottle and examine the scale under

the optical microscope for its structure.

(25) Replace the tube in the exchanger. Connect the steam line at the top and the steam trap at the bottom. Tighten the flange at the top and the fittings at the bottom. Connect the thermocouples and insulate the steam line again.

(26) Clean the heat exchanger and the rest of the equipment using the method described below.

(27) Prepare for another run. Follow steps 1 to 26.

4.5 Cleaning of the heat exchanger

After cracking off and scraping the deposit from the tube, the tube was further cleaned by using steel wool and occasionally, fine emery cloth. It was then further chemically cleaned in a dilute HCl solution in a batch process using a plastic column about 1.5 m high and 4 cm. in diameter The tube was then wiped off and put back in the heat exchanger. Water was filled to about one-third of the tank's height and about 1 L of concentrated HCl solution was added to the tanks with mild air sparging. The pump was started and the discharge valve was wide open to allow rapid cleaning of the tube and other internals of the system. Tap water was added to the tank to top it up and the drain was opened to purge out the remains of the deposit and HCl. The water was allowed to recirculate for about ½ hour. The acidic water was then allowed to drain using the drain valves with air sparging at 10-15 kg/cm^{2}gage to drain any particulates from the system which would otherwise settle at the bottom of the tanks. After the draining, the tanks were refilled with tap water, the pump primed and started again and the draining procedure

repeated. Water samples were drawn and tested for the presence of any dissolved solids using a Cole-Parmer TDS meter, which had a minimum count of 10 mg/L. When the TDS meter showed zero, the cleaning process was judged to be complete.

§ 5. RESULTS AND DISCUSSION

5.1 General Overview

Artificially hardened water was prepared by adding 50 grams each of Technical Grade KH_2PO_4 and $CaCl_2.H_2O$ to about 380 L tap water. The molar concentrations of the total calcium and orthophosphate were thus kept approximately equal at values of about 90 ppm as $CaCO_3$ and 92 ppm as PO_4. If one of these species was fed in much lower amount than the other, its depletion over the course of time would necessitate very frequent additions to keep water quality parameters constant, besides causing many absolute errors in the measurements of concentration. These chemicals were added after making sure that a steady state had been reached, which previous experimentation in clean runs had shown could be reached in about 1-2 hours. It took about one-half to one hour after adding the chemicals to reach the set pH. The fouling run was considered to be started at this point. The nucleation on the tube was normally visible within a few hours of the start, through the pyrex glass section of the heat exchanger. However, sometimes it occurred almost instantly. The nucleation time was not considered to be of any practical significance over the fouling runs which extended from 15 to 100 hours. The on-line filter was used for all medium velocity and low velocity runs. For high velocity runs, the filter was bypassed frequently, as clogging of the filter caused a considerable drop in the flow rate. In case the rotameter was in line, the rotameter setting was also periodically monitored as the flow was maintained as constant as possible by adjusting a manual valve. In the first 12 runs, the presence of suspended solids in the water samples was observed visually after storing the

samples for 2-3 days. For the subsequent runs, all the water samples were filtered using a Gelman 47 mm Filter through 0.45 μm filter papers and no bulk precipitation in the water samples could be observed after that for a few days. The water samples were withdrawn and analysed for total calcium, total phosphate and pH. As the run progressed, if a considerable decrease in concentration was observed, make-up salts were added to keep the water quality parameters constant as described in section 4.4. The pH was maintained constant by the automatic pH controller. A typical plot of the water analysis with time is shown in Figure 5-1. Water analysis data are tabulated in Appendix II-9.

5.2 Variation of the Clean Overall Heat Transfer Coefficient with the Heat Transfer Rate

The variation of the clean overall heat transfer coefficient with the heat transfer rate was determined experimentally by carrying out runs at different velocities (0.19, 0.47, 0.93 m/s) and by varying the steam temperature. The thick tube was used for all these runs. As was expected, the clean overall heat transfer coefficient always increased with the steam temperature. Increasing the steam temperature increased the outside wall temperature and hence the outside heat transfer coefficient increased, leading to an increase in the clean overall heat transfer coefficient. For identical conditions, the clean overall heat transfer coefficient for the thin tube was greater than that for the thick tube because of higher thermal resistance for the thick tube. The slopes of the linear plots of clean overall heat transfer coefficient versus the heat transfer rate, obtained by the least squares fit method are shown in Table 5-1. Average values of the slopes were used in equation (2-9) to correct U_{oc} for the variations in the heat transfer rate.

TABLE 5-1 SLOPES OF U_{oc} VERSUS Q CURVES

Run	v (m/s)	Range of Q (kW)	Slope of U_{oc} vs Q Line ($1/m^2K$)
LV	0.19	5.6-10.1	0.04954
MV	0.47	8.9-13.7	0.04439
HV	0.93	12.6-17.6	0.01931
LVR	0.19	6.1-10.1	0.04560
MVR	0.47	9.7-14.0	0.05200
HVR	0.93	12.9-17.2	0.00721

R = repeat Run L = low velocity M = medium velocity H = high velocity

The effect of the variations in the heat transfer rate on the experimental overall heat transfer coefficient is shown in Figure 5-2 through Figure 5-7. It can be noted that at higher velocities, the variation of the overall heat transfer coefficient with the heat transfer rate is relatively less pronounced than at lower velocities. It was observed that the variation in the heat transfer rate due to the fouling process did not affect the clean overall heat transfer coefficient and, therefore, the calculated fouling resistance appreciably in any of the runs. In all subsequent analysis, the term fouling resistance refers to the "corrected" fouling resistance, calculated by using the clean overall heat transfer value which corresponded to the measured heat flow, as indicated below.

5.3 Fouling Resistance Versus Time

The datalogger was programmed to record the temperatures every hour. As the fouling

progressed, the outlet temperature of the water would tend to decrease. The steam temperature was therefore raised by manually opening the 12 mm needle valve on the steam line gradually, in order to maintain a constant heat flux with time.

From the results of section 5.3 it is evident that fluctuations in Q would produce fluctuations in the clean overall heat transfer coefficient. Thus in evaluating the fouling resistance, it is necessary to ensure that during the dirty overall coefficient measurement at time t, the heat flow is the same as that used for the clean coefficient i.e.:

$$R_f = \frac{1}{U_{od}}\Big|_{Q = Q_t} - \frac{1}{U_{oc}}\Big|_{Q = Q_t} \qquad (5\text{-}1)$$

This R_f value is referred to as the corrected fouling resistance since it uses clean overall heat transfer coefficient corrected to $Q = Q_t$ which may differ slightly from Q_0. The uncorrected fouling resistance was also calculated for each run as follows:

$$R_f = \frac{1}{U_{od}}\Big|_{Q = Q_t} - \frac{1}{U_{oc}}\Big|_{Q = Q_0} \qquad (5\text{-}2)$$

Figure 5-8 compares the corrected and uncorrected fouling resistance versus time curves. The scatter which is probably due to the fluctuations in the heat transfer rate appears to be reduced with the correction, hence in all subsequent results the corrected fouling resistance is used.

The "corrected" and "uncorrected" fouling resistances were calculated for each run. All

three types of behaviours i.e. linear, falling rate and asymptotic were observed. Typical curves are shown in Figures 5-9 to 5-11. The initial fouling rates and the conditions of the runs are summarised in Table 5-2. The concentrations of important ionic species and the activity coefficients are summarised in Table 5-3. The initial fouling rate was determined by applying a linear regression to the initial part of the curve that appeared to be a straight line. The water chemistry was assumed to be constant during this initial part of the run. As well, for this initial period, the removal processes were expected to have the least effect on the net fouling process. In some runs, an initial negative R_f was observed, which is presumably due to roughness effects.

5.4 Reproducibility of the Results

Some runs were repeated to ascertain the degree of reproducibility. In most cases, a reasonable reproducibility could be observed. In fouling experiments, a perfect reproducibility is hard to achieve because of limited direct and indirect control over the large number of the variables involved and experimental errors associated with their measurements. Where the extent of fouling is large, measurement errors are much less significant; by contrast a change in the dirty overall heat transfer coefficient of a few percent due to fouling is difficult to measure accurately.

Runs 3 and 4 were done at almost identical conditions of heavy fouling yielding R_f values of about 0.35 m^2K/kW after 100 hours (Appendix IV). As can be seen from the Table 5-2, the initial fouling rate of Run 4 is only 9% more than that of Run 3. Runs 14 and 19 were done at

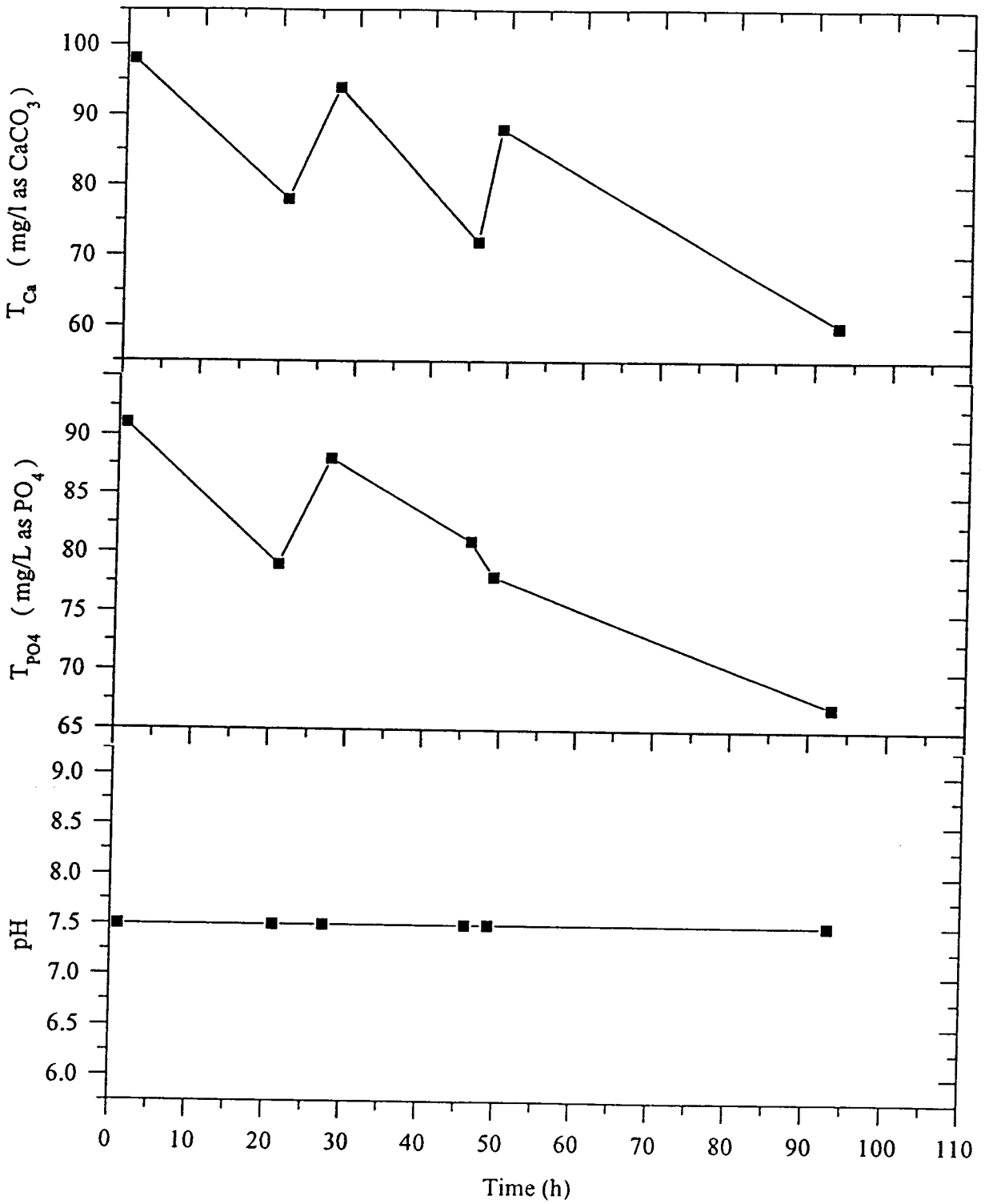

FIGURE 5-1 VARIATION OF WATER CHEMISTRY WITH TIME

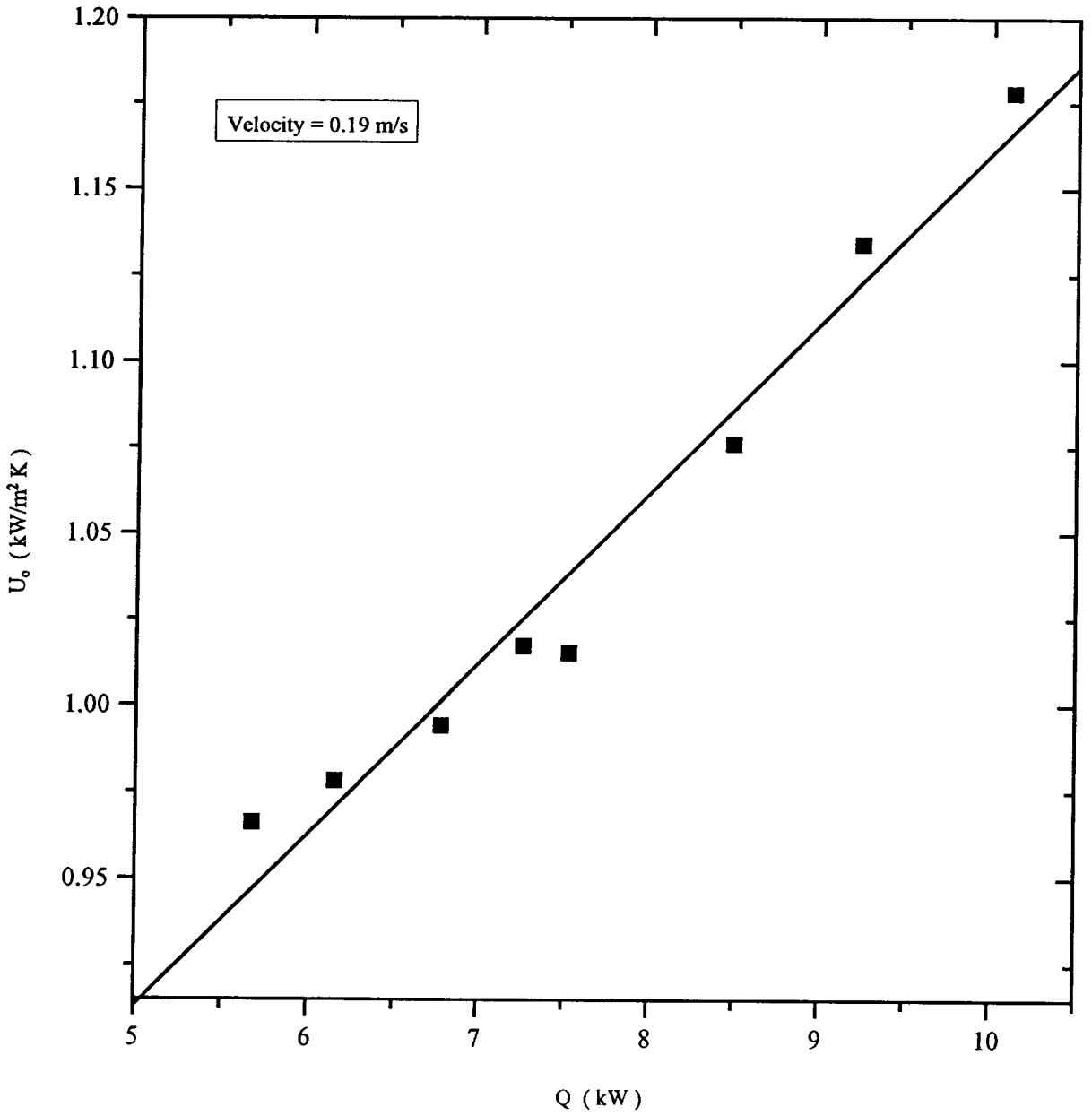

FIGURE 5-2 EFFECT OF THE HEAT TRANSFER RATE ON THE CLEAN OVERALL HEAT TRANSFER COEFFICIENT AT LOW VELOCITY

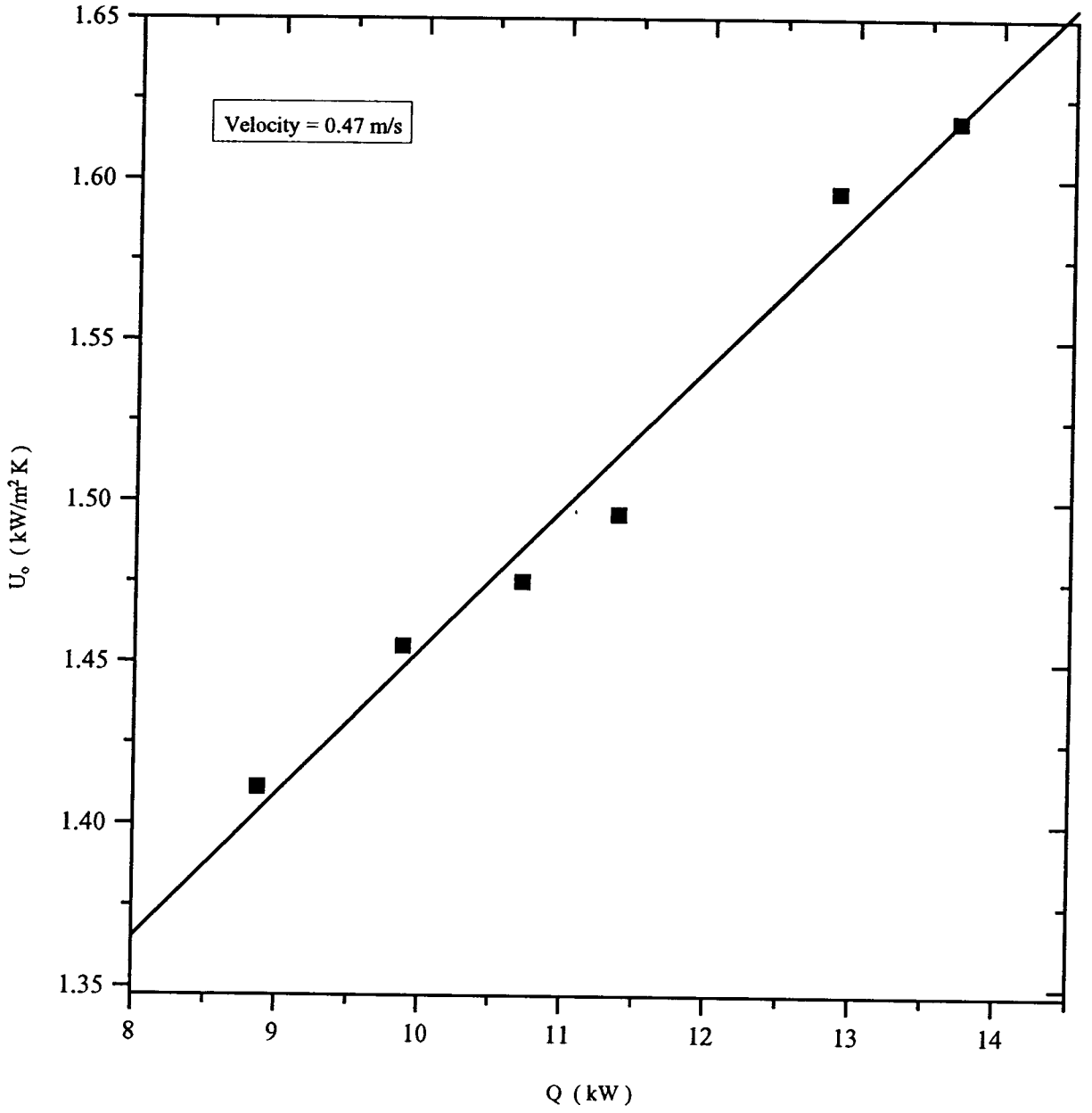

FIGURE 5-3 EFFECT OF THE HEAT TRANSFER RATE ON THE CLEAN OVERALL HEAT TRANSFER COEFFICIENT AT MEDIUM VELOCITY

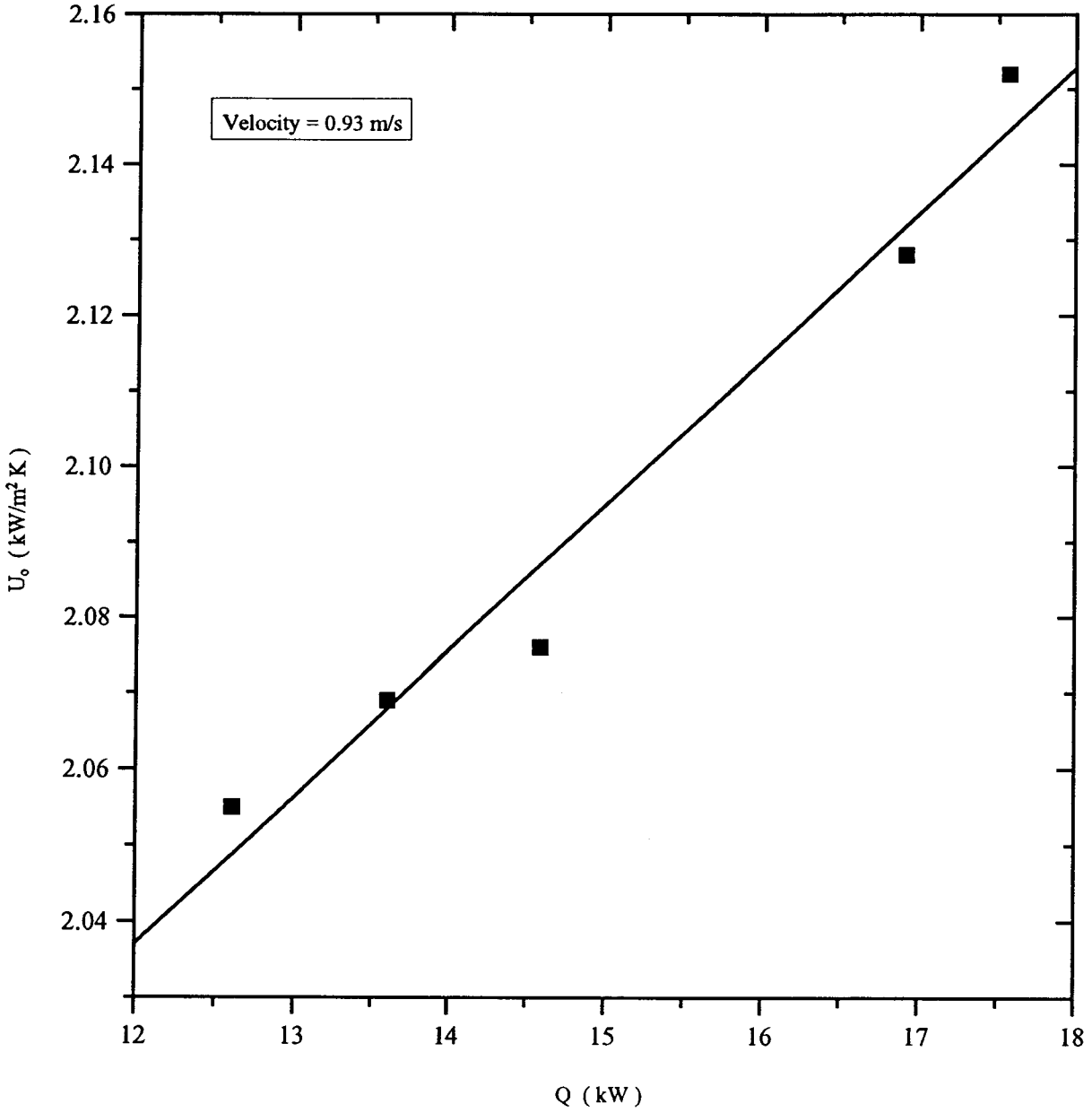

FIGURE 5-4 EFFECT OF THE HEAT TRANSFER RATE ON THE CLEAN OVERALL HEAT TRANSFER COEFFICIENT AT HIGH VELOCITY

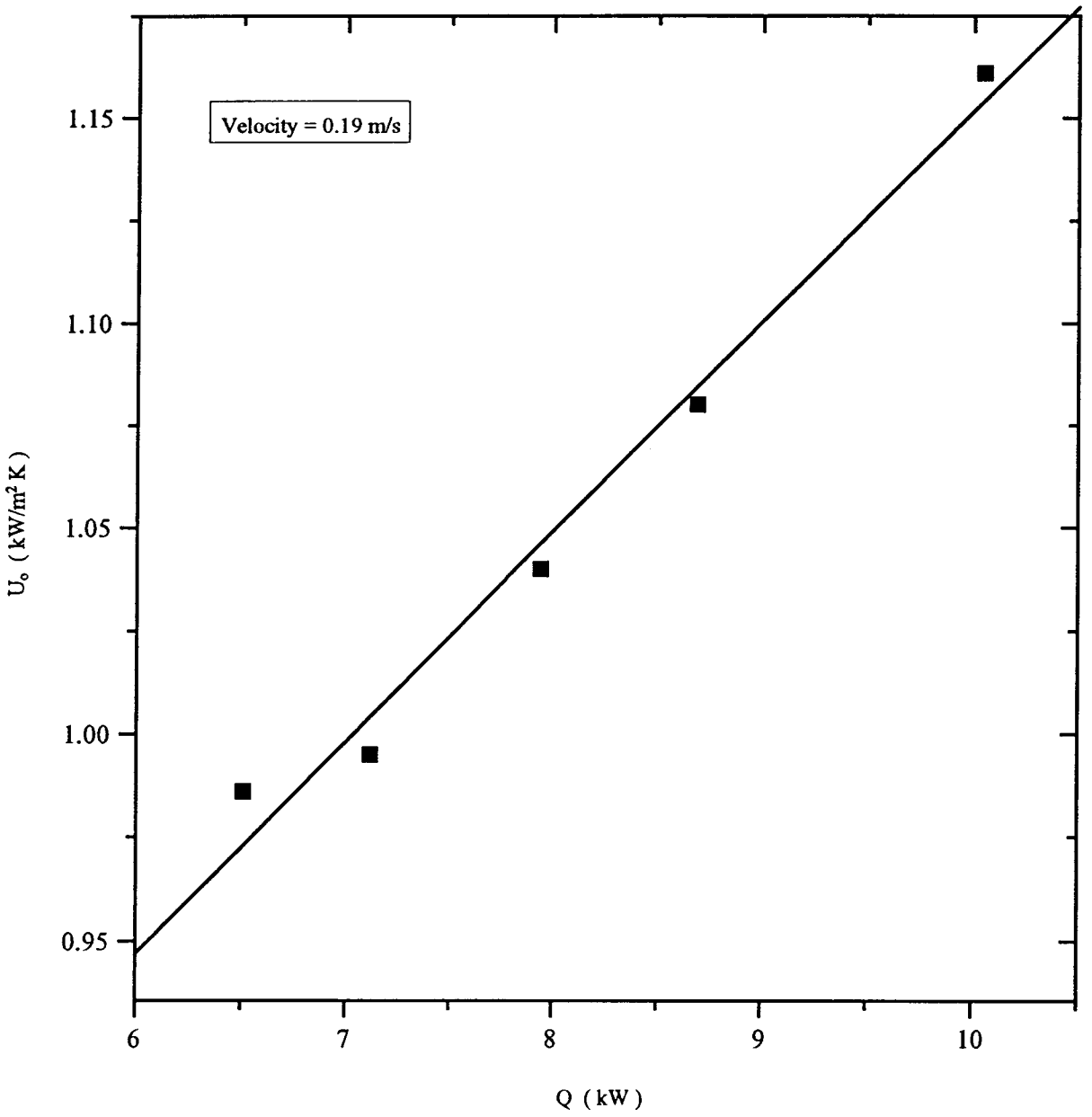

FIGURE 5-5 EFFECT OF THE HEAT TRANSFER RATE ON THE CLEAN OVERALL HEAT TRANSFER COEFFICIENT AT LOW VELOCITY (REPEAT)

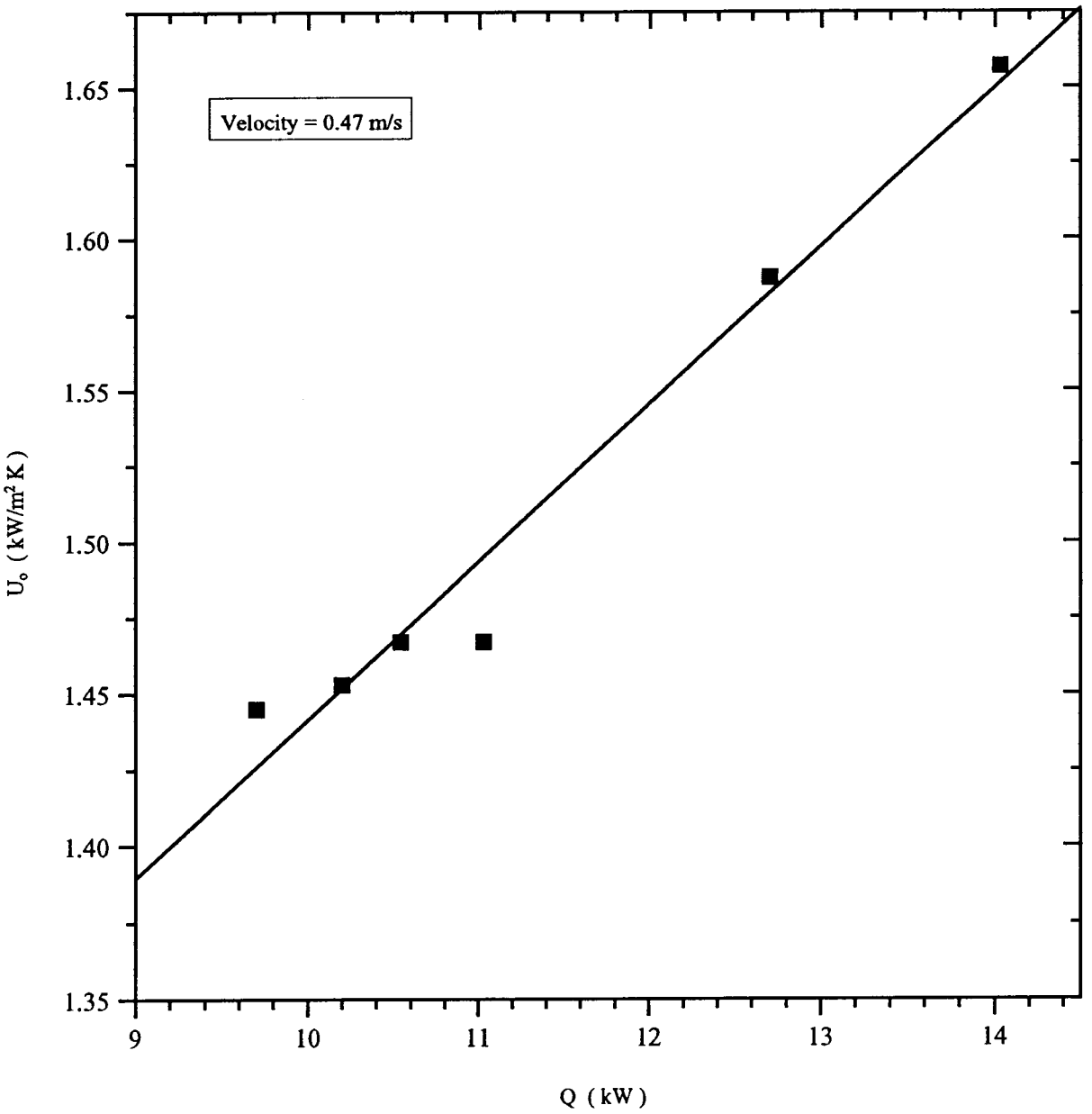

FIGURE 5-6 EFFECT OF THE HEAT TRANSFER RATE ON THE CLEAN OVERALL HEAT TRANSFER COEFFICIENT AT MEDIUM VELOCITY (REPEAT)

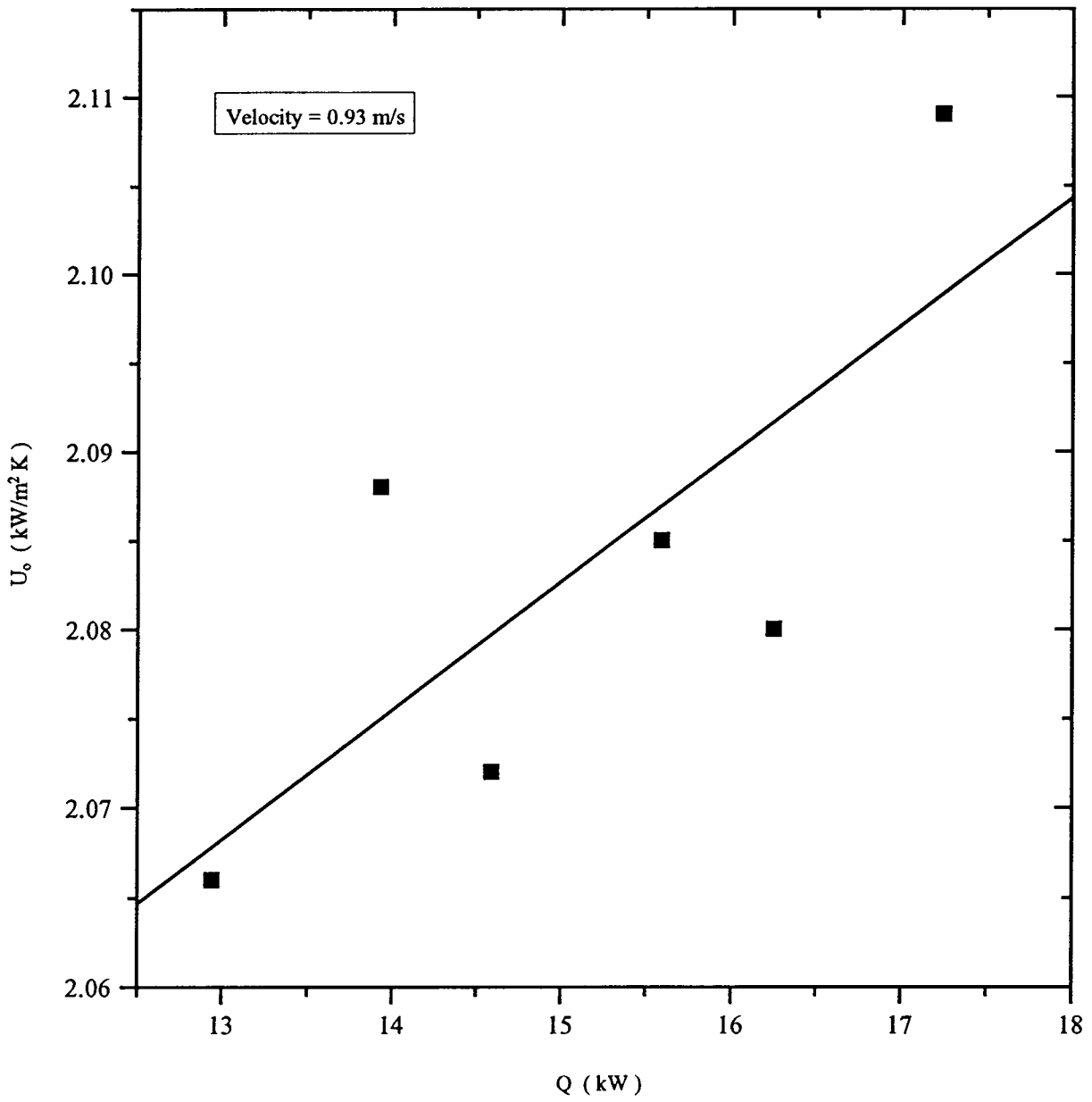

FIGURE 5-7 EFFECT OF THE HEAT TRANSFER RATE ON THE OVERALL HEAT TRANSFER COEFFICIENT AT HIGH VELOCITY (REPEAT)

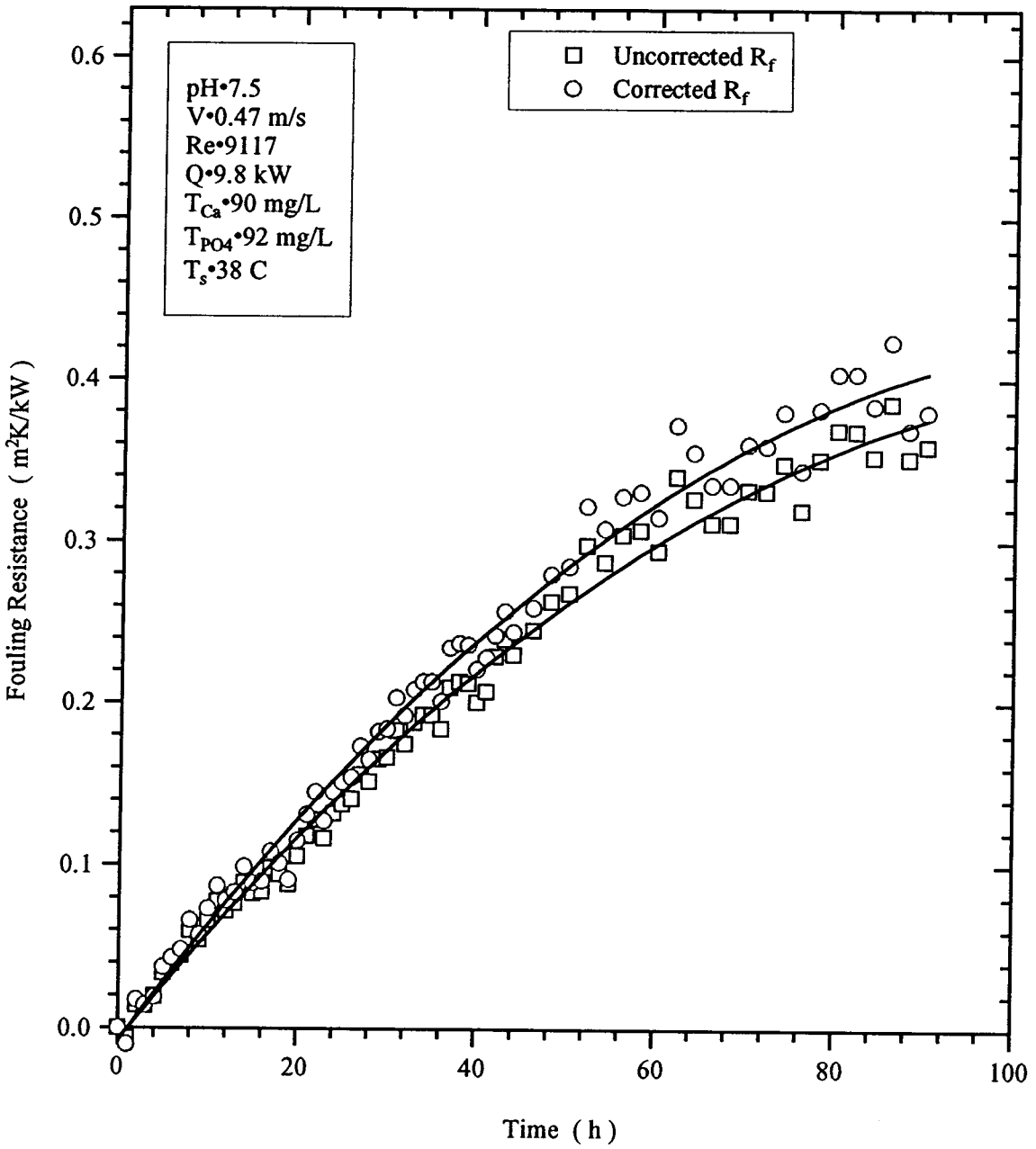

FIGURE 5-8 RUN 3 CORRECTED AND UNCORRECTED FOULING RESISTANCES VS. TIME

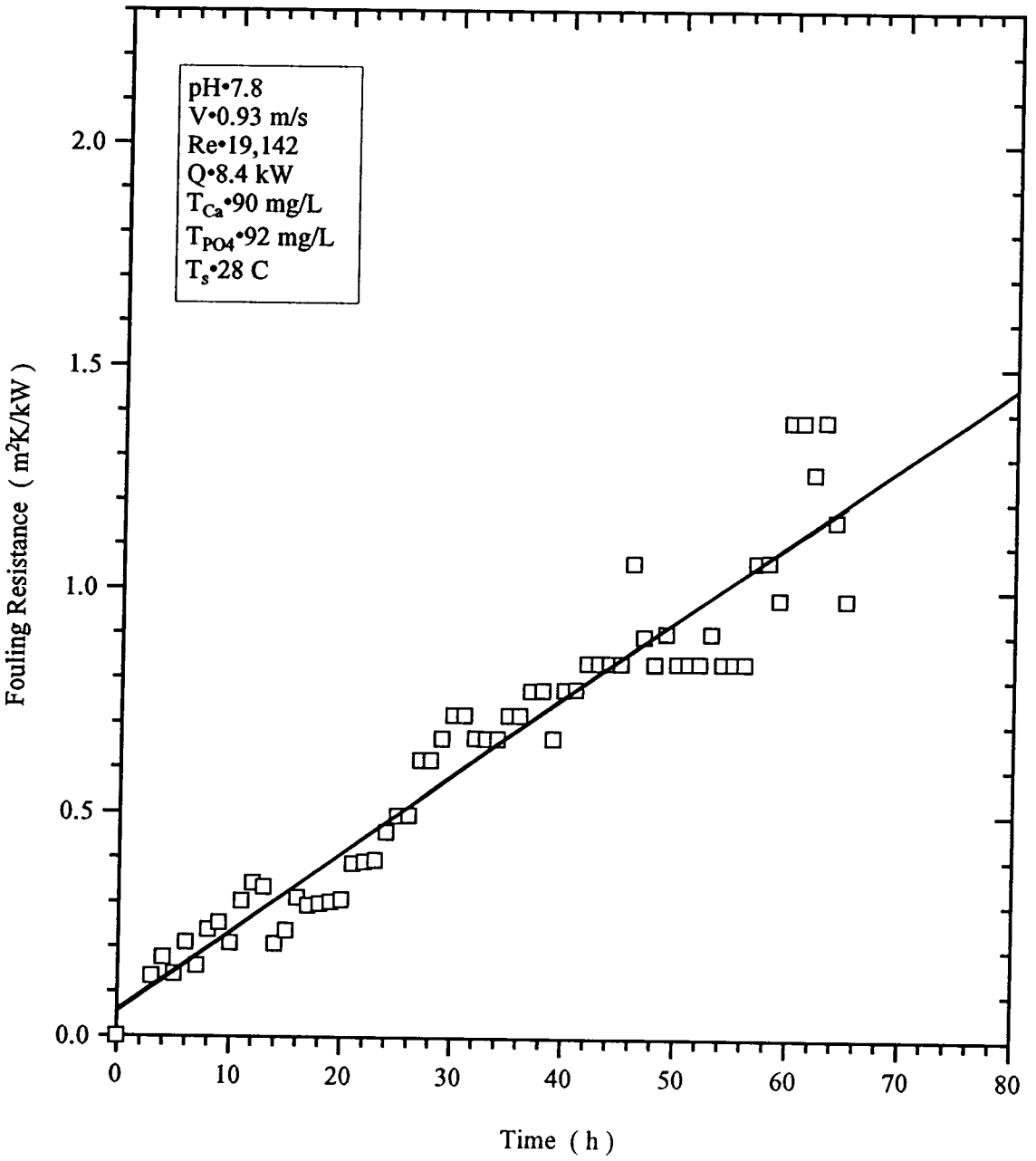

FIGURE 5-9 RUN 11 FOULING RESISTANCE VERSUS TIME (LINEAR TYPE)

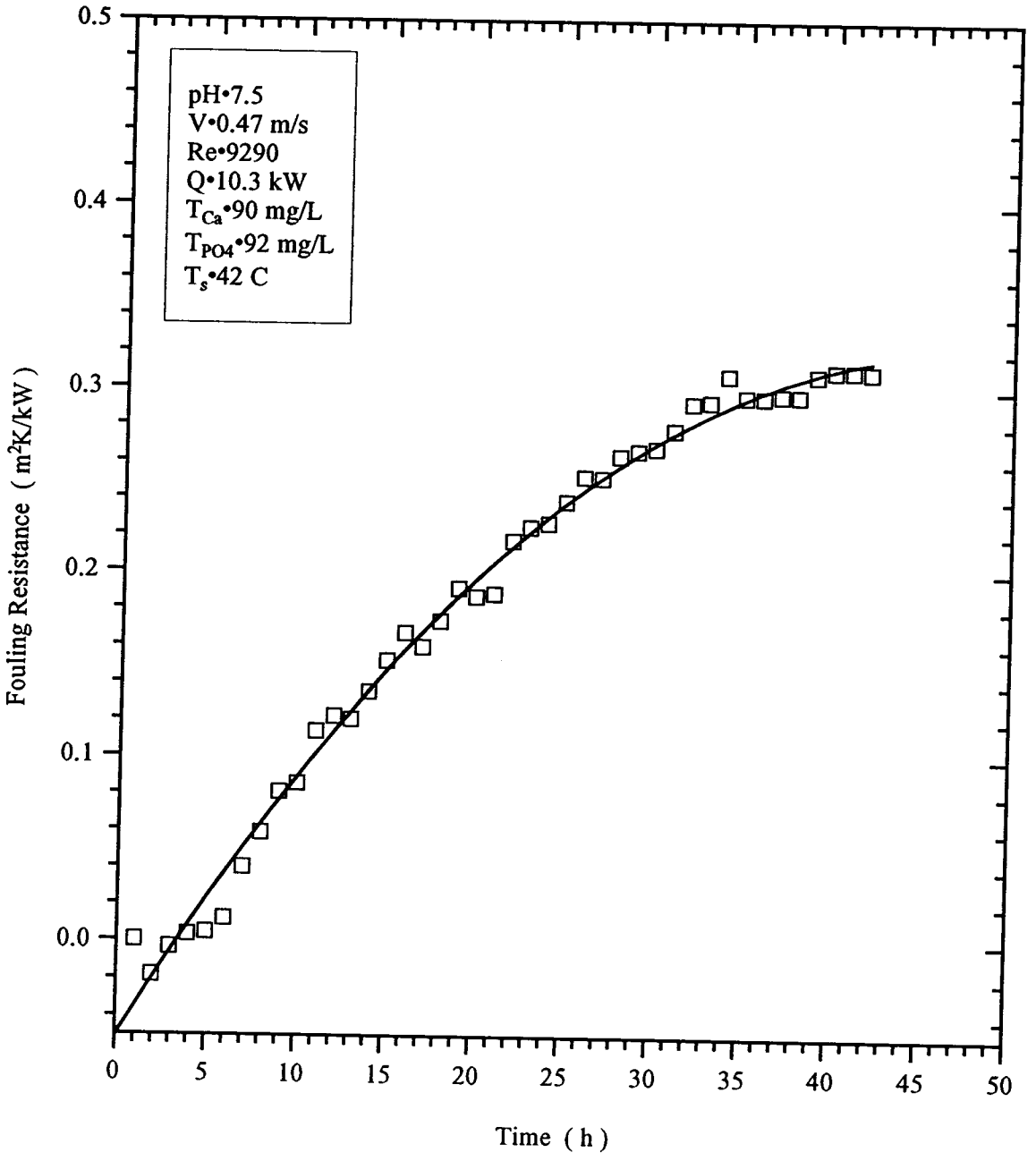

FIGURE 5-10 RUN 21 FOULING RESISTANCE VERSUS TIME (FALLING RATE TYPE)

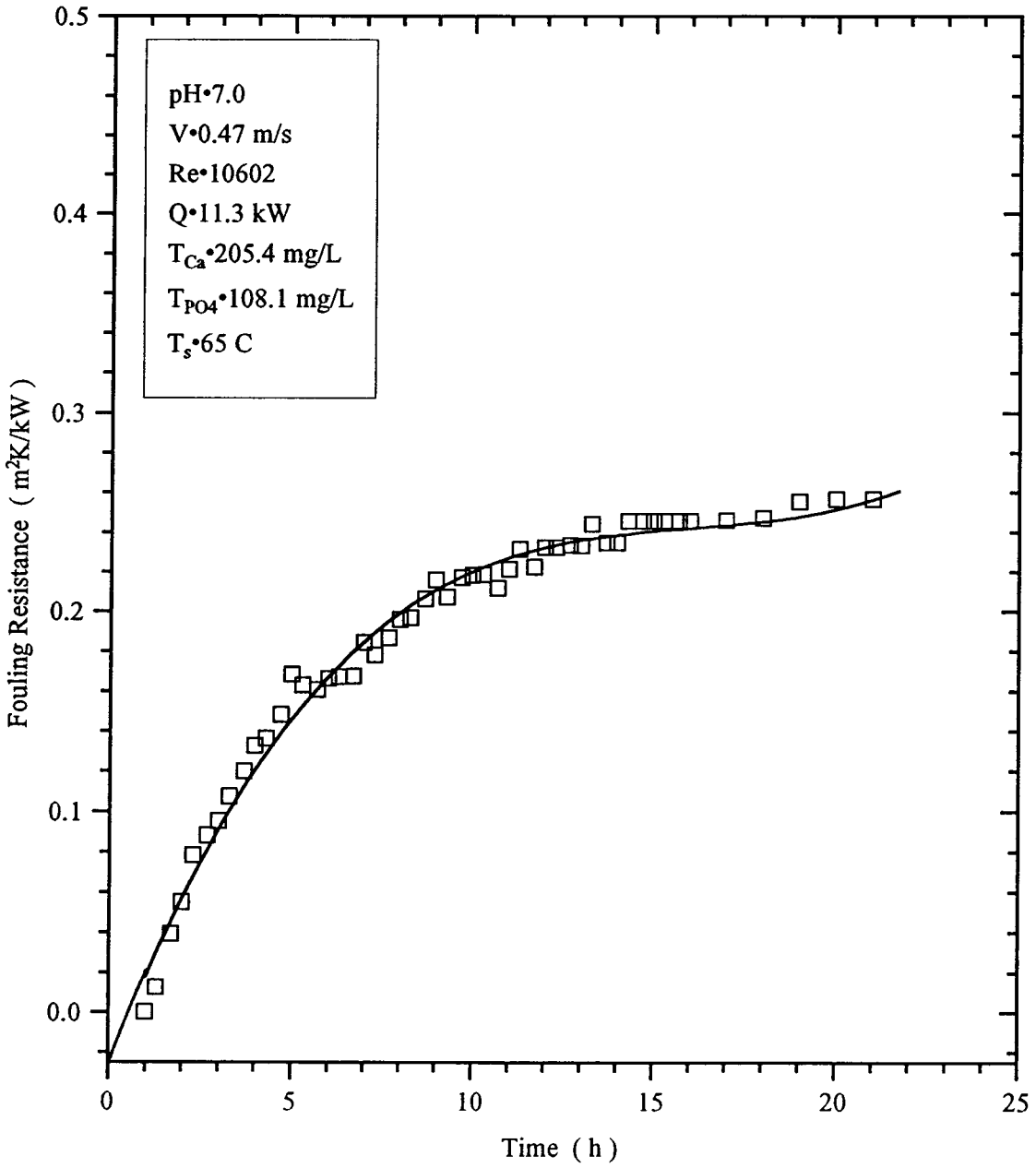

FIGURE 5-11 RUN 23 FOULING RESISTANCE VERSUS TIME (ASYMPTOTIC TYPE)

TABLE 5-2 SUMMARY OF THE RESULTS

Run	pH	Vel (m/s)	Re_b	Q_{avg} (kW)	T_{Ca} (ppm)	T_{PO4} (ppm)	T_s^* (°C)	$(dR_f/d\theta)_{inst}$ (m^2K/kWh)	Comments
2	7.5	0.47	8950	9.0	90	92	52	0.0077	
3	7.5	0.47	9117	9.8	90	92	38	0.0053	Restarted after power failed at t = 1 hour
4	7.5	0.47	9195	10.9	90	92	38	0.0058	
5	7.0	0.93	18,792	12.3	90	92	23	0.0074	
6	7.5	0.2	3612	6.5	90	92	62	0.0027	
7	7.0	0.93	19,777	13.9	90	92	44	0.0016	
8	7.0	0.47	10,120	9.6	90	92	58	0.0030	
9	8.0	0.2	3884	6.1	90	92	69	0.0096	Deposit very sticky and loose
10	8.0	0.93	19968	9.1	90	92	28	0.0692	Fouling very rapid, lasted about 3-4 hrs
11	7.8	0.93	19142	8.4	90	92	28	0.0183	
12	7.3	0.47	10204	8.7	90	92	60	0.0060	
13	6.5	0.47	9729	8.1	90	92	49	-5.6E-5	Negligible fouling observed in 24 hrs
14	6.8	0.47	9856	9.0	90	92	49	-.0009	Negligible fouling observed in 24 hrs
15	7.0	0.93	19,807	12.7	90	92	30		Fouling Rate could not be specified
16	7.5	0.93	19,946	11.0	90	92	43	0.0177	
17	7.5	0.93	19,467	12.5	90	92	21	0.023	
18	7.0	0.19	4028	5.7	90	92	71	0.00127	
19	6.8	0.47	9,213	9.2	92	94	52	-0.0008	Negligible fouling observed in 24 hrs
20	7.5	0.47	10,183	9.7	90	92	87	0.033	

Run	pH	Vel (m/s)	Re_b	Q_{avg} (kW)	T_{Ca} (ppm)	T_{PO4} (ppm)	T_S^* (°C)	$(R_f)_{init}$	Comments
21	7.5	0.47	9290	10.3	90	92	42	0.0120	
22	7.5	0.47	9509	10.4	90	92	50	0.0168	
23	7.0	0.47	10,602	11.3	200	103	65	0.032	
24	7.0	0.47	10,622	9.6	90	184	56	.0237	
25	7.0	0.47	10,577	9.9	90	138	51	0.009	
26	7.0	0.47	10,954	10.2	135	92	57	0.0198	
27	7.0	0.47	10,367	9.5	225	92	55	0.030	
28	7.0	0.47	10,307	9.5	90	230	54	0.028	
29	7.5	0.47	10,290	10.0	100	103	63	0.0188	
30	7.0	0.47	10,415	11.3	100	103	60	0.0027	
31	7.0	0.47	10,748	11.2	93	96	72	0.0007	Negligible fouling observed
32	7.0	0.47	10,457	9.4	400	103	77	0.0307	Deposit very sticky and porous
33	8.0	0.47	10627	10.0	100	103	61	0.0478	

* calculated (see Appendix II)

TABLE 5-3 SUMMARY OF THE CONCENTRATIONS AND ACTIVITY COEFFICIENTS FOR ALL RUNS

Run	pH	Ca (mol/L)	$H_2PO_4^-$ (mol/L)	HPO_4^{2-} (mol/L)	PO_4^{3-} (mol/L)	H^+ (mol/L)	OH^- (mol/L)	f_M	f_D	f_T
2	7.5	$.76 \times 10^{-3}$	$.21 \times 10^{-3}$	$.62 \times 10^{-3}$	$.22 \times 10^{-7}$	$.34 \times 10^{-7}$	$.28 \times 10^{-6}$	.93	.73	.50
3	7.5	$.76 \times 10^{-3}$	$.21 \times 10^{-3}$	$.62 \times 10^{-3}$	$.22 \times 10^{-7}$	$.34 \times 10^{-7}$	$.28 \times 10^{-6}$	.93	.74	.50
4	7.5	$.76 \times 10^{-3}$	$.21 \times 10^{-3}$	$.62 \times 10^{-3}$	$.22 \times 10^{-7}$	$.34 \times 10^{-7}$	$.28 \times 10^{-6}$	.93	.74	.50
5	7.0	$.80 \times 10^{-3}$	$.45 \times 10^{-3}$	$.42 \times 10^{-3}$	$.45 \times 10^{-8}$	$.11 \times 10^{-6}$	$.89 \times 10^{-7}$	.93	.74	.51
6	7.5	$.77 \times 10^{-3}$	$.21 \times 10^{-3}$	$.61 \times 10^{-3}$	$.22 \times 10^{-7}$	$.34 \times 10^{-7}$	$.28 \times 10^{-6}$	.93	.74	.50
7	7.0	$.80 \times 10^{-3}$	$.45 \times 10^{-3}$	$.40 \times 10^{-3}$	$.42 \times 10^{-8}$	$.11 \times 10^{-6}$	$.13 \times 10^{-6}$	.93	.75	.52
8	7.0	$.80 \times 10^{-3}$	$.45 \times 10^{-3}$	$.42 \times 10^{-3}$	$.45 \times 10^{-8}$	$.11 \times 10^{-6}$	$.89 \times 10^{-7}$	.93	.74	.51
9	8.0	$.71 \times 10^{-3}$	$.76 \times 10^{-4}$	$.71 \times 10^{-3}$	$.80 \times 10^{-7}$	$.11 \times 10^{-7}$	$.90 \times 10^{-6}$	.92	.72	.48
10	8.0	$.71 \times 10^{-3}$	$.75 \times 10^{-4}$	$.69 \times 10^{-3}$	$.75 \times 10^{-7}$	$.11 \times 10^{-7}$	$.13 \times 10^{-5}$	.92	.73	.45
11	7.8	$.73 \times 10^{-3}$	$.12 \times 10^{-3}$	$.69 \times 10^{-3}$	$.48 \times 10^{-7}$	$.17 \times 10^{-7}$	$.56 \times 10^{-6}$	.92	.73	.49
12	7.3	$.77 \times 10^{-3}$	$.30 \times 10^{-3}$	$.53 \times 10^{-3}$	$.11 \times 10^{-7}$	$.54 \times 10^{-7}$	$.25 \times 10^{-6}$	.93	.75	.52
13	6.5	$.84 \times 10^{-3}$	$.71 \times 10^{-3}$	$.20 \times 10^{-3}$	$.68 \times 10^{-9}$	$.34 \times 10^{-6}$	$.28 \times 10^{-7}$	.93	.75	.53
14	6.8	$.81 \times 10^{-3}$	$.56 \times 10^{-3}$	$.32 \times 10^{-3}$	$.22 \times 10^{-8}$	$.17 \times 10^{-6}$	$.56 \times 10^{-7}$	.93	.75	.52
15	7.0	$.80 \times 10^{-3}$	$.46 \times 10^{-3}$	$.41 \times 10^{-3}$	$.45 \times 10^{-8}$	$.11 \times 10^{-6}$	$.90 \times 10^{-7}$	.93	.75	.52
16	7.5	$.76 \times 10^{-3}$	$.21 \times 10^{-3}$	$.62 \times 10^{-3}$	$.22 \times 10^{-7}$	$.34 \times 10^{-7}$	$.28 \times 10^{-6}$	.93	.74	.50
17	7.5	$.76 \times 10^{-3}$	$.21 \times 10^{-3}$	$.62 \times 10^{-3}$	$.22 \times 10^{-7}$	$.34 \times 10^{-7}$	$.28 \times 10^{-6}$	.93	.74	.50
18	7.0	$.80 \times 10^{-3}$	$.45 \times 10^{-3}$	$.42 \times 10^{-3}$	$.45 \times 10^{-8}$	$.11 \times 10^{-6}$	$.89 \times 10^{-7}$	.93	.74	.51
19	6.8	$.82 \times 10^{-3}$	$.56 \times 10^{-3}$	$.32 \times 10^{-3}$	$.22 \times 10^{-8}$	$.17 \times 10^{-6}$	$.56 \times 10^{-7}$	.93	.75	.52
20	7.5	$.78 \times 10^{-3}$	$.21 \times 10^{-3}$	$.62 \times 10^{-3}$	$.22 \times 10^{-7}$	$.34 \times 10^{-7}$	$.28 \times 10^{-6}$	.93	.73	.50
23	7.0	$.19 \times 10^{-2}$	$.45 \times 10^{-3}$	$.43 \times 10^{-3}$	$.52 \times 10^{-8}$	$.11 \times 10^{-6}$	$.91 \times 10^{-7}$	.91	.69	.43
24	7.0	$.75 \times 10^{-3}$	$.91 \times 10^{-3}$	$.85 \times 10^{-3}$	$.98 \times 10^{-8}$	$.11 \times 10^{-6}$	$.90 \times 10^{-7}$	.92	.71	.43
25	7.0	$.78 \times 10^{-3}$	$.68 \times 10^{-3}$	$.63 \times 10^{-3}$	$.71 \times 10^{-8}$	$.11 \times 10^{-6}$	$.9 \times 10^{-7}$	.92	.73	.43
26	7.0	$.12 \times 10^{-2}$	$.43 \times 10^{-3}$	$.40 \times 10^{-3}$	$.46 \times 10^{-8}$	$.11 \times 10^{-6}$	$.9 \times 10^{-7}$	.92	.72	.47
27	7.0	$.21 \times 10^{-2}$	$.39 \times 10^{-3}$	$.38 \times 10^{-3}$	$.47 \times 10^{-8}$	$.11 \times 10^{-6}$	$.90 \times 10^{-7}$	.91	.68	.41
28	7.0	$.72 \times 10^{-3}$	$.11 \times 10^{-2}$	$.11 \times 10^{-2}$	$.13 \times 10^{-7}$	$.11 \times 10^{-6}$	$.91 \times 10^{-7}$	.91	.70	.45
29	7.5	$.80 \times 10^{-3}$	$.23 \times 10^{-3}$	$.68 \times 10^{-3}$	$.24 \times 10^{-7}$	$.34 \times 10^{-7}$	$.28 \times 10^{-6}$	.92	.73	.49
30	7.0	$.91 \times 10^{-3}$	$.50 \times 10^{-3}$	$.46 \times 10^{-3}$	$.51 \times 10^{-8}$	$.11 \times 10^{-6}$	$.89 \times 10^{-7}$	.93	.73	.50
31	7.0	$.91 \times 10^{-3}$	$.50 \times 10^{-3}$	$.46 \times 10^{-3}$	$.51 \times 10^{-8}$	$.11 \times 10^{-6}$	$.89 \times 10^{-7}$	.93	.73	.50
32	7.0	$.38 \times 10^{-2}$	$.38 \times 10^{-3}$	$.4 \times 10^{-3}$	$.55 \times 10^{-8}$	$.11 \times 10^{-6}$	$.93 \times 10^{-7}$	.89	.62	.34
33	8.0	$.81 \times 10^{-3}$	$.82 \times 10^{-4}$	$.78 \times 10^{-3}$	$.89 \times 10^{-7}$	$.11 \times 10^{-7}$	$.9 \times 10^{-6}$	.92	.71	.47

identical conditions and virtually no fouling could be observed in about 24 hours. Run 28 differs from Run 8 only with respect to the concentrations of the calcium and the phosphate, but has virtually identical results, the initial fouling rate of Run 28 being about 7% less than that of Run 8. There were, however, some cases where the reproducibility was poorer, e.g. Runs 21 and 22, where the former showed a fouling rate 40% greater than the other, probably due to experimental errors. The wide range of fouling rates measured (0.07 - 0.003 $m^2K/kW.h$) with considerable accuracy indicates the quality of measurements. Rates below about 10^{-3} $m^2K/kW.h$ or fouling resistances below about 0.03 m^2K/kW were subject to large error. All other measurements related to the water chemistry and calibration procedures were repeated until reproducible results of satisfactory accuracy were obtained.

For the clean runs, the reproducibility can be seen in Table 5-1, where the slopes for the repeat runs are within 17% of the original values, except for the runs at highest velocity.

5.5 Explanation for the Type of the Fouling Behavior

The traditional explanation of asymptotic fouling is the Kern-Seaton (10) model which assumes that as the fouling proceeds, the thickness of the fouled deposit increases and the removal term increases until it becomes equal to the deposition term and the net rate of fouling becomes zero. According to this model, all fouling resistance versus time curves should ultimately become asymptotic. However, an interesting observation was made in the present work that in some cases the fouling curve tended to become asymptotic as the calculated outside

tube wall temperature approached 100°C. As well, Barton et. al. (23) reported that asyptotic behaviour occurred at measured wall temperatures above 100°C. This leads to a possibility that the water contained in the pores of the fouled deposit comes in contact with the wall, gets converted into steam continuously and escapes outwardly i.e. away from the tube wall. The deposition of the phosphate salt on the heat exchanger surface occurs after a set of cation(s) and anion(s) combine and nucleate at a particular spot. This subcooled boiling would either assist in removal processes already taking place or tend to reduce transport to the surface and hence reduce the net rate of fouling. It may however be noted that in the case where the heat transfer flux is not constant, the falling surface temperature or the decreasing species concentration can also give rise to a falling rate or even asymptotic behavior. Table 5-4 categorises the different fouling curves obtained and the data suggest that asymptotic behavior may occur when the calculated outside temperature exceeds about 90°C. Further experimentation with a measured wall temperature is essential to confirm this hypothesis.

5.6 Effect of the pH on the Initial Fouling Rate

The pH determines the ionic distribution of the different phosphate and calcium species as described in section 2.6, and since these species participate in the fouling process, it significantly influences the fouling process. As seen in Figures 5-12 and 5-13, the effect of pH on the initial fouling rate is very pronounced at both velocities. On plotting the initial fouling rate versus the pH on a log linear scale, as shown in Figures 5-14 and 5-15, a linear relationship is obtained for both velocities which suggests that, keeping everything else constant:

TABLE 5-4 SHAPES OF THE EXPERIMENTAL FOULING CURVES

Run	Type of Fouling Behavior	Remarks
2	Falling Rate	At the end, T_{wo} = 64°C
3	Falling Rate	At the end, T_{wo} = 82°C
4	Asymptotic	At t = 80 h, T_{wo} = 84°C
5	Falling Rate	At the end, T_{wo} = 63°C
6	Linear	At the end, T_{wo} = 61°C
7	Linear	At the end, T_{wo} = 39°C
8	Falling Rate	At the end, T_{wo} = 65°C
9	Falling Rate	At the end, T_{wo} = 69°C
10	Asymptotic	At t = 7 h, T_{wo} = 97°C
11	Negligible	At the end T_{wo} = 105°C
12	Negligible	At the end T_{wo} = 66°C
13	Negligible	At the end T_{wo} = 49°C
14	Negligible	At the end T_{wo} = 47°C
15	Negligible	At the end T_{wo} = 36°C
16	Asymptotic	At t = 20 h, T_{wo} = 92°C
17	Asymptotic	At t = 20 h, T_{wo} = 78°C
18	Negligible	At the end T_{wo} = 76°C
19	Negligible	At the end T_{wo} = 50°C
20	Asyptotic	At t = 20 h, T_{wo} = 105°C
21	Falling Rate	At the end T_{wo} = 81°C
22	Falling Rate	At the end T_{wo} = 78°C
23	Asymptotic	At t = 15 h, T_{wo} = 96°C
24	Asymptotic	At t = 15 h, T_{wo} = 81°C
25	Falling Rate	At the end, T_{wo} = 64°C
26	Falling Rate	At the end, T_{wo} = 81°C
27	Asymptotic	At t = 15 h, T_{wo} = 86°C
28	Falling Rate	At the end, T_{wo} = 80°C
29	Asymptotic	At t = 10 h, T_{wo} = 83 °C
30	Negligible	At the end, T_{wo} = 73°C
31	Negligible	At the end, T_{wo} = 71°C
32	Asymptotic	At t = 12 h, T_{wo} = 97 °C
33	Asymptotic	At t = 10 h, T_{wo} = 93 °C

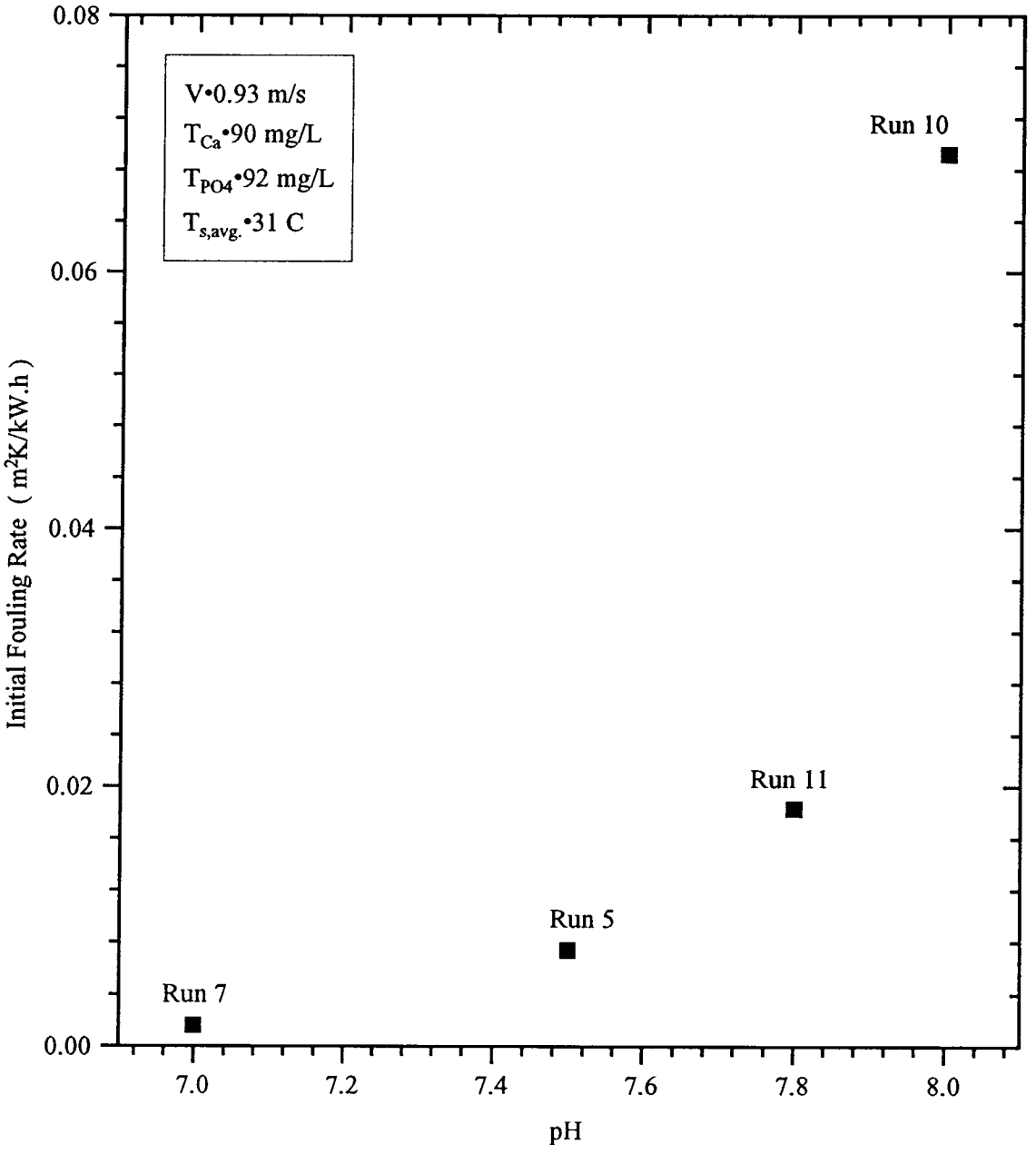

FIGURE 5-12 pH VERSUS INITIAL FOULING RATE AT HIGH VELOCITY

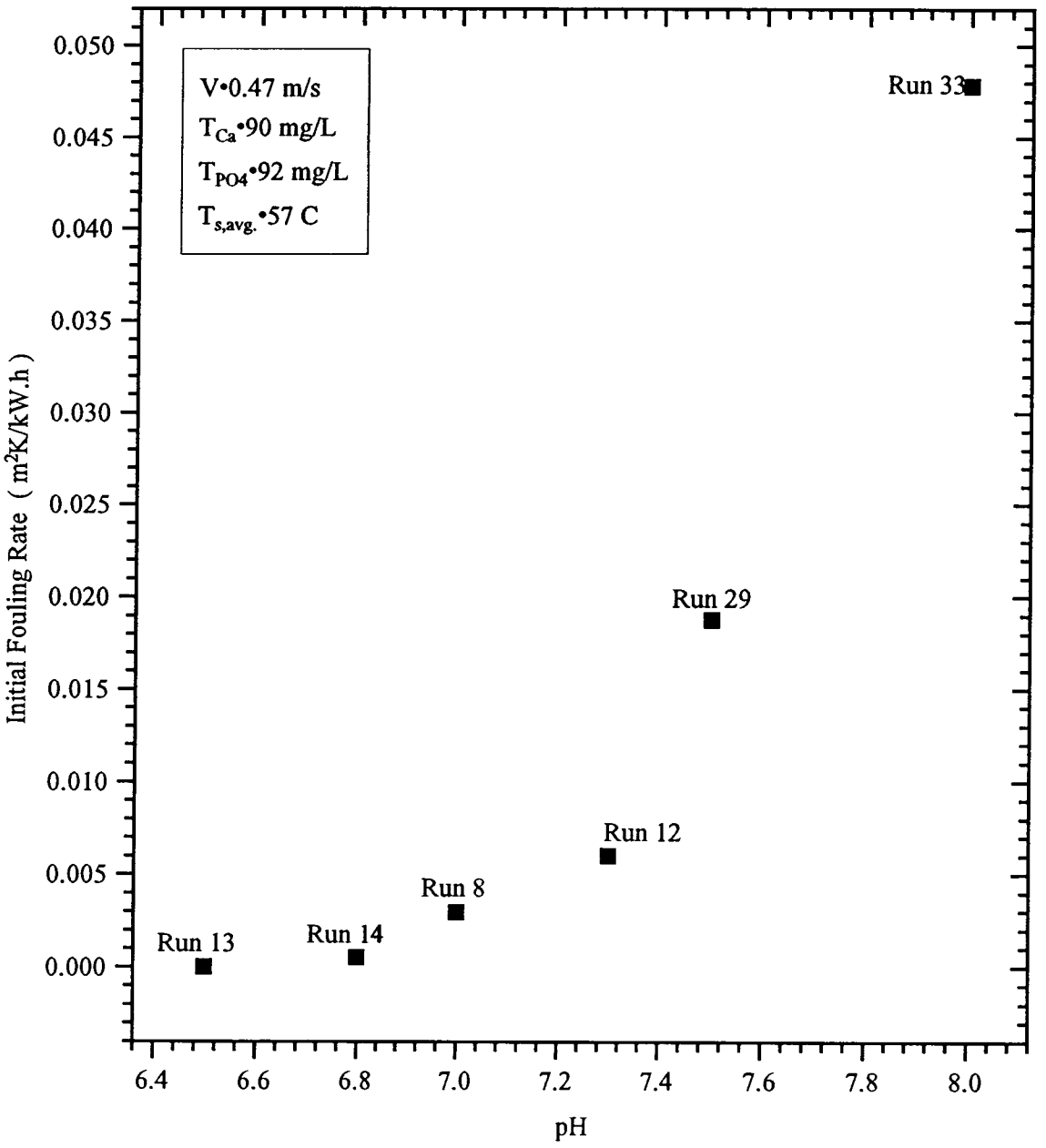

FIGURE 5-13 pH VERSUS INITIAL FOULING RATE AT LOW VELOCITY

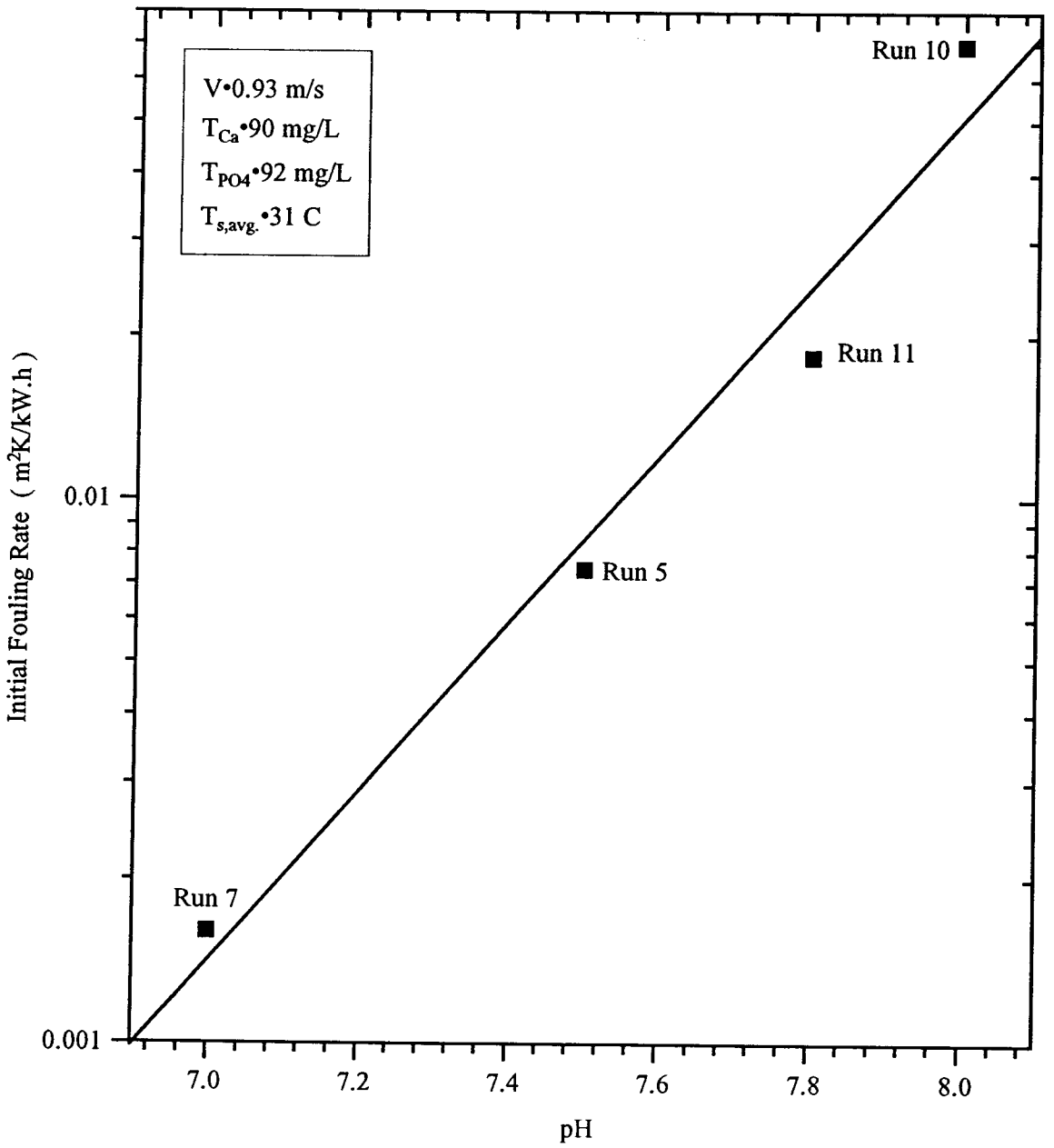

FIGURE 5-14 pH VERSUS LOG OF INITIAL FOULING RATE AT HIGH VELOCITY

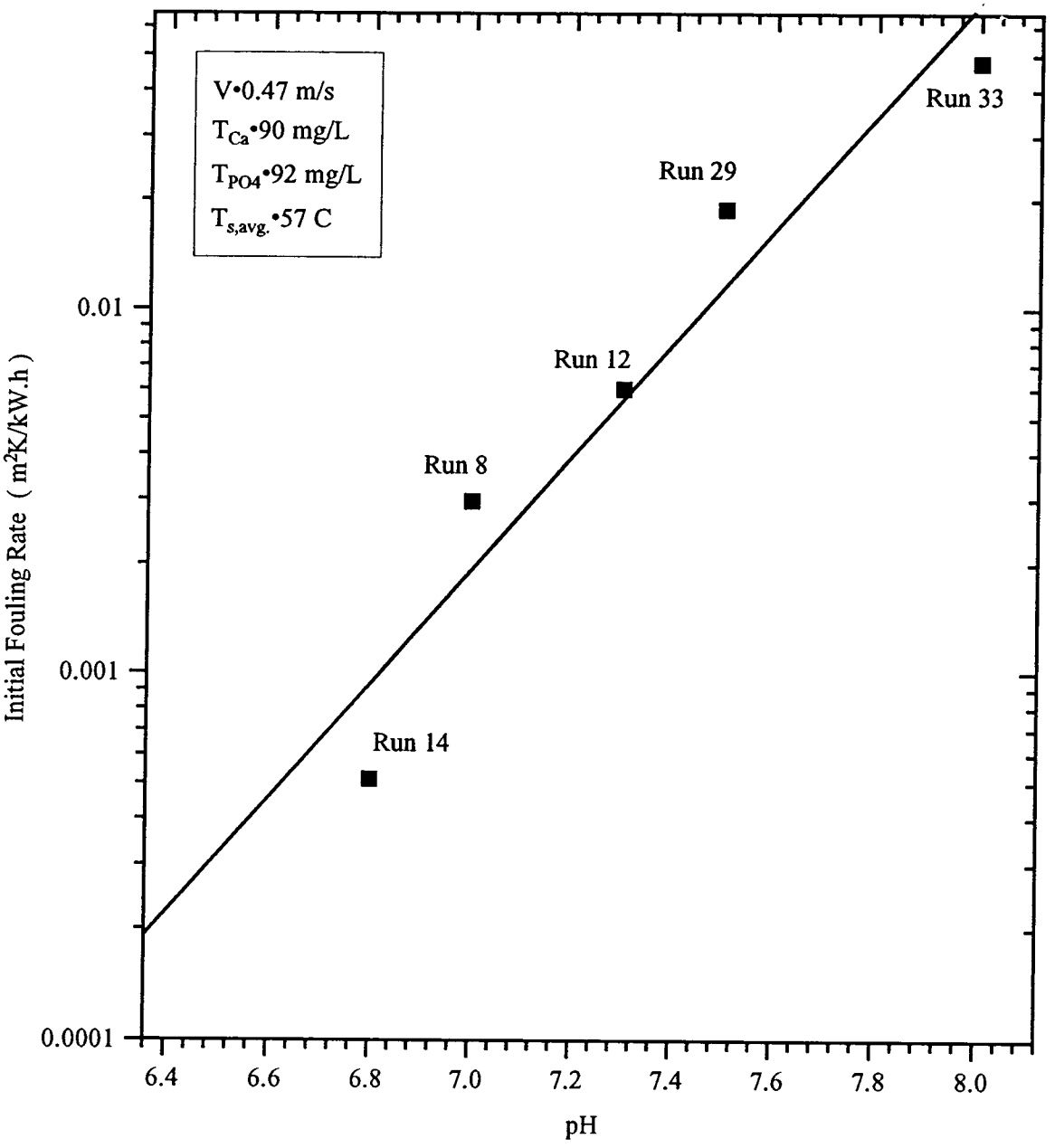

FIGURE 5-15 pH VERSUS LOG OF INITIAL FOULING RATE AT LOW VELOCITY

Log_{10} { Initial Fouling Rate } = a.pH + b

where a and b are constants. It follows from above that:

Initial Fouling Rate $\propto$ $(OH^-)^a$

At v = 0.47 m/s a = 1.562, while at v = 0.93 m/s a = 1.557.

Such a drastic effect of pH on the fouling rate has also been observed by other authors (3,4,9). In the power station condensers using water containing dissolved orthophosphate of the order of about 10 ppm where the fouling process occurs in relatively much longer time periods, a pH reduction of about 1 unit resulted in variation of the rate of fouling by about an order of magnitude. Figures 5-14 and 5-15 show increases in rate of a factor of 16 and 43 respectively as pH increases from 7 to 8.

This similarly strong effect of pH on the fouling rate at low concentrations of phosphate and calcium of about 10 ppm and 100 ppm, respectively (i.e. practical situations), and at relatively higher concentrations in the present case indicates that pH plays a most critical role in the fouling phenomena.

As mentioned in section 2-6, pH affects the distribution of ionic species and also the concentration of hydroxyl ions. It can be seen from Figure 2-3 that at a fixed total phosphate content increasing pH increases the concentration of both PO_4^{3-} and OH^- ions drastically, while the concentration of HPO_4^{2-} does not change much from pH 7 to 8. The strong effect of pH in

this range indicates that either OH^- or PO_4^{3-} or both are playing an important role in the fouling process. Figure 5-21 shows the data on pH effect (total phosphate content fixed) expressed as fouling rate versus calculated PO_4^{3-} concentration. The linearity of plot indicates strongly that it is the PO_4^{3-} ion concentration which dictates the fouling rate, and hence the deposit should contain TCP, OCP or HAP rather than DCPD.

5.7 Effect of the Velocity on the Initial Fouling Rate

The velocity has an effect on both deposition and removal processes and hence its effect on the net fouling rate (or the measured fouling rate) is somewhat complicated. Runs were carried out at three different annular velocities of 0.19, 0.47 and 0.93 m/s. The average bulk and film Reynolds numbers were calculated at the average bulk and average film temperatures, respectively, and covered the range of about 3,500 to 20,000 and 7,000 to 30,000 respectively.

The variation of the initial fouling rate with velocity is shown in the Figure 5-16. At pH 8.0 and 7.5, a consistent rise in the initial fouling rate with the velocity is observed. This suggests that in the range of velocity tested transport processes are important in determining initial fouling rates. However, more data are needed at higher velocities to assess the effect of the velocity on the fouling process. In a similar study done by Knudsen (9) at higher velocities in the range of 0.9 -2.44 m/s, it was found that the fouling rate over the first 100 to 200 hours decreased with increases in the velocity. Since at infinite velocity, the deposition would be prevented and at very low velocities the fouling resistance is non-zero, the velocity vs. fouling

rate curve should have a maximum point at some velocity, say v_{max}. Below this velocity, the fouling rate should increase with the velocity and above that, the opposing trend should be followed. It should be noted that the initial rates of the present work extend to significant R_f values, and hence are not restricted to the events involved in the initiation of fouling (Figure 5-9).

The effect of the velocity on the fouling rate can be explained as follows. At a particular scale-water interface temperature and composition of the water, the rate of fouling is the net difference between the deposition and the removal process. In a simplified approach, where surface integration is neglected, the deposition term is directly proportional to the mass transfer coefficient k_D, which is almost directly proportional to the velocity. The removal processes are functions of shear stress, which is proportional to the square of the velocity. If the removal process is also assumed to be independent of the thickness of the deposit, the fouling rate as function of velocity alone can be expressed by the following simplified expression:

$$f(v) = k_1 v - k_2 v^2 \tag{5-3}$$

where k_1 and k_2 are constants that depend on the water chemistry and the deposit characteristics, respectively. On differentiating the above expression, the velocity at which the fouling is maximum can be derived as follows:

$$v_{max} = \frac{k_1}{2k_2} \tag{5-4}$$

It can be easily noted that the velocity at which the fouling becomes zero is exactly twice

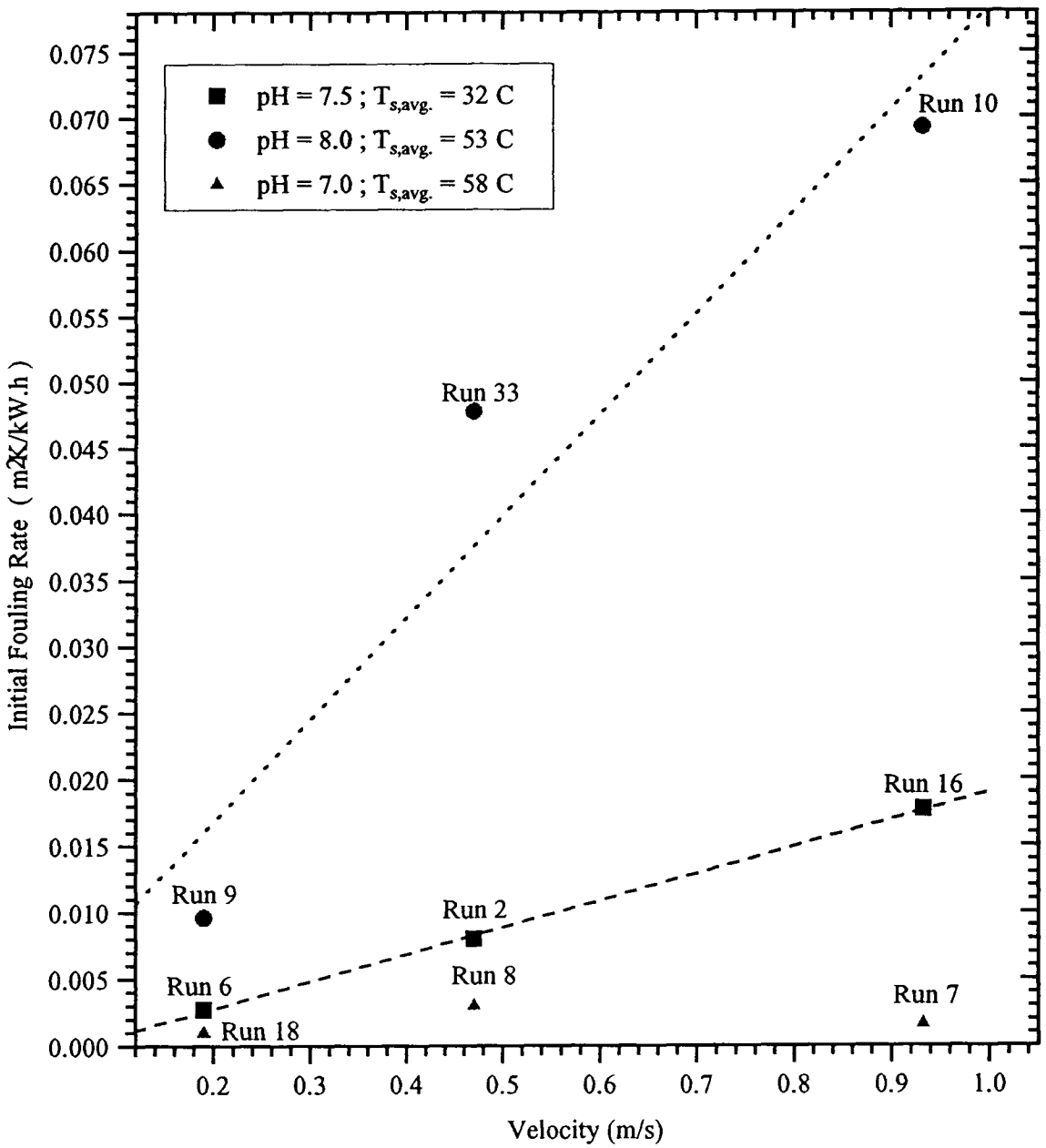

FIGURE 5-16 VELOCITY VERSUS INITIAL FOULING RATE

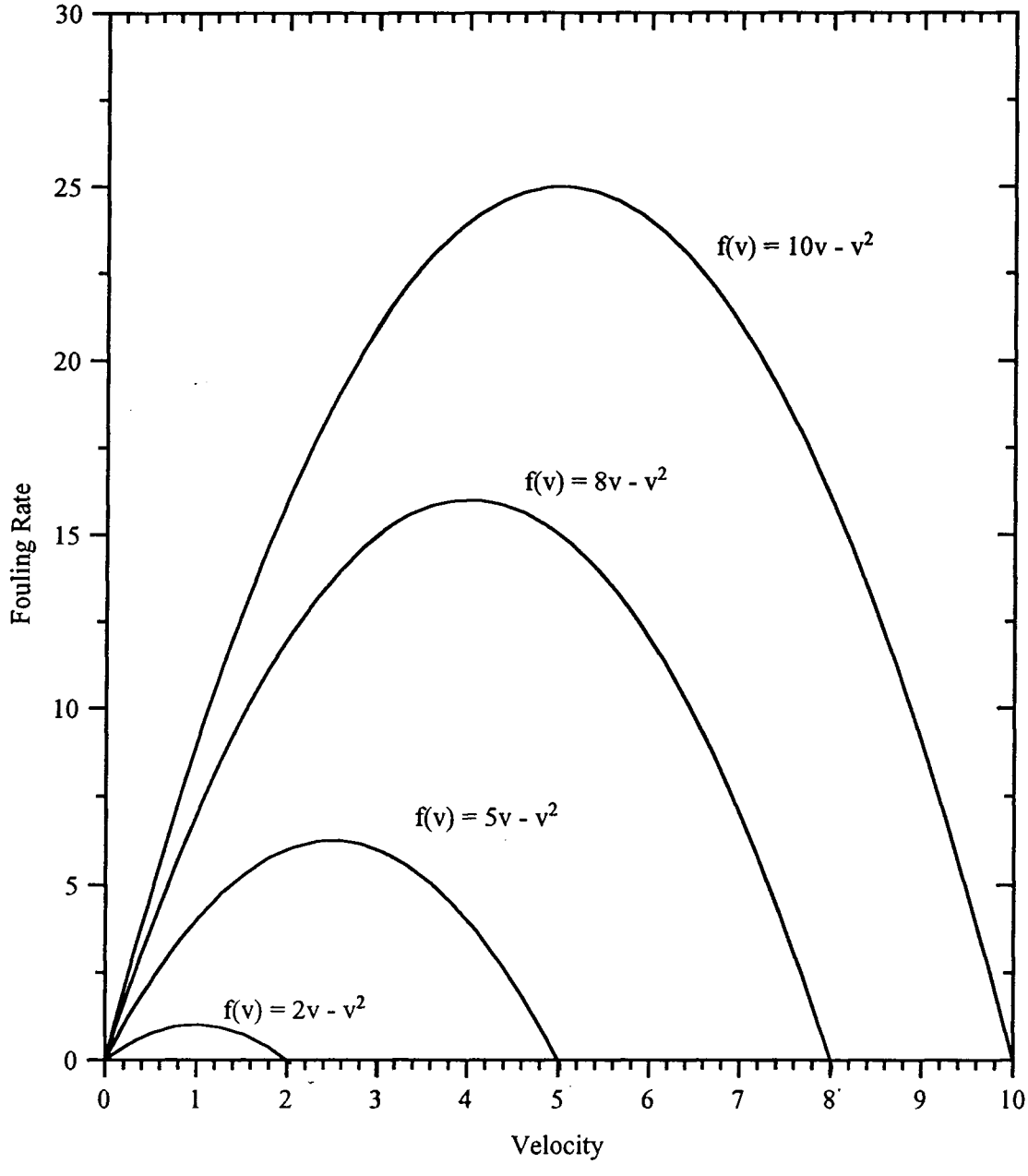

FIGURE 5-17 QUALITATIVE PRESENTATION OF THE VARIATION OF FOULING RATE WITH VELOCITY

v_{max}. It can be concluded that if the deposition term is much greater than the removal term or the ratio of k_1 to k_2 is very large, v_{max} will increase with k_1/k_2 and the rate will increase with respect to the velocity. This is true of diffusion-controlled deposition where the deposits loosely adhere to the heat transfer surface. In the case where the ratio is not very large, i.e. the deposition term is not much greater than the removal term, the fouling rate may decrease with increasing velocity. This is shown qualitatively in Figure 5-17 by considering four arbitrary cases in which the removal term is the same, but the deposition term varies. An arguement can also be made that in the absence of removal processes, and where both mass transfer and surface integration affect the deposition process, that the initial fouling rate may either increase or decrease with velocity.

5.8 Effect of the Surface Temperature on the Initial Fouling Rate

The surface temperatures were calculated on the basis of the one-dimensional steady state heat conduction equation. Since a fairly good agreement between the calculated and the experimental clean overall heat transfer coefficient was found (Appendix II), the calculated surface temperatures were regarded as a good representation of the actual surface temperatures. If the fouling phenomena was purely diffusion controlled in the ranges of variables studied, the surface temperature would have little effect on the deposition rate. The surface temperature effects the fouling process mainly in the following two ways:

1) It affects the crystallization rate constant which is often found to follow an Arrhenius

type relationship.

2) It affects the properties of the fluid in contact with the heat transfer surface, namely viscosity, thermal conductivity, specific heat and density of the fluid and hence affects the convective mass transfer coefficient.

The effect of the surface temperature on the initial rate of fouling can be seen from Figure 5-18, where $\ln(\dot{R}_{fi})$ is plotted against T^{-1}. A near linear relationship is obtained. The slope of the straight line obtained by applying a linear regression is 4139. The activation energy of the precipitation reaction occurring on the solid-fluid interface calculated from the value of the slope is 8.2 kcal/mol, which is between the values of 10.5 kcal/mol and 4.5 kcal/mol for the precipitation of DCPD reported by Nancollas (21).

From Tables 5-2 and 5-7, comparing Runs 3 and 20, it can be seen that increasing surface temperature from 38°C to 87°C increases the calculated diffusive mass transfer coefficient k_D by about 11% only, but the measured initial fouling rate increases by about 6 times, which indicates that the surface reaction rather than mass transfer effectively controls the fouling process in this range of temperature.

5.9 Effect of Concentrations of Species on the Initial Fouling Rate

Since the potentially scale forming species i.e. calcium and orthophosphate ions have to diffuse from the bulk fluid and then react at the heat transfer surface, their bulk concentrations

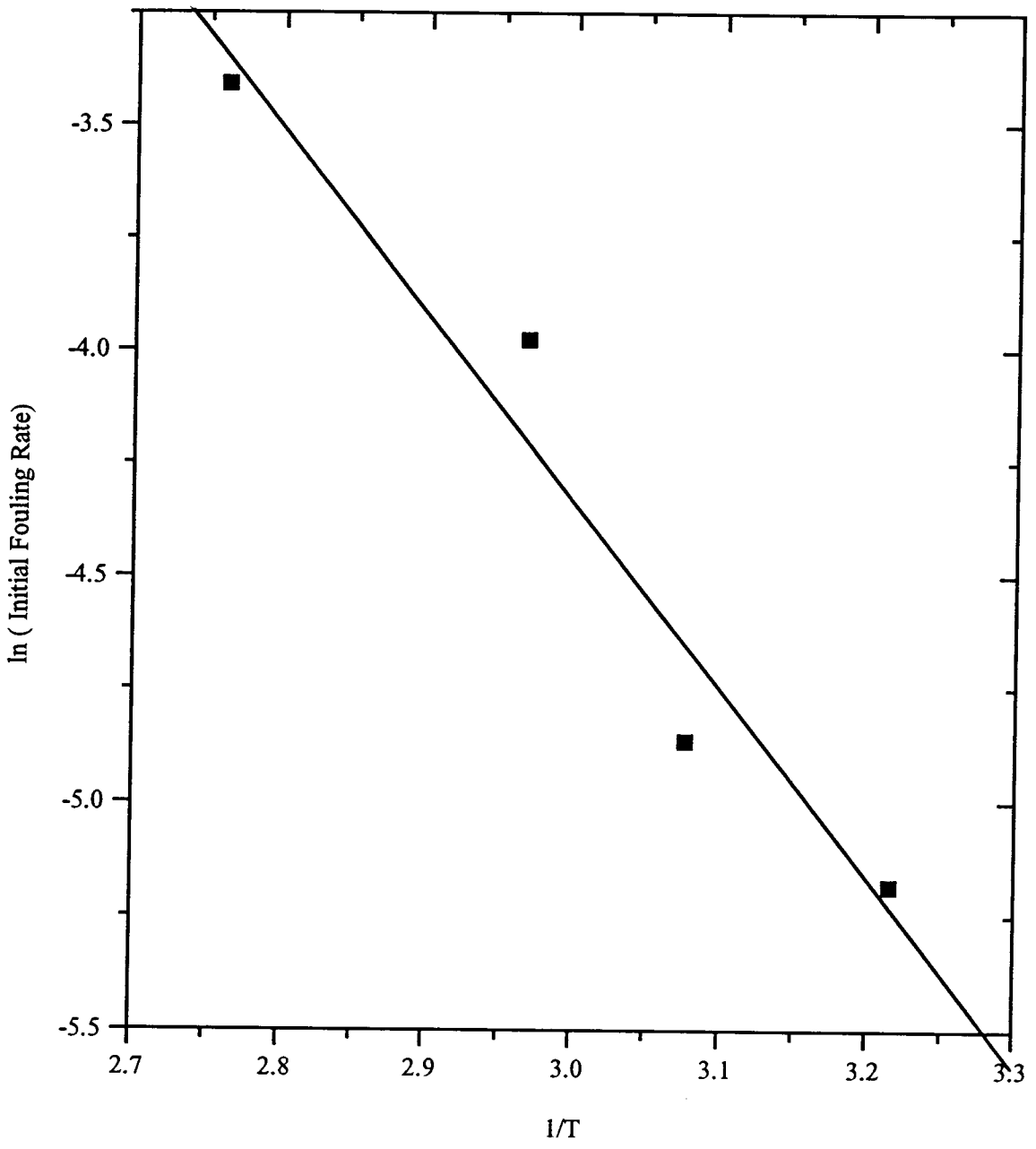

FIGURE 5-18 ARRHENIUS PLOT OF INITIAL FOULING RATE WITH ABSOLUTE TEMPERATURE

have a direct bearing on the rate of fouling. This is evident in Figure 5-19 and 5-20, where the initial rate of fouling is plotted against the concentrations of the total phosphate and calcium ions at fixed pH. It can be noted that increasing the calcium concentration increased the initial fouling rate in a near linear relationship. However, increasing the total phosphate concentration appeared to increase the initial fouling rate more markedly. A log-log plot of initial fouling rate versus phosphate concentration yielded a straight line with a slope of about 2.6. Hence, it was concluded that keeping all other variables constant:

$$\dot{R}_{fi} \propto T_{Ca} T_{PO4}^{2.6} \tag{5-5}$$

It is interesting to note that Ferguson et. al (31) in their study to model the kinetics of calcium phosphate precipitation at various concentration levels of carbonate, formulated the following expression from purely empirical observations:

$$\frac{dC_{PO4}}{d\theta} = (-\frac{4.1}{C_{T,CO3}}) C_{PO4}^{2.7} \tag{5-6}$$

where C's denote the concentrations in millimol/L and θ is in hours. The tests were done at slightly alkaline pH as in the present study. The kinetic exponent 2.7 indicated a strong sensitivity of the reaction rate to the phosphate concentration.

5-10 Characteristics of the Deposit

After a run was completed, the equipment was shut down and the water drained. The deposit, if it appeared very sticky, was 'baked' for a few minutes before pulling the tube out.

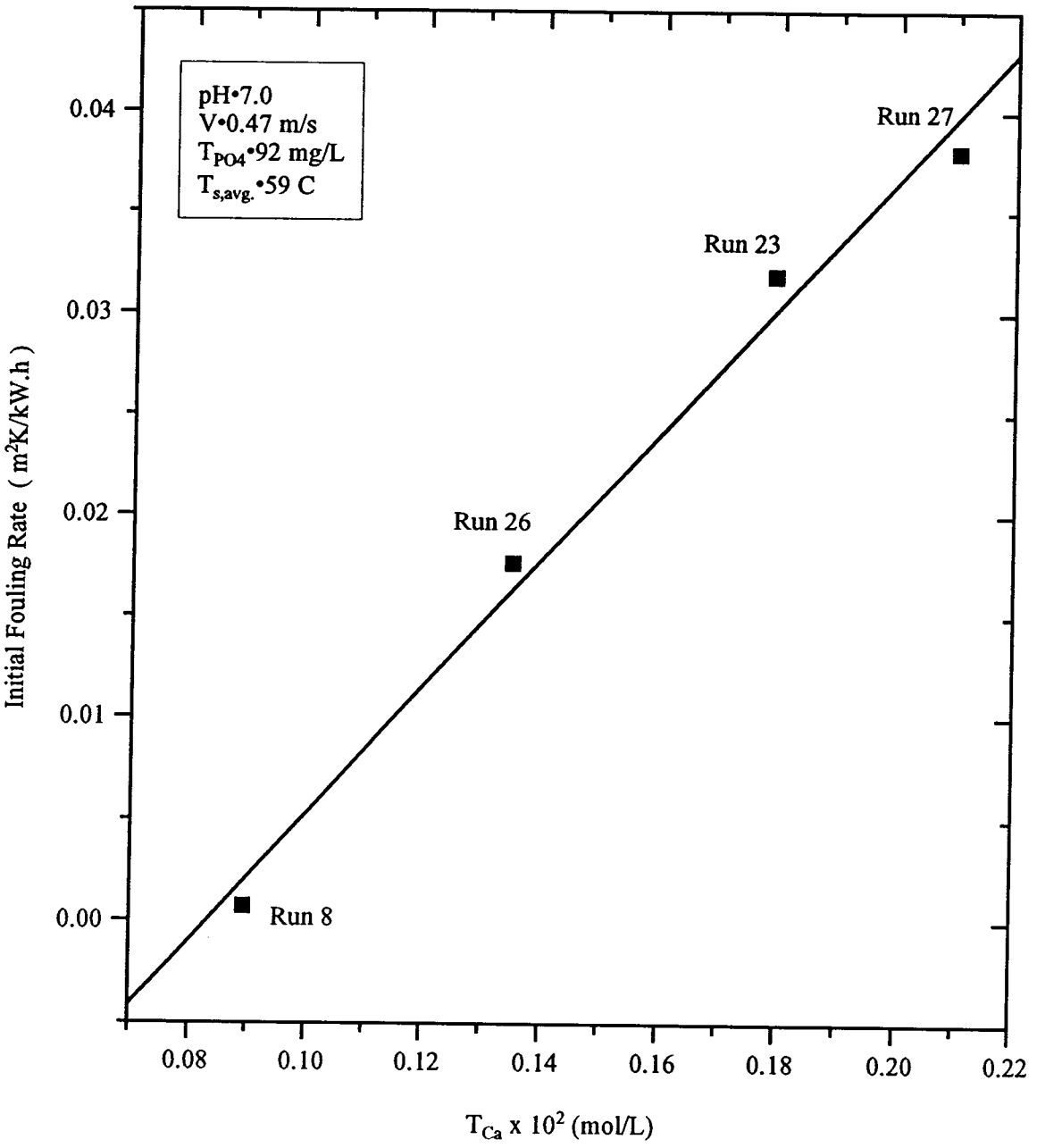

FIGURE 5-19 VARIATION OF FOULING RATE WITH TOTAL CALCIUM

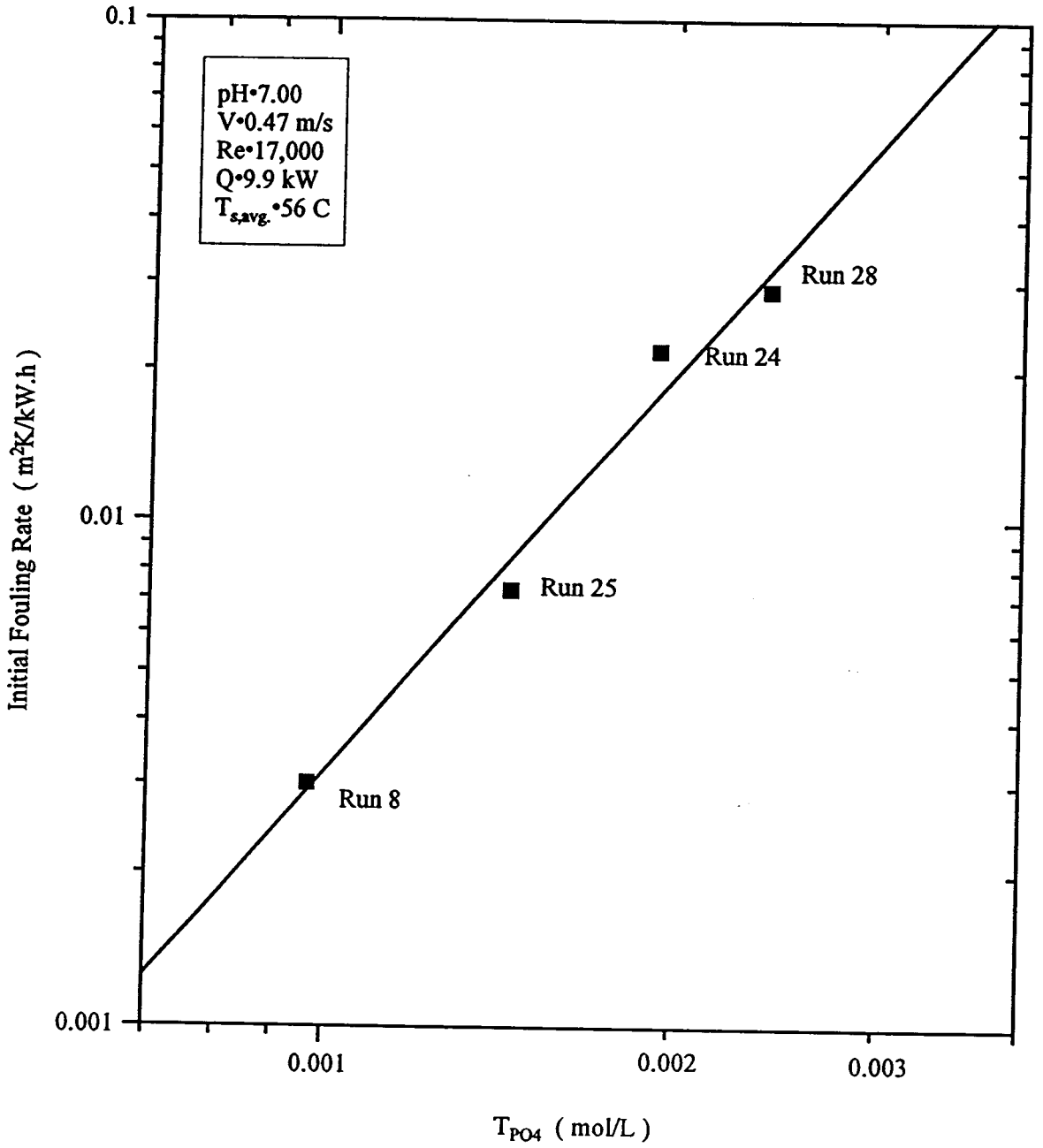

FIGURE 5-20 VARIATION OF INITIAL FOULING RATE WITH TOTAL PHOSPHATE CONCENTRATION

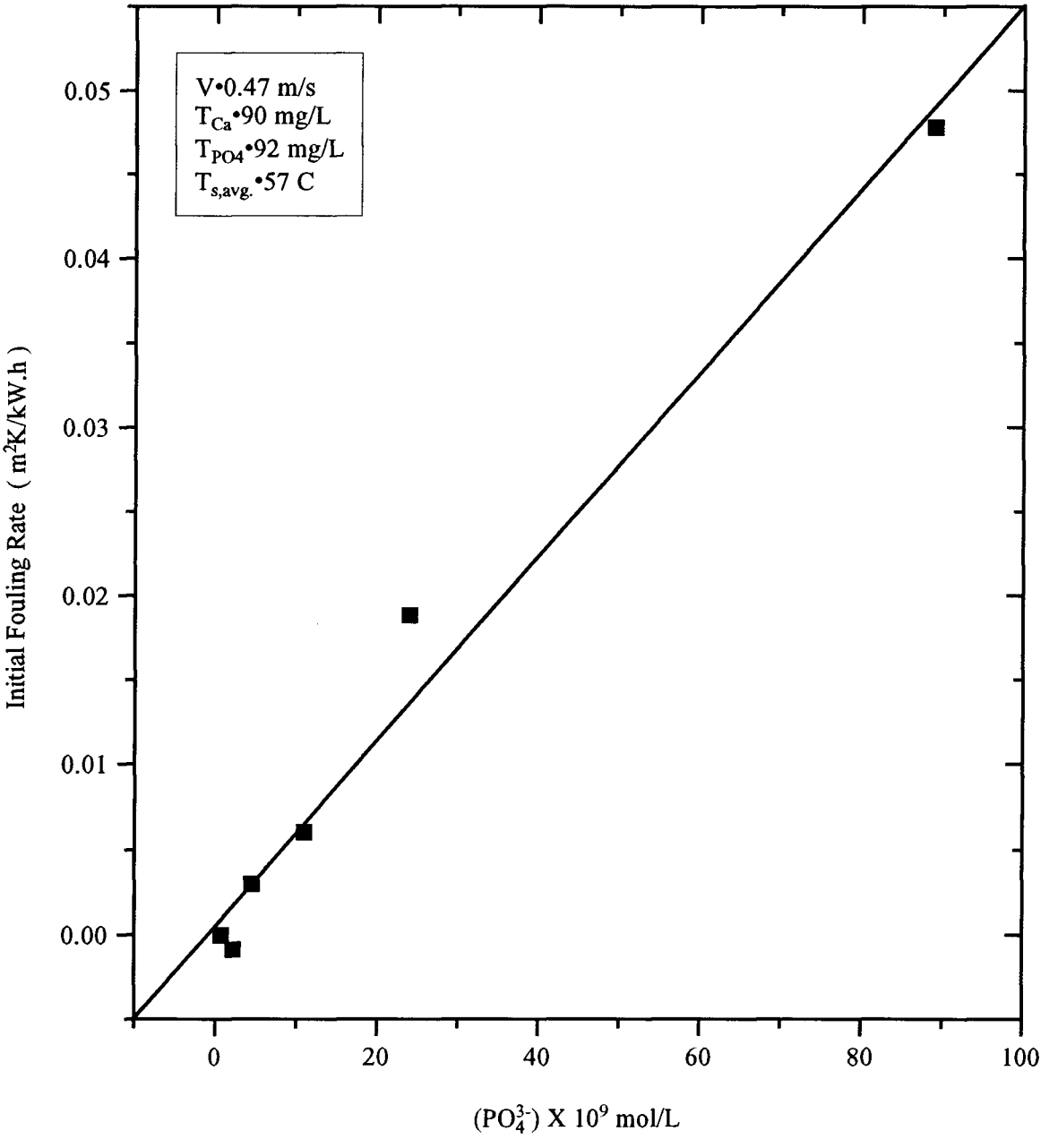

FIGURE 5-21 EFFECT OF CALCULATED (PO_4^{3-}) CONTENT ON INITIAL FOULING RATE AT pH 6.5 TO 8.0

It was observed that the thickness of the scale increased with the distance from the water entrance. The deposits were, in most cases, cream colored, hard and brittle. They were porous and compressible, and generally had very weak adhesion with the surface of the tube. Deposits could be easily scraped off with a spatula, leaving little spots of residue behind on the tube. In other cases, however, the deposits were wet, sticky and tightly adherent to the wall of the tube.

The deposits were sent to an external laboratory for the determination of the chemical composition. The ICP analysis gave results that are shown in Table 5-5. The samples were finally powdered, homogenised and dissolved in a solvent before analysis. It can be seen that the Ca/P molar ratio varies considerably from one sample to the other. However, the reproducibility of this method is poor, as is evident from the analysis for Run 5, where the Ca/P ratio is 11% higher in the original analysis than in the repeat.

Comparing Tables 5-5 and 5-6 suggests the following:

1) DCPD is not the only phase precipitating in any of the runs listed in Table 5-5.
2) A number of phases may be precipitating simultaneously giving rise to molar Ca/P ratios that are different from the Ca/P ratios for DCPD, OCP or ACP, the precursors to the formation of HAP.
3) The transformation of the initially precipitated phases to the final phase (HAP) has not taken place, since the Ca/P ratio is less than 1.66.

The deposit analysis is consistent with the interpretation of pH effects through Figure

TABLE 5-5 ICP ANALYSIS OF THE DEPOSIT SAMPLES

Sample	% Ca (by mass)	% P (by mass)	Mass ratio of Ca to P	Molar Ratio of Ca to P
Run 2	31.78	20.29	1.566	1.214
Run 2R	31.85	19.54	1.630	1.263
Run 5 (repeat)	32.29	19.39	1.665	1.291
Run 3	32.52	18.88	1.722	1.335
Run 4	33.98	19.03	1.786	1.384
Run 5	33.54	18.50	1.810	1.404
Run 6	34.03	18.70	1.820	1.410
Run 7	33.64	18.30	1.840	1.425
Run 1A	25.17	13.12	1.920	1.487
Run 4A	33.92	18.50	1.830	1.421
Run 5A	34.05	18.45	1.850	1.430

TABLE 5-6 Ca/P MOLAR RATIOS FOR VARIOUS CALCIUM PHOSPHATES

Name	Chemical Formula	Ca/P Molar Ratio
dicalcium phosphate dihydrate	$CaHPO_4.2H_2O$	1.00
anhydrous dicalcium phosphate	$CaHPO_4$	1.00
octacalcium phosphate	$Ca_8H_2(PO_4)_6.5H_2O$	1.33
tricalcium phosphate	$Ca_3(PO_4)_2$	1.50
hydroxyapatite	$Ca_5(PO_4)_3(H)$	1.67

5-21, which indicated the key importance of PO_4^{3-} concentration.

5.11 Comparison with Previous Studies

Knudsen et. al (9) carried out experimental work to determine the effect of adding corrosion inhibitors to cooling water. They also studied the effects of pH, velocity, surface temperature and the material of the heating surface on the fouling rate. The conditions of their experiments were as follows:

pH = 6.5 - 7.0

Velocity = 0.91 - 2.44 m/s

T_s = 328 - 344 K = 55 - 71 °C

T_{Ca} = 650 ppm as $CaCO_3$

T_{PO4} = 5 ppm as PO_4

The fouling rates obtained were of the order of about 10^{-4} m^2K/kWh. The fouling rates obtained in the present work were of the order of 10^{-1} - 10^{-3} m^2K/kWh. This can be explained by the fact that higher pH and phosphate concentrations were used in the present work. However, it is interesting to note that the trends in the variations of the fouling rates are to some extent similar. An increase in the surface temperature led to an increase in the fouling rate. The effect of the pH on the fouling rate was also remarkable, with fouling increasing drastically with a change in the pH of 0.5 units. In contrast to the present work, an increase in the velocity resulted in a decrease in the initial fouling rates presumably due to higher velocities used in their

work. All three types of fouling behavior i.e. linear, falling rate and asymptotic were observed in both studies. No firm conclusions on the fouling mechanisms were given regarding these trends.

Barton et al (23) carried out experiments with a double pipe heat exchanger at a fixed pH of 5.6 -5.7 , so that only dicalcium phosphate dihydrate (DCPD) was precipitated. Their experimental conditions were as follows:

T_{Ca} = 250 ppm as $CaCO_3$

T_{PO4} = 1900 ppm as PO_4

Re = 10,000 - 5,500

Q/A = 5.2 - 5.9 W/cm^2

Their deposition rates varied between 0.7 and 7.0 $mol/cm^2.s$. The fouling rates were of the order of about 0.06 $m^2K/kW.h$, which is similar in magnitude to a few of the runs in the present work. The fouling rate became zero after the metal-scale interface temperature had exceeded 100 °C, while the solution was still supersaturated with respect to DCPD. No further increase in the fouling resistance could be observed even after the addition of reactants and increases in the surface temperature. No explanation was offered for this. This observation, which is supported by similar observations in the present work, suggests the possibility of the steam participating in the removal processes. A rigorous mathematical model was proposed by them to predict the fouling rates. Under the very limited range of conditions (pH= 5.6-5.7, T_s= 80°C, Re = 5500-10,000) tested, it was concluded that both mass transfer and

heterogenous reaction kinetics controlled the deposition process. The drawbacks of their research are as follows:

1) Their experimental measurements of the deposition rates were highly irreproducible and varied by as much as a factor of 10.
2) The density and thermal conductivity values were not specified.
3) The value of the reaction rate constant was arbitrarily obtained by adjustment so that the observed deposition rate equalled the calculated deposition rate.
4) The model does not account for the deposition kinetics of other phases of the calcium phosphates as is commonly observed in normal practice.

Little comparison of this study with the present work is possible.

Parry et al (3) studied the problem of phosphate scaling in power station condensers. The circulating water analysis was as follows:

T_{Ca} = 400 ppm as $CaCO_3$

T_{PO4} = 9 ppm as PO_4

pH = 8.4

The high pH was found to be the major factor responsible for the high rate of the fouling. On reducing the pH to about 7.00 - 7.5, a 97% - 99% reduction in the scaling extent was observed. The rate of scaling was also found strongly dependent on the pH and the surface temperature of the condenser tubes. These observations are both supported by the present study. In a related work (4), Humphris mentioned that considerable fouling occurred in similar

condensers at a pH of 7.2 and phosphate concentration of 16 ppm as PO_4.

5.12 Calculation of the Rate of Fouling if Limited by Diffusion

It is possible to make a rough estimate of the maximum possible rate of fouling assuming that it is a purely diffusion controlled process. The molar rate of the mass transfer, M_A, in such a case is given by:

$$\dot{M}_A = k_D(C_{Ab} - C_{Ai}) \tag{5-7}$$

where C_{Ab} and C_{Ai} are the bulk and interfacial concentrations of limiting reactant A and k_D is the diffusive mass transfer coefficient. The value of k_D can be calculated using the following expression (30):

$$k_D = 0.027 v Re^{-0.17} Sc^{-0.667} \tag{5-8}$$

where the fluid properties are evaluated at the average conditions between the phase surface and the bulk fluid, i.e. at the film temperature.

The maximum rate will occur if $C_{Ai} \ll C_{Ab}$ and can be neglected. Hence, it follows from equation (5-7) that:

$$\dot{w} \approx k_D C_{Ab} m_A \tag{5-9}$$

where m_A is the molecular weight of the species precipitating.

The maximum rate of fouling can be calculated using equation (2-22) as:

$$(\frac{dR_f}{d\theta})_{max} \approx \frac{k_D C_{Ab} m_A}{\rho_f k_f} \qquad (5\text{-}10)$$

The average values of density and thermal conductivity used in the above equation were obtained from this work (Tables II-2 and II-3) as 1470 kg/m^3 and 1.039 W/m.K respectively.

Phosphate will be the limiting reactant irrespective of whether one of DCPD, OCP, ACP or HAP precipitates. One mole of phosphorus yields one mole of DCPD, two moles of phosphorus yield one mole of ACP, 3 moles of phosphorus yield one mole of OCP and HAP each, or 1 mole of phosphorus yields 136 g, 155 g (approx.), 164 g, 167 g of DCPD, ACP, OCP and HAP respectively. Since these numbers are quite close to each other, it can be said that one mole of phosphorus will yield approximately 156 g (average of the above numbers) of the deposit.

Table 5-7 shows the calculated values of the fouling rates if limited by the diffusion. The calculated values are somewhat uncertain because of variations in scale density and thermal conductivity measurements (Appendix II). The use of average values of scale density (1470 kg/m^3) and thermal conductivity (1.039 W/mK) might be a contributing factor for the experimental rates to exceed the calculated values. In five runs the calculated transport limited rate exceeds the measured rate by a factor of 3 or more. This would indicate that chemical reaction limits the rate in some cases. The fact that the experimental rates are within $\pm$50% of the transport limited calculated rates in ten runs suggests that the transport effects will be significant. Given the uncertainities involved the evidence from these calculations suggests that

TABLE 5-7 CALCULATION OF FOULING RATES IF NOT LIMITED BY SURFACE REACTION

Run	k_D (x 10^4 m/s)	T_{PO4} (x10^5 mol/L)	$(dR_f/dt)_{Calc}$	$(dR_f/dt)_{exp}$	Ratio
2	0.314	97	0.011	0.0077	1.43
3	0.303	97	0.0107	0.0053	2.02
4	0.305	97	0.0108	0.0058	1.86
5	0.521	97	0.0188	0.0074	2.5
6	0.153	97	0.0054	0.0027	2.0
7	0.551	97	0.0195	0.0016	12.2
8	0.322	97	0.011	0.0030	3.6
9	0.156	97	0.0057	0.0096	0.59
10	0.534	97	0.0189	0.0692	0.27
11	0.529	97	0.0188	0.0183	1.03
12	0.324	97	0.0115	0.0060	1.91
13	0.313	97	0.011	-5.6E-5	Not defined
14	0.314	97	0.011	-.0009	Not defined
16	0.550	97	0.0195	0.0177	1.1
17	0.524	97	0.0186	0.0231	0.81
18	0.158	97	0.0056	0.001	5.6
19	0.314	97	0.011	-.0008	-
20	0.350	97	0.0124	0.033	0.38
21	0.310	97	0.011	.0120	9.2
22	0.310	96	0.011	.0168	0.65
23	0.310	108	0.0123	0.032	0.38
24	0.310	193	0.022	0.0237	0.93
25	0.310	145	0.0165	0.009	1.83
26	0.310	97	0.011	0.0198	0.56
27	0.310	97	0.028	0.04	0.70
28	0.310	242	0.011	0.028	0.39
29	0.327	108	0.01145	0.0188	0.59
30	0.323	108	0.0118	0.0027	4.24
31	0.333	108	0.0120	0.0007	16.85
32	0.339	108	0.0116	0.0307	0.39
33	0.328	108	0.0124	0.0478	0.23

a mixed control situation exists where both transport and crystallization reaction influence the fouling rate.

5-13 Correlation for the Prediction of the Fouling Rates

All the variables studied can be correlated by observing from Figures (5-13) to (5-20) that:

$$\dot{R}_{fi} \propto T_{Ca} T_{PO4}^{2.6} v e^{-\frac{4139}{T_s}} (OH^-)^{1.45} \qquad (5\text{-}11)$$

in the following range of variables:

0.9×10^{-3} mol/L $< T_{Ca} < 2.1 \times 10^{-3}$ mol/L

10^{-3} mol/L $< T_{PO4} < 2.5 \times 10^{-3}$ mol/L

0.2 m/s $< v <$ 1.0 m/s

$6.5 <$ pH < 8.0

30°C $< T_s <$ 75°C

Thus by plotting $\dot{R}_{fi}$ versus the R.H.S. of the above equation and applying a linear regression, an empirical value of the proportionality constant, K_p, can be obtained. This value of K_p is used to predict the initial fouling rates for various Runs. From Figure 5-22, the value of the proportionality constant is obtained as 2.39×10^{28}. Figure 5-23 shows a plot of predicted versus experimental fouling rates. A linear regression is applied to this plot, the slope of the straight line is 1.03, indicating that this simplified correlation may be useful in predicting the

initial fouling rates over the range 0.002 to 0.07 $m^2K/kW.h$. Table 5-8 compares the values of experimental and predicted initial fouling rates.

The empirical correlation is given in terms of the velocity and the measured or readily calculated water quality parameters i.e. total phosphate, calcium hardness and hydroxyl ion concentration available from the pH measurement. A more fundamental relation could perhaps be found based on Figure 5-21, however for application one would have to solve the ionic equilibrium equations for PO_4^{3-}.

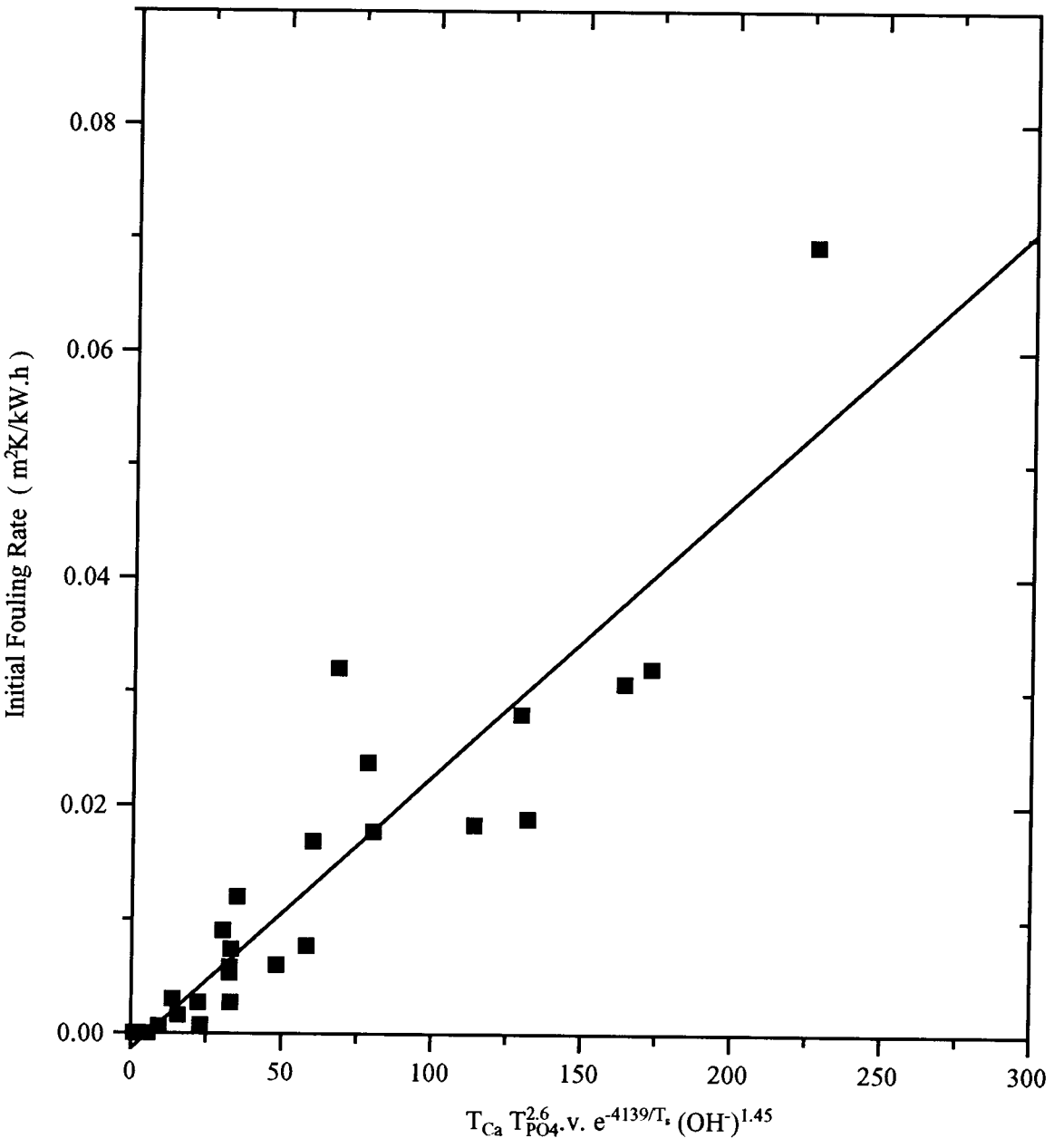

FIGURE 5-22 PLOT OF INITIAL FOULING RATE VS.$T_{Ca}\ T_{PO4}^{2.6}.v.e^{-4139/T_s}(OH)^{-1.45}$

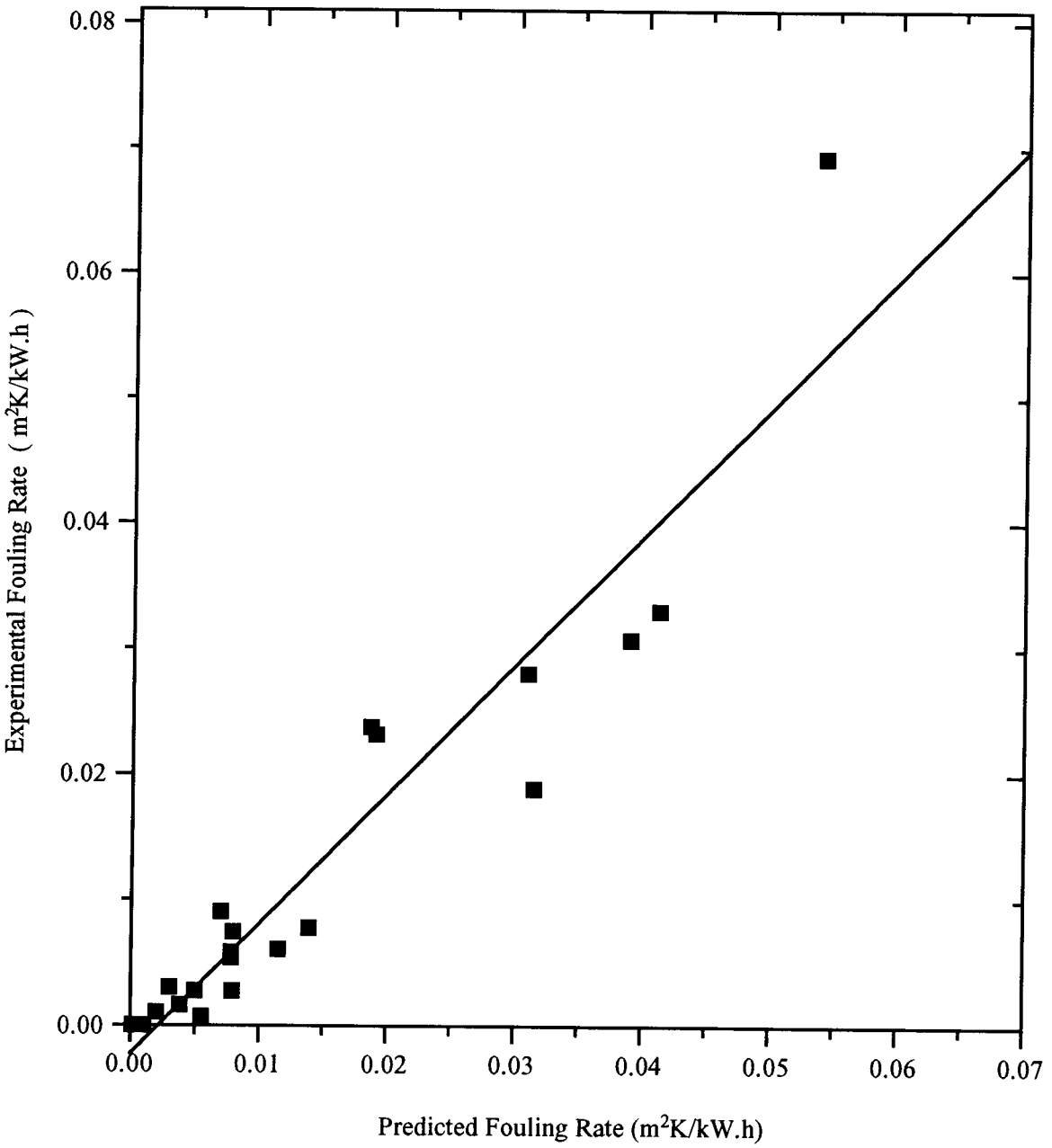

FIGURE 5-23 PREDICTED VERSUS EXPERIMENTAL INITIAL FOULING RATE

TABLE 5-8 EXPERIMENTAL AND PREDICTED INITIAL FOULING RATES

Run	Experimental $\dot{R}_{fi}$	$T_{Ca}\ T_{PO4}^{2.6} v\ \exp(-4139/T_a)(OH^-)^{1.45}$	Predicted $\dot{R}_{fi}$
2	0.0077	58.18	0.0139
3	0.0053	32.79	0.0078
4	0.0058	58.18	0.0078
5	0.0074	33.04	0.00796
6	0.0027	33.10	0.0079
7	0.0016	15.84	0.0038
8	0.0030	13.91	0.003
9	0.0026	240.76	0.058
10	0.0692	226.7	0.054
11	0.0183	113.92	0.027
12	0.0060	48.3	0.0115
13	-5.6 E-5	1.83	4E-4
14	-0.0009	0.85	2E-4
16	0.0177	80.09	0.019
17	0.0231	30.05	0.007
18	0.00127	9.4	0.002
19	-0.0008	5.64	0.001
20	0.033	172.7	0.0413
21	0.0120	54.0	0.0129
22	0.0168	58.0	0.0139
23	0.032	68.0	0.016
24	0.0237	78.18	0.0187
25	0.009	30.46	0.007
26	0.0198	20.08	0.048
27	0.03	31.02	0.007
28	0.028	129.25	0.0031
29	0.0188	131.87	0.003151
30	0.0027	22.40	0.005
31	0.0007	23.10	0.0055
32	0.0307	163.85	0.039
33	0.0478	446.7	0.1067

§ 6. CONCLUSIONS AND RECOMMENDATIONS

8.1 Conclusions

The fouling of heat exchanger surfaces in the presence of calcium and orthophosphate ions was studied. The fouling process was found to be a strong function of pH, as has been observed in similar studies (3,4,9). At a fixed total phosphate content, this data could be expressed either as a linear increase in rate with the calculated PO_4^{3-} content, or a power law dependence on OH^-. Surface temperature also had a noticeable effect on the initial rates of fouling, which indicated that surface reaction processes were also participating in determining the overall fouling rate. The temperature dependence was consistent with the crystallisation kinetics literature. Increases in the velocity increased the initial fouling rate in a linear fashion. The concentration of phosphate and calcium species also affected fouling considerably. The phosphate effect was non-linear. In conclusion, the overall rate of fouling was found to be mass-transfer and surface reaction controlled in the region of variables tested.

In the absence of accurate kinetic expressions being available and the structure and composition of the deposit not known completely, an empirical model has been presented which correlates all the variables studied in the present work. This model predicts with a reasonable degree of accuracy the initial fouling rates, which vary by a factor of about 100 in the range of variables studied. The slope and intercept of the straight line obtained by applying a linear regression to the predicted versus experimental initial fouling rate data are 1.03001 ± 0.08153

and -0.00225, respectively. The coefficient of regression is 94.27%, indicating a significant degree of correlation between the experimental and predicted fouling rates. The clean overall heat transfer coefficient was found to be a linear function of the heat transfer rate over the range of heat transfer rates studied. The variations in the heat transfer rates due to fouling did not make much impact on the overall clean heat transfer coefficient in most cases.

All three types of fouling behavior i.e. linear, falling rate and asymptotic were obtained. In the cases where the fouling became asymptotic, it was found that the calculated surface temperatures were high and approached 90-100°C. A hypothesis has been proposed linking the net fouling rate to the generation of steam at the metal-scale interface. This would have to be checked in a modified test section in which wall temperatures could be measured directly. Pressure drop results are discussed in Appendix II-6.

The physical and chemical properties of the deposits as well as the adhesion to the tube varied from run to run. Measured scale densities varied from 1118.9 to 1775.4 kg/m^3. A rough value of deposit thermal conductivity of 1.039 W/mK was estimated from thickness and fouling resistance measurements at the end of a number of runs. The Ca/P ratio varied over the range 1.214 to 1.487, which suggested that more than one species was precipitating. Analysis suggests that the final conversion to HAP had not taken place.

8.2 Recommendations

Several modifications were carried out to improve the original set-up. However, the present apparatus and procedures should be modified in order to yield more information about the fouling process. The following modifications in the equipment are required to generate experimental data of practical importance:

1) The storage capacity of the supply tanks should be increased so that monitoring the water chemistry is not needed. At present, the monitoring of water chemistry is very time consuming and it makes specifying the concentrations of species difficult for a particular run.
2) Thermocouples should be installed to measure the wall temperature. This will help in specifying the surface temperature more realistically. The surface temperature is a very important parameter affecting almost all types of fouling and should be measured accurately.
3) A bigger pump should be installed so that an annular velocity of greater than 1 m/s is obtained.
4) The present rotameter should be replaced with one capable of measuring higher flow rates.
5) Automatic control systems to measure and control the water bulk, inlet and outlet (to the heat exchanger) temperatures should be installed to keep the heat flux constant throughout a run. The present set up needs 24-hr manual supervision.
6) A high temperature cut-off system should be installed on the steam line to protect the

equipment against the following emergencies:

a) Excessive leakage causing major water loss

b) Accidental shut off / surging of the pump motor

c) Accidental closure / failure of the cooling water

Presently the equipment is protected against power failure only. Steam supply is cut off as soon as the power fails and doesn't resume automatically when the power comes back.

7) A flow control valve should be installed on the recirculating water discharge line because the online filter gets plugged resulting in a decreased flow.

8) The entire piping system should be replaced with a new one to avoid leaks that are a perpetual problem in the present equipment.

On the operations side, the pH probe should be closely watched for a loss in performance and the thermocouples should be calibrated periodically on a regular basis.

Further work is needed in this relatively unexplored area of phosphate fouling. Future studies should aim at widening the understanding of the various aspects of phosphate fouling; characterising the deposit, studying its structure and physical properties. Runs should be done for longer durations to generate data regarding the occurrence of linear vs. asymptotic fouling. The role of velocity in the removal process should be analyzed more thoroughly by conducting experiments at higher velocities. The possibility of the steam acting as a "removal agent" in the cases where the outside wall temperature exceeds 100 °C should be further investigated, which

would lead to a better understanding of the removal process. And last but not least, analytical models should be developed in order to predict the fouling rates as a function of various variables.

§ 7. NOMENCLATURE

Notation	Description	Units
A	temperature dependent constant	
A_i	inside area of the tube	m^2
A_{lm}	logarithmic mean surface area	m^2
A_o	outside area of the tube	m^2
A_{fi}	outside area of the fouled layer	m^2
A_{fo}	outside area of the fouled layer	m^2
B_1	constant	
C_1-C_7	constants	
C_i	concentration of the species i	mol/L
C(0)	concentration of the calcium at time=0	mol/L
C_p	specific heat	kJ/kg.K
C_{pc}	specific heat of the water	kJ/kg.K
C_{ph}	specific heat of the steam	kJ/kg.K
D_e	equivalent diameter of the annular space	m
D_{fi}	inside diameter of the fouled layer	m
D_{fo}	outside diameter of the fouled layer	m
D_{si}	inside diameter of the shell	m
D_{ti}	inside diameter of the tube	m
D_{to}	outside diameter of the tube	m

D_{AB}	diffusivity	m^2/s
e	charge on an electron	F
f_i	friction factor of the inner surface of the annular space	
f_o	friction factor for the outer surface of the annular surface	
f_M	activity coefficient of the monovalent ion	
f_D	activity coefficient of the divalent ion	
f_T	activity coefficient of the trivalent ion	
F	volumetric flow rate	m^3/s
g	acceleration due to the gravity	m/s^2
G	a parameter defined by the equation ()	
h_{ci}	convective inside heat transfer coefficient	$kW/m^2.K$
h_{co}	convective outside heat transfer coefficient	$kW/m^2.K$
k	Boltzmann's constant	
k_c	thermal conductivity of the water	kW/m.K
k_D	diffusive mass transfer coefficient	m/s
k_h	thermal conductivity of the steam condensate	kW/m.K
k_f	thermal conductivity of the foulant	W/m.K
k_m	thermal conductivity of the metal wall	W/m.K
K_1	first dissociation constant of the phosphoric acid	
K_2	second dissociation constant of the phosphoric acid	
K_3	third dissociation constant of the phosphoric acid	
K_w	ionic product of the water	

K_4 - K_7	association constants for the reactions described by the equations (2-36) to (2-39)	
$\bar{K}_1$ - $\bar{K}_7$	equilibrium constants based on activities	
K_{sp1}	solubility product of DCPD	$(mol/L)^2$
K_{sp2}	solubility product of TCP	$(mol/L)^5$
K_{sp3}	solubility product of OCP	$(mol/L)^7$
K_{sp4}	solubility product of HAP	$(mol/L)^9$
l	distance between the manometer tappings on the heat exchanger	m
L	length of the heat exchanger in contact with the water	m
$\dot{m}$	gross rate of mass deposition	kg/s
m_A	molecular weight of species A	
m_c	mass flow rate of the cold fluid (water)	kg/s
$\dot{m}_r$	rate of mass removal	kg/s
$\dot{m}_{net}$	net rate of mass deposition	kg/s
M	a constant representing the mechanical strength of the deposit	
M_A	molar rate of mass transfer	mol/L
M_i	molality of the component i	mol/L
N	Avogadro's number	
P(0)	concentration of the phosphate at time=0	mol/L
P_o	total pressure (gravity and fluid) at the location z=0	N/m^2

P_L	total pressure (gravity and static) at the location z=L	N/m^2
Q	rate of heat transfer	kW
r	radial distance from the axis of the heat exchanger	m
r_{si}	inner radius of the shell	m
r_{ti}	inner radius of the tube	m
r_{to}	outer radius of the tube	m
R	rotameter setting	
Re_b	Reynolds number for the water bulk	
Re_i	Reynolds number at the inner surface of the annular space	
Re_o	Reynolds number at the outer surface of the annular space	
Re_s	Reynolds number for the steam condensate	
Re_f	Reynolds number for the film	
R_f	fouling resistance	$m^2.K/kW.h$
R_{fi}	inside fouling resistance	$m^2.K/kW.h$
R_{fo}	outside fouling resistance	$m^2.K/kW.h$
R_f^*	asymptotic fouling resistance	$m^2.K/kW.h$
R_m	thermal resistance of the metal wall	K/kW
R_f	thermal resistance of the fouled layer	K/kW
R_{fu}	uncorrected fouling resistance	$m^2.K/kW.h$
R_{fc}	corrected fouling resistance	$m^2.K/kW.h$
R_s	thermal resistance of the steam	K/kW
R_t , R_T	total thermal resistances	K/kW

R_w	water side thermal resistance	K/kW
s	slope of the Q vs. U_{oc} curve	
S	supersaturation potential	
T	absolute temperature	K
T_{Ca}	total calcium content of the solution	ppm as $CaCO_3$
T_{PO4}	total phosphate content of the solution	ppm as PO_4
T_c	temperature of the cold stream (water)	°C
T_{cb}	bulk temperature of the water stream	°C
T_{ci}	temperature of the incoming stream of the water	°C
T_{co}	temperature of the outgoing stream of the water	°C
T_h	temperature of the hot stream (steam)	°C
T_{hi}	temperature of the incoming stream of the steam	°C
T_{ho}	temperature of the outgoing stream of the steam	°C
T_{hb}	average bulk temperature of the steam	°C
T_s	scale water interface temperature	°C
T_{wo}	metal water interface temperature	°C
TWP	total wetted perimeter	m
U_o	overall heat transfer coefficient based on the outside area	$kW/m^2.K$
U_{oc}	clean overall heat transfer coefficient	$kW/m^2.K$
U_{od}	dirty (or fouled) overall heat transfer coefficient	$kW/m^2.K$
v	(average) velocity of the water stream	m/s
V	recirculating volume	

V_r	residual water left in the tanks	L
V_p	internal volume of the piping	cm^3
V_{sg}	internal volume of the specific gravity bottle	cm^3
V_{avg}	average volume drained out by the pump	L
$\dot{w}$	mass deposited per unit area per unit time	$kg/m^2.s$
wc	weight of calcium salt make-up	g
wp	weight of phosphate salt make-up	g
W_1	weight of the empty specific gravity bottle	g
W_2	weight of the empty specific gravity bottle + saturated water	g
W_3	weight of the empty specific gravity bottle + sample	g
W_4	weight of the empty specific gravity bottle + sample + saturated water	g
W_5	weight of the empty specific gravity bottle + pure water	g
W_F	rate of the condensation of the steam	
x_f	deposit thickness	mm
x_{favg}	average thickness of the deposit	mm
z	axial distance from the bottom of the heat exchanger	m
z_i	charge on the species i	
(i)	concentration of the species i	mol/L

Dimensionless Groups

Pr	Prandtl number, $C_p\mu/k$

Nu	Nusselt number, hD/k	
Re	Reynolds number, $\rho vD/\mu$	
Sc	Schmidt number, $\mu/\rho D_{AB}$	

Greek Letters	Description	
α_i	part of total phosphate present as species i	
β_i	degree of supersaturation	
Γ	rate of weight condensation of the steam per unit inside perimeter of the tube	kg/m.s
ϵ	dielectric constant	
Δ	difference between two values of a variable	
Δh	height differential of the manometer	cm
ΔT_{lm}	log mean temperature difference	°C
κ	ratio of the outer diameter of the tube and the inner diameter of the shell	
π	constant=3.1415....	
θ	time	h
θ_c	time constant	h
θ_d	delay time	h
λ	constant	
λ_s	heat of vaporisation (or condensation) of the steam	kJ/kg
μ	viscosity	$N.s/m^2$

μ_c	viscosity of the water	$N.s/m^2$
μ_h	viscosity of the steam condensate	$N.s/m^2$
ρ_c	density of the water	kg/m^3
ρ_h	density of the steam condensate	kg/m^3
ρ_f	density of fouled deposit	kg/m^3
ρ_m	density of the manometric fluid	$kg.m^3$
τ_{rz}	liquid shear stress at any location (r,z)	N/m^2

Subscripts	Description
d	dirty or fouled
avg	average
b	bulk
i	inside
in	incoming
o	outside
out	outgoing
m	metal
max	maximum

Abbreviations	Description
ACP	amorphous calcium phosphate

ADCP	anhydrous dicalcium phosphate
C	centigrade
DCPD	dicalcium phosphate dihydrate
DPHE	double pipe heat exchanger
g, mg	gram, milligram
h	hour
HP	horsepower
HAP	hydroxyapatite
HTRI	Heat Transfer Research Incorporated
ICP	Inductively Coupled Plasma
ID	inside diameter
kW	kilowatt
K	Kelvin
L, mL	liter, milliliter
m, cm, mm	meter, centimeter, millimeter, nanometer
M	molar
min	minute
OCP	octacalcium phosphate
OD	outside diameter
PVC	polyvinyl chloride
s	second
SS	stainless steel

TCP	tricalcium phosphate
TDS	total dissolved solids
TEMA	Tubular Exchangers Manufacturers Association
TWP	total wetted perimeter

§ 8. REFERENCES

1) Epstein, N.,"Fouling in Heat Exchangers". Proceedings of sixth International Heat Transfer Conference, Vol.6, p. 235-253, August 1978.

2) Hasson, D.,"Precipitation Fouling". Fouling of Heat Transfer Equipment, Somerscales, E. and Knudsen, J.G. (Editors), Hemisphere Publishing Corporation, p. 527-568, 1981.

3) Parry, D.J., Hawthorn, D. and Rantell, A.,"Fouling of Power Station Condensers within the Midlands Region of the C.E.G.B.". Fouling of Heat Transfer Equipment, Somerscales, E. and Knudsen, J.G., (Editors), Hemisphere Publishing Corporation, p. 569-585, 1981

4) Humphris, T.H.,"The Control of Phosphate Scaling in the Power Station Condensers", Central Engineering Research Laboratories, Fouling of Heat Transfer Equipment, Somerscales, E. and Knudsen, J.G. (Editors), Hemisphere Publishing Corporation, 1981

5) Strauss, S.D. and Puckorius, P.R.,"Cooling Water Treatment for control of Scaling, Fouling and Corrosion", Power, June 1984, p. S5-S24.

6) Chenoweth, J.M.,"Final Report of the HTRI/TEMA Joint Committee to review the Fouling Section of the TEMA Standards". Heat Transfer Engineering, Vol. 11, No. 1, p. 73-107, 1990

7) Thackery, P.A.,"The Cost of Fouling in Heat Exchangers Plant". Proceedings of the Conference "Fouling- Science or Art",Surrey, Guildford, England, March 27-28, 1979

8) Knudsen, J.G.,"Coping with Cooling Water Fouling in the Heat Exchangers", Heat Transfer Philadelphia 1989, A.I.Ch.E. Symposium Series 269, Volume 85, 1989

9) Knudsen, J.G., et. al.,"Fouling Characteristics of Cooling Tower Water Containing Phosphate Corrosion Inhibitors", Proceedings of the 1987 ASME-JSME Thermal Engineering Joint Conference, Honolulu, p. 109-115, 1987.

10) Kern, D.G. and Seaton, R.E.,"A theoretical Analysis of Thermal Surface Fouling". British Chemical Engineering, Vol. 4, p.258, May 1959

11) Kern, D.G. and Seaton R.E.," Surface Fouling.....How to Calculate Limits", Chemical Engineering Progress, Vol. 55, p. 71, June 1959

12) Varsanik, R.G.," The Nature and Control of Calcium Orthophosphate Deposition in

Cooling Water Systems", Materials Performance, December 1975, p. 16-22.

13) Davies, C.W.," Ion Association ", Butterworths, London, 1962

14) Nancollas, G.H.," Interactions in Electrolyte Solutions ", Elsevier, Amsterdam, 1966

15) Nancollas, G.H., Amzad, Z. and Koutsoukos, P.,"Calcium Phosphates - Speciation, Solubility and Kinetic Considerations", Chemical Modelling in Aqueous Systems, E.A. Jenne (Ed.) ACS Symposium Series, Vol. 93, 1979.

16) Butler, J.N.," Solubility and pH Calculations ", Addison-Wesley Publishing Company, Inc., Second Edition, 1973

17) Brown, W.E., Solubilities of Phosphates and Other Sparingly Compounds", Environmental Phosphorous Handbook, Griffith E.J., Beeton A., Spencer J.M., Mitchell D.T. (Eds.), John Wiley, N.Y.

18) Abbona, F.," Crystallization of Calcium and Magnesium Phosphates from Solutions of Low Concentrations ", Journal of Crystal Growth ", Vol. 104, 1990, p. 661-671

19) Cowan, J.C. and Weintritt, D.J.," Water Formed Scale Deposits ", Gulf Publications, Texas, 1976

20) Nancollas, G.H.," Kinetics of Crystal Growth from Solutions", Journal of Crystal Growth, Volume 3, No. 4, 1968, p. 335-339

21) Marshall, R.W. and Nancollas, G.H.," The Kinetics of Crystal Growth of Dicalcium Phosphate Dihydrate", The Journal of Physical Chemistry, Volume 73, No. 11, November 1969

22) Nancollas, G.H.," The Growth of Crystals in Solution", Advances in Colloid and Interface Science, Volume 10, 1979, p. 215-252

23) Barton, K.P., Chapman, T.W., and Lund, D.," Rate of Precipitation of Calcium Phosphate on Heated Surfaces", Biotechnology Progress, Volume 1, No.1, March 1985, p.39-45

24) "Standard Methods of Chemical Analysis", Welcher, F.J. (Ed.), D. Van Nostrand Corporation Inc., Princeton, N.J., Sixth Edition. Vol. No. 2, 1963, p. 2399

25) " Standard Methods for the Examination of Water and the Wastewater", Twelfth Edition, APHA, AWWA, WPCF, 1965.

26) Perry, R.H. and Green, D.," Perry's Chemical Engineer's Handbook ", Sixth Edition, Mc Graw Hill Publications, 1984

27) Wiegand, J.H.," Annular Heat Transfer Coefficient for the Turbulent Flow ", Transactions A.I.Ch.E., Vol. 41, 1945, p. 147

28) Bird, R.B., Stewart, W.E. and Lightfoot, W.E.," Transport Phenomena ", John Wiley and Sons, New York, 1960

29) Incropera, F.P. and Dewitt, D.P.,"Fundamentals of Heat and Mass Transfer", Second Edition, John Wiley and Sons, New York, 1985

30) Treybal, R.E.," Mass Transfer Operations", Third Edition, Mc Graw Hill Publications, 1980

31) Ferguson, J.F., Jenkins, D. and Eastman, J.," Calcium Phosphate Precipitation at Slightly Alkaline pH", WPCF Journal, Vol.45, No.4, April 1973

32) Sheikholeslami, R.," Tube Material and Augmented Surface Effects in Heat Exchanger Scaling", M.A.Sc. Thesis, 1984

APPENDIX I.

CALIBRATION CURVES

I.1 Calibration of the Rotameter

The calibration of the rotameter was done by measuring the time taken by the water to fill a 60-litre tank. The volumetric flow rates were obtained for the rotameter readings corresponding to 10, 20, 30, 50, 80 and 100 . The calibration procedure was repeated several times to ensure accuracy. A plot was then drawn and a linear regression was applied to fit a straight line through the points. The calibration curve is shown in Figure I-1.

I.2 Calibration Curve for the Phosphate Determination

A standard phosphate solution was prepared by dissolving 219.5 mg reagent grade Potassium Dihydrogen Phosphate in one litre distilled water. The solution is diluted to various extents. 35 mL of a solution is mixed with 10 mL of vandate-molybdate reagent and 5 mL of distilled water to give a final volume of 50 mL. After about 15 minutes, the absorbance was measured using a spectrophotometer at 470 nm wavelength and 1-cm optical path length. A linear regression was applied to yield a straight line shown in Figure I-2.

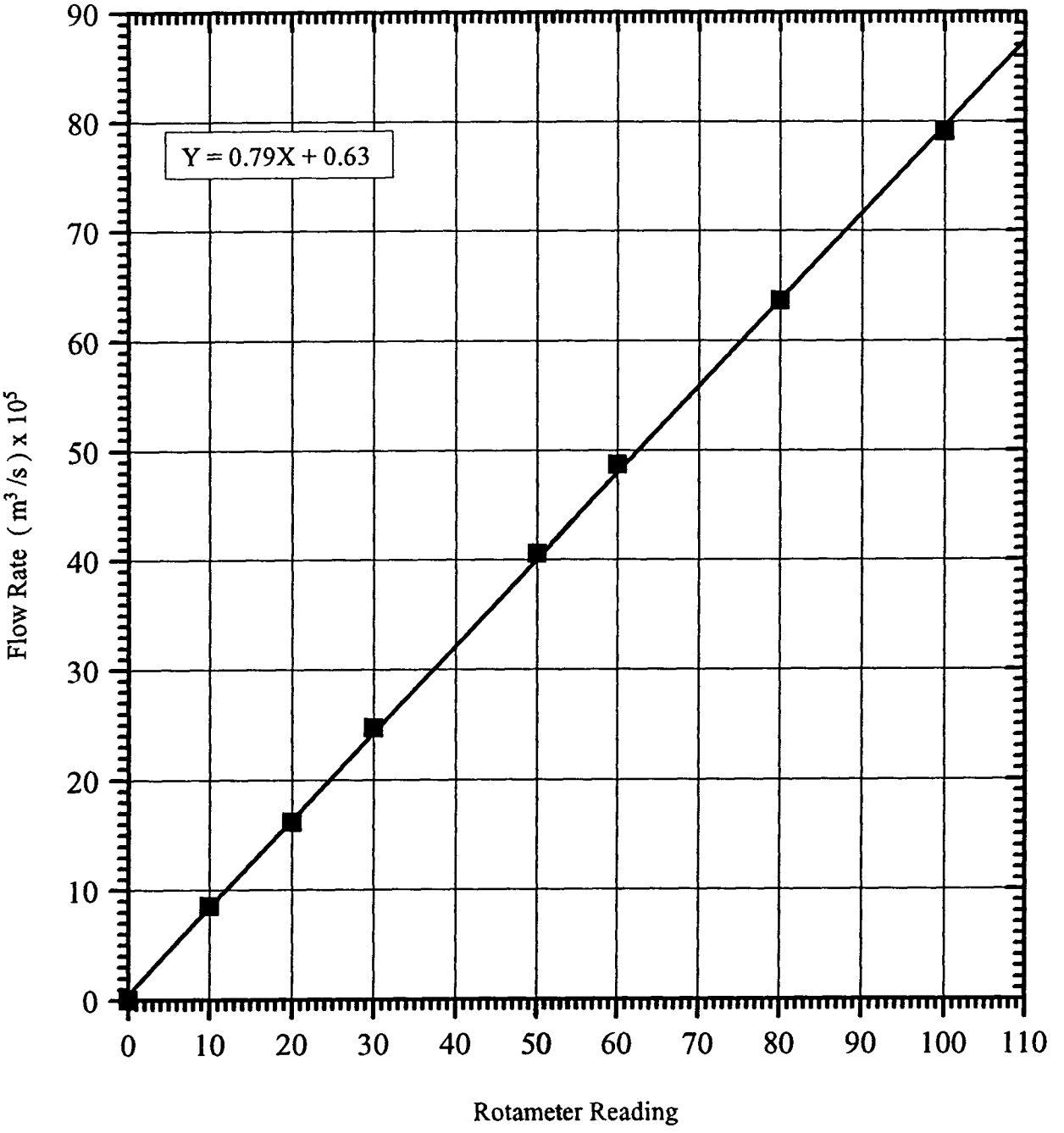

FIGURE I-1 ROTAMETER CALIBRATION CURVE

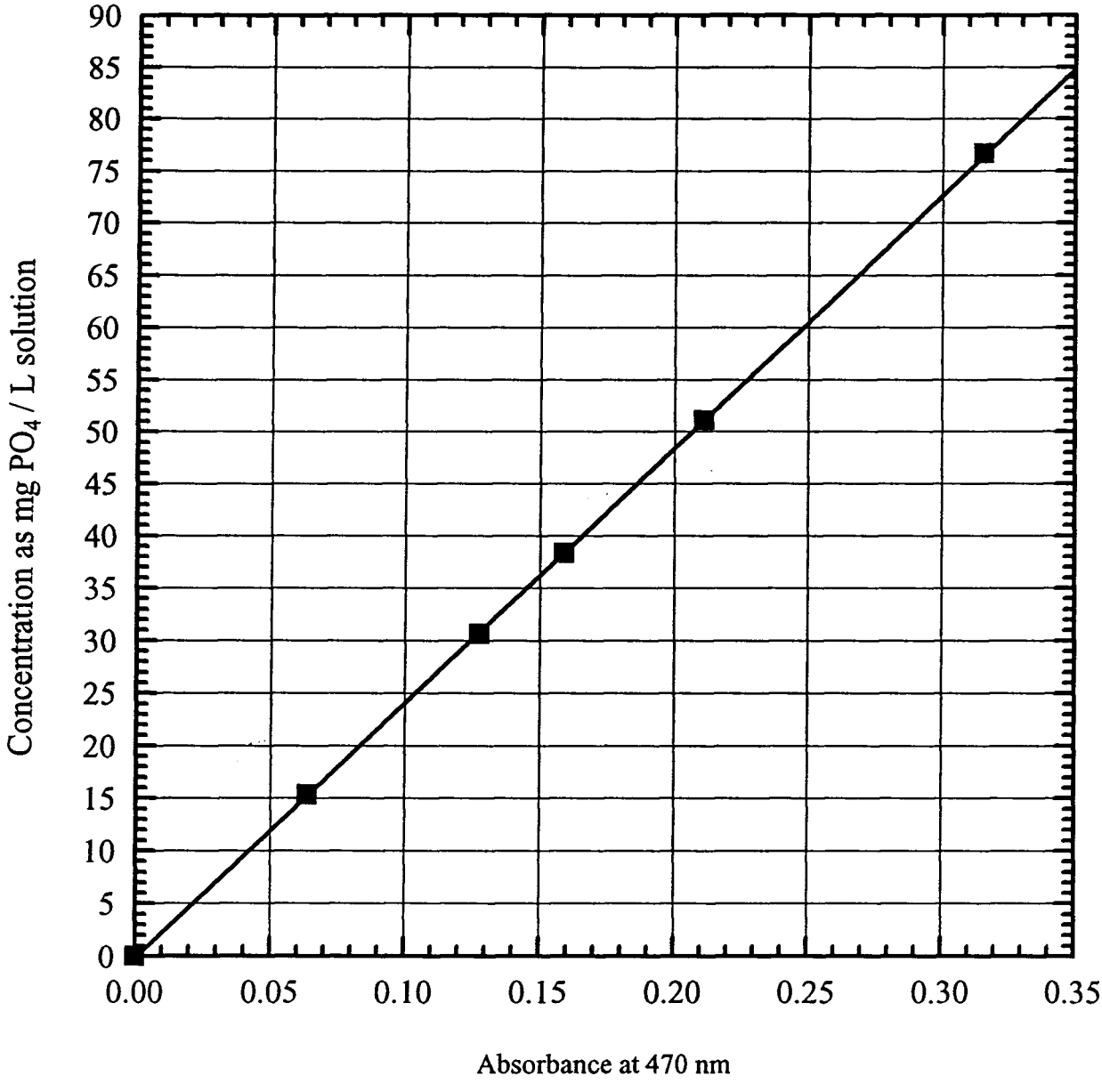

FIGURE I-2 CALIBRATION CURVE FOR THE MEASUREMENTS OF PHOSPHATE CONCENTRATION

APPENDIX II.

SAMPLE CALCULATIONS

II.1 Calculation of the Rate of the Heat Transfer

The rate of heat transfer at any instant of time was calculated using:

$$Q = \dot{m}_w C_p (\Delta T)_c \qquad \text{(II-1)}$$

where:

$\dot{m}_w$ = mass flow rate

C_{pc} = specific heat at the average bulk temperature of the water

ΔT_c = Rise in the temperature of the water

and $\dot{m}$ is related to the volumetric flow rate as follows:

$$\dot{m} = \rho \times F \qquad \text{(II-2)}$$

The datalogger was programmed to give the output temperatures for J-type thermocouples. The volumetric flow rate was determined by noting the rotameter reading and by using the calibration curve.

The density and specific heat of water at the bulk temperature were determined using the following relationships by applying a polynomial regression to the available literature data (29):

$$\rho \left(\frac{kg}{m^3}\right) = -0.3269\ T_{cb} + 1005.4 \qquad \text{(II-3)}$$

$$C_p \left(\frac{kJ}{kg°C}\right) = -0.000108\ T_{cb} + 4.1818 \qquad \text{(II-4)}$$

where T_{cb} is in degrees centigrade.

II.2 Determination of the Dirty Overall Heat Transfer Coefficient

The dirty overall heat transfer coefficient, based on the outside area of the inner tube of the DPHE was calculated as follows:

$$U_{od} = \frac{Q}{A_o \Delta T_{lm}} \qquad \text{(II-5)}$$

where A_o is given by:

$$A_o = \pi D_o L \qquad \text{(II-6)}$$

and the log mean temperature was calculated using:

$$\Delta T_{lm} = \frac{T_{co} - T_{ci}}{\ln \frac{T_{hb} - T_{co}}{T_{hb} - T_{ci}}} \qquad \text{(II-7)}$$

where T stands for temperature and subscripts c, h, i and o denote the cold, the hot, the incoming and the outgoing flows. The average of the inlet and outlet steam temperatures was used.

II.3 Determination of the Fouling Resistance

The fouling resistance as a function of time was calculated using:

$$R_f = \frac{1}{U_{od}} - \frac{1}{U_{oc}} \qquad \text{(II-8)}$$

where U_{od} is the dirty overall heat transfer coefficient at any instant of time.

II.4 Calculation of the Theoretical Overall Heat Transfer Coefficient

The overall heat transfer coefficient is determined by calculating individually the inside and outside heat transfer coefficients and the thermal resistance of the metal wall, using equation (2-3). A computer program, Figure III-1, is used to facilitate the calculations.

The following relationship is employed in calculating the outside heat transfer coefficient (27):

$$(Nu)_o = \frac{h_o D_e}{k_c} = (0.023)\, Re_c^{0.8}\, Pr^{0.4} \left(\frac{D_{so}}{D_{si}}\right) \qquad \text{(II-9)}$$

The physical properties of water are evaluated using the following expressions where T is in Kelvin (29):

$$\rho_c \left(\frac{kg}{m^3}\right) = \frac{1000.}{1.22961 - 0.0018T_c + 3.483\times10^{-6}T_c^2} \quad \text{(II-10)}$$

$$\mu_c \left(\times10^6 \frac{kg}{ms}\right) = 65816.344 - 418.2856T_c + 0.67255T_c^2 \quad \text{(II-11)}$$

$$k_c \left(\times10^6 \frac{kW}{mK}\right) = -278.316 + 4.4628T_c - 0.00499T_c^2 \quad \text{(II-12)}$$

$$Pr_c = 460.768 - 2.891T_c + 0.00458T_c^2 \quad \text{(II-13)}$$

The above equations are taken from pure water data (25), and do not reflect the presence of the added chemicals.

The thermal resistance of the metal wall is determined using:

$$R_m = \frac{\ln\left(\frac{D_{to}}{D_{ti}}\right)}{2\pi k_m L} \quad \text{(II-14)}$$

The inside heat transfer coefficient for the condensing steam is evaluated using the following equation for Re < 2100 (26):

$$\left(\frac{h_i}{C_{ph}G}\right)\left(\frac{C_{ph}\mu_h}{k_h}\right) = \frac{5.35}{\frac{4\cdot\Gamma}{\mu_h}} \quad \text{(II-15)}$$

The Reynolds number is defined as:

$$Re_s = \frac{4\Gamma}{\mu_h} \tag{II-16}$$

and:

$$G = \frac{\Gamma}{\left(\frac{3\mu_h\Gamma}{\rho_h^2 g}\right)^{\frac{1}{3}}} = \left(\frac{W_F\rho^2 g}{29.6 D_{ti}\mu_h}\right)^{\frac{1}{3}} \tag{II-17}$$

$$\Gamma = \frac{W_F}{\pi D_{ti}} \tag{II-18}$$

The physical properties are that of the condensate at the average steam temperature and are evaluated using the following expressions (25):

$$\rho_h\ (kg/m^3) = \frac{1000.0}{0.68523 + 0.000958 T_h^2} \tag{II-19}$$

$$\mu_h\ (\times 10^6 \frac{kg}{ms}) = 4032.3786 - 17.26126 T_h + 0.0193 T_h^2 \tag{II-20}$$

$$C_{ph}(\times 10^6\ \frac{kJ}{kgK}) = 6.17287 - 0.01149 T_h + 1.67\ X\ 10^{-5} T_h^2 \tag{II-21}$$

$$k_h\ (\times 10^6 \frac{kW}{mK}) = -446.29124 + 5.57289 T_h - 0.00684 T_h^2 \tag{II-22}$$

$$h_f \left(\frac{kJ}{kg}\right) = 2306.62 + 2.31058T_h - 0.00655T_h^2 \qquad \text{(II-23)}$$

The rate of mass condensation is evaluated using:

$$W_F = \frac{Q}{\lambda_s} \qquad \text{(II-24)}$$

The overall heat transfer coefficient is evaluated using equation (2-3). A comparison of the experimental and theoretical clean overall heat transfer coefficients is shown in Table II-1.

II.5 Determination of the Wall Temperature and the Scale Water interface Temperature

The average wall temperatures and the scale-water interface temperatures throughout a run were evaluated using the steady-state, one-dimensional (radial) process of heat transfer for concentric cylinders with negligible contact thermal resistance.

The following equation expresses the heat transfer:

$$Q = \frac{(T_{h,avg} - T_{wi,avg})}{\frac{1}{A_i h_i}} = \frac{(T_{wi,avg} - T_{wo,avg})}{R_m} = \frac{(T_{wo,avg} - T_{c,avg})}{\frac{1}{h_o}} \qquad \text{(II-25)}$$

It follows from the above equation:

Table II-1 Comparison of the Theoretical and Experimental Clean Overall Heat Transfer Coefficients

Run	v (m/s)	T_c (°C)	T_h (°C)	Q (kW)	U_{th} (kW/m^{2}K)	U_{exp} (kW/m^{2}K)
2	0.47	21.1	102.3	10.55	1.550	1.191
3	0.47	19.6	107.0	9.38	1.278	1.208
4	0.47	22.4	119.6	12.72	1.559	1.189
5	0.93	23.2	105.3	13.28	1.927	1.376
6	0.19	20.0	102.6	7.00	1.009	0.883
7	0.93	26.3	124.6	13.27	1.606	1.417
8	0.47	25.9	113.1	9.36	1.278	1.242
9	0.19	21.8	102.1	6.24	0.926	0.900
10	0.93	29.0	111.6	13.90	2.008	1.390
11	0.93	25.0	114.6	14.60	1.939	1.377
12	0.47	25.7	107.7	8.36	1.214	1.251
13	0.47	23.1	101.9	9.04	1.366	1.222
14	0.47	24.7	103.1	9.03	1.372	1.300
15	0.93	25.1	104.6	11.62	1.741	1.409
16	0.93	26.7	124.5	13.93	1.695	1.407
17	0.93	27.9	131.5	17.90	2.058	1.361
18	0.19	24.8	102.9	5.68	0.867	0.920
19	0.47	20.9	106.0	9.04	1.265	1.219
29	0.47	27.2	101.1	10.03	1.616	1.590
30	0.47	24.3	103.6	11.21	1.682	1.557
31	0.47	25.4	111.1	11.20	1.558	1.577
32	0.47	27.1	113.9	10.19	1.400	1.610
33	0.47	29.9	111.1	12.52	1.835	1.572

$$T_{wo,avg} = T_{h,avg} - Q \cdot R_t \tag{II-26}$$

where:

$$R_t = \frac{\ln(\frac{D_{to}}{D_{ti}})}{2\pi k_m L} + \frac{1}{h_i A_i} = R_m + R_s \tag{II-27}$$

and the temperature of the scale/water interface is then:

$$T_{s,avg} = T_{h,avg} - Q \cdot R_T \tag{II-28}$$

where:

$$R_T = R_t + \frac{R_f}{A_o} \tag{II-29}$$

The temperature gradients and the heat transfer resistances are shown qualitatively in Figure II-1. The calculated scaling temperature is subject to some uncertainty, as it relies on equation (II-5) for h_i.

II.6 Determination of Reynolds and Schmidt Numbers

The equivalent diameter of the DPHE was calculated using the following relationship:

$$D_e = 4.\frac{Net\ Free\ Area}{Total\ Wetted\ Perimeter} = D_{si} - D_{to} \tag{II-30}$$

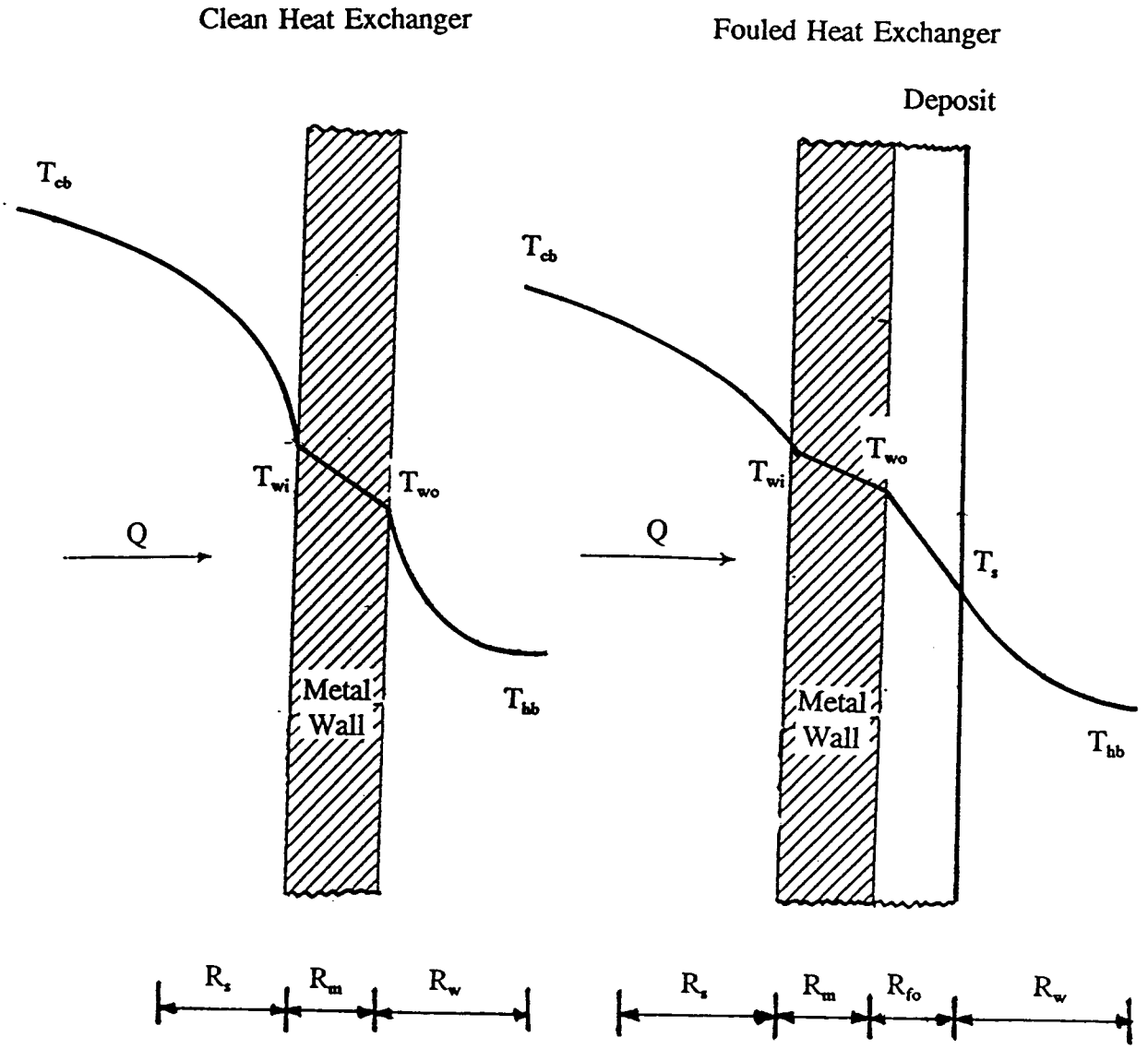

FIGURE II-1 TEMPERATURE GRADIENTS AND HEAT TRANSFER RESISTANCES

Reynolds numbers, based on the bulk and film temperature were calculated using:

$$Re_b = \frac{\rho_{cb} v D_e}{\mu_{cb}} \tag{II-31}$$

$$Re_f = \frac{\rho_{cf} v D_e}{\mu_{cf}} \tag{II-32}$$

where ρ, V and μ are the density, the velocity and the viscosity of the water and the film temperature is evaluated as:

$$T_f = \frac{T_{cb} + T_s}{2} \tag{II-33}$$

As mentioned in section 5-2, the overall heat transfer coefficient at a particular velocity is a function of the heat duty, which is, in turn, a function of the bulk steam temperature. Since it was not possible to maintain the exact same heat duty throughout the length of a run, the clean overall heat transfer coefficient was also a function of the heat duty. Therefore, in equation (2-8), the clean overall heat transfer coefficient was corrected for the variations in the heat duty as follows:

$$U_{oc}(t) = U_{oc}(0) + s \cdot [Q(t) - Q(0)] \tag{II-34}$$

These corrected values of the clean overall heat transfer coefficients were substituted in equation (2-8) to give the corrected values of the fouling resistances.

II.7 Determination of the Chemical Composition, Density and the Thermal Conductivity of the Deposit

The chemical composition of the deposit, mainly the Ca/P ratio, was determined by Acme Analytical Laboratories Limited, Vancouver using the Inductively Coupled Plasma Technique. In this technique, 200 g of the sample to be analysed is fused with 1.2 g of $LiBO_2$ and is dissolved in 100 mL of 5 % HNO_3. The results of the analysis are presented in the Table 5-5. The Ca/P molar ratio of the deposit was variable, indicating that different phosphate phases may be present in the deposit samples.

The density of the deposit was determined using a specific gravity bottle. The relationship used to calculate the density is derived below:

Let:

ρ = Density of pure water at the temperature of the experiment

ρ_1 = Density of water saturated with the calcium phosphate

ρ_f = Density of the (foulant) sample

V_{sg} = Internal Volume of the specific gravity bottle at the temperature of the experiment

W_1 = Weight of the empty bottle

W_2 = Weight of the empty bottle + saturated water

W_3 = Weight of the empty bottle + sample

W_4 = Weight of the empty bottle + saturated water + sample

W_5 = Weight of empty bottle + pure water

The volume of the specific gravity bottle is given as:

$$V_{sg} = \frac{W_5 - W_1}{\rho} \tag{II-35}$$

The density of the sample is given as

$$\rho_f = \frac{Weight\ of\ the\ sample}{Volume\ of\ the\ sample} = \frac{W_4 - W_2}{V_s} \tag{II-36}$$

and the volume of the sample is calculated as:

$$V_s = V - \frac{(W_4 - W_3)}{\rho_1} \tag{II-37}$$

where the density of the saturated water is given as:

$$\rho_1 = \frac{W_2 - W_1}{V} \tag{II-38}$$

Combining equations (II-34) to (II-37) yields:

$$\rho_s = \frac{W_4 - W_2}{(\frac{W_5 - W_1}{\rho}) \cdot [\ 1 - \frac{W_4 - W_3}{W_2 - W_1}\ ]} \tag{II-39}$$

Table II-2 lists the calculated values of density of the scale for some of the runs. The average value used for calculation purposes was 1470 kg/m^3.

The thermal conductivity of the deposit is determined using equation, assuming steady state one-dimensional heat conduction through concentric cylinders. As an approximation, the thermal conductivity is calculated as:

$$k_f = \frac{(x_f)_{avg}}{R_f} \qquad \text{(II-40)}$$

where x_{favg} is the thickness of the scale averaged over the length of the tube and R_f is the (corrected) fouling resistance at the end of a run. Table II-3 shows the calculated values of thermal conductivity of the scale for 8 runs. The average value used for calculation purposes was 1.039 W/mK, which agrees well with the value reported in literature (3).

II.8 Calculations for the Total System Volume

The total system volume was calculated by adding up the volume of the twin tanks and the internal volume of the piping. Since the volumes of the tanks were not known, these were determined by measuring the time taken to empty the tanks at a fixed flow rate of the water, which was drained instead of being recirculated back to the tanks. This was repeated thrice and an average was taken. However, the pump lost suction before all the water was drained, and the residual volume of the water was therefore determined by measuring the height and the diameter of the residual water columns left in the both tanks. The total volume was calculated by adding up all three volumes as expressed by:

TABLE II-2 CALCULATION FOR THE SCALE DENSITY

Run	W_1 (g)	W_2 (g)	W_3 (g)	W_4 (g)	W_5 (g)	ρ_f (kg/m^3)
2	21.3215	46.8432	23.1210	48.0103	46.8432	1795.4
8	18.3385	43.6350	21.4745	45.5030	43.6350	1469.5
9	20.7200	45.7355	21.5220	46.2490	45.7355	1775.4
12	20.7035	45.9555	22.2195	46.7570	45.9555	1118.9
26	19.5940	44.8347	21.8080	45.8040	44.8347	1189.6

TABLE II-3 CALCULATED THERMAL CONDUCTIVITIES OF THE SCALE

Run	x_{favg} (mm)	R_f (m^{2}K/kW)	k_f (W/mK)
3	0.375	0.3592	1.04
4	0.450	0.3227	1.39
20	0.25	0.180	1.39
23	0.30	0.246	1.22
24	0.2	0.219	0.91
25	0.1	0.109	0.92
26	0.2	0.2027	0.99
27	0.15	0.3358	0.45

$$V_t = V_{avg} + V_r + V_p \qquad \text{(II-41)}$$

II.9 Water Analysis Calculations

Table II-5 summarises water chemistry data for various Runs. The total orthophosphate was determined by either using the calibration curve, Figure I-2 or the following calibration equation:

$$T_{PO4}\left(\frac{mg}{L}\ as\ PO_4\right) = 242.19 \times Absorbance_{470\ nm} \qquad \text{(II-42)}$$

The total calcium was determined by measuring the volume of EDTA consumed and using the following expression:

$$T_{Ca}\left(\frac{mg}{L}\ as\ Ca\right) = \frac{A \times B \times 400.8}{C} \qquad \text{(II-43)}$$

$$T_{Ca}\left(\frac{mg}{L}\ as\ CaCO_3\right) = \frac{A \times B \times 1000.0}{C} \qquad \text{(II-44)}$$

where:

A = Volume of EDTA consumed in mL

B = mg of $CaCO_3$ equivalent to 1 mL EDTA

C = Volume of the sample in mL

The total potassium was calculated by adding up the potassium added as KH_2PO_4 and as KOH, at the start of a run.

$$Total\ Potassium = M_1 + M_2 + M_3 \qquad \text{(II-45)}$$

where:

M_1 = Moles of potassium added as KH_2PO_4

M_2 = Moles of potassium added (as KOH) from tank 1

M_3 = Moles of potassium added (as KOH) from tank 1

Table II-4 summarises the water analysis data for some of the runs.

11.10 Calculations for the Pressure Drop and the Shear Stresses

The pressure drop across a 0.6 m long section of the DPHE is measured by a U-tube manometer containing a Meriam Blue Fluid that is immiscible in water and has a specific gravity of 1.75.

For an incompressible fluid flowing in an annular space, the following expression can be written (24):

$$0 = \frac{P_o - P_L}{L} - \frac{1}{r}\frac{d(r\bar{\tau}_{rz})}{dr} \qquad \text{(II-46)}$$

Integrating the above expression yields:

TABLE II-4 WATER ANALYSIS DATA

Run	Sample #	Time (h)	T_{Ca} (ppm $CaCO_3$)	T_{PO4} (ppm PO_4)	pH	Comments
2	1	24	70		7.5	No salt make-up
3	1	1	98	91	7.5	Make-up after 27 and 49 hrs
	2	21	78	79	7.5	
	3	27.5	94	88	7.5	
	4	46	72	81	7.5	
	5	49	88	78	7.5	
	6	93	60	67	7.5	
4	1	2.5	88	83	7.5	Make-up after 25 and 50 hrs
	2	23	58	68	7.5	
	3	30	78	81	7.5	
	4	48	60	72	7.5	
5	1	0.5	90	93	7.5	Make-up after 24 hrs
	2	23	68	77	7.5	
	3	30	80	86	7.5	
	4	47	66	77	7.5	
6	1	22	54	68	7.5	No salt make-up
2R	1	0	98	92	7.5	Make-up after 18 hrs
	2	15.5	75	64	7.5	
9	1	0.5	68	72	7.4	No salt make-up
	2	52	26	52	7.4	
10	1	3	32	52	7.0	No salt make-up
11	1	0	26	52	6.5	No salt make-up
	2	16	10	28	37	
12	1	0.5	66	75	7.00	No salt make-up
	2	23	26	47	7.15	
	3	55	20	49	7.25	

TABLE II-4 WATER ANALYSIS DATA (CONTD.)

Run	Sample #	Time (h)	T_{Ca} (ppm $CaCO_3$)	T_{PO4} (ppm PO_4)	pH	Comments
13	1	0	90	87	6.4	No fouling observed
14	1	0		93		No salt make-up
	2	26		88		
15	1	0.5	94	95	7.2	No salt make-up
	2	20	82	88	7.2	
18	1	0.5	92	88	7.0	No salt make-up
	2	7.5	84	85	7.0	
	3	70	50	65	7.0	
23	1	0.5	190	101	7.0	
	2	4.5	182	-	7.0	
	3	6.5	178	92	7.0	
	4	20	150	69	7.0	
24	1	0.5	92	165	7.0	No salt make-up
	2	7.0	82	158	7.0	
	3	21	64	152	7.0	
25	1	0.5	92	137	7.0	No salt make-up
	2	19	72	127	7.0	
26	1	0.5	136	95	7.0	No salt make-up
	2	16	114	81	7.0	
27	1	0.5	210	91	7.0	No salt make-up
	2	6	204	86	7.0	
	3	26	190	74	7.0	
28	1	0.5	88		7.0	No salt make-up
	2	24	66		7.0	

$$\tau_{rz} = \left(\frac{P_o - P_L}{2L}\right) + \frac{B_1}{r} \qquad \text{(II-47)}$$

In order to determine constant B_1 , it can be said that the maximum in the velocity profile lies at some plane $r=\lambda R$, where:

$$B_1 = -\frac{(P_o - P_L)\,(\lambda R)^2}{2L} \qquad \text{(II-48)}$$

hence,

$$\tau_{rz} = \frac{(P_o - P_L)R}{2L} \cdot \left[\frac{r}{R} - \lambda^2\left(\frac{R}{r}\right)\right] = \tau_o \cdot \left[\frac{r}{R} - \lambda^2\frac{R}{r}\right] \qquad \text{(II-49)}$$

where:

$$\lambda = \sqrt{\frac{1 - \kappa^2}{2\ln\frac{1}{\kappa}}} \qquad \text{(II-50)}$$

The maximum of τ_{rz} is at $r = \kappa R$. Hence,

$$\tau_{rz}\big|_{r=\kappa R} = \tau_o\left[\kappa - \frac{1 - \kappa^2}{2\kappa\ln\frac{1}{\kappa}}\right] \qquad \text{(II-51)}$$

II.10.1 Calculation of Theoretical ΔP

A force balance on the fluid flowing in the heat exchanger gives:

$$(P_o - P_L)\pi(r_{si}^2 - r_{to}^2) = 2\pi L(\frac{1}{2}\bar{\rho}v^2)[r_{si}f_o - r_{to}f_i] \quad \text{(II-52)}$$

where:

$$\bar{\rho} = \frac{\rho_{cb}+\rho_f}{2} \quad \text{(II-53)}$$

and f_i and f_o are the friction factors for the outside surface of the tube and the inside surface of the shell, both assumed to be hydraulically smooth. Their values are given by Blausius expression (24):

$$f_i = \frac{0.0791}{Re_f^{0.25}} \quad \text{(II-54)}$$

and:

$$f_o = \frac{0.0791}{Re_{cb}^{0.25}} \quad \text{(II-55)}$$

II.10.2 Calculation of Experimental ΔP

An expression for experimental ΔP can easily be derived in terms of the height differential of the manometric fluid and is provided below:

$$\Delta P_e = (\rho_m - \rho)g\Delta h \quad \text{(II-56)}$$

where Δh is the difference in the heights of the manometric fluid.

Figures II-2 and II-3 show the effect of velocity on calculated and experimental pressure

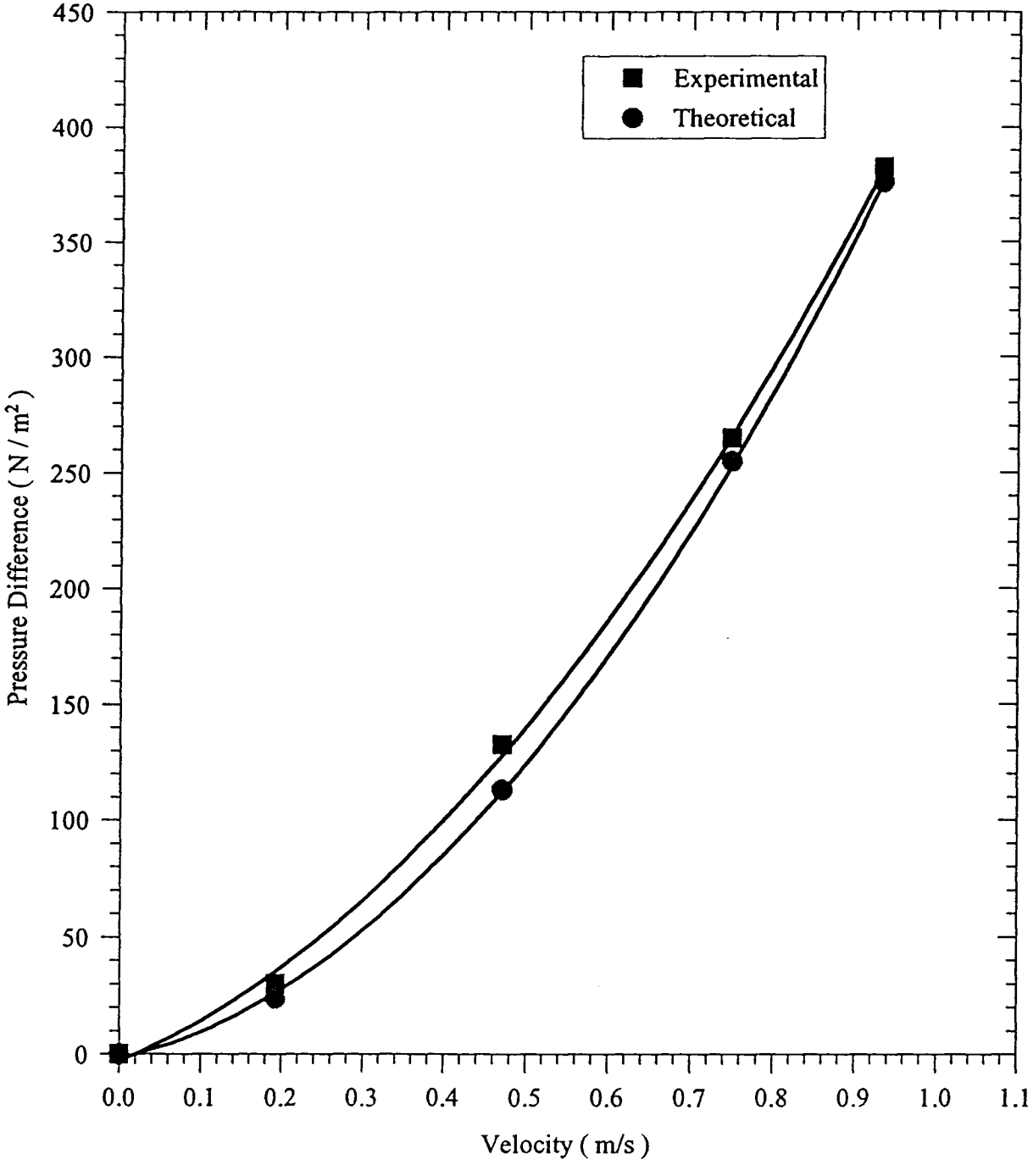

FIGURE II-2 EFFECT OF THE VELOCITY ON THE CALCULATED AND THE EXPERIMENTAL PRESSURE DROP ACROSS THE DPHE

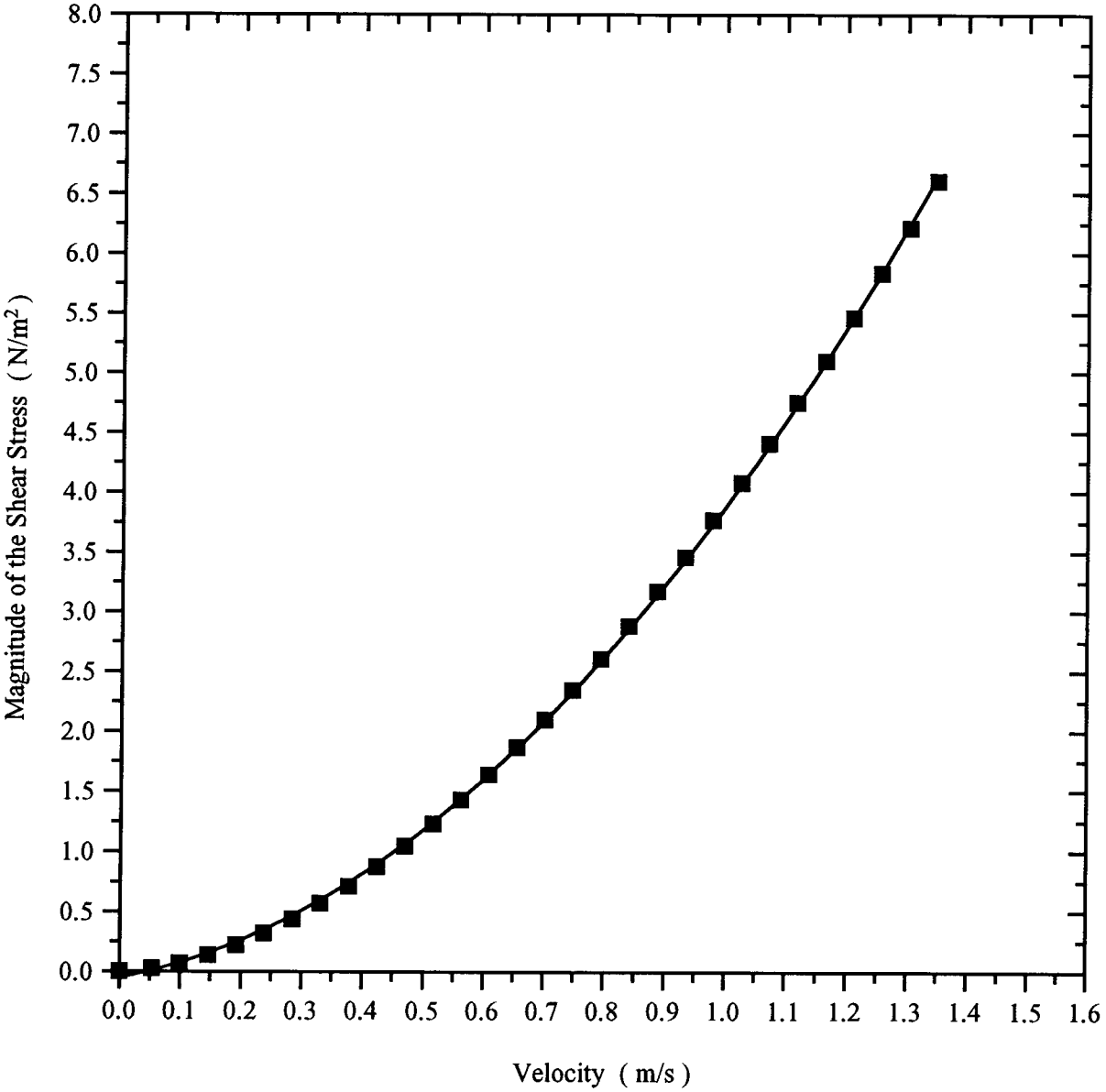

FIGURE II-3 EFFECT OF THE VELOCITY ON THE CALCULATED SHEAR STRESS

drop and shear stress for the clean condition.

II.10 Numerical Sample Calculation Using Run 2

Run 2 was carried out at the following conditions, at a rotameter setting of 50 . At time=1 h, the temperature readings were:

T_{ci} = 16.8 °C

T_{co} = 22.4 °C

T_{hb} = (107.2 + 106.9) / 2 = 107.05 °C = 380.21 K

T_{cb} = (22.4 + 16.8) / 2 = 19.6 °C = 292.76 K

Applying equations (II-3), (I-1) and (II-4):

ρ_b =998.78 kg/m^3

F = 40.13 x 10^{-5} m^3/s

C_p = 4.1797 kJ/kg°C

Using equation (II-1):

Q = (40.13 x 10^{-5}) (998.78) (4.1797) (22.4 - 16.8) = 9.38 kW

ΔT_{lm} = (22.4 - 16.8) / ln {(107.05 - 22.4) / (107.05 - 16.8)} = 87.42 °C

$A_o = \pi$ (19.1 x 10^{-3}) (1.4) = 8.4 x 10^{-2} m^2

Hence, the overall heat transfer coefficient can be calculated using equation (II-5):

$U_{oc} = 9.38 / \{(0.084)\ (87.4)\} = 1.278\ kW/m^2K$

Similarly, at t = 10.0 h:

$U_{od} = 1.141\ kW/m^2K$

$Q = 8.88\ kW$

Assuming the clean overall heat transfer coefficient to be independent of the heat transfer rate, the uncorrected fouling resistance can be calculated as:

$(R_f)_u = 1 / 1.141 - 1 / 1.278 = 0.09395\ kW/m^2K$

However, the clean overall heat transfer coefficient depends on the rate of heat transfer as shown in Figures (5-2) to (5-7). The average slope of the clean overall heat transfer coefficient versus heat transfer straight line, at this velocity, is 0.048 . From equation (2-9):

$U_{oc} = 1.278 + 0.048\ (8.88 - 9.38) = 1.254\ kW/m_2K$

Hence, the corrected fouling resistance, denoted by R_{fc} , is calculated as:

$R_{fc} = 1/1.141 - 1/1.262 = 0.079\ kW/m^2K$

The physical properties of water are evaluated at the bulk temperature using equations (II-10) to (II-13) as:

$\mu_c = 1006.2 \times 10^{-6}\ Ns/m^2$

$K_c = 600.282 \times 10^{-6}\ kW/mK$

$Pr = 7.09$

$Re_c = (19.0 \times 10^{-3}) (0.47) (998.78) / 1006.2 \times 10^{-6} = 8864.3$

Hence, the outside heat transfer coefficient is calculated using equation (II-9):

$h_o = (600.3 \times 10^{-6}) / 19.0 \times 10^{-3}) (0.023) (8864)^{0.8} (7.09)^{0.4} (1.99)^{0.45}$

$= 3.124 \text{ kW/m}^2\text{K}$

The physical properties for the steam condensate are evaluated using equations (II-19) to (II-23):

$h_f = 2238.82 \text{ kJ/kg}$

$\rho_h = 953.7 \text{ kg/m}^3$

$\mu_h = 260.02 \text{ kg/m.s}$

$C_{ph} = 4.2182 \text{ kJ/kg°C}$

$K_h = 683.7 \times 10^{-6} \text{ kW/m.K}$

The mass rate of the condensation of the steam is calculated using equation (II-24):

$W_F = 9.38 / 2238.8 = 4.1897 \times 10^{-3} \text{ kg/s}$

The parameter Γ, defined by equation (II-18) is evaluated as follows:

$\Gamma = 4.1897 \times 10^{-3} / \{(3.1415) (13.7 \times 10^{-3})\} = 9.73 \times 10^{-2} \text{ kg/m.s}$

The Reynolds number is given according to equation (II-16):

$Re_h = 4 \times 9.73 \times 10^{-2} / 260.0 \times 10^{-6} = 1498 < 2100$ (laminar regime)

Hence, the parameter G defined by equation (II-17) is calculated as:

$G = [(4.1897 \times 10^{-3})^2 (953.7)^2 (9.8) / \{(29.6) (13.7 \times 10^{-3})^2 (260. \times 10^{-6})\}]^{1/6}$

$= 476.85$

The Prandtl number is given below:

$Pr = (4.2182) (260. \times 10^{-6}) / (683.7 \times 10^{-6}) = 1.60$

By plugging the above numerical values in equation (II-15), the value of the inside heat transfer coefficient is obtained as:

$h_i = (4.2182) (476.85) (5.35) / \{(1.60) (1497.6)\} = 4.479$ kW/m^{2}K

The thermal resistance of the metal wall is calculated using equation (II-14):

$R_m = \ln (19.1/13.7) / \{(2.0) (3.1415) (16.1 \times 10^{-3}) (1.4)\} = 2.3464$ K/kW

By substituting the above values in equation (2-3), the clean overall heat transfer coefficient is obtained as follows:

$1 / U_o = 1 / \{4.479 (13.7/19.1)\} + 1 / 3.124 + \{(2.3464) (6.025 \times 10^{-2})\}$

or, $U_o = 1.207$ kW/m^{2}K

The following calculation sums up the thermal resistances of steam and the metal wall, both in series, at time = 1 h:

$R_t = 1/ \{(4.479) (6.025 \times 10^{-2})\} + 2.3464 = 6.0526$ K/kW

The outside wall temperature can be calculated according to the equation (II-26):

$T_w = 107.05 - (9.38) (6.05257) = 50.2$ °C

The total thermal resistance at time = 10 h is made up of the resistances offered by steam, metal and water, all in series and can be calculated by adding them up:

$R_T = 2.3464 + 1 / \{(4.633) (6.025 \times 10^{-2})\} + 0.079/0.084 = 6.869$ K/kW

Therefore, the scale-water interface temperature is calculated according to equation (II-28):

$T_s = 112.8 - (8.88) (6.869) = 51.8$ °C

and the wall temperature is calculated as:

$T_w = 112.8 - (8.88) (5.929) = 60.2$ °C

The Reynolds number, at the film temperature, is evaluated as below:

$Re_f = (19.0 \times 10^{-3}) (0.47) (994.4) / 545.4 \times 10^{-6} = 16281.2$

The following Table II-5 summarises the experiments done to calculate the volume of the water pumped before the suction was lost:

TABLE II-5 DETERMINATION OF THE TOTAL SYSTEM VOLUME

Rotameter Reading	Volumetric Flow Rate (m^3/s)	Time taken to Empty the Tanks (s)	Volume ($x\ 10^3\ m_3$)
46	37.14×10^{-5}	1178	437
56	44.27×10^{-5}	967	428
64	51.50×10^{-5}	855	432

Hence, V_{avg} is calculated as:

$V_{avg} = (440 + 428 + 437) / 3.0 = 435$ liters

When the pump lost suction, there was 5 cm high water column left at the bottom of both the tanks, having upper and lower diameters of 48.3 cm and 45.7 cm, respectively. Hence the residual volume is calculated as:

$V_r = 2 \times 3.1415 \times 46.5^2 / 4 \times 51\ cm^3 \approx 18$ l

The piping is essentially made up of about 12.2 m of 2.54 cm ID and 6.1 m of 3.81 cm ID. Hence the internal volume of the piping is calculated as:

$V_p = 3.1415 (0.0127^2 \times 12.2 + 0.0191^2 \times 6.1)\ m^3 \approx 13$ l

Hence the total system volume is calculated as:

$V = 435 + 18 + 13 = 466$ l

Water Analysis

10 ml of vandate-molybdate reagent was added to 35 ml of sample # 1 for run 3 and finally diluted to 50 ml. The absorbance at 470 nm and 1 cm path length was measured using spectrophotometer as being 0.3741. From Figure I-2:

T_{PO4} (as mg/l PO_4) = 90.6

50 ml of the sample # 1 for run 3 was titrated against EDTA. The volume of EDTA consumed was 4.9 cc. Hence, according to the equation (II-43), the total Ca-hardness is:

T_{Ca} (as mg/l Ca) = 4.9 X 1 X 400.8 / 50 = 39.3

The total potassium concentration, (K), for the run 3 was calculated by summing up the potassium added as KH_2PO_4 and as KOH, at the start of a run as follows:

(K) = (50 / 136.1 + 20 x 0.01 + 11 x 0.58 x .04) / 380 = 2.1646×10^{-3} mol/l

Pressure Drop

The pressure drop across a 0.6 m length of the heat exchanger is evaluated by calculating the friction factors using the Blausius equation:

$f_i = 0.0791 / (16281)^{1/4} = 7.003 \times 10^{-3}$

$f_o = 0.0791 / (8864)^{1/4} = 8.152 \times 10^{-3}$

$\Delta P_t = (2)\ (0.6)\ (0.5)\ (996.6)\ (0.47)^2$

$\cdot\ [\{(.00955)\ (7.005 \times 10^{-3}) + (.0191)\ (8.15 \times 10^{-3})\} / \{(.0191)^2 - (.00955)^2)\}]$

$\Delta P_t = 107.6\ N/m^2$

The experimental pressure drop is calculated using equation (II-56):

$\Delta P_e = (1750 - 1000)(9.81)(1.7 \times 10^{-2}) = 124.95\ N/m^2$

The experimental pressure drops as a function of velocity are listed in the following Table II-6:

TABLE II-6 EXPERIMENTAL PRESSURE DROP AT VARIOUS VELOCITIES

Rotameter Reading	Velocity (m/s)	Manometric Δh (cm.)	ΔP (N/m^2)
20	0.1926	0.4	29.93
50	0.4704	1.8	132.44
80	0.7481	3.6	264.87
100	0.9333	5.2	382.59

APPENDIX III

COMPUTER PROGRAMS

The following pages list six computer programs that were used to process the experimental data. The first computer program, Figure III-1, calculates, as functions of time, the heat transfer rate, the log mean temperature difference, the dirty overall heat transfer coefficients, the uncorrected and corrected fouling resistances; the wall, scale surface, water bulk, steam bulk temperatures and their averages and standard deviation over the entire length of the run. Also calculated are the bulk and the Reynolds numbers over the entire length of a run. The second computer program, Figure III-2, calculates the concentrations of the various phosphate and calcium ionic species as functions of pH and temperature. The activity coefficients and the ionic strength of the solution are calculated using an iterative procedure. The output for the programs III-1 and III-2 are listed only for Run 2. For all other runs the output of the computer programs III-1 and III-2 has been bound in a supplemental volume to the thesis which is available from Dr. A.P. Watkinson. The third computer program, Figure III-3, calculates the distribution of the phosphate species as a function of pH neglecting the ion pair complexing and assuming all the activity coefficients to be unity. The fourth one, Figure III-4, calculates the theoretical inside and the outside heat transfer coefficients and, therefore, the theoretical overall heat transfer coefficient as functions of the temperatures, geometry, velocity and the heat flux. The fifth one, Figure III-5, calculates, at a particular velocity, the theoretical and the experimental pressure drops across the heat exchanger and the theoretical shear stress as functions of temperatures and the geometry of the heat exchanger. The sixth one calculates the theoretical and experimental

pressure drops and the shear stress as functions of the velocity, geometry and the temperature under "no steam" conditions.

FIGURE III-1 COMPUTER PROGRAM TO CALCULATE THE EXPERIMENTAL FOULING RESISTANCES AS A FUNCTION OF TIME

```
C     THIS PROGRAM CALCULATES THE EXPERIMENTAL FOULING RESISTANCE
C     AS A FUNCTION OF TIME
C     T1 AND T2 DENOTE THE OUTLET AND INLET TEMPERATURES OF WATER IN
C     DEGREE C, T3 AND T4 DENOTE THE INLET AND OUTLET TEMPERATURES
C     OF THE STEAM, LMTD DENOTES LOG MEAN TEMPERATURE DIFFERENCE.
C     POSTSCRIPTS C AND H DENOTE WATER AND STEAM RESPECTIVELY. P, CP,
C     H, U, K DENOTE DENSITY, SPECIFIC HEAT, HEAT OF VAPORISATION,
C     THERMAL CONDUCTIVITY HAVING UNITS OF kg/m**3, kJ/kgK, kJ/kg,
C     kW/mK, RESPECTIVELY. TC AND TH DENOTE THE AVG BULK TEMPERATURES
C     TS DENOTES THE CALCULATED SCALE WATER INTERFACE TEMPERATURE.
C     RFC AND RFU DENOTE THE CORRECTED AND UNCORRECTED FOULING
C     RESISTANCES HAVING UNITS OF m**2K/kW. TRE DENOTES THE TOTAL
C     THERMAL RESISTANCE. UOC AND UOD DENOTE THE OVERALL CLEAN AND
C     DIRTY HEAT TRANSFER COEFFICIENTS HAVING UNITS kW/m**2K
C     M DENOTES THE SLOPE OF THE Q VS. UOC STRAIGHT LINE.

      REAL LMTD,M,KH,NREC,NREF,KS
      INTEGER RUN
      DIMENSION TIME(134),T1(134),T2(134),T3(134),T4(134),DT(134)
      DIMENSION LMTD(134),PC(134),CPC(134),Q(134),UOD(134),TWALL(134)
      DIMENSION RFC(134),RFU(134),TS(134),TC(134),TRE(134),TH(134)
      DIMENSION UOC(134),PH(134),HF(134),UH(134),CPH(134),KH(134)
      DIMENSION WH(134),T(134),G(134),PRH(134),HS(134),HI(134)
      SUMTC=0.0
      SUMTH=0.0
      SUMQA=0.0
      SUMTS=0.0

C     F IS THE FLOW RATE OF WATER IN m**3/s
C     N IS THE NUMBER OF THR OBSERVATIONS FOR THE RUN

      READ(5,1) RUN,F,M,N
1     FORMAT(I3,E8.2,F7.6,I3)
2     FORMAT(F7.4,2F4.1,2F5.1)
      DO 10 I=1,N
      READ(5,2) TIME(I),T1(I),T2(I),T3(I),T4(I)
      TH(I)=(T3(I)+T4(I))/2.0
      TC(I)=(T1(I)+T2(I))/2.0
      CPC(I)=(-0.000108)*TC(I)+4.181817
      PC(I)=(-0.326893)*TC(I)+1005.445464
      DT(I)=T1(I)-T2(I)
      SUMTC=SUMTC+TC(I)
      SUMTH=SUMTH+TH(I)
      LMTD(I)=DT(I)/LOG((TH(I)-T2(I))/(TH(I)-T1(I)))
      Q(I)=(DT(I)*PC(I)*CPC(I)*F)
      UOD(I)=Q(I)/(0.084*LMTD(I))
      UOC(I)=UOD(1)+M*(Q(I)-Q(1))
      RFU(I)=1./UOD(I)-1./UOD(1)
      RFC(I)=1./UOD(I)-1./UOC(I)

C     TO CALCULATE THEORETICAL STEAM SIDE THERMAL RESISTANCE, HI

      PH(I)=1000./(0.68523+0.000958*(TH(I)+273.))
      HF(I)=2306.62+2.31058*(TH(I)+273.)-0.00655*(TH(I)+273.)**2
      UH(I)=(4032.3786-17.26126*(TH(I)+273.)+0.0193*(TH(I)+273.)**2)/
     *1000000.
      CPH(I)=6.17287-0.01149*(TH(I)+273.)+1.67E-05*(TH(I)+273.)**2
      KH(I)=(-446.29124+5.57289*(273.+TH(I))-0.00684*(273.+TH(I))**2)/
     *1000000.
```

```
      WH(I)=Q(I)/HF(I)
      T(I)=WH(I)/(3.1415*(13.7/1000.))
      G(I)=((WH(I)**2*PH(I)**2*9.81)/(29.6*(13.7/1000.)**2*UH(I)))**(0
     *.3333333)
      PRH(I)=(CPH(I)*UH(I)/KH(I))
      HI(I)=(((CPH(I)*G(I))/PRH(I))*5.35/(4.0*T(I)/UH(I)))
      AI=3.1415*1.4*(13.7/1000.)
      AO=3.1415*1.4*(19.1/1000.)

C     TO CALCULATE TOTAL THERMAL RESISTANCE,TRE, IN DEG K/kW

      RM=LOG(19.1/13.7)/(2.0*3.1415*16.1/1000.*1.4)
      TRE(I)=RM+RFC(I)/0.084+1./(HI(I)*AI)
      TS(I)=TH(I)-Q(I)*TRE(I)
      SUMTS=SUMTS+TS(I)
      SUMQA=SUMQA+Q(I)
      SWRE=RM+1./(HI(I)*AI)
      TWALL(I)=TH(I)-SWRE*Q(I)
10    CONTINUE
      WRITE(6,3)
3     FORMAT(' DT   TC    TH      LMTD  TIME Q     UOD    RFC    RFU    TS
     *TWALL HI   ')
4     FORMAT(F4.1,1X,F4.1,1X,F5.1,1X,F5.1,1X,F4.1,1X,F5.2,1X,F5.3,
     *1X,F6.4,1X,F5.3,1X,F5.1,1X,F5.1,1X,F5.3)
      Z=0.0
      DO 7 I=1,N
      WRITE(6,4) DT(I),TC(I),TH(I),LMTD(I),TIME(I),
     *Q(I),UOD(I),RFC(I),RFU(I),TS(I),TWALL(I),HI(I)
      Z=Z+1.
7     CONTINUE
      AVGTC=SUMTC/Z
      AVGTH=SUMTH/Z
      AVGQA=SUMQA/Z
      AVGTS=SUMTS/Z
      SWA=0.0
      SFA=0.0
      SBA=0.0
      DO 8 I=1,N
      SWA=SWA+(TC(I)-AVGTC)**2
      SFA=SFA+(Q(I)-AVGQA)**2
      SBA=SBA+(TS(I)-AVGTS)**2
8     CONTINUE
      SDTW=SQRT(SWA)/Z
      SDQA=SQRT(SFA)/Z
      SDTS=SQRT(SBA)/Z
      WRITE(6,40)
40    FORMAT(//,'  SDTW       SDQA     SDTS ')
      WRITE(6,20) SDTW,SDQA,SDTS
20    FORMAT(F8.4,3X,F7.4,2X,F7.4)
      WRITE(6,5)
5     FORMAT(//,'  TC(avg)   TH(avg.)   Q(avg.)   TS(avg.)   ')
30    FORMAT(2X,F4.1,6X,F5.1,4X,F4.1,5X,F5.1)
      WRITE(6,30) AVGTC,AVGTH,AVGQA,AVGTS

C     TO CALCULATE THE FILM AND BULK REYNOLDS NUMBER DENOTED BY
C     NREF AND NREC, RESPECTIVELY

      UC=(65816.34444-418.2856*(AVGTC+273.)+0.67255*(AVGTC+273.)**2)/1
     *000000.
      PB=1000./1.002
```

```
      DE=(38.1-19.1)/1000.
      V=F/((3.1415/4.)*((38.1/1000.)**2-(19.1/1000.)**2))
      NREC=DE*V*PB/UC
      TF=(AVGTS+AVGTC)/2.
      UFA=(4032.3786-17.26126*(TF+273.)+0.0193*(TF+273.)**2)/1000000.
      PF=1000.0/(1.+(TF+273.-285.)*.0002)
      NREF=DE*V*PF/UFA
      WRITE(6,50) NREF,NREC
50    FORMAT(//,'  NREF=',F8.1,7X,'NREC=',F8.1)
      STOP
      END
```

FIGURE III-2 COMPUTER PROGRAM TO CALCULATE THE CONCENTRATION OF VARIOUS SPECIES AND THE ACTIVITY COEFFICIENTS

```
      PROGRAM BPREP

C      THIS PROGRAM CALCULATES CONCENTRATIONS AND ACTIVITY COEFFICIENTS
C      AT THE BULK TEMPRATURE AND  GIVEN PH, TCA AND TPO4

      IMPLICIT REAL(A-Z)
      REAL K1,K2,K3,K4,K5,K6,K7,KW,I,II,K,KSP

C      ALL CONCENTRATIONS ARE IN mol/L. Z IS THE NO. OF ITERATIONS

      TPO4=96.67E-5
      TCA=89.5E-5
      PH=7.50
      CL= 1.93E-3
      K=4.335E-3
      EPS=.00001
      Z=0.0

C      TC IS THE AVERAGE WATER BULK TEMPERATURE,T IS THE AVERAGE
C      STEAM TEMPERATURE IN DEG.K

      TH=52.+273.16
      TC=20.+273.16

C      INITIAL APPROXIMATION FOR THE IONIC STRENGTH

      I=0.5*(9.*TPO4+4.*TCA+K+CL+10.**(-1.*PH))

C      CALCULATE ACTIVITY COEFFICIENTS AT THE FILM TEMPERATURE
C      USING EXTENDED FORM OF THE DEBYE-H:UCKEL EQUATION
C      PROPOSED BY DAVIES FOR I < 0.2 MOLE/LITER

100   FM=10.0**(-2620.7/TC**1.5*(SQRT(I)/(1+SQRT(I))-0.3*I))
      FD=10.0**(-10482.8/TC**1.5*(SQRT(I)/(1+SQRT(I))-0.3*I))
      FT=10.0**(-23586.3/TC**1.5*(SQRT(I)/(1+SQRT(I))-0.3*I))

C      CALCULATE VARIOUS EQUILIBRIUM CONSTANTS AT THE BULK TEMPERATURE

      K1=10.**(423.23/TC-3.5903)/(FM**2)
      K2=10.**(141.08/TC-7.617)/FD
      K3=10.**(211.62/TC-12.845)*FD/(FM*FT)
      K4=10.**(-282.156/TC+2.2935)*FD
      K5=10.**(-775.93/TC+4.022)*FD
      K6=10.**(-987.5/TC+6.047)*(FD**2)
      K7=10.**(-634.85/TC+8.585)*FD*FT/FM
      KW=10.**(-2609.9/TC-5.18)/(FM**2)

C      CALCULATE THE H+ & OH- CONCENTRATIONS IN mol/L

      H=10.**(-1.*PH)/FM
      OH=KW/H

C      CALCULATE VARIOUS CONSTANTS C1,C2,C3,C4,C5,C6

      C1=(1.+(K1/H)+(K1*K2/(H**2))+(K1*K2*K3/H**3))/(1.+K4*OH)
      C2=(TCA-TPO4)/(1.+(K4*OH))
      C3=1.+(K4*OH)
      C4=(K5*K1/H)+(K6*K1*K2/H**2)+(K7*K1*K2*K3/H**3)
```

```
      C5=((C2*C4)+(C3*C1))/(C1*C4)
      C6=((C2*C3)-TCA)/(C1*C4)
      H3PO4=0.5*(SQRT((C5**2)-(4.0*C6))-C5)
      H2PO4=(K1*H3PO4)/H
      HPO4=(K1*K2*H3PO4)/(H**2)
      PO4=(K1*K2*K3*H3PO4)/(H**3)
      CA=C2+(C1*H3PO4)
      CAOH=K4*OH*CA
      CAH2PO=(K5*K1*H3PO4*CA)/H
      CAHPO4=(K6*K1*K2*CA*H3PO4)/(H**2)
      CAPO4=(K7*K1*K2*K3*CA*H3PO4)/(H**3)

C     CALCULATE THE IONIC STRENGTH OF SOLUTION USING ABOVE VALUES

      II=I
      I=0.5*(4.0*CA+9.0*PO4+CAOH+CAH2PO+CAPO4+H2PO4+4.0*HPO4+K+CL+H
     *+OH)
      Z=Z+1.
      DI=ABS((I-II)/II)*100.
      IF(DI.LE.EPS) GOTO 110
      GOTO 100
110   WRITE(6,120) K1,K2,K3,K4,K5,K6,K7,KW
120   FORMAT('   K1  ','  K2   ','  K3   ','   K4  ',2X,4(E8.3,2X
     *),//,'   K5  ','  K6   ','  K7   ','    KW  ',2X,4(E8.3,2X)/)
      WRITE(6,130) H,OH,CA,CAOH,CAH2PO,CAHPO4,CAPO4
130   FORMAT( '   H   ','  OH   ','   CA  ',10X,3(E8.3,2X)//,
     *' CAOH ',' CAH2PO','  CAHPO4  ','CAPO4   ',4(E8.3,2X)/)
      WRITE(6,140) H3PO4,H2PO4,HPO4,PO4,I,II,Z
140   FORMAT(' H3PO4 ',' H2PO4 ','  HPO4 ','   PO4 ',4(2X,E8.3),//
     *'   I   ','  II   ','  Z    ',8X,2(2X,E13.8),2X,F3.1/)
      WRITE(6,150) FM,FD,FT
150   FORMAT('   FM   ','  FD   ','  FT   ',7X,3(2X,F5.4),/)

C     CHECK FOR THE ELECTONEUTRALITY OF THE SOLUTION

      SPOS=2.*FD*CA+FM*(CAOH+CAH2PO+K+H)
      SNEG=3.*FT*PO4+2.*FD*HPO4+FM*(CAPO4+H2PO4+CL+OH)
      TCA=CA+CAOH+CAH2PO+CAHPO4+CAPO4
      TPO4=H3PO4+H2PO4+HPO4+PO4+CAH2PO+CAHPO4+CAPO4

C     TO CALCULATE THE SUPERSATURATION POTENTIAL W R T VARIOUS
C     SPECIES

      KSP=1.05E-8*EXP(943.47/TC)/FD**2
      SDCPD=CA*HPO4-KSP
      SHAP=CA**5*PO4**3*OH-1.8E-58/(FD**5*FT**3*FM)
      STCP=CA**3*PO4**2-1.15E-29/(FD**3*FT**2)
      SOCP=CA**4*PO4**3*H-1.25E-47/(FD**4*FT**3*FM)

C     CALCULATE THE DEGREE OF SUPERSATURATION WRT VARIOUS SPECIES

      DDCPD=CA*HPO4/KSP
      DHAP=CA**5*PO4**3*OH/(1.8E-58/(FD**5*FT**3*FM))
      DTCP=CA**3*PO4**2/(1.15E-29/(FD**3*FT**2))
      DOCP=CA**4*PO4**3*H/(1.25E-47/(FD**4*FT**3*FM))
      WRITE(6,151) DDCPD,DHAP,DTCP,DOCP
151   FORMAT(' DDCPD  DHAP    DTCP   DOCP ',4(1X,E9.2)/)
      WRITE(6,200) SDCPD,SHAP,STCP,SOCP
200   FORMAT(' SDCPD  SHAP    STCP   SOCP ',4(1X,E9.2)/)
      WRITE(6,155) SPOS,SNEG
```

```
155   FORMAT (' SPOS = ',E8.3,2X,' SNEG = ',E8.3/)
      WRITE(6,112) PH,TCA,TPO4
112   FORMAT(' PH = ',F3.1,8X,'  TCA = ',E8.2,8X,'    TPO4 = ',E8.2/)
      STOP
      END
```

FIGURE III-3 COMPUTER PROGRAM TO CALCULATE THE CONCENTRATION OF VARIOUS PHOSPHATE SPECIES

```
C     THIS PROGRAM CALCULATES THE CONCENTRATIONS OF THE PHOSPHATE
C     ASSUMING NO CALCIUM PHOSPHATE ION COMPLEXING

      REAL K1,K2,K3
      DATA K1,K2,K3/6.09E-3,6.33E-8,4.29E-13/

C     ALL CONCENTRATIONS ARE IN mol/L
C     ALL ACTIVITY COEFFICIENTS ARE ASSUMED TO BE UNITY

      TPO4=1.184E-2
      TCA=1.210E-2

C     CALCULATE THE (H+) CONCENTRATION

      H=10**(-PH)

C     CALCULATE THE CONCENTRATIONS OF THE VARIOUS SPECIES

      PO4=TPO4/(1.0+H/K3+H**2/(K3*K2)+H**3/(K3*K1*K2))
      HPO4=H/K3*PO4
      H2PO4=H/K2*HPO4
      H3PO4=H/K1*H2PO4
      WRITE(6,100) PO4,HPO4,H2PO4,H3PO4,PH
100   FORMAT(1X,'   PO4   ',E8.2,'  HPO4 ',E8.2,
     *   '   H2PO4  ', E8.2,'  H3PO4  ',E8.2,'  PH   ',F4.1)
      END
```

FIGURE III-4 COMPUTER PROGRAM TO CALCULATE THE OVERALL HEAT TRANSFER COEFFICIENTS

```
C     THIS PROGRAM CALCULATES THE OVERALL THEORETICAL HEAT TRANFER
C     COEFFICIENTS FOR THE D P H E IN kW/m*mK

      REAL KC,KH,NREC,K,NREH,J

C     INPUT VARIABLES ARE HEAT TRANSFER RATE(Q), OUTSIDE AND INSIDE
C     DIAMETERS OF THE ANNULAR SPACE(DO, DI), VELOCITY(V) AND THE
C     AVERAGE BULK TEMPERATURES OF STEAM AND WATER (TH, TB). UNITS
C     ARE kW, m, m/s AND DEGREE KELVIN, RESPECTIVELY. POSTSCRIPTS
C     H AND C DENOTE STEAM AND WATER, RESPECTIVELY

      Q=09.38
      TH=273.16+107.
      TC=273.16+19.6
      ROT=50.0

C     CALCULATE THE FLUID PROPERTIES AT THE BULK TEMPERATURE
C     PRC DENOTES THE BULK PRANDTL NUMBER AND VISCOSITY(UC), THERMAL
C     CONDUCTIVITY(KC) AND DENSITY(PC) OF WATER AT THE BULK TEMP.
C     HAVE UNITS OF Nm/s*s, kW/mK AND kG/m**3 RESPECTIVELY

      UC= (65816.3444-418.2856*TC+0.67255*TC**2)/1000000.
      KC=(-278.3159+4.4628*TC-0.00499*TC**2)/1000000.
      PRC=460.7678-2.8906*TC+0.00458*TC**2

C     CALCULATE THE WATER SIDE HEAT TRANSFER COEFFICIENT (HO) USING
C     WIEGAND CORRELATION FOR TURBULENT FLOW IN ANNULI. DE DENOTES
C     EQUIVALENT DIAMETER

      DO=38.1/1000.0
      DI=19.1/1000.
      V=.009259*ROT+.007398
      DE=DO-DI
      NREC= DE*V*PC/UC
      HO=(KC/DE)*(0.023)*NREC**0.8*PRC**0.4*(DO/DI)**0.45

C     CALCULATE THE WATER SIDE COEFFICIENT (HOG) USING GNIELINSKI
C     CORRELATION FOR TURBULENT FLOW IN CIRCULAR PIPES

      J=1./((1.82*0.4342*LOG(NREC)-1.64)**2)
      HOG=( KC/DE)*((J/8.)*(NREC-1000.)*PRC)/(1.+12.7*(J/8.)**0.5*(PRC
     1**0.6666-1.))

C     CALCULATE THE FLUID PROPERTIES AT THE STEAM TEMP.(TH), T IS IN K
C     HFH DENOTES THE HEAT OF VAPORISATION IN kJ/kg

      PH=1000./(1.22961-0.0018*TH+3.483E-6*TH**2)
      HFH=2306.62+2.31058*TH -0.00655*TH**2
      UH=(4032.3786-17.26126*TH+0.0193*TH**2)/1000000.
      CPH=6.17287-0.01149*TH+1.67E-05*TH**2
      KH=(-446.29124+5.57289*TH-0.00684*TH**2)/1000000.
      WH=Q/HFH
      T=WH/(3.1415*(13.7/1000.))
      NREH=4.0*T/UH
      G=((WH**2*PH**2*9.81)/(29.6*(13.7E-03)**2*UH))**(0.33333)
      PRH=(CPH*UH/KH)
      HI=(((CPH*G)/PRH)*5.35/(4.0*T/UH))

C     THE FOLLOWING STEPS CALCULATE RESISTANCE OF THE METAL WALL (RM)
```

```
C     K DENOTES THE THERMAL CONDUCTIVITY OF THE METAL WALL

      K=16.1/1000.
      RM=LOG(19.1/13.7)/(2.0*3.1415*1.40*K)
      AO=3.1415*(19.1/1000.)*1.40

C     CALCULATE OVERALL HEAT TRANSFER COEFFICIENT FROM THE INDIVIDUAL
C     HEAT TRANSFER COEFFICIENTS

      UO=1./(1./(HI*(DO/DI))+RM*AO+1./HO)
      WRITE (6,100) HI,HO,NREH,HOG,UO
100   FORMAT ('HI = ',1X,F7.4,//,'HO = ',1X,F7.4,//,'NREH = ',1X,
     1F6.1,//,'HOG = ',1X,F7.4,//,'UO = ',1X,F7.4)
      STOP
      END
```

FIGURE III-5 COMPUTER PROGRAM TO CALCULATE THE SHEAR STRESSES AND THE PRESSURE DROPS

```
C     THIS PROGRAM CALCULATES THE REMOVAL SHEAR STRESSES AND
C     PRESSURE DROP ACROSS THE HEAT EXCHANGER

      REAL NREF,NREC,K,KD
      INTEGER RUN

C     ROT IS THE ROTAMETER READING, F IS THE VOLUMETRIC FLOW RATE IN
C     m**3/s, INPUT TEMPERATURES ARE IN DEGREE C. DELHE IS THE
C     MANOMETRIC HEIGHT DIFFERENTIAL IN cm. V IS THE VELOCITY IN m/s

      ROT=50.
      TC=19.6
      TH=50.9
      DELHE=5.0
      TC=TC+273.16
      TH=TH+273.16
      F=(0.79032*ROT+0.63147)/100000.
      V=4.0*F/(3.1415*((38.1/1000.)**2-(19.1/1000.)**2))
      RI=(19.1/2.)/1000.
      RO=(38.1/2.)/1000.
      DE=2.*(RO-RI)

C     CALCULATE THE AVG. FILM TEMP. IN DEG. K

      TF=0.5*(TC+TH)

C     FIND LIQUID DENSITY (P) AND VISCOSITY (U) AS FUNCTION OF
C     TEMPERATURE. UNITS OF DENSITY AND VISCOSITY ARE kg/cm**3,Nm/s**2

      PF=1000./(1.+(TF-285.)*0.0002)
      PC=1000./1.002
      UF=(4032.3786-17.26126*TF+0.0193*TF**2)/1000000.
      UC=(65816.34444-418.2856*TC+0.67255*TC**2)/1000000.

C     FIND BULK & FILM REYNOLDS NUMBERS & SCHMIDT NUMBER (SC)

      NREF=V*DE*PF/UF
      NREC=V*DE*PC/UC

C     DIFFUSION COEFFICIENT OF ALL THE IONS IS APPROXIMATED
C     AS 10.**-9 m**2/s AT 25 DEG. CENTIGRADE

      SC=UF/(PF*1.E-09)

C     CALCULATE MASS TRANSFER COEFFICIENT (KD) IN THE FILM
C     UNITS ARE m/s

      KD=0.023*V*NREF**(-0.17)*SC**(-0.666)

C     CALCULATE DELPE, THE EXPERIMENTAL PRESSURE DIFFERENCE IN N/m**2

      DELPE=(1750.-1000.)*9.81*DELHE/100.

C     CALCULATE DELPT, THE THERETICAL PRESSURE DIFFERENCE IN N/m**2

      FI=.0791/(NREF**.25)
      FO=.0791/(NREC**.25)
      DELPT=2.*0.6*0.5*PF*V**2*(RI*FI+RO*FO)/(RO**2-RI**2)
```

```
C     CALCULATE TRZ, SHEAR STRESSES AT THE SCALE LIQUID INTERFACE
C     UNITS ARE N/m**2

      TO=DELPT*RO/(2.*0.6)
      K=RI/RO
      TRZ=TO*(K-(1.-K**2)/(2.*K*LOG(1./K)))
      WRITE(6,100) KD,DELPE,DELPT,TRZ,NREC,NREF,FI,FO,V,UF,PF
100   FORMAT (1X,'   KD    DELPE  DELPT   TRZ  ',4(1X,E9.3))
      STOP
      END
```

FIGURE III-6 COMPUTER PROGRAM TO CALCULATE THE SHEAR STRESS AND THE PRESSURE DROP AS A FUNCTION OF VELOCITY

```
C     THIS PROGRAM CALCULATES THE REMOVAL SHEAR STRESSES AND
C     PRESSURE DROP ACROSS THE HEAT EXCHANGER UNDER NO STEAM CONDITION
C     FOR DIFFERENT FLOW RATES OF WATER

      REAL NREC,K,KD
      INTEGER RUN

C     ROT IS THE ROTAMETER READING, F IS THE VOLUMETRIC FLOW RATE IN
C     m**3/s, INPUT TEMPERATURES ARE IN DEGREE C. DELHE IS THE
C     MANOMETRIC HEIGHT DIFFERENTIAL IN cm. V IS THE VELOCITY IN m/s

      ROT=0.0
10    ROT=ROT+5.0
      TC=20.0
      TC=TC+273.16
      F=(0.79032*ROT+0.63147)/100000.
      V=4.0*F/(3.1415*((38.1/1000.)**2-(19.1/1000.)**2))
      RI=(19.1/2.)/1000.
      RO=(38.1/2.)/1000.
      DE=2.*(RO-RI)

C     FIND LIQUID DENSITY (P) AND VISCOSITY (U) AS FUNCTION OF
C     TEMPERATURE. UNITS OF DENSITY AND VISCOSITY ARE kg/cm**3,Nm/s**2

      PC=1000./1.002
      UC=(65816.34444-418.2856*TC+0.67255*TC**2)/1000000.

C     FIND BULK & FILM REYNOLDS NUMBERS & SCHMIDT NUMBER (SC)

      NREC=V*DE*PC/UC

C     CALCULATE DELPE, THE EXPERIMENTAL PRESSURE DIFFERENCE IN N/m**2

C     CALCULATE DELPT, THE THERETICAL PRESSURE DIFFERENCE IN N/m**2
C     FR DENOTES THE FRICTION FACTOR

      FR=.0791/(NREC**.25)
      DELPT=4.*0.6*0.5*PC*V**2*FR/DE

C     CALCULATE TRZ, SHEAR STRESSES AT THE SCALE LIQUID INTERFACE
C     UNITS ARE N/m**2

      TO=DELPT*RO/(2.*0.6)
      K=RI/RO
      TRZ=TO*(K-(1.-K**2)/(2.*K*LOG(1./K)))

      WRITE(6,100) ROT,V,NREC,DELPT,TRZ
100   FORMAT ('ROT   = ',F5.1,//,'VEL   = ',F6.4,//,'NREC  = ',E10.3,
     *//,'DELPT = ',E10.3,//,'TRZ   = ',E10.3,////)
      IF (ROT.LE.140.) GOTO 10
      GOTO 200
200   STOP
      END
```

APPENDIX IV

FOULING CURVES

The remainder of the fouling curves are shown in Figures IV-1 to IV-29. The outputs of the computer programs III-1 and III-2 for Run 2 are listed in Figures IV-30 and IV-31. The actual data points, temperatures etc. for each run are bound in a supplemental volume, available from Dr. A.P. Watkinson.

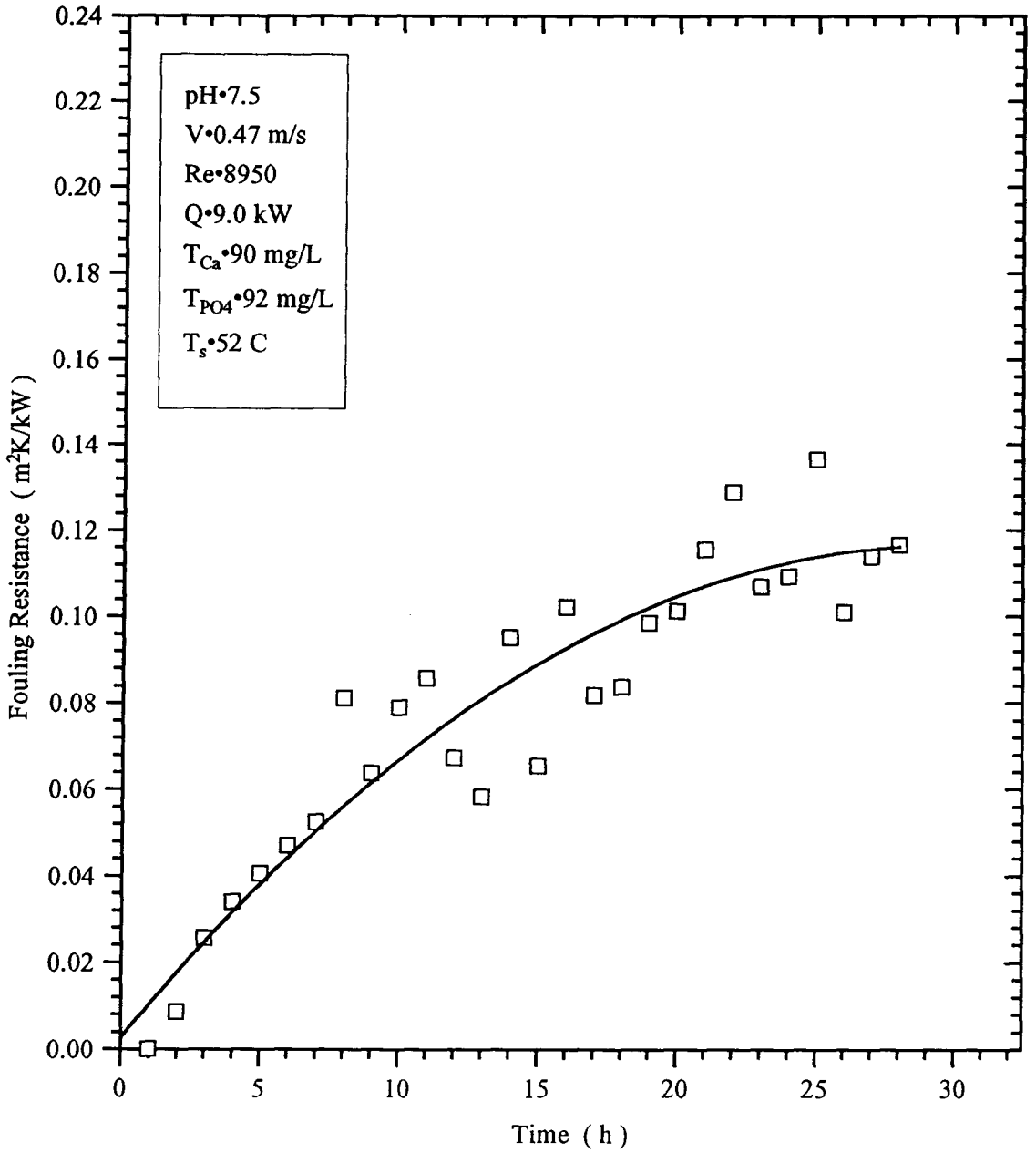

FIGURE IV-1 RUN 2 FOULING RESISTANCE VERSUS TIME

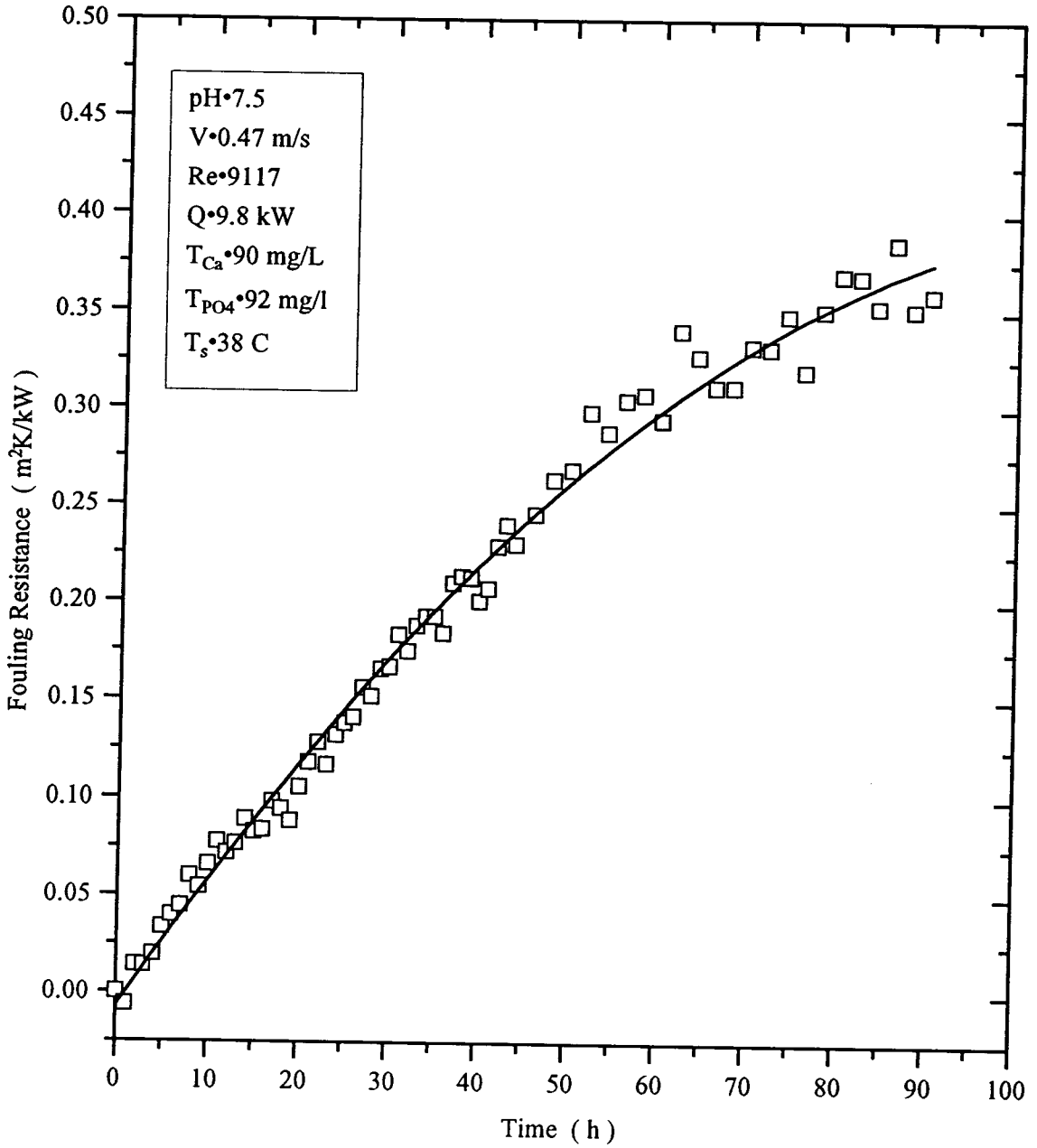

FIGURE IV-2 RUN 3 FOULING RESISTANCE VERSUS TIME

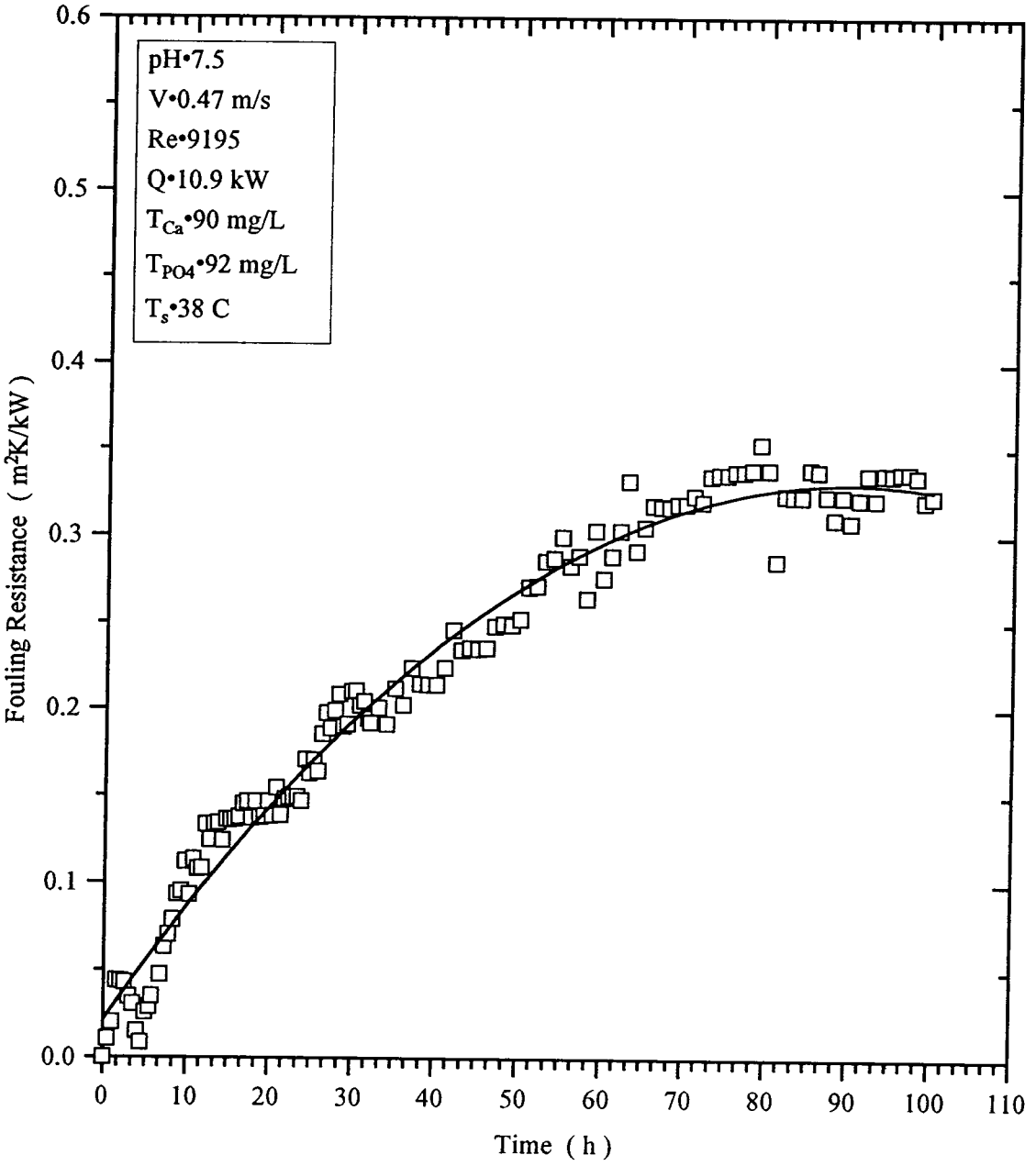

FIGURE IV-3 RUN 4 FOULING RESISTANCE VERSUS TIME

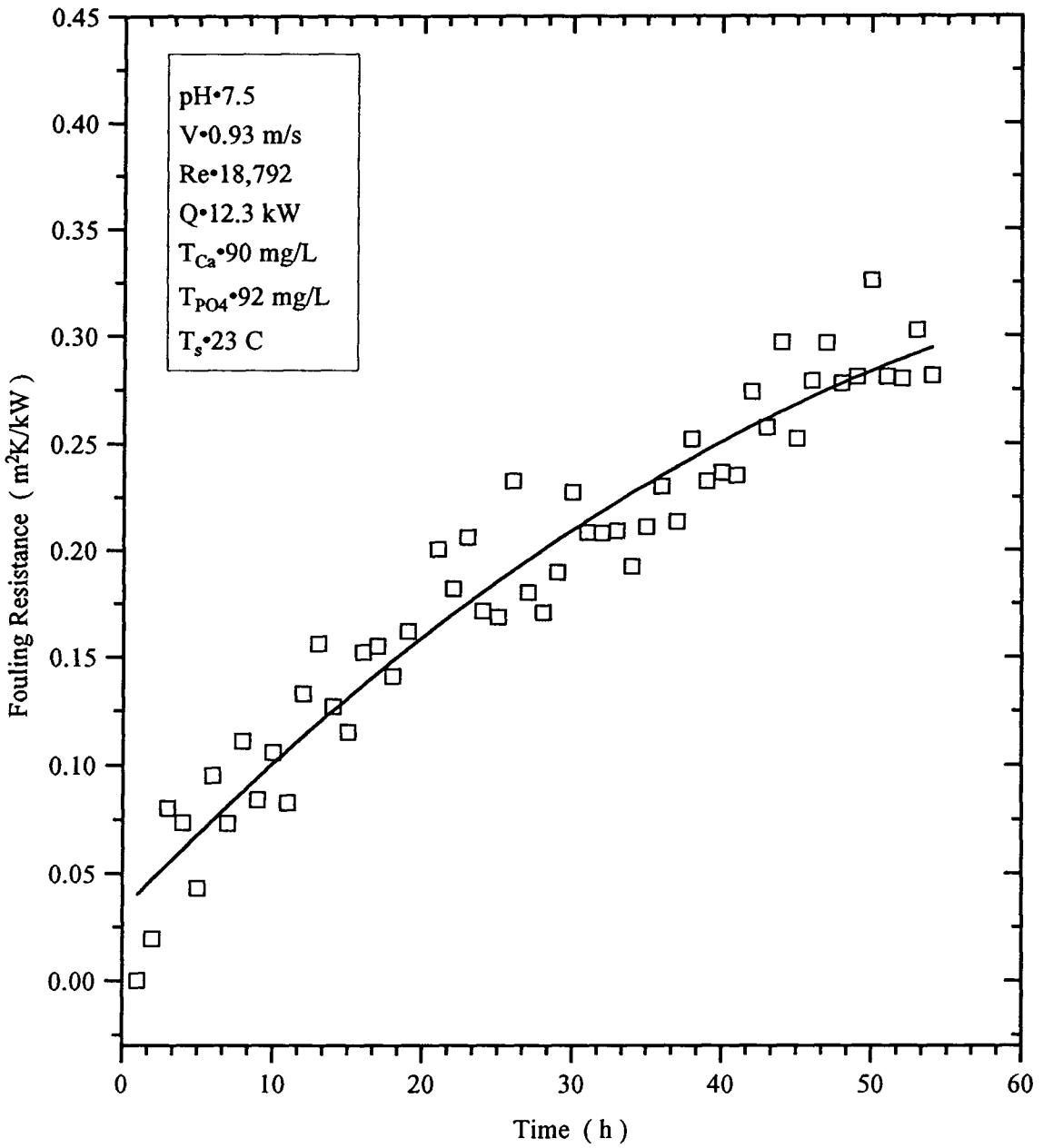

FIGURE IV-4 RUN 5 FOULING RESISTANCE VERSUS TIME

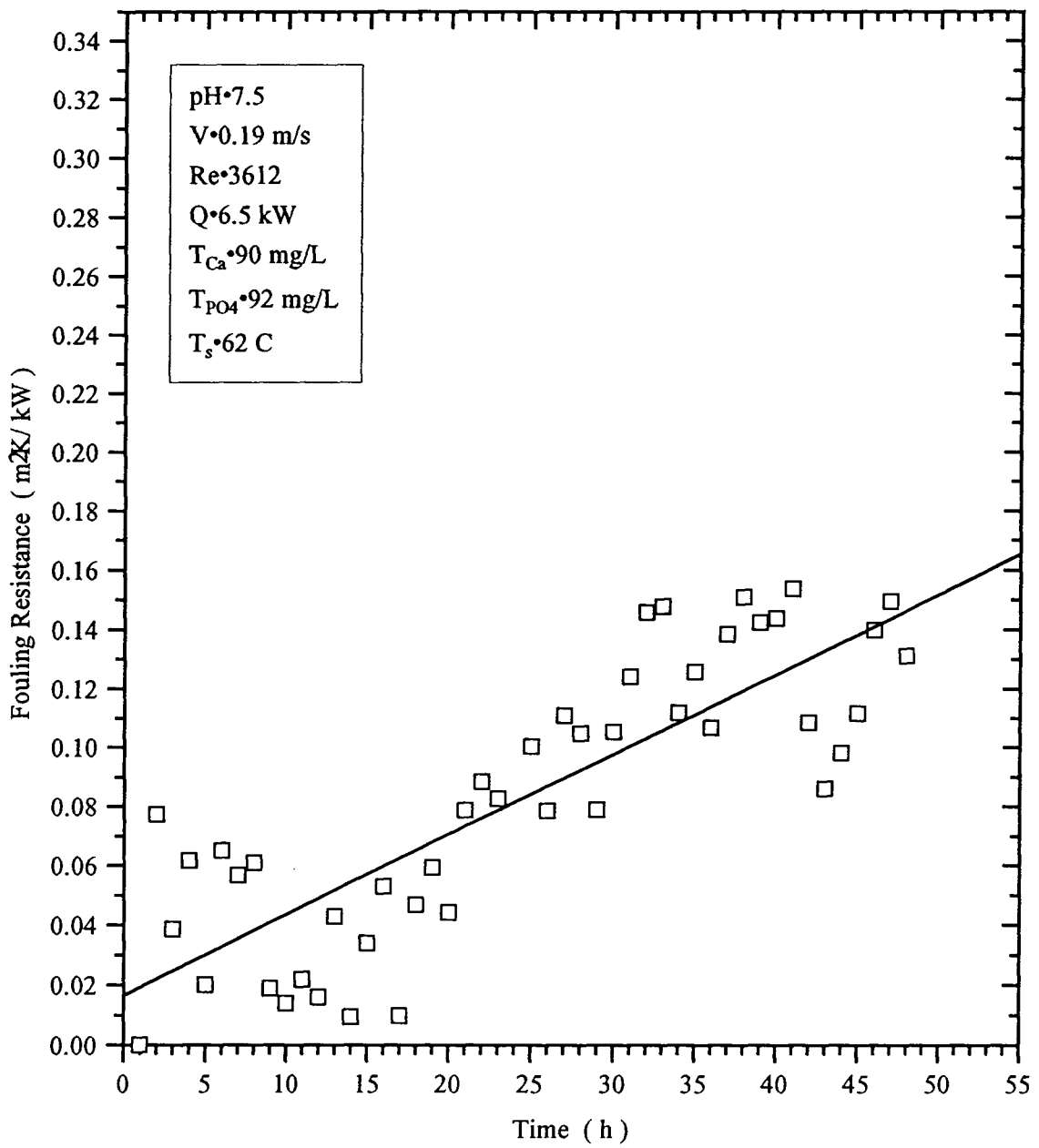

FIGURE IV-5 RUN 6 FOULING RESISTANCE VERSUS TIME

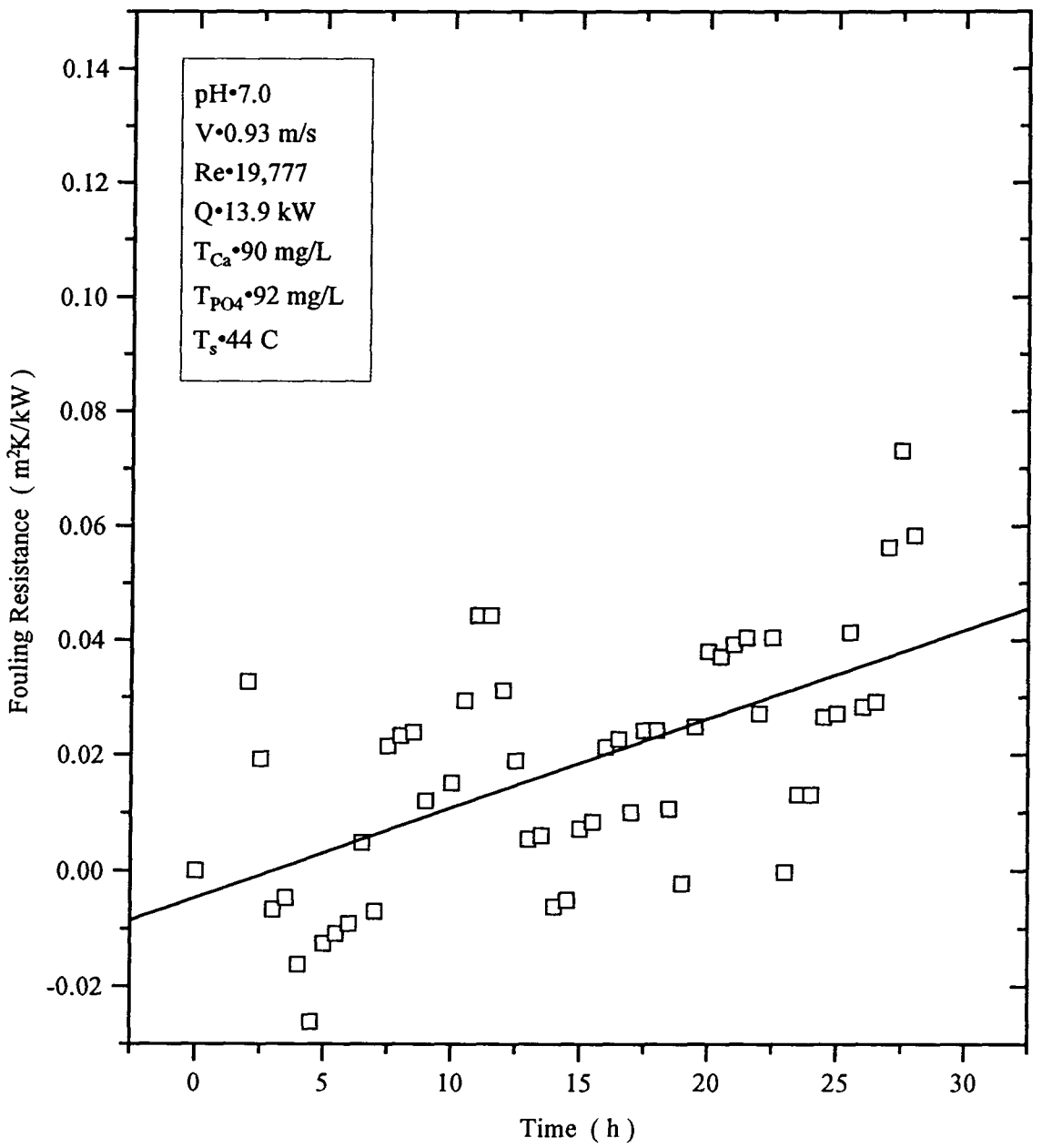

FIGURE IV-6 RUN 7 FOULING RESISTANCE VERSUS TIME

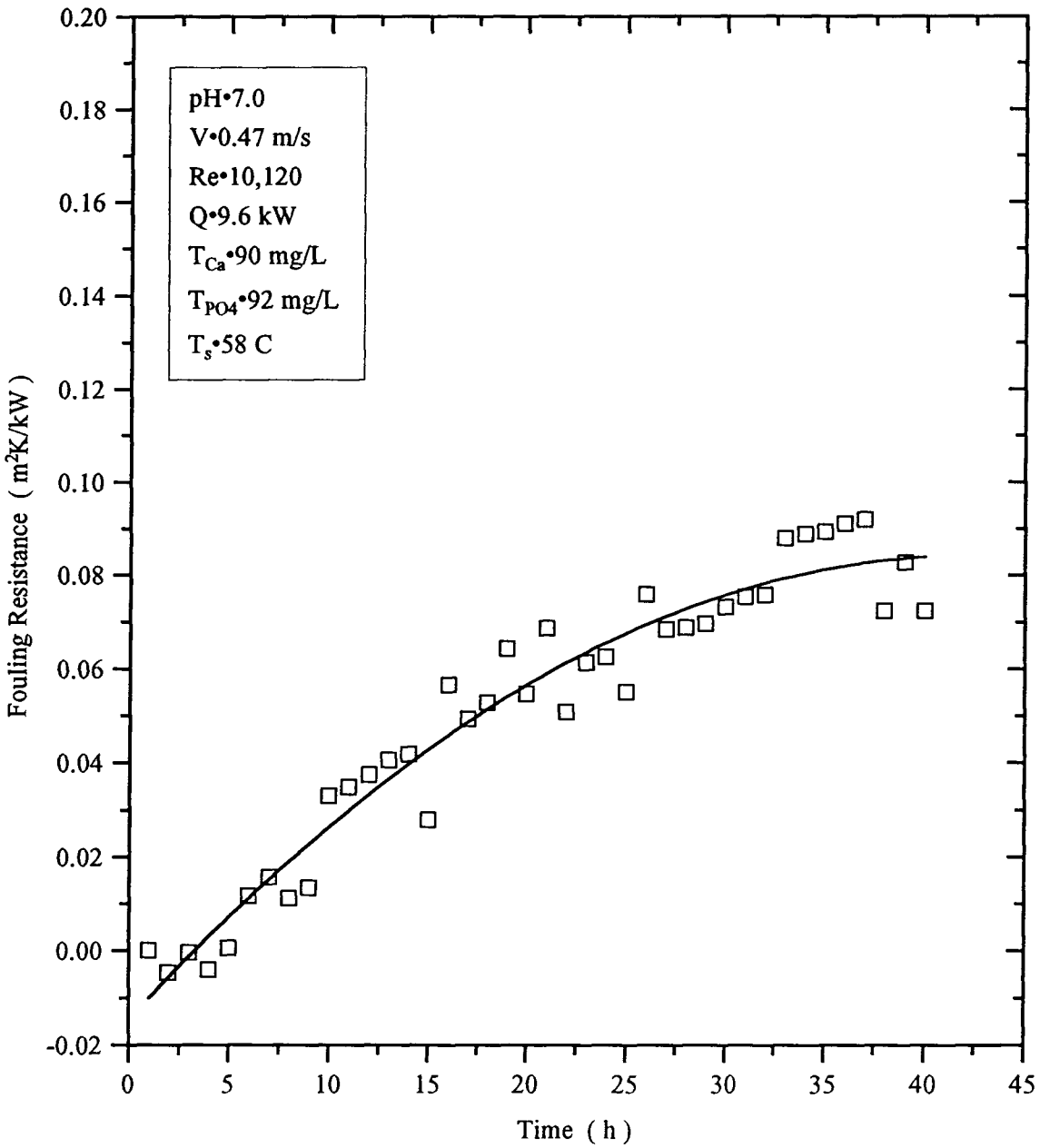

FIGURE IV-7 RUN 8 FOULING RESISTANCE VERSUS TIME

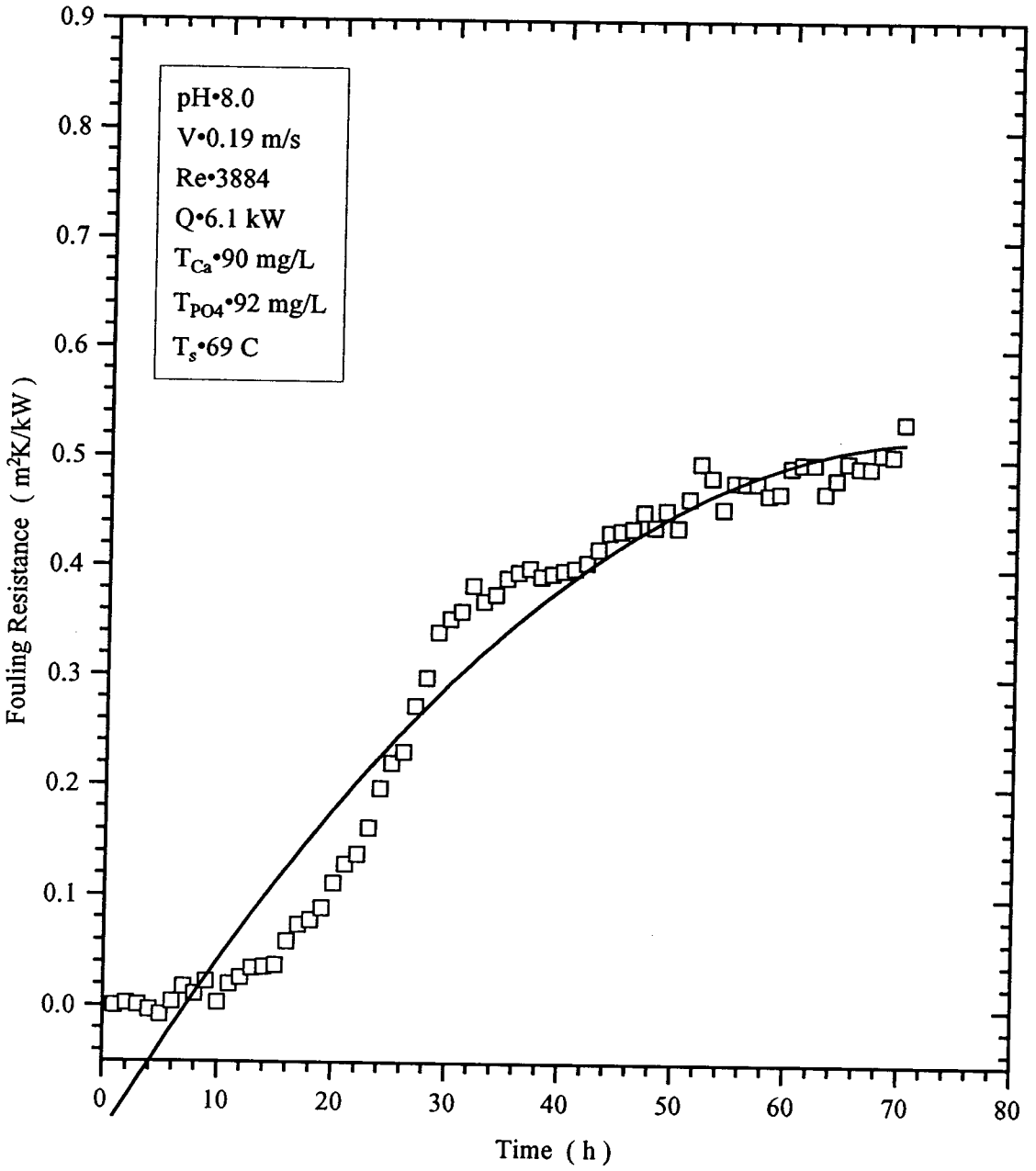

FIGURE IV-8 RUN 9 FOULING RESISTANCE VERSUS TIME

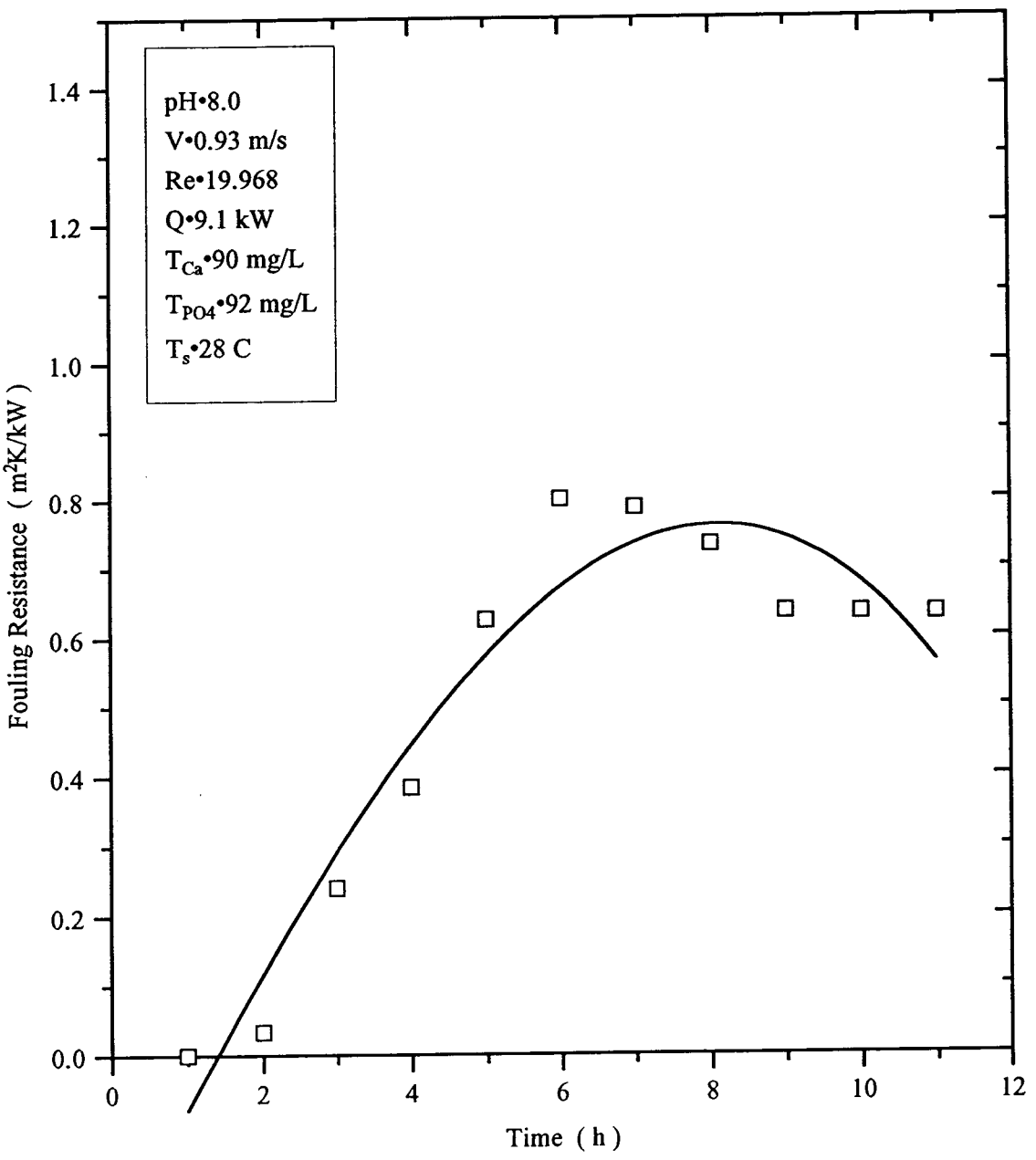

FIGURE IV-9 RUN 10 FOULING RESISTANCE VERSUS TIME

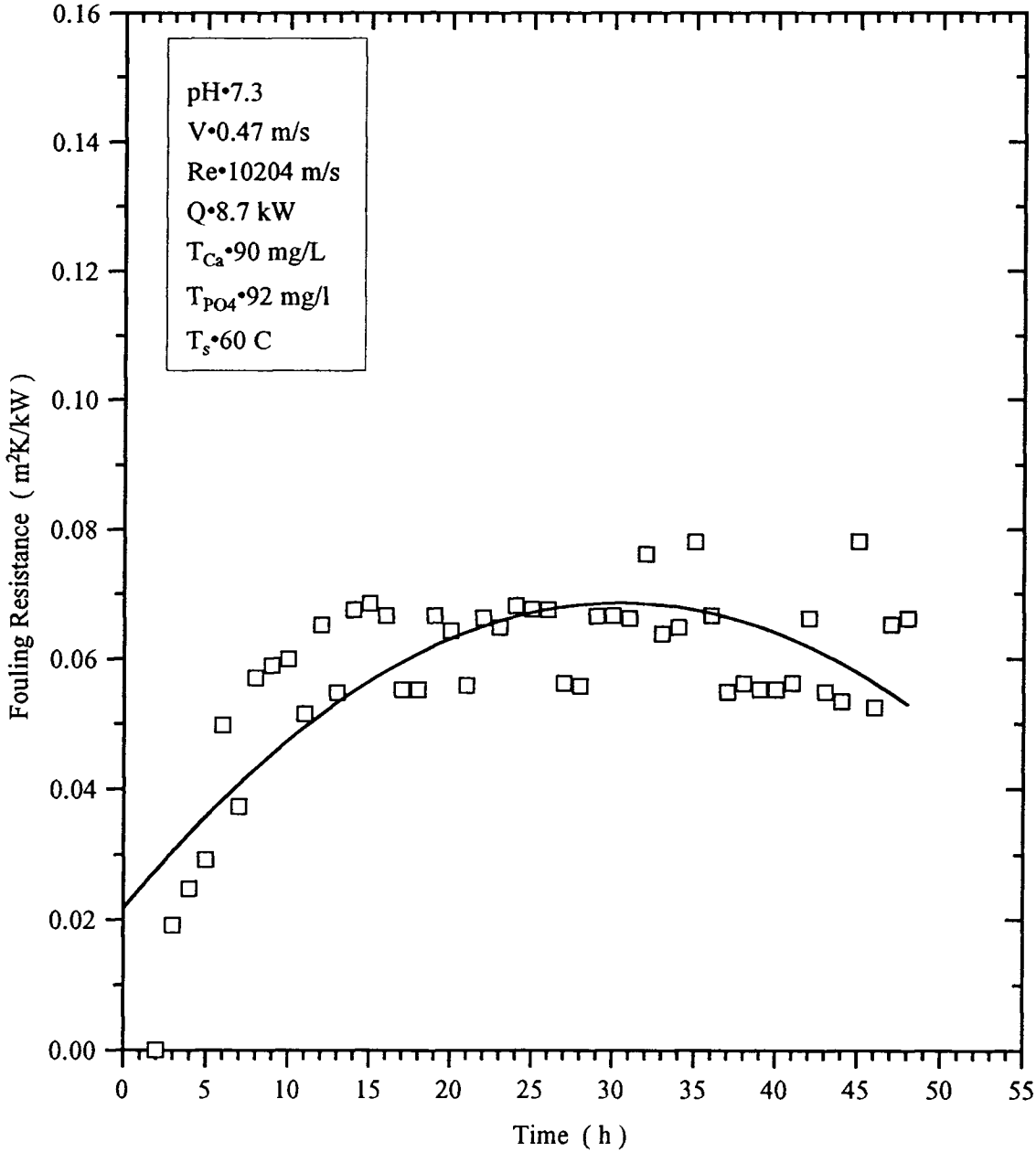

FIGURE IV-10 RUN 12 FOULING RESISTANCE VERSUS TIME

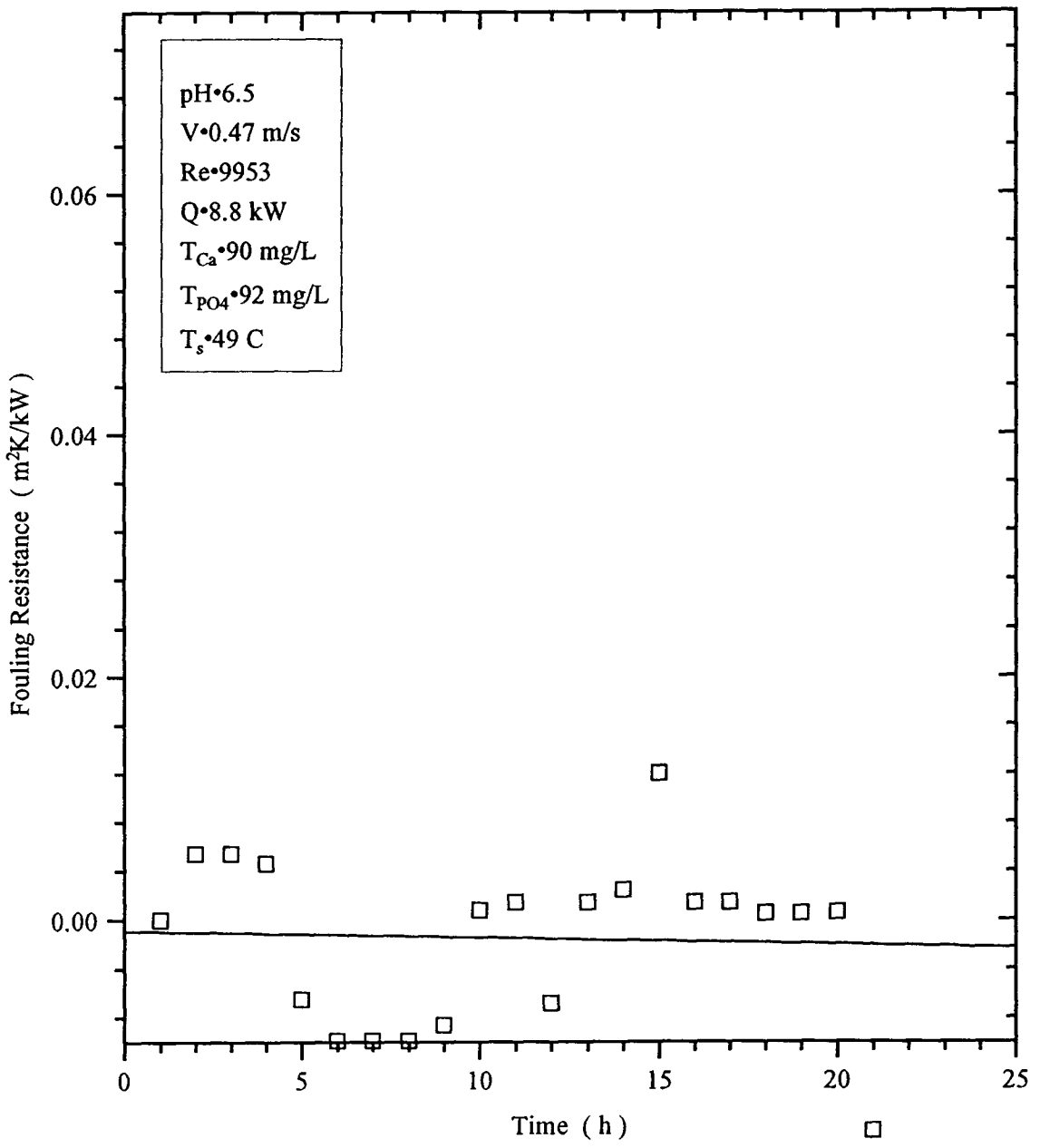

FIGURE IV-11 RUN 13 FOULING RESISTANCE VERSUS TIME

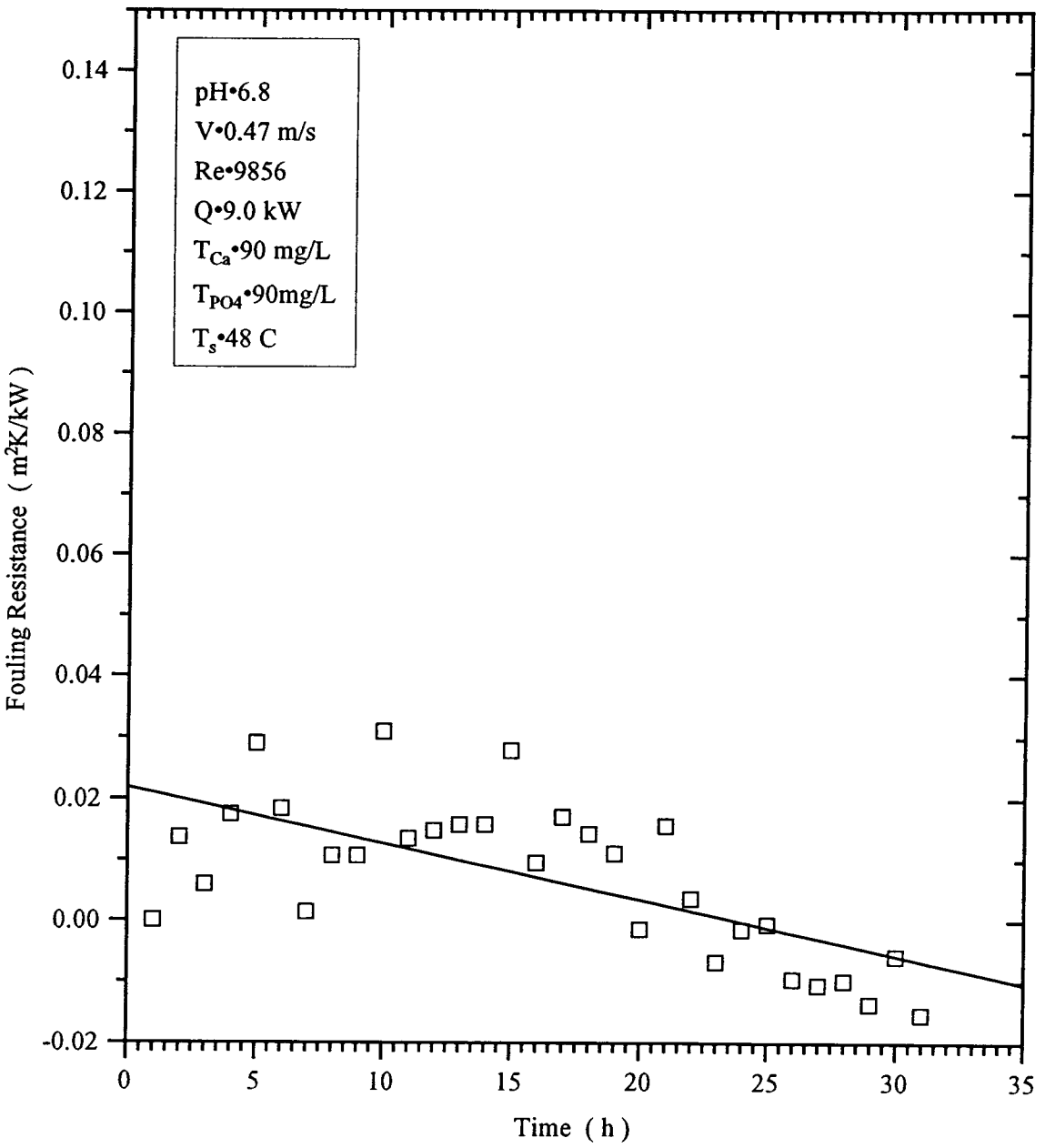

FIGURE IV-12 RUN 14 FOULING RESISTANCE VERSUS TIME

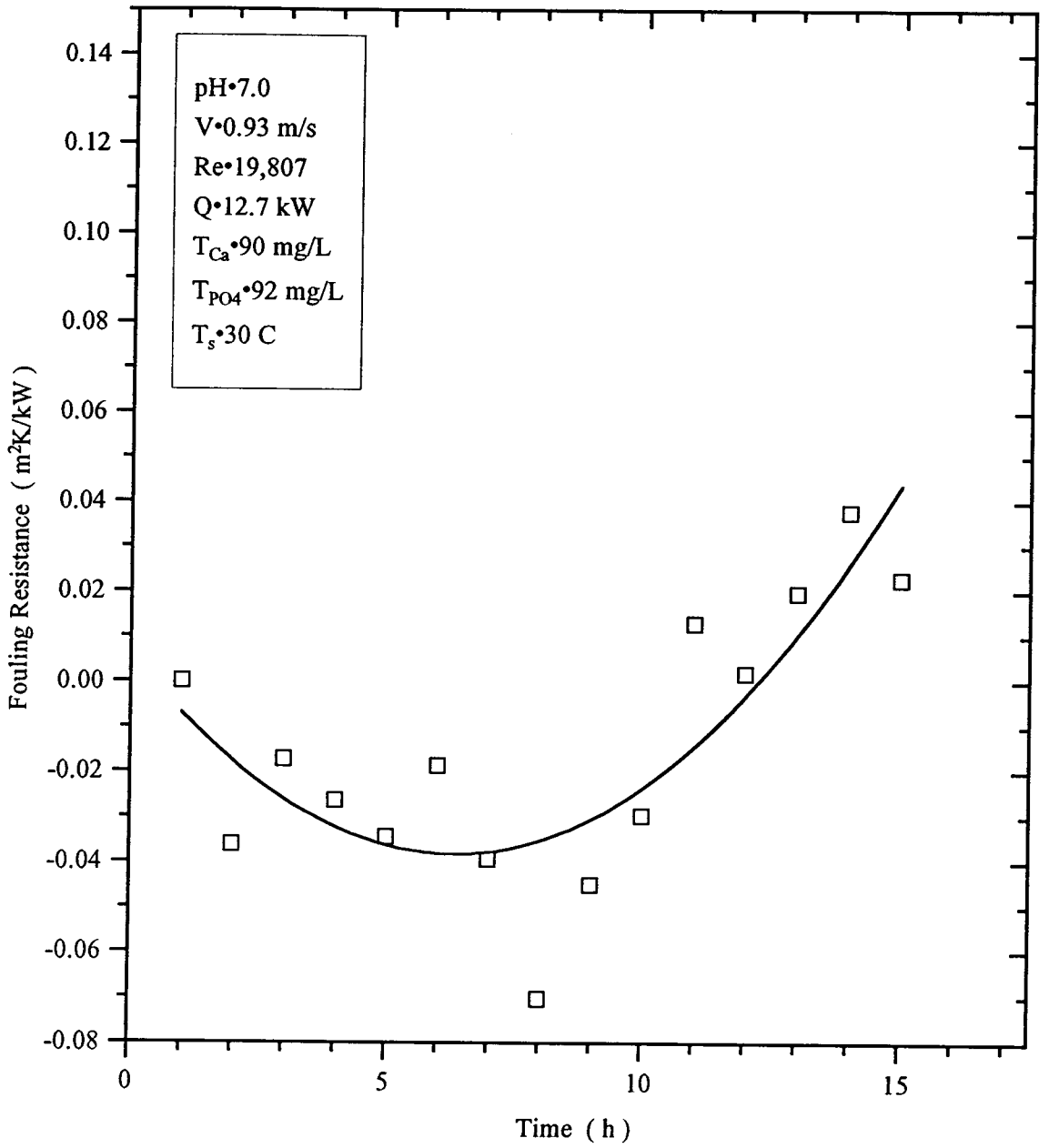

FIGURE IV-13 RUN 15 FOULING RESISTANCE VERSUS TIME

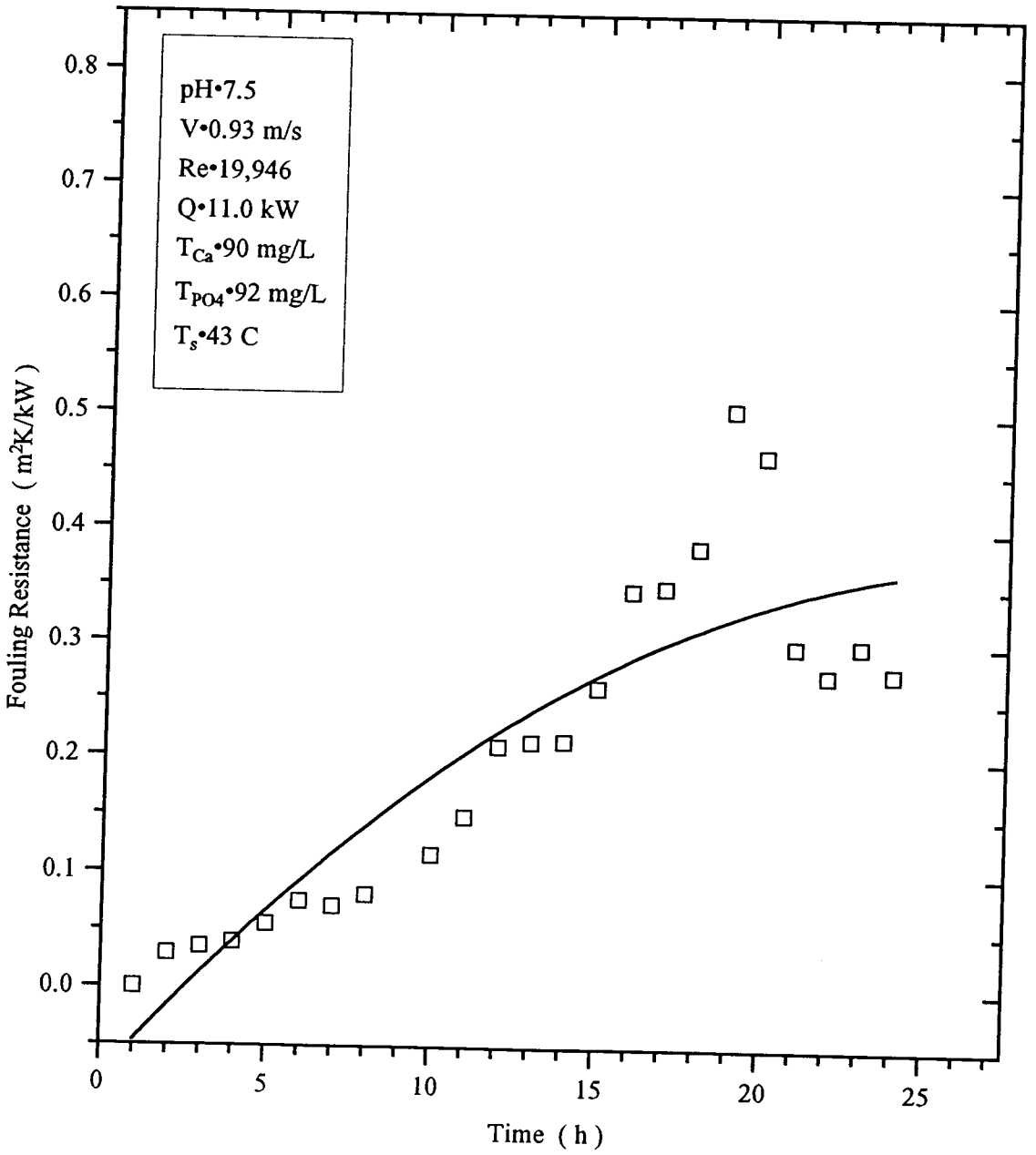

FIGURE IV-14 RUN 16 FOULING RESISTANCE VERSUS TIME

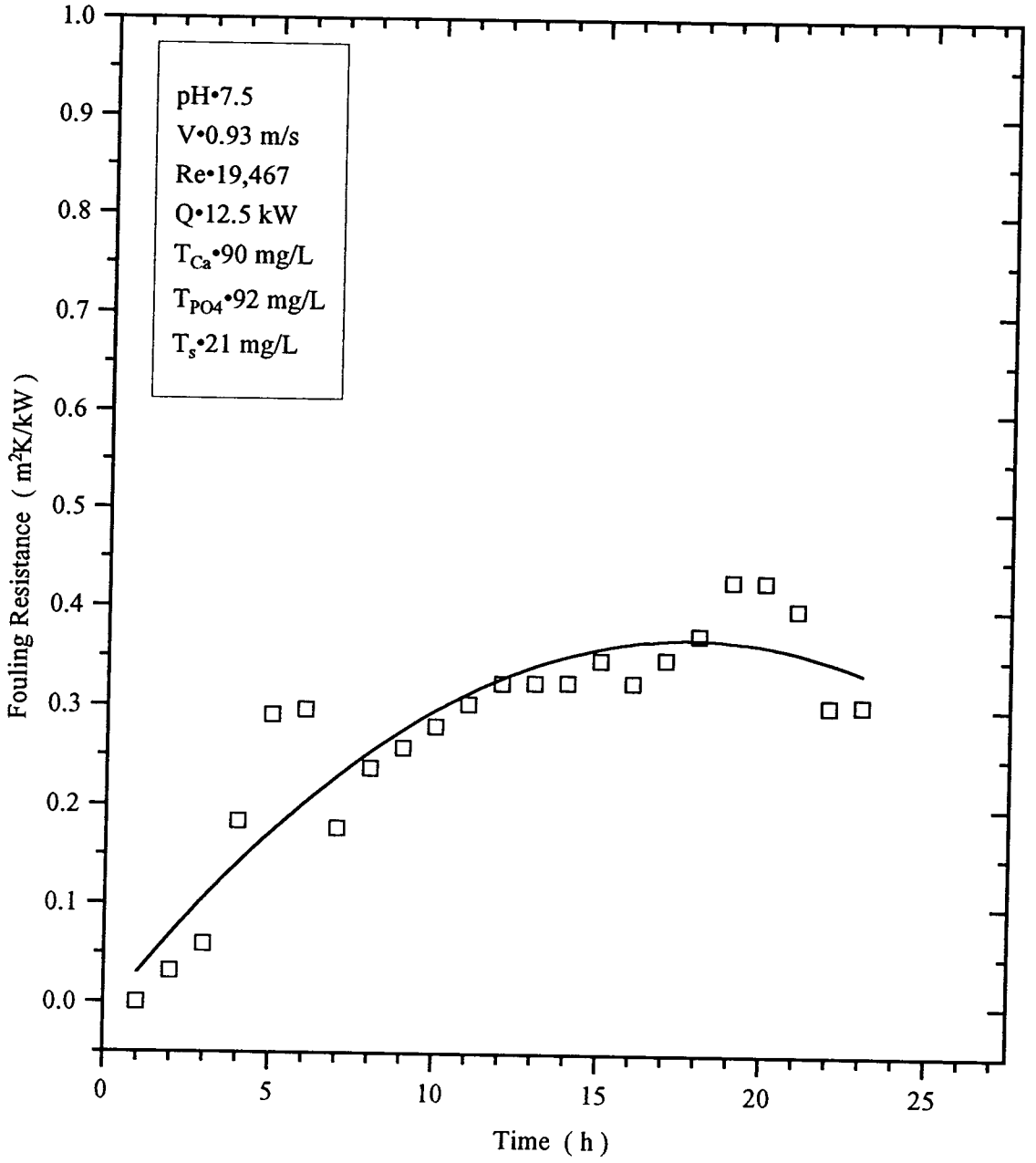

FIGURE IV-15 RUN 17 FOULING RESISTANCE VERSUS TIME

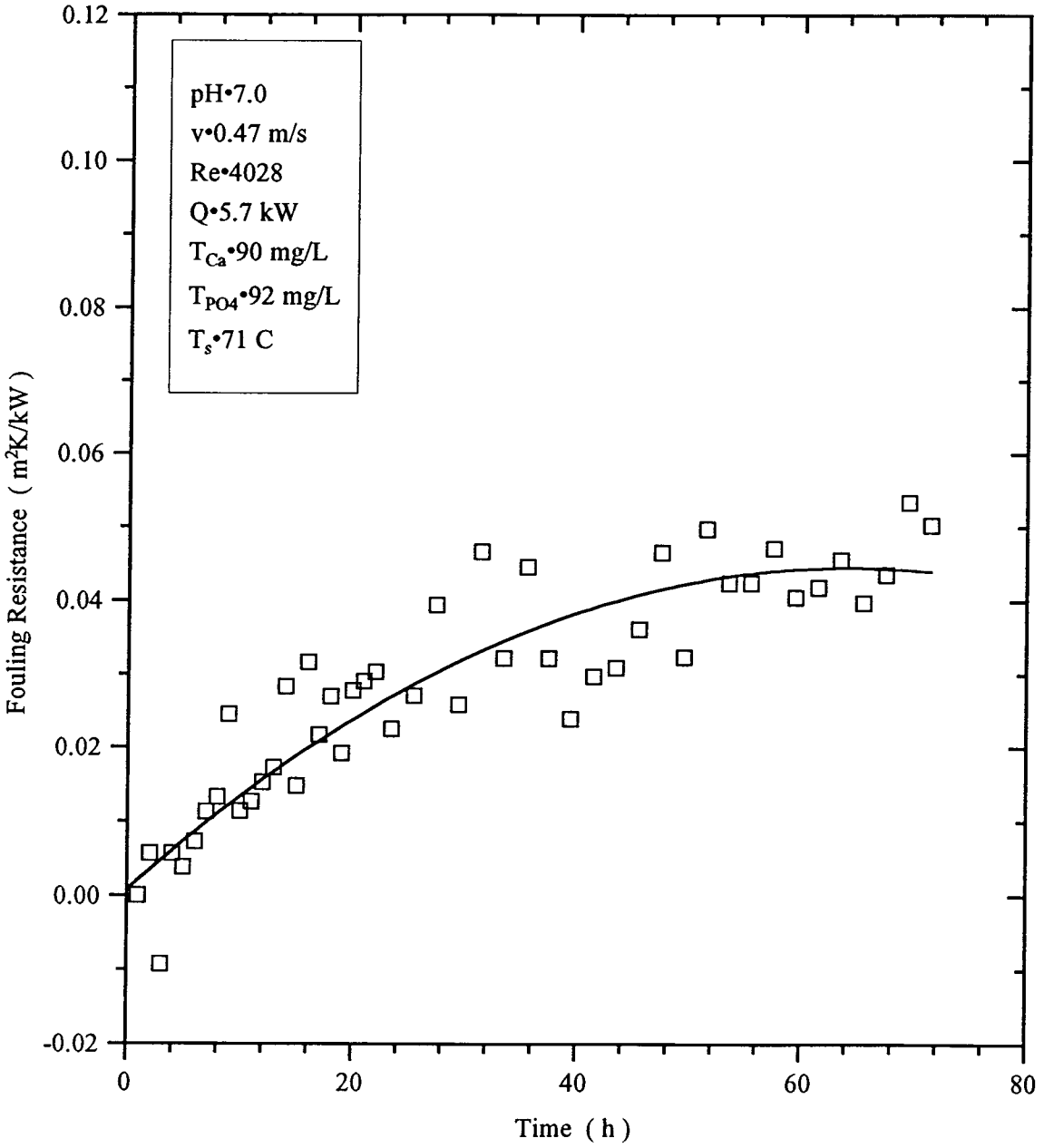

FIGURE IV-16 RUN 18 FOULING RESISTANCE VERSUS TIME

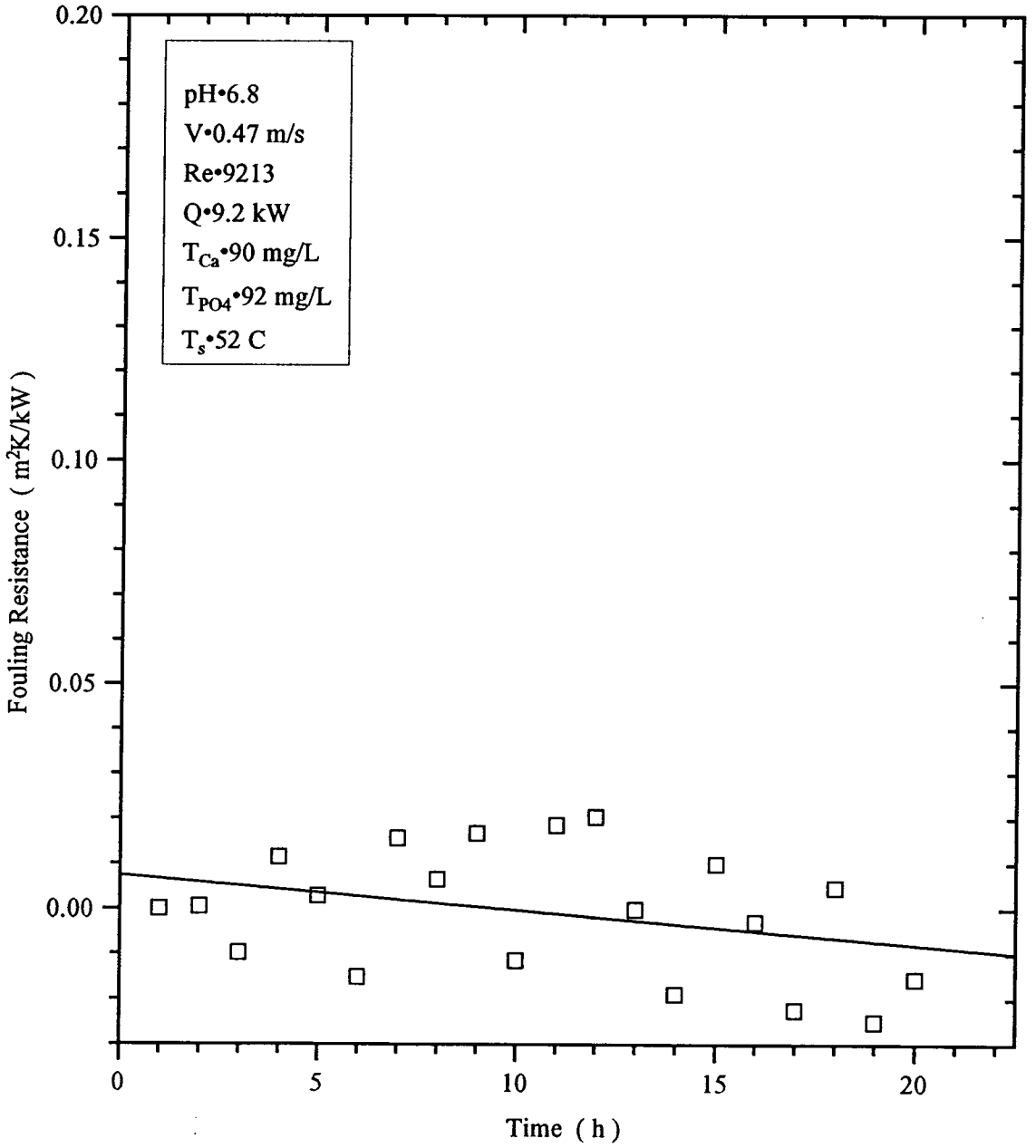

FIGURE IV-17 RUN 19 FOULING RESISTANCE VERSUS TIME

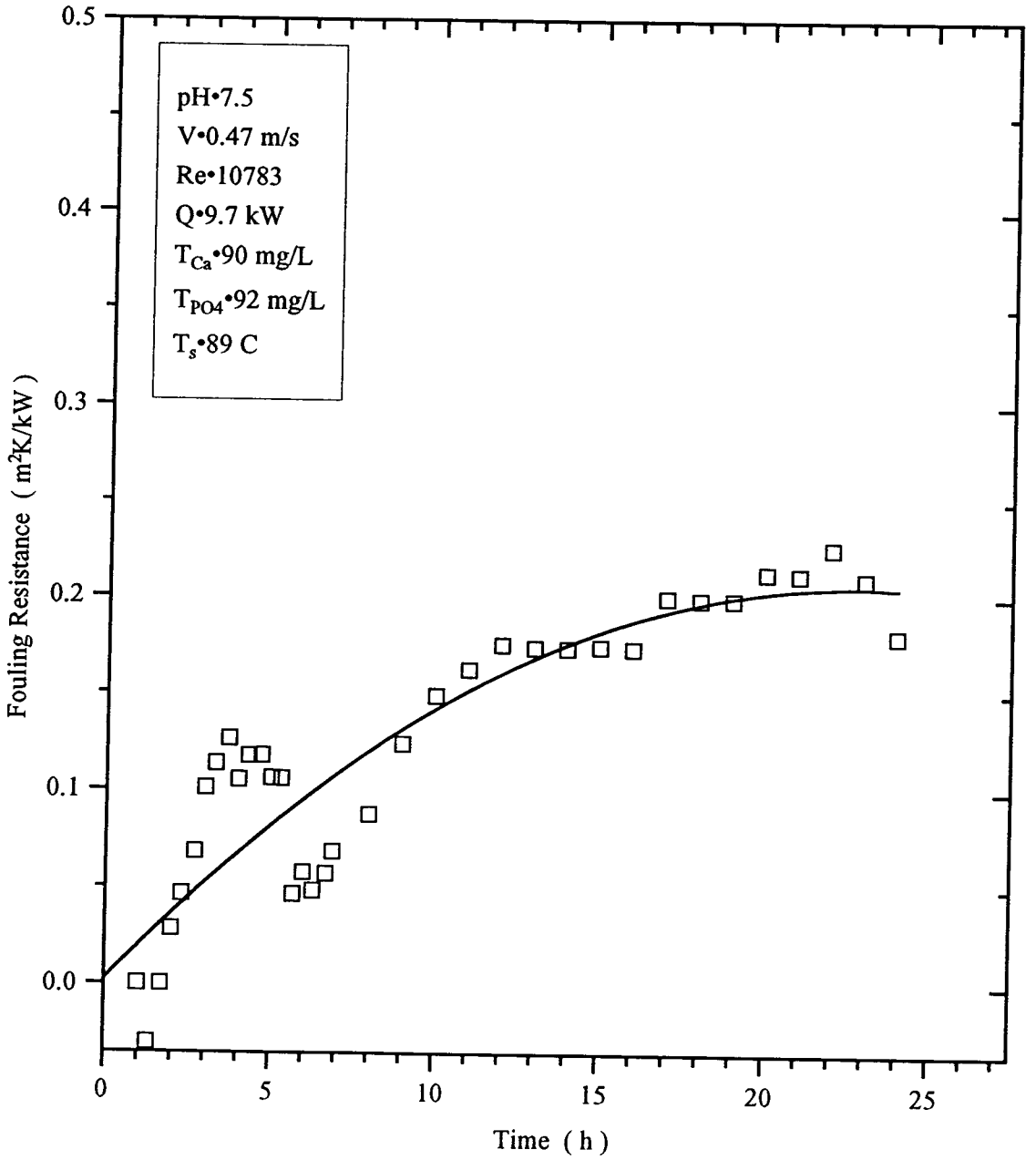

FIGURE IV-18 RUN 20 FOULING RESISTANCE VERSUS TIME

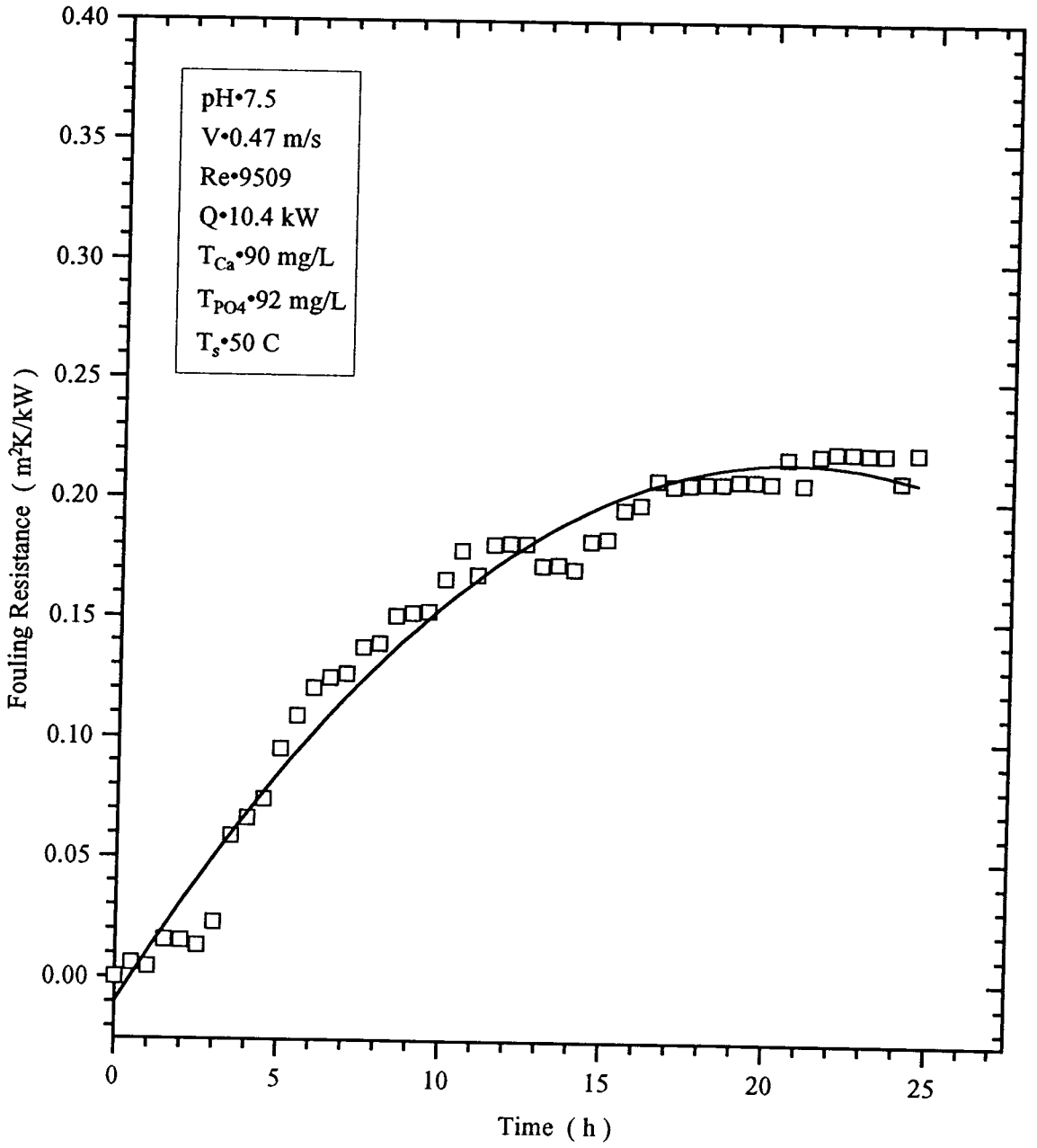

FIGURE IV-19 RUN 22 FOULING RESISTANCE VERSUS TIME

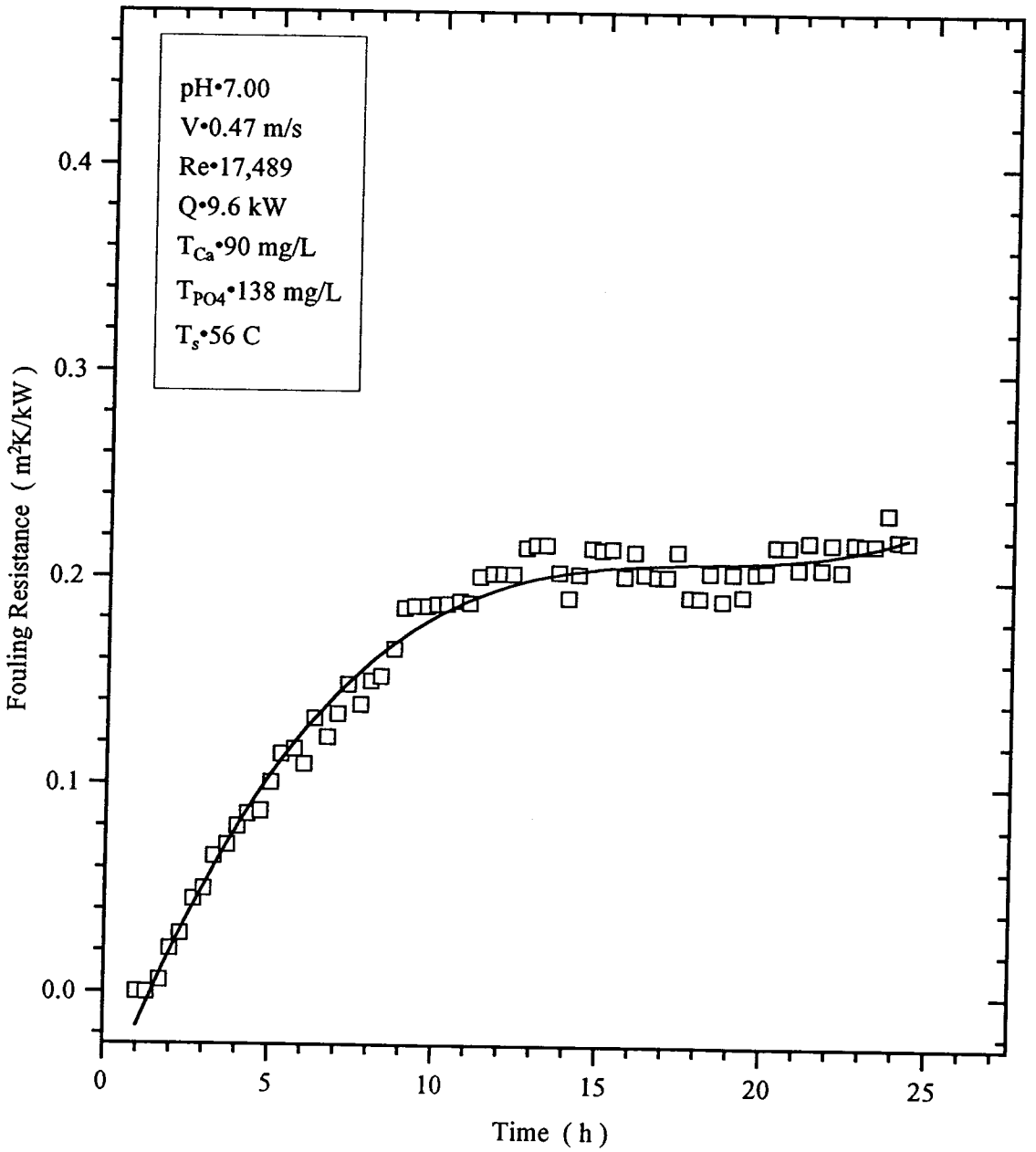

FIGURE IV-20 RUN 24 FOULING RESISTANCE VERSUS TIME

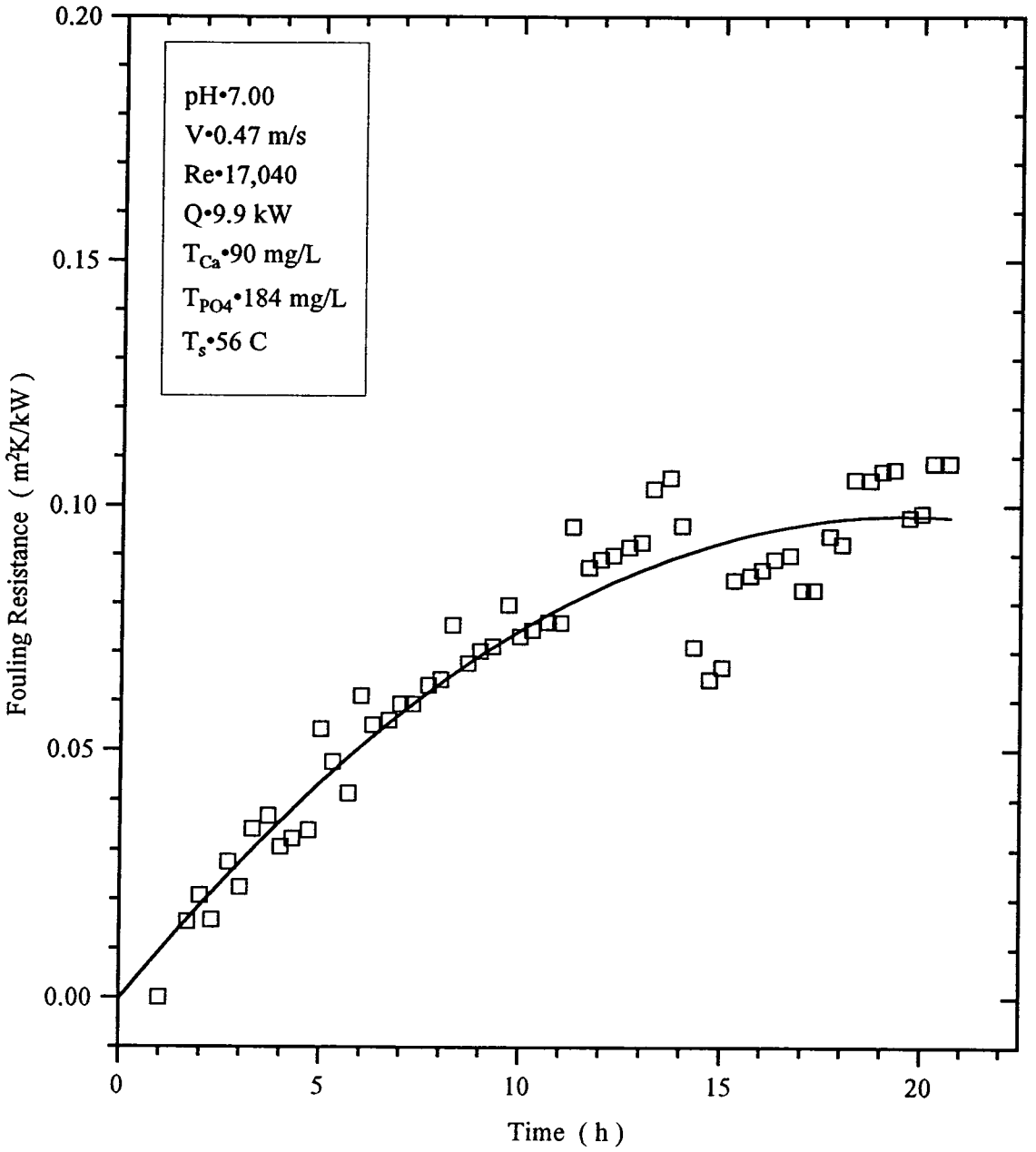

FIGURE IV-21 RUN 25 FOULING RESISTANCE VERSUS TIME

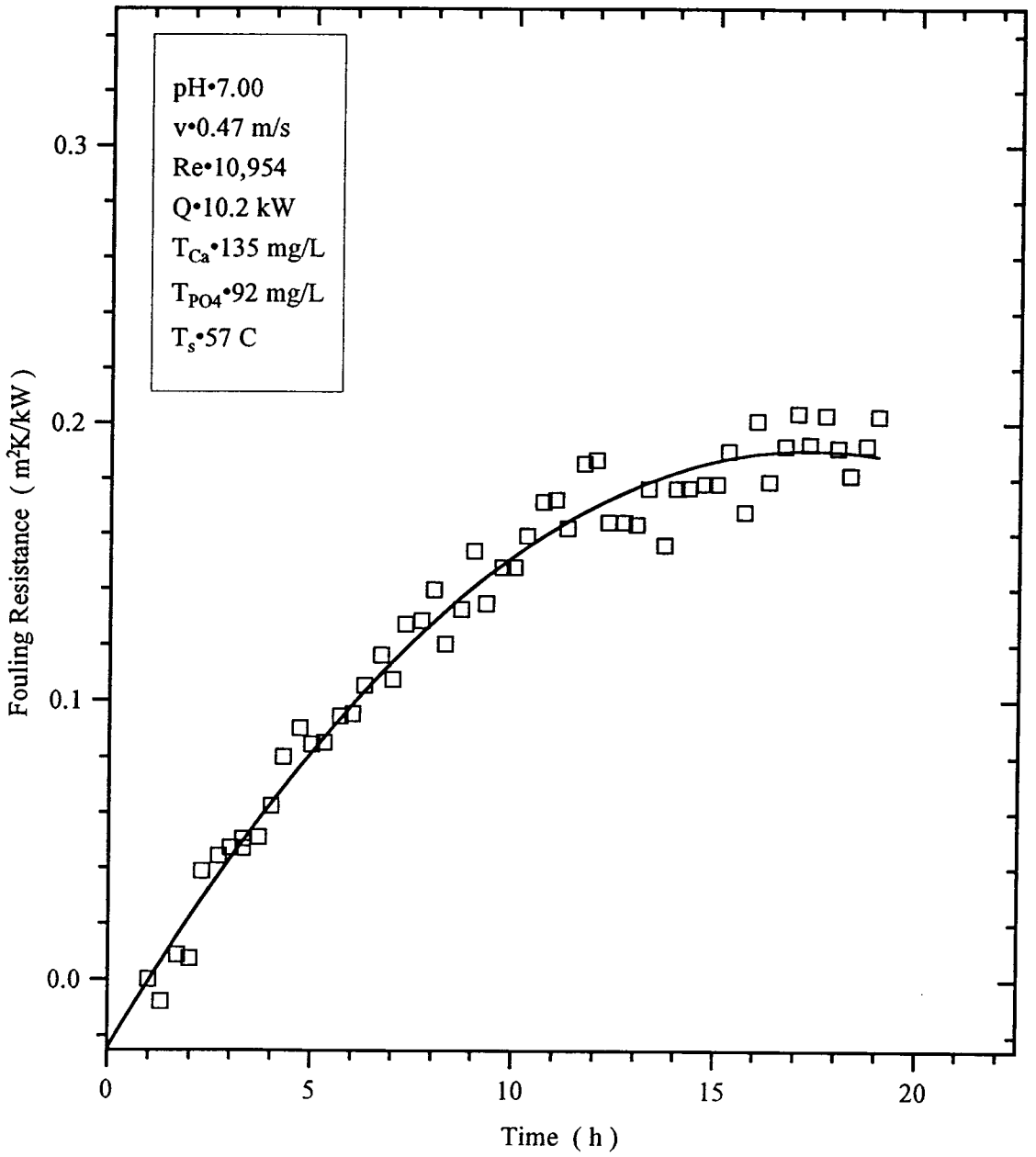

FIGURE IV-22 RUN 26 FOULING RESISTANCE VERSUS TIME

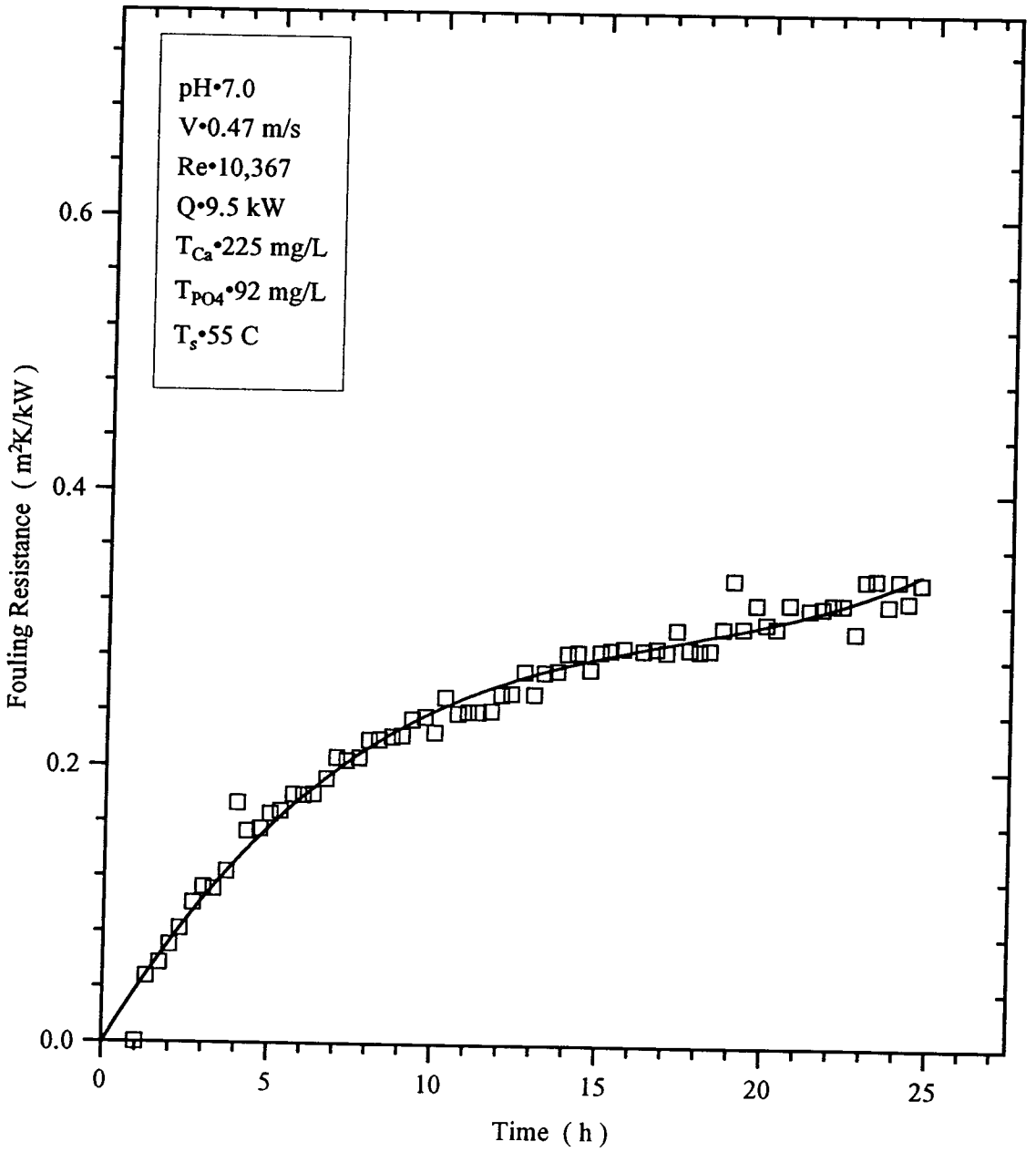

FIGURE IV-23 RUN 27 FOULING RESISTANCE VERSUS TIME

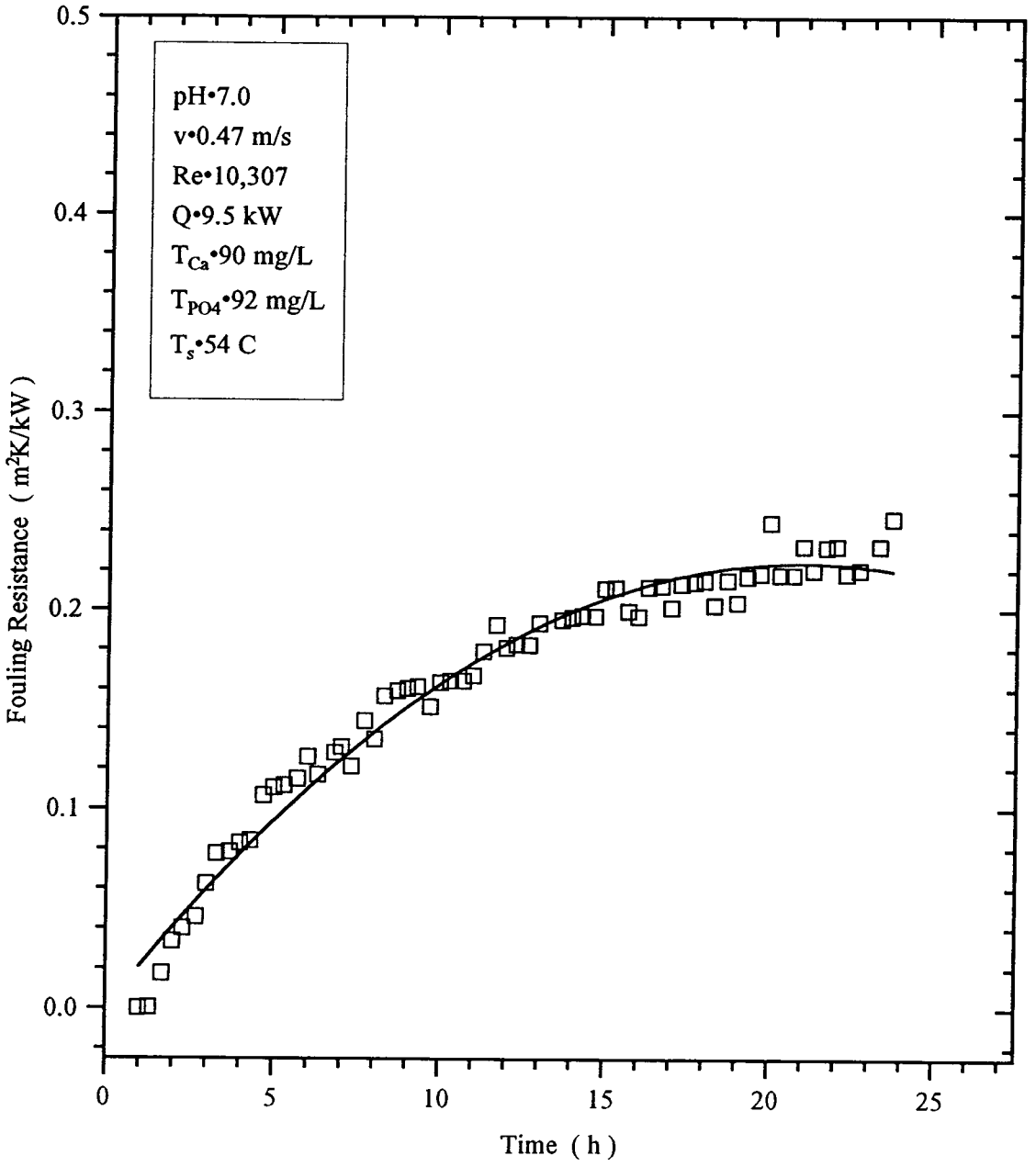

FIGURE IV-24 RUN 28 FOULING RESISTANCE VERSUS TIME

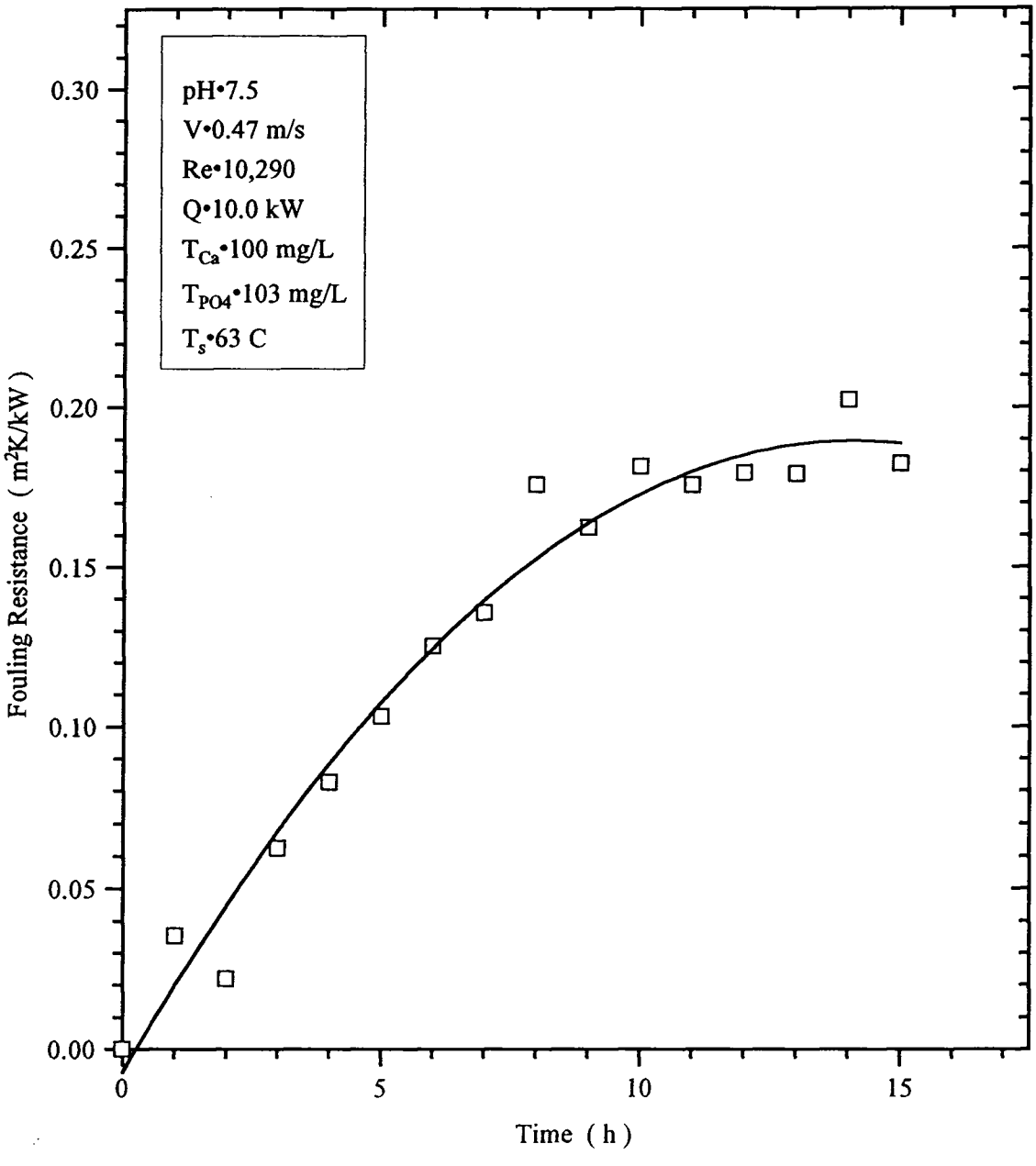

FIGURE IV-25 RUN 29 FOULING RESISTANCE VERSUS TIME

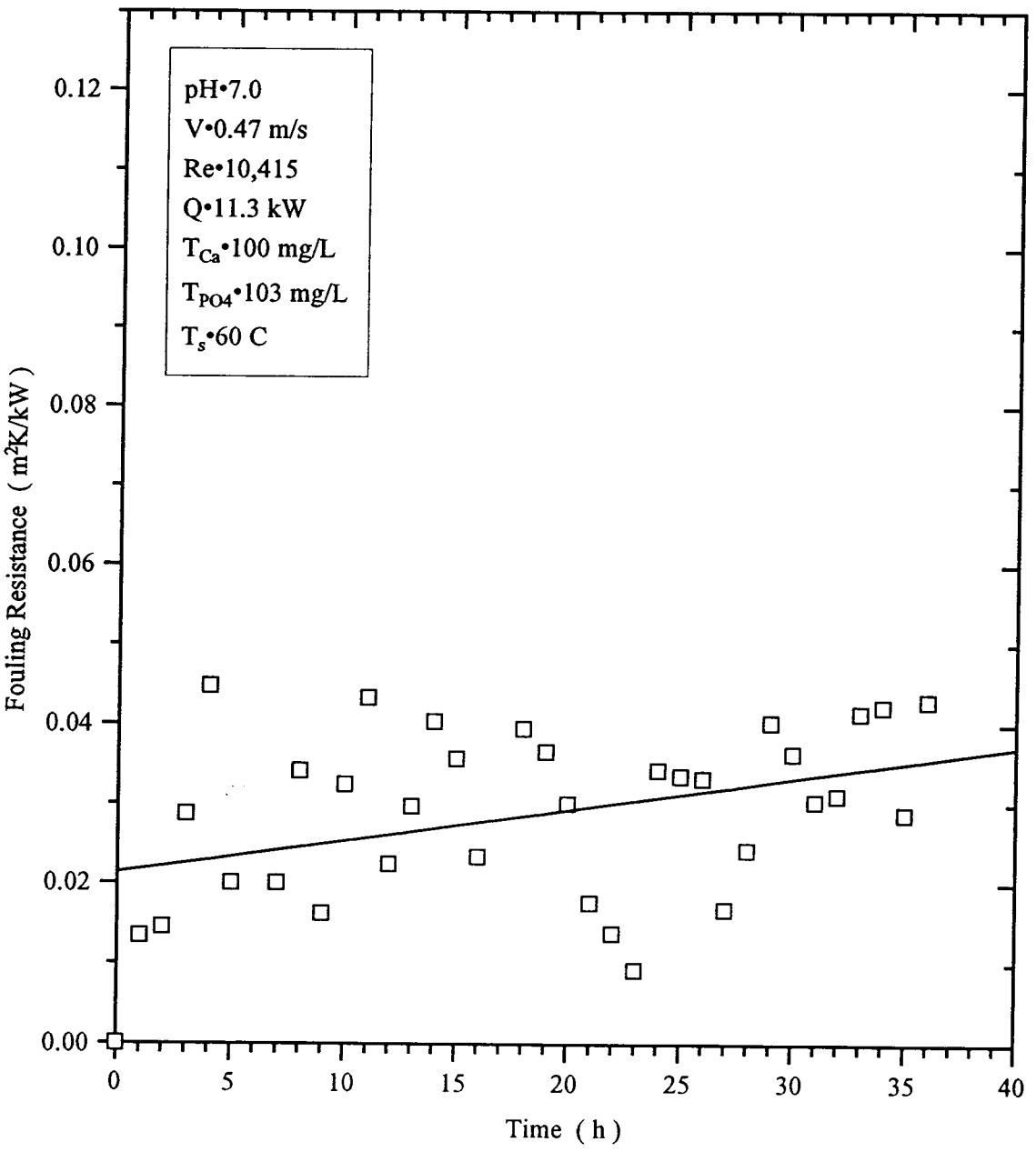

FIGURE IV-26 RUN 30 FOULING RESISTANCE VERSUS TIME

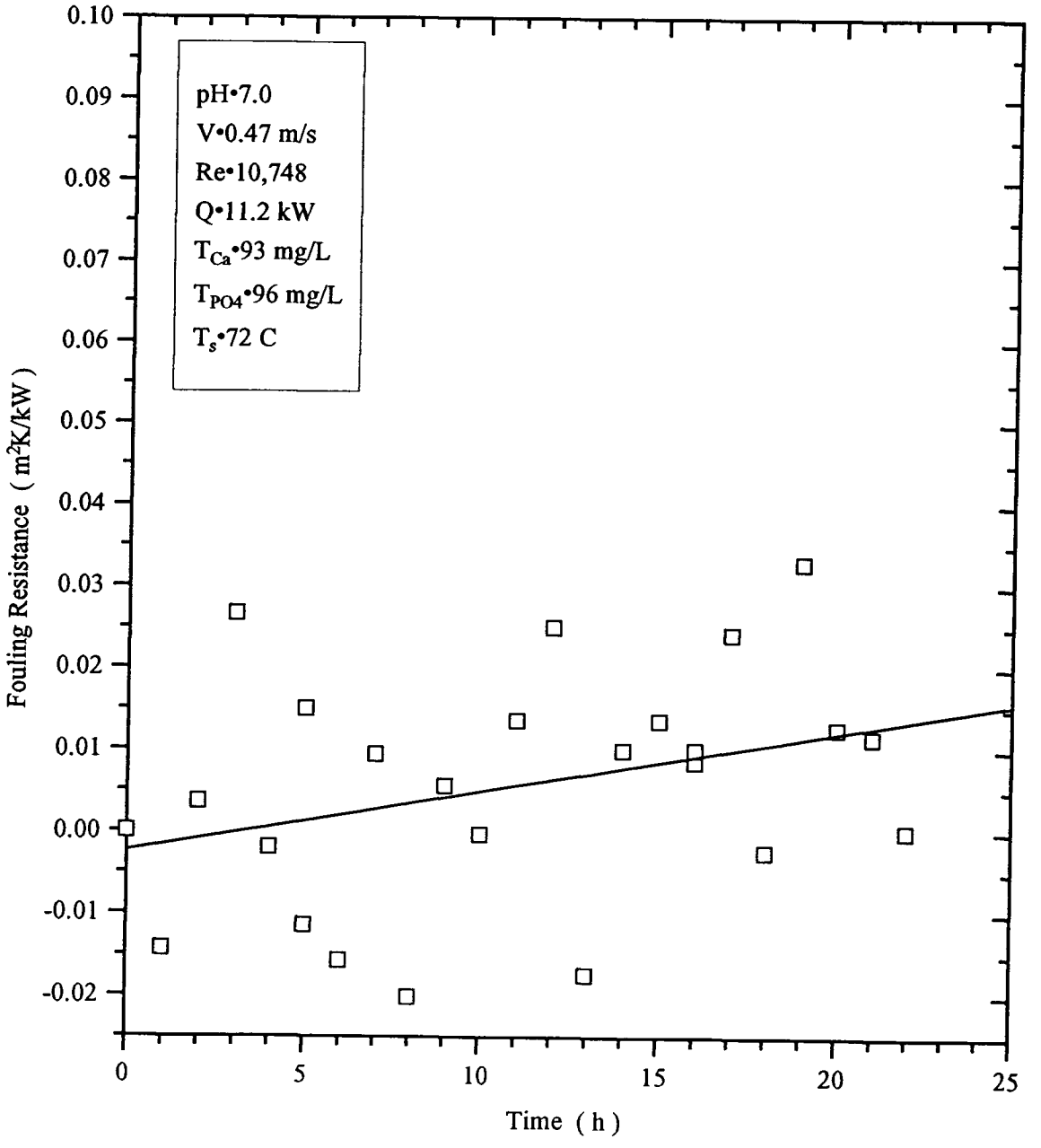

FIGURE IV-27 RUN 31 FOULING RESISTANCE VERSUS TIME

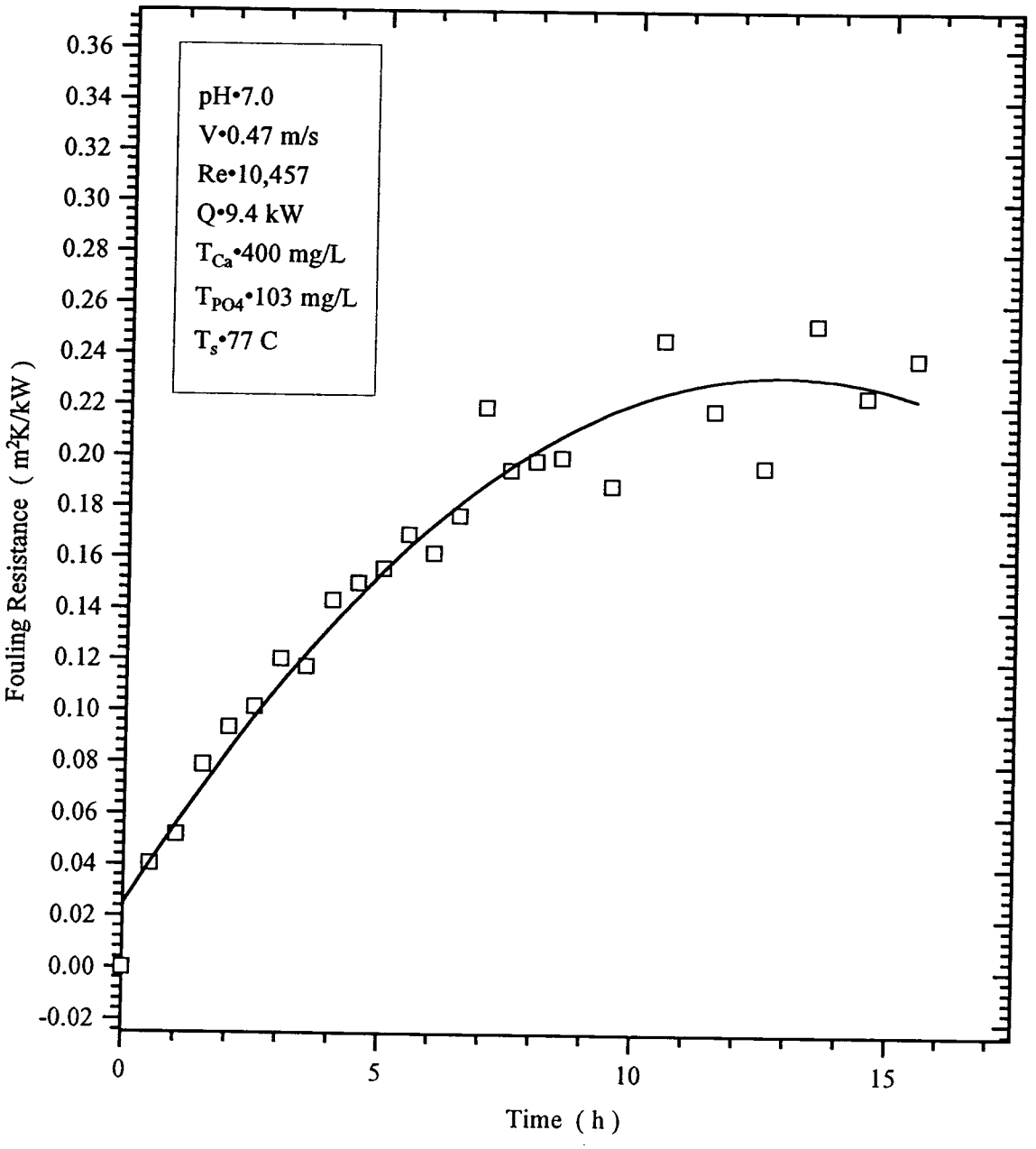

FIGURE IV-28 RUN 32 FOULING RESISTANCE VERSUS TIME

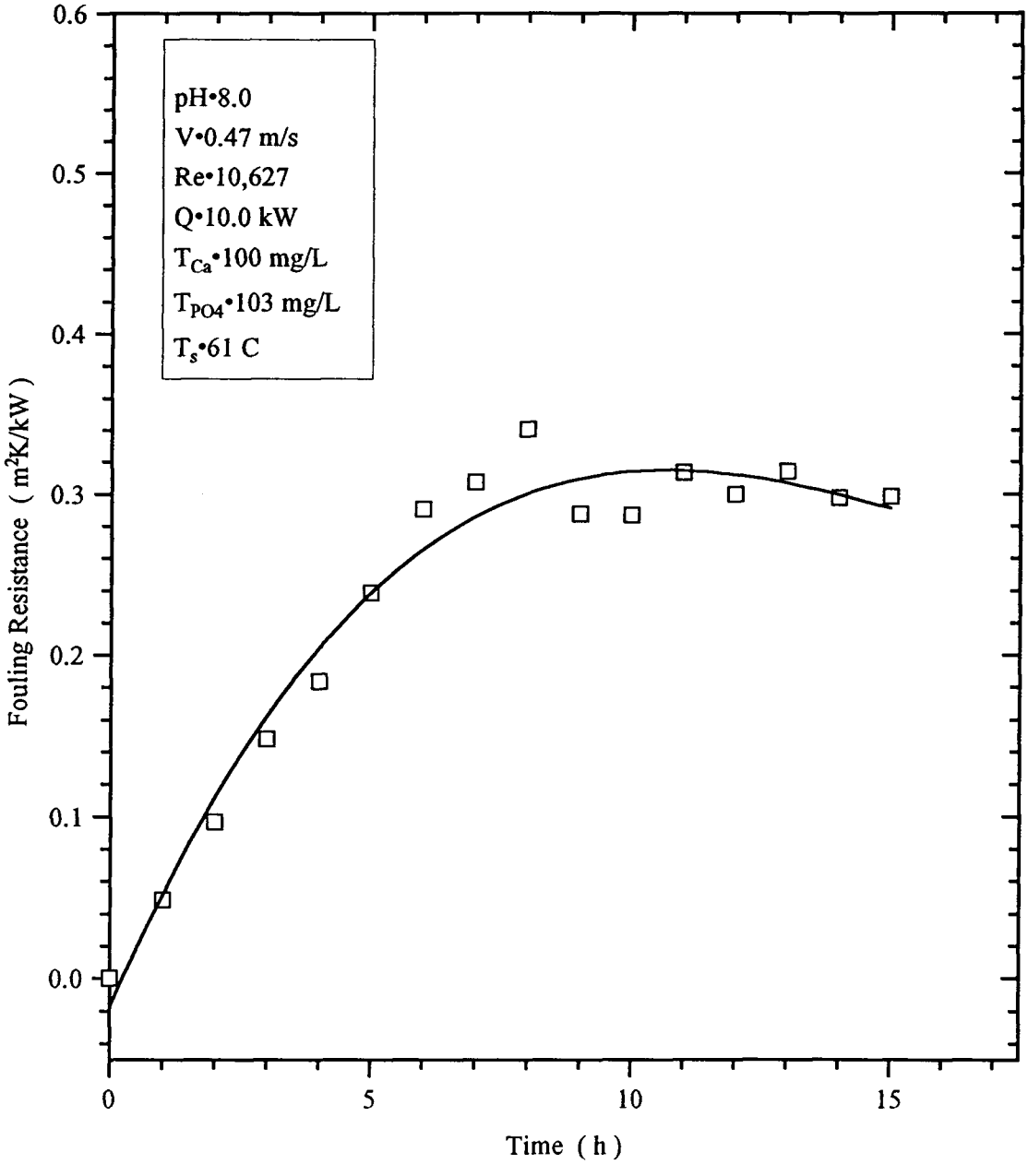

FIGURE IV-29 RUN 33 FOULING RESISTANCE VERSUS TIME

DT	TC	TH	LMTD	TIME	Q	UOD	RFC	RFU	TS	TWALL	HI
5.6	19.6	107.0	87.4	1.0	9.38	1.278	0.0000	0.000	50.2	50.2	4.477
5.5	20.1	107.4	87.3	2.0	9.21	1.256	0.0085	0.013	50.9	51.9	4.509
5.4	20.1	108.3	88.1	3.0	9.05	1.222	0.0256	0.036	51.2	54.0	4.548
5.4	20.1	109.1	89.0	4.0	9.05	1.210	0.0340	0.044	51.3	55.0	4.559
5.4	20.0	109.8	89.7	5.0	9.05	1.200	0.0405	0.050	51.3	55.6	4.567
5.4	20.0	110.4	90.4	6.0	9.05	1.191	0.0470	0.057	51.3	56.4	4.575
5.4	20.0	111.1	91.0	7.0	9.05	1.183	0.0525	0.063	51.4	57.1	4.583
5.2	20.0	111.7	91.7	8.0	8.71	1.131	0.0811	0.101	51.7	60.2	4.649
5.4	20.1	112.3	92.2	9.0	9.05	1.168	0.0637	0.074	51.6	58.5	4.599
5.3	20.0	112.8	92.7	10.0	8.88	1.141	0.0790	0.094	51.7	60.1	4.633
5.3	20.0	113.4	93.4	11.0	8.88	1.132	0.0857	0.101	51.8	60.9	4.641
5.5	20.1	113.8	93.8	12.0	9.21	1.170	0.0673	0.072	51.5	58.9	4.589
5.6	20.2	114.1	93.9	13.0	9.38	1.189	0.0583	0.058	51.5	58.0	4.565
5.3	19.9	114.3	94.4	14.0	8.88	1.120	0.0951	0.110	51.8	61.8	4.652
5.6	20.0	114.8	94.7	15.0	9.38	1.179	0.0654	0.065	51.4	58.7	4.572
5.3	19.8	115.0	95.1	16.0	8.88	1.111	0.1022	0.117	51.7	62.5	4.659
5.5	19.9	115.3	95.4	17.0	9.22	1.150	0.0818	0.087	51.5	60.5	4.606
5.5	19.9	115.6	95.6	18.0	9.22	1.148	0.0837	0.089	51.6	60.7	4.609
5.4	20.1	116.1	96.0	19.0	9.05	1.122	0.0985	0.109	51.9	62.5	4.643
5.4	20.1	116.4	96.3	20.0	9.05	1.119	0.1013	0.111	51.9	62.9	4.647
5.3	20.0	116.6	96.5	21.0	8.88	1.095	0.1155	0.131	52.1	64.3	4.678
5.2	20.0	116.6	96.6	22.0	8.71	1.073	0.1288	0.149	52.1	65.5	4.708
5.4	20.2	117.1	96.9	23.0	9.05	1.112	0.1069	0.117	52.1	63.6	4.655
5.4	20.1	117.3	97.1	24.0	9.05	1.109	0.1092	0.119	52.0	63.8	4.656
5.2	19.9	117.3	97.4	25.0	8.71	1.065	0.1365	0.157	52.1	66.2	4.716
5.5	20.1	117.6	97.5	26.0	9.21	1.125	0.1010	0.106	51.8	62.9	4.631
5.4	20.1	117.8	97.6	27.0	9.05	1.103	0.1139	0.124	52.1	64.3	4.662
5.4	19.9	117.8	97.9	28.0	9.05	1.100	0.1166	0.127	51.9	64.4	4.663

SDTW	SDQA	SDTS
0.0216	0.0349	0.0763

TC(avg)	TH(avg.)	Q(avg.)	TS(avg.)
20.0	113.8	9.0	51.6

NREF= 16392.2 NREC= 8950.8

Figure IV-30 Output of Computer Program III-1 for Run 2

```
  K1     K2      K3       K4     .833E-02  .996E-07  .120E-11  .157E+02
  K5     K6      K7       KW     .174E+02  .257E+03  .104E+07  .965E-14
  H      OH      CA               .342E-07  .282E-06  .756E-03
CAOH   CAH2PO  CAHPO4   CAPO4    .336E-08  .278E-05  .120E-03  .170E-04
H3PO4  H2PO4   HPO4     PO4      .867E-09  .211E-03  .616E-03  .216E-07
  I      II      Z                .49417354E-02  .49417689E-02  4.0
  FM     FD      FT               .9257  .7344  .4993
DDCPD  DHAP    DTCP    DOCP    0.96E+00  0.96E+11  0.17E+04  0.30E+03
SDCPD  SHAP    STCP    SOCP   -0.21E-07  0.70E-45  0.20E-24  0.11E-42
SPOS = .331E-02    SNEG = .277E-02
PH = 7.5           TCA = 0.89E-03           TPO4 = 0.97E-03
```

Figure IV-31 Output of Computer Program III-2 for Run 2